SAIMM
THE SOUTHERN AFRICAN INSTITUTE OF MINING AND METALLURGY
VOLUME 121 NO. 8 AUGUST 2021

Developing the mining industry's future leaders

SAIMM, bringing together world-class knowledge and a professional community to drive African solutions for a sustainable future.

SAIMM is focused on nurturing the future leaders of Southern Africa's minerals industry


This image was kindly supplied by the Minerals Council South Africa

We provide a collaborative multistakeholder platform that connects minerals professionals throughout the region and across the globe. With our technical capacity, contemporary industry insights and global reach and alliances, SAIMM is able to help Southern African individuals and corporates raise the bar across the minerals industry.

LINK TO VIDEO

Our offerings are structured around four key pillars, each of which is fundamentally focused on Africa.

International professional relevance

SAIMM maintains its international professional relevance through its experienced team, extensive membership base, far-reaching network and concerted industry involvement.

Information and resource portal

The wealth of information housed within SAIMM ensures our members have access to relevant, accurate and modern information relevant to our industry.

Convening capacity

We help to stimulate debate, foster collaboration and inspire change.

Training and development

We pride ourselves on the world-class technical events and training sessions we host, each of which is designed to equip our members with valuable networks and experiences that fuel their professional development.

Membership

Student	**Associate**	**Member** MSAIMM	**Fellow** FSAIMM	**Company Affiliate**	**Corporate Partner**
For 3rd+ year students who want access to world-class knowledge and a professional network.	For young working professionals (18+ years) in the industry who are looking for access to modern insights, a professional network and/or a mentor to help you navigate your career.	For working professionals in the industry looking for access to modern, innovative knowledge and engagement with specialists and peers on current industry topics.	For 35+ years, senior professionals with 5+ years experience and 5+ years as a SAIMM member – apply to become a fellow with international recognition and ability to sign off on specialist work.	For small companies associated with the industry looking for access to current, modern knowledge and a professional network to engage.	For large corporates looking to provide their qualifying employees with access to world-class, modern knowledge, and platforms to engage the broader industry and communities.

SAIMM is the platform to facilitate this collaboration. Join us.

For all general enquiries, please contact Sam Moolla, who heads up the team.
email-sam@saimm.co.za

SAIMM
THE SOUTHERN AFRICAN INSTITUTE OF MINING AND METALLURGY

OFFICE BEARERS AND COUNCIL FOR THE 2020/2021 SESSION

Honorary President

Mxolisi Mgojo
President, Minerals Council South Africa

Honorary Vice Presidents

Gwede Mantashe
Minister of Mineral Resources, South Africa

Ebrahim Patel
Minister of Trade, Industry and Competition, South Africa

Blade Nzimande
Minister of Higher Education, Science and Technology, South Africa

President

V.G. Duke

President Elect

I.J. Geldenhuys

Senior Vice President

Z. Botha

Junior Vice President

W.C. Joughin

Incoming Junior Vice President

E Matinde

Immediate Past President

M.I. Mthenjane

Co-opted to Office Bearers

S. Ndlovu
G.R. Lane

Honorary Treasurer

W.C. Joughin

Ordinary Members on Council

B. Genc
G.R. Lane
K.M. Letsoalo
T.M. Mmola
G. Njowa
S.J. Ntsoelengoe
S.M. Rupprecht
N. Singh
A.G. Smith
M.H. Solomon
A.J.S. Spearing
S.J. Tose
M.I. van der Bank
A.T. van Zyl
E.J. Walls

Co-opted Members

Z. Fakhraei

Past Presidents Serving on Council

N.A. Barcza
R.D. Beck
J.R. Dixon
H.E. James
R.T. Jones
A.S. Macfarlane
C. Musingwini
S. Ndlovu
J.L. Porter
S.J. Ramokgopa
M.H. Rogers
D.A.J. Ross-Watt
G.L. Smith
W.H. van Niekerk

G.R. Lane–TPC Mining Chairperson
Z. Botha–TPC Metallurgy Chairperson

S.F. Manjengwa–YPC Chairperson
A.T. Chinhava–YPC Vice Chairperson

Branch Chairpersons

Johannesburg	D.F. Jensen
Namibia	N.M. Namate
Northern Cape	I. Lute
Pretoria	S. Uludag
Western Cape	A.B. Nesbitt
Zambia	D. Muma
Zimbabwe	C.P. Sadomba
Zululand	C.W. Mienie

PAST PRESIDENTS

*Deceased

* W. Bettel (1894–1895)
* A.F. Crosse (1895–1896)
* W.R. Feldtmann (1896–1897)
* C. Butters (1897–1898)
* J. Loevy (1898–1899)
* J.R. Williams (1899–1903)
* S.H. Pearce (1903–1904)
* W.A. Caldecott (1904–1905)
* W. Cullen (1905–1906)
* E.H. Johnson (1906–1907)
* J. Yates (1907–1908)
* R.G. Bevington (1908–1909)
* A. McA. Johnston (1909–1910)
* J. Moir (1910–1911)
* C.B. Saner (1911–1912)
* W.R. Dowling (1912–1913)
* A. Richardson (1913–1914)
* G.H. Stanley (1914–1915)
* J.E. Thomas (1915–1916)
* J.A. Wilkinson (1916–1917)
* G. Hildick-Smith (1917–1918)
* H.S. Meyer (1918–1919)
* J. Gray (1919–1920)
* J. Chilton (1920–1921)
* F. Wartenweiler (1921–1922)
* G.A. Watermeyer (1922–1923)
* F.W. Watson (1923–1924)
* C.J. Gray (1924–1925)
* H.A. White (1925–1926)
* H.R. Adam (1926–1927)
* Sir Robert Kotze (1927–1928)
* J.A. Woodburn (1928–1929)
* H. Pirow (1929–1930)
* J. Henderson (1930–1931)
* A. King (1931–1932)
* V. Nimmo-Dewar (1932–1933)
* P.N. Lategan (1933–1934)
* E.C. Ranson (1934–1935)
* R.A. Flugge-De-Smidt (1935–1936)
* T.K. Prentice (1936–1937)
* R.S.G. Stokes (1937–1938)
* P.E. Hall (1938–1939)
* E.H.A. Joseph (1939–1940)
* J.H. Dobson (1940–1941)
* Theo Meyer (1941–1942)
* John V. Muller (1942–1943)
* C. Biccard Jeppe (1943–1944)
* P.J. Louis Bok (1944–1945)
* J.T. McIntyre (1945–1946)
* M. Falcon (1946–1947)
* A. Clemens (1947–1948)
* F.G. Hill (1948–1949)
* O.A.E. Jackson (1949–1950)
* W.E. Gooday (1950–1951)
* C.J. Irving (1951–1952)
* D.D. Stitt (1952–1953)
* M.C.G. Meyer (1953–1954)
* L.A. Bushell (1954–1955)
* H. Britten (1955–1956)
* Wm. Bleloch (1956–1957)
* H. Simon (1957–1958)
* M. Barcza (1958–1959)
* R.J. Adamson (1959–1960)
* W.S. Findlay (1960–1961)
* D.G. Maxwell (1961–1962)
* J. de V. Lambrechts (1962–1963)
* J.F. Reid (1963–1964)
* D.M. Jamieson (1964–1965)
* H.E. Cross (1965–1966)
* D. Gordon Jones (1966–1967)
* P. Lambooy (1967–1968)
* R.C.J. Goode (1968–1969)
* J.K.E. Douglas (1969–1970)
* V.C. Robinson (1970–1971)
* D.D. Howat (1971–1972)
* J.P. Hugo (1972–1973)
* P.W.J. van Rensburg (1973–1974)
* R.P. Plewman (1974–1975)
* R.E. Robinson (1975–1976)
* M.D.G. Salamon (1976–1977)
* P.A. Von Wielligh (1977–1978)
* M.G. Atmore (1978–1979)
* D.A. Viljoen (1979–1980)
* P.R. Jochens (1980–1981)
* G.Y. Nisbet (1981–1982)
  A.N. Brown (1982–1983)
* R.P. King (1983–1984)
  J.D. Austin (1984–1985)
  H.E. James (1985–1986)
  H. Wagner (1986–1987)
* B.C. Alberts (1987–1988)
* C.E. Fivaz (1988–1989)
* O.K.H. Steffen (1989–1990)
* H.G. Mosenthal (1990–1991)
  R.D. Beck (1991–1992)
* J.P. Hoffman (1992–1993)
* H. Scott-Russell (1993–1994)
  J.A. Cruise (1994–1995)
  D.A.J. Ross-Watt (1995–1996)
  N.A. Barcza (1996–1997)
* R.P. Mohring (1997–1998)
  J.R. Dixon (1998–1999)
  M.H. Rogers (1999–2000)
  L.A. Cramer (2000–2001)
* A.A.B. Douglas (2001–2002)
  S.J. Ramokgopa (2002-2003)
  T.R. Stacey (2003–2004)
  F.M.G. Egerton (2004–2005)
  W.H. van Niekerk (2005–2006)
  R.P.H. Willis (2006–2007)
  R.G.B. Pickering (2007–2008)
  A.M. Garbers-Craig (2008–2009)
  J.C. Ngoma (2009–2010)
  G.V.R. Landman (2010–2011)
  J.N. van der Merwe (2011–2012)
  G.L. Smith (2012–2013)
  M. Dworzanowski (2013–2014)
  J.L. Porter (2014–2015)
  R.T. Jones (2015–2016)
  C. Musingwini (2016–2017)
  S. Ndlovu (2017–2018)
  A.S. Macfarlane (2018–2019)
  M.I. Mthenjane (2019–2020)

Honorary Legal Advisers
MH Attorneys

Auditors
Genesis Chartered Accountants

Secretaries
The Southern African Institute of Mining and Metallurgy
Fifth Floor, Minerals Council South Africa
5 Hollard Street, Johannesburg 2001 • P.O. Box 61127, Marshalltown 2107
Telephone (011) 834-1273/7 • Fax (011) 838-5923 or (011) 833-8156
E-mail: journal@saimm.co.za

Typeset and Published by
The Southern African Institute of Mining and Metallurgy
P.O. Box 61127
Marshalltown 2107
Telephone (011) 834-1273/7
Fax (011) 838-5923
E-mail: journal@saimm.co.za

Printed by
Camera Press, Johannesburg

Advertising Representative
Barbara Spence
Avenue Advertising
Telephone (011) 463-7940
E-mail: barbara@avenue.co.za

ISSN 2225-6253 (print)
ISSN 2411-9717 (online)

Directory of Open Access Journals
INDEXED IN DOAJ

SAIMM
JOURNAL OF THE SOUTHERN AFRICAN INSTITUTE OF MINING AND METALLURGY
VOLUME 121 NO. 8 AUGUST 2021

Contents

Research and its qualities†

On a summer day at the University of Chicago several years ago Larry McEnerney, then Director of the University's Writing Program, gave a lecture on 'The craft of writing effectively'. It was to a class of graduate students in the social and natural sciences. From the outset, McEnerney challenged widely held views on writing. Writing, he said, is mistakenly taught as a process governed by rules. 'Stop thinking about rules; start thinking about readers' and 'use writing to help [one] self think', he urged the class. McEnerney then identified the most important quality that marks all effective writing. But he did so only after he had ticked off qualities that we all readily attach to good writing:

'Yeh, your writing needs to be *clear*. Sure, [it] needs to be *organized* . . . to be *persuasive*. But more than anything else [it] needs to be *valuable*' [my emphasis].

As he ticks off each quality, McEnerney writes it on the blackboard. Each quality sits above the preceding one; *valuable*, unlined, stands out at the top of the list. To emphasize the point he ends, 'The other stuff doesn't matter if it is not valuable'.

Writing in some form—as a report or an academic paper, for example—closes off most bodies of research that we undertake. It is no coincidence, then, that the defining quality that McEnerney attaches to effective *writing* is echoed in effective or good research. That echo reverberates in the question, 'What is research?', or more specifically, 'What characterizes good *research*?' There are, however, different pitches to the echo depending on who you are. To hear them one needs to clarify research in the context of the SAIMM and its membership.

The Institute serves three engineering disciplines—mining, extractive metallurgy, and physical metallurgy or allied branches in material science. These disciplines divide the Institute along lines of *subject*. Another division cuts across these lines, setting members apart *within* their disciplines. This is the division that separates engineers in industry from academics at universities. It is marked, but it is not impervious: some members—a minority—may switch 'camps', even temporarily, depending on whether the problem at hand is framed by an industrial or academic/scholarly need. Being a member of one or other camp is not in itself grounds for discrimination. What is important, however, is the different sense each camp attaches to what is valuable in research. We all know that, as a rule, engineers in industry place value on practical applications. They will view research favourably if it cuts costs or brings in profit; if it introduces measures that secure the safety of workers or that reduce harm to the environment; or if it raises productivity, improves efficiencies, or sets out new possibilities. Value here also has a dimension in time: the value of research might well change when judged in the short, medium, or long term. These values inform research conducted in industry. One thinks of what passed/passes as research at the former Anglo Research and at Mintek. They also inform, and this is far-reaching, the engineer as *reader*—'value lies with the reader' is a point that McEnerney makes. Here we face a dilemma that lingers at the core of the *Journal* of the SAIMM: many of the papers published in the Journal are written by academics, who invoke a different set of criteria, including a different sense of value, when judging the worth of a paper. Their papers will reflect these criteria, and this will not sit comfortably with the other group, which is also the larger.

Compounding this problem between camps is a blight *within* the academic camp. To appreciate it we need to take stock of how academics view research. What for the academic constitutes 'good' research, where 'good' refers to a standard? (I am discounting the notion of excellence, which connotes

---

†This editorial arose out of introductory remarks I made at a meeting of the Publications Committee in March this year. It owes much to the discussion that followed those remarks. I am indebted particularly to Dick Stacey and Rodney Jones for their thoughts in personal communications following that meeting. I trust that I have not misrepresented them. I have had many hours of discussion with two senior colleagues—Hurman Eriç, Chamber of Mines Professor of Extractive Metallurgy, and David Lewis-Williams, Professor Emeritus of Cognitive Archaeology, both of them at the University of the Witwatersrand.

Journal Comment *(continued)*

'excelling'—pre-eminence or superiority—and therefore practices of comparison and performance.) All of science is marked primarily by asking questions. *Good* science or research asks questions of significance, questions that address a key, if not fundamental, concern, questions that look for insight. Nothing is trivial about them—profound might be no exaggeration: In the beginning is the question. Value for the academic consists primarily in the 'reach' of these questions. That is not to say that industry does not ask significant questions. Its questions differ not by degree but in class. Questions are less likely to be fundamental than applied, they are less about understanding fundamental processes than about feasibility at the industrial scale. Business and industrial criteria frame the applied category; it is they that impart significance to the questions asked. Not so in academia. Asking the right question is what some academics call 'Research, with a capital R'. There is no algorithm, rubric, or procedure to finding that question. It is up to chance. One can stack the odds, however; for chance, in Louis Pasteur's memorable phrase, 'favours the prepared mind'.

Not only is finding the right question difficult, but preparing one's mind is hard work, and that contributes to the poor quality of many papers produced at universities. This quality reflects inferior research. The greater part of preparing one's mind is reading extensively, both within and without one's field of study. The effort is huge. That we understand English brings little comfort. But not knuckling down to the effort is only part of the problem. The other part is the element of blissful ignorance. The English historian Eric Hobsbawm, in an interview with Simon Schama, a fellow historian, summed it up poignantly when he despaired of historians' (read engineers' and researchers') 'using the by-products, not the thinking'. What are the by-products of our profession? I suggest they consist in two activities that, properly engaged, support good research/Research. They are method and procedure, which is coupled with technique. Method, as implied in the philosophical label 'scientific method' and understood by eminent scholars, refers to the logic we use to validate a thesis or hypothesis, to argue a case, or to work to a solution. (Method is not to be confused with methodology, which is the study of method, an activity that exercises the minds of philosophers.) any of the engineers with whom I have engaged have only a passing knowledge of the logical processes they use to arrive at technical answers. At best, they are unaware of how they think but get it right, or they hide behind statistical tests in the mistaken belief that rigour leads to objective truths; at worst, they run foul of the asymmetries and rules in logical structures. Flawed logic calls into question the validity of research. Nevertheless, papers demonstrating flawed logic continue to be submitted for publication. Some of them slip through the net of peer review and make it to press.

Whereas method is abstract and remote for engineers, empirical procedures are concrete and reassuring. They set out which tests will be conducted, how these tests will be run, and the techniques (the instruments) that will be used. How many engineers know that all these activities are governed by theory—theory appropriate to the principles underlying a technique *and* theory appropriate to the problem that is the object of a study? Yet the Publications Committee receives papers in which procedures and techniques are disconnected from the problem. It is as if understanding (from theory and principles) and judgment have been suspended. But like specious arguments, procedures, techniques and their inscriptions (graphs and tables) display the trappings of science. They dazzle researchers as much as these practitioners hope to dazzle readers. The satirical BAHFest (Festival of Bad Ad Hoc Hypotheses) plays on this sophistry (much as the Ig Nobel prize 'celebrates' 'trivial questions pursued as research'). The misuse of method and procedure is, I suggest, the 'by-product' that, along with asking trivial questions, displaces thinking in poor research.

I have not mentioned communication, the writing of academic papers. It stands apart from questions, methods and procedures in that it does not correlate with good or bad research. Bad writing, however, might well relegate good research to the peripheries of science, if not to oblivion—unless a sympathetic editor, looking through the mist of text and discerning forms of value, gives the authors a chance to redeem themselves.

The papers in this issue of the Journal are not collected around a theme. There may be something here that, consequently, interests a broad section of readers. Ask yourself what value you attach to the point or points of interest you find in any of the papers.

P. den Hoed

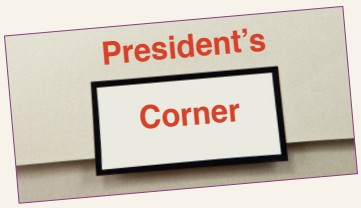

Discovering Rare Earth Elements

'All truths are easy to understand once they are discovered; the point is to discover them.' – Galileo Galilei

With the approaching SAIMM event focusing on rare earth elements (REEs) in October 2021, I have decided to utilize my final address to discuss REEs, which in my opinion remain a potential game-changer in the Southern African mining and industrial landscape.

The purpose of the SAIMM's Rare Earths International Conference is to provide more information on all aspects of REEs including mining, extraction, and industrial applications. Before we can delve into the complexities of REEs, we must first understand what they are.

The first element to be considered an REE was in a rock excavated in Sweden in 1788. The element, yttrium, was considered 'rare' as it had never been discovered before and at the time the geological term 'earth' defined minerals that were acid-soluble.

There are 17 REEs, all of which are metals and are often found together due to their similar properties. Fifteen of these elements are found in the range in atomic numbers from 57 [lanthanum (La)] to 71 [lutetium (Lu)], commonly referred to as the lanthanides. In addition, yttrium (Y, atomic number 39) and scandium (Sc, atomic number 21) are also commonly regarded as REEs because they share chemical and physical similarities and affinities with the lanthanides. The following periodic table illustrates where the REEs can be found.

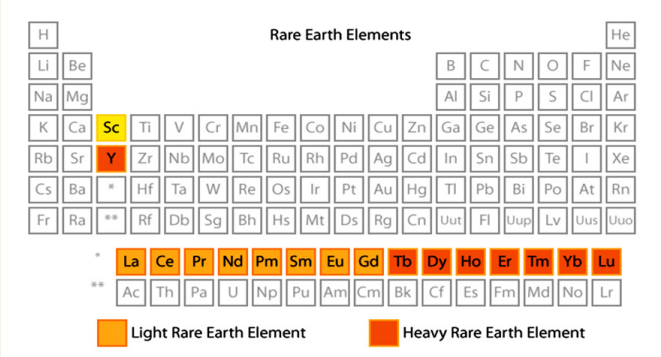

The global extraction of REEs has increased significantly since the early 1960s to the extent that they are no longer technically 'rare'. This increase in production has been driven by an increased demand for REEs, brought about by corresponding technological advances as well as new environmental engineering applications. REEs are widely used in rechargeable batteries, including those in mobile phones, and are thus a critical part of our daily lives. This rechargeable property is also used in the current fleet of electrical and hybrid vehicles. As such, they provide us with a vital tool to combat greenhouse gas emissions from diesel and petrol engines. With further technological and eco-sustainability advances, the demand for REEs is bound to increase in the future.

REE production is currently dominated by China. In 2020, China produced around 140 000 metric tons of REEs; the USA following far behind at 38 000 metric tons. China is also the largest consumer of these metals, which are used in the manufacturing of electronic products for local and international markets.

Although REEs are not 'rare' in terms of their average crustal abundance, concentrated deposits of REEs are limited in number. Southern Africa is fortunate to have a globally significant REE Mineral Resource inventory, including the Steenkampskraal Mine, located in Western Province, which contains one of the world's highest grade REE Mineral Reserves.

Considering the combination of quality REE mineral resource assets and our long-established industrial sector, the potential for developing REE-focused industrial sectors in Southern Africa appears to be promising.

I therefore encourage all our readers and members to participate in the SAIMM's up-and-coming REE conference. Get informed and involved in REEs. They will continue to touch our daily lives and change the world around us.

V.G. Duke
President, SAIMM

Evolution of oxide and nitride inclusions during processing of stainless steel

Y. Kacar[1], D. Kruger[2], and P.C. Pistorius[1]

Affiliation:
[1]Center for Iron and Steelmaking Research, Department of Materials Science and Engineering Carnegie Mellon, University, Pittsburgh, PA, U.S.A.
[2]Columbus Stainless Pty Ltd, South Africa .

Correspondence to:
C. Pistorius

Email:
pistorius@cmu.edu

Dates:
Received: 7 Oct. 2019
Revised: 23 Dec. 2020
Accepted: 21 Apr. 2021
Published: August 2021

How to cite:
Kacar, Y., Kruger, D., and Pistorius, P.C. 2021
Evolution of oxide and nitride inclusions during processing of stainless steel.
Journal of the Southern African Institute of Mining and Metallurgy, vol. 121, no. 8, pp. 379–384

DOI ID:
http://dx.doi.org/10.17159/2411-9717/923/2021

ORCID:
C. Pistorius
https://orcid.org/0000-0002-2966-1879

Synopsis

Because of its superior properties, stainless steel has been widely used for many applications. Nonmetallic inclusions can influence the quality of stainless steel products. A set of samples was used to track the response of inclusion composition during processing of a heat of titanium-bearing 18% chromium steel, from deoxidation after decarburization, to the solidified slab. The oxide inclusions responded as expected to additions of deoxidizers and calcium treatment, changing from silica to alumina and spinels, and then to calcium aluminates. The samples confirmed that titanium nitride can nucleate on liquid calcium aluminate during steel solidification.

Keywords
stainless steel, inclusion, oxides, titanium nitride precipitation, solidification.

Introduction

Nonmetallic inclusions that can be present in stainless steels include oxides, nitrides, and sulphides (Park and Kang, 2017). In this work we studied changes in oxide inclusions and the associated formation of titanium nitride and niobium carbonitride during processing of a ferritic stainless steel (containing 18% Cr). The investigation was based on a previous study that considered the change in oxide inclusions when processing a similar ferritic stainless steel in the same plant (Kruger and Garbers-Craig, 2017).

Background

The stainless steel production route typically includes melting of raw materials in an electric arc furnace (EAF), removing excess carbon by argon-oxygen decarburization (AOD) or vacuum decarburization, establishing the final temperature and composition of the liquid steel by ladle treatment, and continuous casting (Washko and Aggen, 1990). During processing, the steel can pick up nitrogen from the use of nitrogen during decarburization (in production of austenitic grades), from raw materials and exposure to the atmosphere, or nitrogen can be added intentionally. In ferritic stainless steel (based on binary Fe-Cr alloys), titanium is frequently added to bind nitrogen as titanium nitride.

In such steels, titanium nitride (TiN) normally precipitates during solidification. Titanium nitride inclusions are very hard – indeed, titanium nitride coatings extend the life of cutting tools – and such hard inclusions play an important role in microcrack formation in steel (Fairchild, Howden, and Clark, 2000). Inclusion shape is also important (*ibid.*). Because of its high entropy of melting, titanium nitride typically forms as faceted (cubic) particles with sharp corners during solidification (Fu *et al.*, 2017). The effect of angular inclusions on the mechanical behaviour of the steel can be strong: In bearing steels the deleterious effect of 6 µm TiN inclusions on the fatigue life of steel is equivalent to that of 25 µm globular oxide inclusions (Monnot, Heritier, and Cogne, 1988).

For the steel considered in this work, both titanium nitride and niobium carbonitride are expected to form during solidification: Figure 1 shows the predicted precipitation of these phases. The composition used in this calculation is that of the steel in the tundish (as measured in this work); see the sample labelled 'Tundish' in Table I (more detailed sample descriptions are provided in the section 'Steel samples'). The expected phases were calculated with Thermo-Calc (Andersson *et al.*, 2002) using the

Table I

Compositions of steel samples studied in this work (mass percentages); sample descriptions are provided in the 'Steel samples' section

Sample	C	Al	S	Ca	N	Ti	Nb	Mn	Si
AOD	0.013	0.003	0.0040	0.000	0.009	0.000	0.000	0.46	0.4
L1	0.016	0.095	0.0030	0.000	0.011	0.000	0.377	0.45	0.37
L3	0.015	0.048	0.0010	0.003	0.015	0.207	0.308	0.45	0.49
Tundish	0.015	0.034	0.0010	0.002	0.018	0.184	0.390	0.45	0.5
Slab	0.015	0.035	0.0010	0.002	0.017	0.159	0.412	0.45	0.5

Others: 18% Cr; balance Fe

TCFE9 database. Two conditions were considered: equilibrium, and Scheil-type solidification (with full mixing in the liquid, and no diffusion in the solid phases). Under equilibrium conditions, only titanium nitride would form upon solidification (Figure 1), but under Scheil conditions (severe microsegregation), niobium carbonitride would form during the last stages of solidification. The results presented later in this paper demonstrate that niobium carbonitride did form in these steel samples.

Microsegregation of niobium and titanium during solidification is the result of both an equilibrium effect (partitioning of these elements to the remaining liquid during solidification) and a kinetic effect (limited diffusion in the solid). Strong partitioning of niobium and titanium is confirmed by the partition coefficients between liquid and ferrite, as listed in Table II (calculated with Thermo-Calc and TCFE9 for the onset of solidification of the same steel composition as in Figure 1). The partition coefficient is the equilibrium ratio of the concentration (expressed as a mass percentage) of the element in the solid to its concentration in the liquid. Values far from unity indicate strong partitioning. As the table shows, little partitioning of chromium, silicon, and manganese occurs during solidification (their partition coefficients are close to unity), but titanium and niobium partition strongly to the liquid, as do carbon, nitrogen, and sulphur. Strong partitioning enhances the formation of titanium nitride and niobium carbonitride, as studied in the work reported here.

Literature survey: titanium nitride formation in stainless steel

In previous work, it was found that magnesium spinel inclusions (chemical composition: solid solution based on $MgAl_2O_4$) are present in liquid 11% Cr stainless steel that was deoxidized with aluminium (Kruger and Garbers-Craig, 2017). Alumina (Al_2O_3) is the initial oxide inclusion product that forms upon deoxidation of the steel, but tends to transform to spinel during ladle processing. The transformation can occur by transfer of magnesium from the slag to the oxide, with a low concentration of dissolved magnesium in the steel as the reaction intermediate (Kumar and Pistorius, 2018).

If spinel forms it can nucleate titanium nitride (TiN) during solidification (Fujimura *et al.*, 2011; Park, 2011; Kruger and Garbers-Craig, 2017). The small lattice misfit between spinel and TiN is stated to promote such nucleation (Park, 2011). Precipitation of titanium nitride is promoted not only by the presence of spinel nuclei, but also by strong partitioning of titanium and nitrogen to the remaining liquid during solidification (Fu *et al.*, 2017; Capurro and Cicutti, 2018).

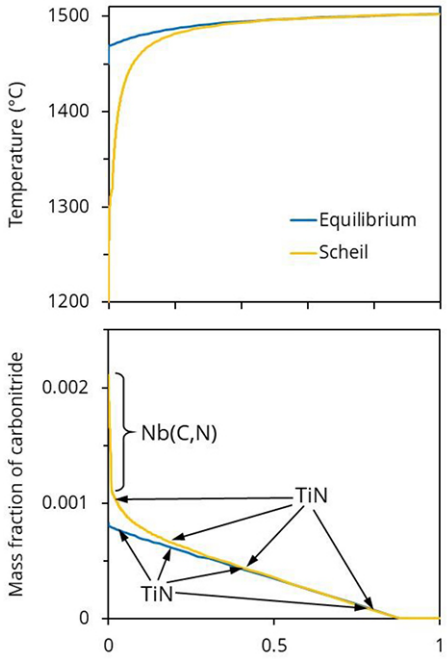

Figure 1—Calculated solidification behaviour (upper figure) and nitride and carbonitride formation (for steel with the 'tundish' composition, Table I) under equilibrium and Scheil conditions

Table II

Equilibrium partition coefficients between ferrite and liquid of elements in 18% chromium steel (at the start of solidification; liquidus temperature 1501°C; steel of 'tundish' composition in Table I). Calculated with Thermo-Calc

Cr	Si	Mn	Ti	Nb	C	N	S
1.01	0.95	0.84	0.34	0.15	0.21	0.27	0.10

Partitioning increases the concentrations of titanium and nitrogen in the last liquid that remains between ferrite dendrites.

If it forms, titanium nitride can in turn act as a nucleant for ferrite solidification in the equiaxed zone of the solidifying metal. Titanium nitride can nucleate ferrite despite the large lattice disregistry (17%) between the (111) plane of TiN and the (110) plane of ferrite: a Kurdjumov-Sachs orientation relationship between TiN and surrounding ferrite grains was found in 17% chromium steel after solidification (Fu *et al.*, 2017). The ability of TiN to nucleate ferrite is in line with the observation that the as-solidified ferrite grain size is smaller in steels with higher titanium concentrations (Park, 2011).

However, some studies showed that inclusions other than spinel can also nucleate titanium nitride. Observed nuclei included alumina (Wang *et al.*, 2013) and – in steels with negligible Al concentrations – oxides and sulphides containing magnesium (Michelic *et al.*, 2015). The ability of oxides other than spinel to nucleate titanium nitride is potentially of importance in controlling the extent and size of titanium nitride precipitation in finished steel products. To study possible nucleation by non-spinel inclusions, in this work steel samples were examined from various stages of stainless steel processing. Steel refining during these stages caused the composition of the oxide inclusions to change, from silicates (after decarburization

and deoxidation with ferrosilicon) to spinel (after deoxidation with aluminium), and finally to calcium aluminates (after calcium treatment). In addition, inclusions were examined to detect possible niobium carbonitride precipitation: titanium nitride can act as a substrate for carbonitride formation upon further solidification (Michelic *et al.*, 2015). Titanium nitride and niobium carbonitride are not expected to form while the steel is fully liquid (Figure 1), and so would not affect castability of the steel (that is, the unimpeded flow of steel through caster nozzles, unaffected by solid inclusions). However, formation of these hard phases during solidification can affect the quality of the cast product, so the distribution of these phases – and how these are affected by possible nucleation on oxides – is of great interest.

The primary aim of the work presented here was to test whether oxide inclusions with different compositions can nucleate titanium nitride during solidification. In particular, we investigated whether titanium nitride can form on liquid calcium aluminates (present after calcium treatment), in addition to the previously documented nucleation of titanium nitride by spinels (which was expected to occur in samples taken before calcium treatment).

Titanium nitride stability

Figure 1 shows that titanium nitride is expected to form during solidification. To illustrate why this phase would not form in the liquid steel at temperatures above the melting point, Figure 2 gives the calculated solubility of TiN in the steel at two temperatures: 1505°C (just above the liquidus temperature) and 1550°C. The steel composition was taken to be that of the tundish sample in this work (sample 'Tundish' in Table I), except that the nitrogen and titanium concentrations were varied. The TiN solubility was calculated with Thermo-Calc (Andersson *et al.*, 2002). For steel compositions above the solubility curve, TiN can form in the liquid by the reaction:

$$[Ti] + [N] \rightarrow < TiN > \qquad [1]$$

In this reaction, the species in square brackets are dissolved in the steel, and the angle brackets indicate the solid phase.

Figure 2 illustrates that the actual steel composition lies below the solubility curve at both 1550°C and 1505°C. Since the latter temperature is just above the liquidus temperature, these curves emphasise the prediction of Figure 1, that TiN is expected to form below the liquidus temperature after some solidification has occurred.

Experimental work

Steel samples

The process route involved melting in an electric arc furnace (EAF), decarburization followed by deoxidation in an AOD vessel, ladle treatment, and continuous casting. During the plant trial, lollipop samples of liquid steel were taken after different process steps to investigate inclusion evolution. The samples from the AOD vessel to tundish were taken from the same heat, whereas the slab sample was from a different (but similar) heat. The sequence of events is illustrated in Figure 3. As shown in Figure 3, three samples (L1, L2, and L3) were taken at different stages of ladle processing: L1 was taken after deoxidation (with Al) and addition of niobium, L2 was taken after addition of titanium, and L3 after calcium treatment. The sample labelled 'T' was taken from the tundish during subsequent continuous casting, and the slab sample was taken after solidification.

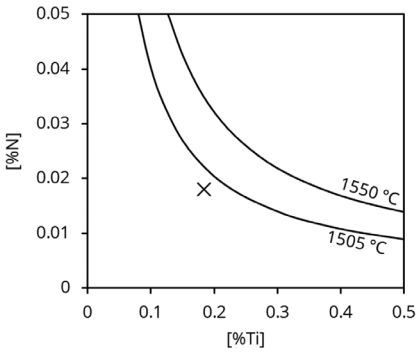

Figure 2—Calculated TiN solubility – at two temperatures – in steel with a similar composition to that studied in this work, but with variable Ti and N concentrations. The actual steel composition in the tundish is indicated by the cross

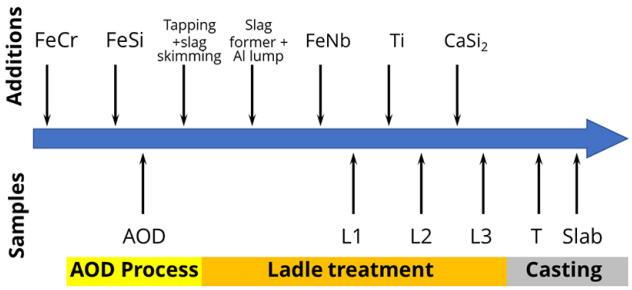

Figure 3—Sequence of events during steel production, showing additions and taking of samples. Sample descriptions are provided in the 'Steel samples' section

After decarburization in the AOD vessel, ferrosilicon was added for deoxidation and recovery of chromium from slag. The resulting silica-rich slag was skimmed off the steel before ladle treatment to prevent reoxidation and to increase alloy yield. Slag formers and aluminium lump (for deoxidation) were added subsequently. Ferroniobium was added after aluminium deoxidation; the first ladle sample was taken after this addition. Low-Al titanium scrap (98–99% Ti) was then added, and another sample taken. Some 3–4 minutes after titanium addition, calcium silicide was added for inclusion modification, and another sample taken. Five minutes of soft stirring was applied after injection of calcium silicide.

Sample analysis

Samples were polished metallographically and inclusions were analysed by automated scanning electron microscopy. Imaging and energy-dispersive X-ray (EDX) analysis were performed at an accelerating voltage of 10 kV. The instrument used a silicon drift detector with a thin window (Moxtek AP3.3). Inclusions were detected using backscattered electron imaging. Brightness levels in the backscattered electron images were standardized by setting the brightness of aluminium tape to 70 (on the dimensionless brightness scale of 0–255 used by the instrument) and that of steel to 170 (Tang, Ferreira, and Pistorius, 2017). An example of the brightness levels in a complex inclusion is shown in Figure 4. All features with brightness levels less than a set threshold of 130 were analysed. This ensured that oxide and titanium nitride inclusions were detected. EDX counts were converted to mass percentages by using the Merlet algorithm (Merlet, 1994). The minimum size of oxide and nitride inclusions

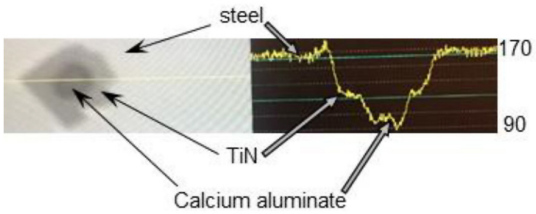

Figure 4—Example of (left) a backscattered electron (BSE) image of an inclusion (TiN around calcium aluminate) in steel, with a line scan of BSE brightness (right)

detected was approximately 1 µm. As shown later, niobium carbonitride inclusions were brighter than the steel matrix, and were evaluated by manual analysis.

Results: Inclusion changes during processing

Inclusion compositions and typical inclusion images are given in Figure 5, with average inclusion sizes (apparent size, from polished sections) and number of inclusions detected per unit area shown in Figure 6. In Figure 5, inclusion compositions are plotted as mole fractions. To show the distribution of compositions, the size of each triangular symbol is scaled proportionately to the area fraction of inclusions with a particular composition – larger triangles indicate that inclusions of that composition were more common. Although multiple elements were analysed in the inclusions in each sample, in general the inclusions contained a small set of major elements. Because quantitative analysis of oxygen and nitrogen is not reliable for micrometre-sized inclusions, the compositions are shown in terms of the metallic elements. For example, inclusions in the sample taken after deoxidation with aluminium (Figure 5b) contained mostly MgO and Al_2O_3, with CaO in a few cases; these are shown as Mg, Al, and Ca in the ternary composition plot.

Manual SEM analysis was used to confirm identification of specific inclusion types that were detected by automated inclusion analysis. For example, inclusions in the sample taken after titanium addition (Figure 5c) contained titanium nitride – which was identified from its brightness in the backscattered electron image (brighter than oxides containing Mg and Al; darker than the steel matrix), the presence of titanium, and the absence of oxygen. Similarly, niobium carbonitride (which is expected to form during the last stages of solidification of the samples; see Figure 1) was identified from its brightness (brighter than the steel matrix), presence of niobium and carbon (at higher than background levels), and absence of oxygen.

In the AOD process, oxygen diluted with argon is blown into the metal bath to decarburize the crude stainless steel. Some chromium is oxidized in the process and is taken up by the slag; ferrosilicon is added for deoxidation and chromium recovery from slag at the end of the AOD process. The resulting inclusions were mainly SiO_2, containing some traces of manganese (Figure 5a).

During subsequent ladle treatment, addition of aluminium converted the inclusions to alumina and spinel (Figure 5b). The conversion from silica to alumina occurred because aluminium has a higher affinity for oxygen than does silicon (Turkdogan, 1983). The added aluminium also deoxidized the steel more deeply, forming new oxide inclusions from the previously

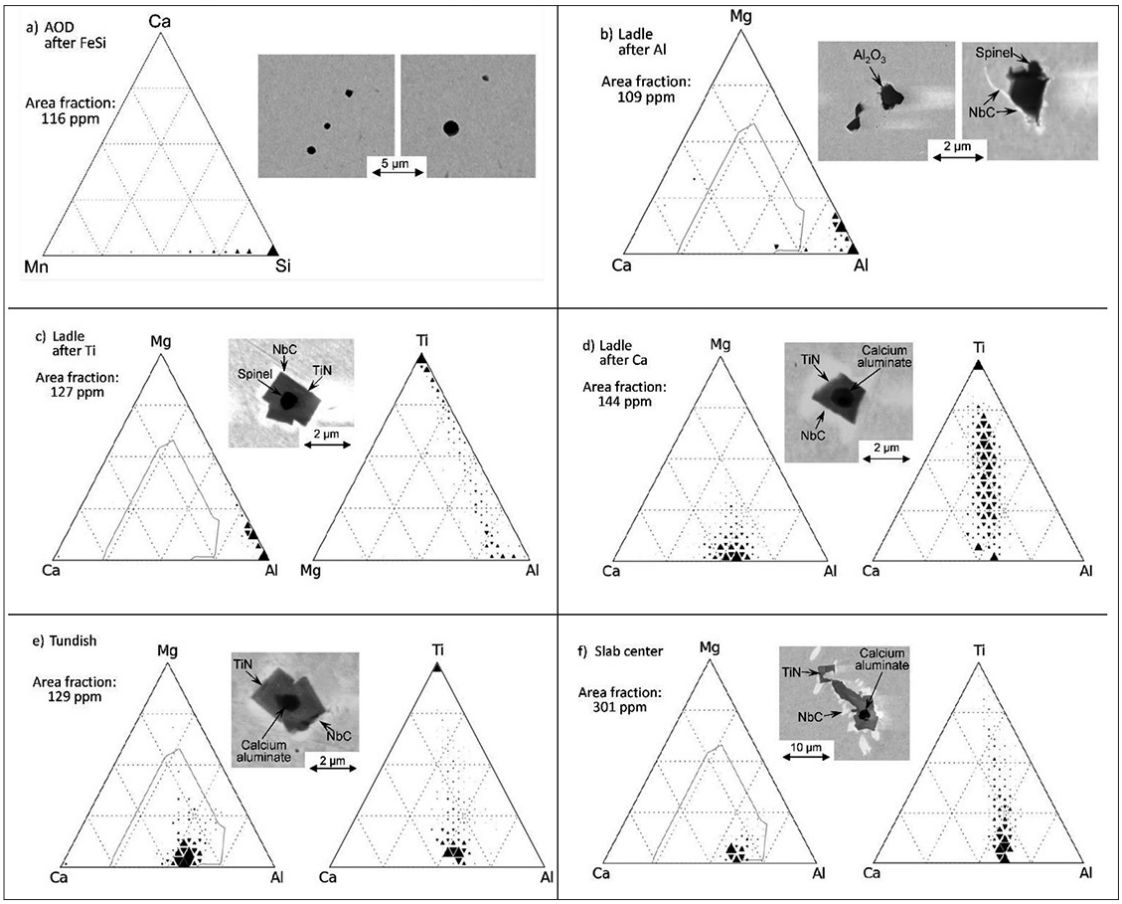

Figure 5—Distributions of inclusion compositions (in mole fractions), with examples of inclusions, for samples taken from different stages of steel processing

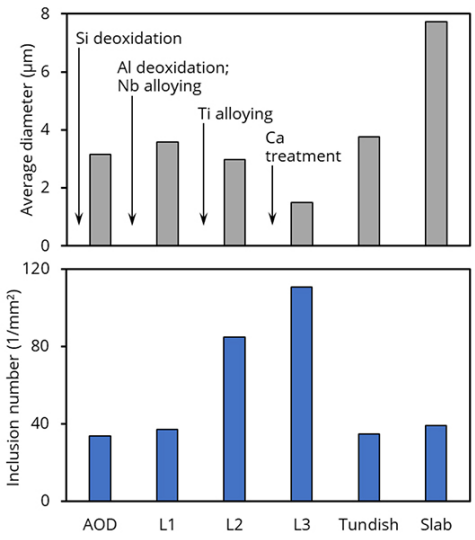

Figure 6—Changes in the average size of inclusions in samples from different stages of steel processing (upper graph), together with the number of inclusions detected (lower graph). Sample numbering corresponds to the sequence shown in Figure 3

dissolved oxygen. Although it is possible to produce stainless steels that are deoxidized with silicon only, deeper deoxidation by aluminium has several advantages:

- Ferrosilicon frequently contains some aluminium; even small aluminium concentrations can change the deoxidation product from silica to alumina and spinel (Todoroki *et al.*, 2001). Uncontrolled formation of alumina and spinel would cause clogging of caster nozzles if these oxides were left untreated. Intentional aluminium additions help to eliminate the variability in the deoxidation product caused by varying aluminium concentrations in ferrosilicon.
- If this steel grade were deoxidized with only silicon, addition of titanium would result in the formation of Ti_2O_3 or Ti_3O_5: that is, the steel would be titanium-deoxidized.

To test whether titanium oxide would form in this steel in the absence of dissolved aluminium, the equilibrium phases in steel with a composition shown in Table I were calculated, but without aluminium and with a total oxygen content of 30 ppm (by mass), for a temperature of 1550°C. The calculation was performed with FactSage 7.3 using the FSstel and FToxid databases (Bale *et al.*, 2016). The equilibrium oxide was predicted to be Ti_2O_3, with 17 ppm oxygen remaining in solution. If titanium additions were made to steel that was not deoxidised with aluminium, formation of titanium oxide would lower the titanium yield. Another side effect is that some of the resulting titanium oxide inclusions would float out in the mould during continuous casting. Titanium oxide pick-up by the mould can lead to formation of solid perovskite in the mould flux, affecting lubrication in the continuous caster mould (Mukongo, Pistorius, and Garbers-Craig, 2004).

Dissolved aluminium that remained in the steel after deoxidation further reacted with MgO in slag or refractory, transferring dissolved magnesium into the steel. The dissolved magnesium reacted with alumina inclusions to convert these to Al_2O_3-MgO inclusions (Kumar and Pistorius, 2018). MgO is only slightly soluble in Al_2O_3 (the atomic ratio of Mg to Al in Al_2O_3 at saturation is 1.1×10^{-4} at 1530°C) (Roy and Coble, 1968). Because of the near-zero solubility of MgO in Al_2O_3, any MgO pick-up caused the formation of spinel, a solid solution based on $MgAl_2O_4$. In addition to deoxidation with aluminium, the steel was alloyed with niobium before the first ladle sample was taken. Figure 5b shows that some niobium carbonitride was detected in the immediate vicinity of the alumina-spinel inclusions. Based on solidification calculations (similar to those reported in Figure 1), the niobium carbonitride precipitated during solidification of the steel sample.

Titanium alloying did not change the oxide inclusions – these remained a mixture of alumina and spinel (Figure 5c). However, titanium nitride precipitation was evident after titanium addition to the liquid steel. Figure 5c shows an example of titanium nitride precipitated on a spinel inclusion, surrounded by niobium carbonitride. This spatial relationship reflects the precipitation sequence shown by Figure 1 – during solidification, titanium nitride nucleated first (on the existing alumina and spinel inclusions), followed by niobium carbonitride formation during the last stages of solidification. The Mg-Al-Ti ternary plot in Figure 5c illustrates a continuous range of inclusion compositions, ranging from oxides (alumina and spinel) to TiN. This distribution reflects the random intersection of the sample polishing plane with inclusions containing both oxide and TiN.

Subsequent calcium treatment successfully converted the alumina and spinel inclusions to calcium aluminates containing some MgO (Figure 5d). Figure 6 shows that the size of the inclusions (oxides surrounded by titanium nitride) decreased after calcium treatment, with a corresponding increase in the number of inclusions. This has also been observed upon calcium treatment of aluminium-killed (non-stainless) steels; the decrease is caused by formation of nuclei of calcium oxide and calcium sulphide, from which the calcium aluminates grow (Ferreira, 2018). Oxide inclusion compositions that lie within the thin grey boundary in the Mg-Ca-Al diagrams would be more than 50% liquid at 1550°C – this boundary was calculated in previous work, using the MgO-CaO-Al_2O_3 phase diagram (Verma *et al.*, 2012). This is the case for the last ladle sample (as well as the tundish and slab samples), demonstrating the success of calcium treatment in converting the solid alumina and spinel inclusions to liquid calcium aluminates.

The inclusions in subsequent samples (tundish and slab, Figure 5e and 4f) are similar in composition. The inclusions consist of calcium aluminate surrounded by titanium nitride and niobium carbide. However, the inclusions in the tundish sample are somewhat larger than those in the last ladle sample, reflecting coarsening of the calcium aluminates by collision and agglomeration (Ferreira, 2018) and also some additional nitrogen pick-up (Table I). The nitrides in the slab are much larger (Figure 5f; note the difference in magnification), reflecting the much longer slab solidification time compared with the lollipop samples taken from the liquid steel.

Discussion

This set of samples confirmed that titanium nitride can nucleate on different oxide inclusions, and not just on spinels. Titanium nitride was found around spinel, alumina, and liquid calcium aluminate inclusions. Based on these results, the sizes of titanium nitride inclusions in solidified steel would depend on the number density of oxide inclusions (if fewer oxides are present, fewer titanium nitrides would form and grow larger),

the nitrogen concentration in the steel, and solidification rate. The combination of nitrogen pick-up during steel processing (Table I), reduction in the number density of oxides, and slower solidification cause the nitrides in the slab to be much coarser than in any of the samples taken from liquid steel. Macrosegregation would also affect the size and concentration of inclusions. Preliminary investigations indicated that the nitride inclusions in samples taken from near the slab surface were smaller than those from the centre of the slab, indicating a possible microsegregation effect.

Since the titanium nitrides and niobium carbonitrides formed during solidification, these would not have affected the castability of the liquid steel. Steel castability depends on the concentration and physical state of inclusions that are present in the liquid steel. From these analyses, the liquid steel contained liquid calcium aluminates (after calcium treatment), which would have ensured good castability.

Conclusions

The additions of deoxidizers and calcium during processing of an 18% Cr ferritic stainless steel resulted in the expected change in the composition of the oxide inclusions – from silica after deoxidation with ferrosilicon to alumina and spinel after deoxidation with aluminium, and finally to calcium aluminates upon calcium treatment. However, the major phase in the inclusions in the solidified samples was titanium nitride, not oxides. Titanium nitride was found to precipitate on calcium aluminates, and not just on spinels (with subsequent growth of niobium carbidonitride on the titanium nitride). The observed inclusion morphology is consistent with the expected changes during solidification (based on Thermo-Calc predictions); only oxide inclusions were present in the liquid steel; titanium nitride formed during solidification, followed by niobium carbide during the last stages of solidification.

Nucleation of titanium nitride on oxide inclusions implies that the number density and spatial distribution of nitrides would be dictated by the number and spatial distribution of oxides during steel solidification; the volume fraction of nitrides depends on nitrogen concentration. The net result is that, in the heat studied in this work, relatively coarse nitrides were present in the slab sample.

Acknowledgements

Support of this work by the Center for Iron & Steelmaking Research at Carnegie Mellon University and by Columbus Stainless Pty Ltd is gratefully acknowledged. The authors would like to acknowledge use of the Materials Characterization Facility at Carnegie Mellon University under grant no. MCF-677785. Dirk Kruger gratefully acknowledges travel support by the School on Production of Clean Steel, hosted by the Southern African Institute of Mining and Metallurgy in 2016.

References

Andersson, J.O., Helander, T., Höglund, L., Shi, P., and Sundman, B. 2002. Thermo-Calc & DICTRA, computational tools for materials science. *Calphad*, vol. 26, no. 2. pp. 273–312.

Bale, C.W., Bélisle, E., Chartrand, P., Decterov, S.A. Eriksson, G., Gheribi, A.E. Hack, K., Jung, I.-H., Kang, Y.-B., Melançon, J.,Pelton, A.D., Petersen, S., Robelin, C., Sangster, J., Spencer, P., and VanEnde, M.-A. 2016. FactSage thermochemical software and databases, 2010–2016. *Calphad*, vol. 54. pp. 35–53.

Capurro, C., and Cicutti, C. 2018. Analysis of titanium nitrides precipitated during medium carbon steels solidification. *Journal of Materials Research and Technology*, vol. 7, no. 3. pp. 342–249.

Fairchild, D.P., Howden, D.G., and Clark, W.A.T. 2000. The mechanism of brittle fracture in a microalloyed steel: Part I. Inclusion-induced cleavage. *Metallurgical and Materials Transactions A*, vol. 31, no. 3. pp. 641–652.

Ferreira, M.E. 2018. Inclusions size distributions after calcium treatment in low carbon aluminum killed steels. PhD thesis, Carnegie Mellon University.

Fu, J., Nie, Q., Qiu, W., Liu, J. and Wu, Y. 2017. Morphology, orientation relationships and formation mechanism of TiN in Fe-17Cr steel during solidification. *Materials Characterization*, vol. 133. pp. 176–184

Fujimura, H., Tsuge, S., Komizo, Y., and Nishizawa, T. 2001. Effect of oxide composition on solidification structure of Ti added ferritic stainless steel. *Tetsu-to-Hagané*, vol. 87, no. 11. pp. 707–712.

Kumar, D. and Pistorius, P.C. 2018. Rate of MgO pickup in alumina inclusions in aluminum-killed steel. *Metallurgical and Materials Transactions B*, vol. 50. pp. 181–191.

Kruger, D. and Garbers-Craig, A.M. 2017. Characteristics and modification of non-metallic inclusions in titanium-stabilized AISI 409 ferritic stainless steel. *Metallurgical and Materials Transactions B*, vol. 48, no. 3. pp. 1514–1532.

Merlet, C. 1994. An accurate computer correction program for quantitative electron probe microanalysis. *Mikrochimica Acta,* vol. 114/115. pp. 363–376.

Michelic, S.K., Loder, D., Reip, T., Ardehali Barani, A., and Bernhard, C. 2015. Characterization of TiN, TiC and Ti(C,N) in titanium-alloyed ferritic chromium steels focusing on the significance of different particle morphologies. *Materials Characterization*, vol. 100. pp. 61–67.

Monnot, J., Heritier, B., and Cogne, J.Y. 1988. Relationship of melting practice, inclusion type, and size with fatigue resistance of bearing steels. *Effect of Steel Manufacturing Processes on the Quality of Bearing Steels*, ASTM STP 987. J.J.C. Hoo (ed.). American Society for Testing and Materials, Philadelphia, PA. pp. 149–165.

Mukongo, T., Pistorius, P.C., and Garbers-Craig, A.M. 2004. Viscosity effect of titanium pick-up by mould fluxes for stainless steel. *Ironmaking and Steelmaking*, vol. 31. pp. 135–143.

Park, J.H. 2011. Effect of inclusions on the solidification structures of ferritic stainless steel: Computational and experimental study of inclusion evolution. *Calphad*, vol. 35. pp. 455–462.

Park, J.H. and Kang, Y. 2017. Inclusions in stainless steels – a review. *Steel Research International*, vol. 87, no. 12. 1700130, 26 pp.

Roy, S.K. and Coble, R.L. 1968. Solubilities of magnesia, titania and magnesium titanate in aluminum oxide. *Journal of the American Ceramic Society*, vol. 51. pp. 1–6.

Tang, D., Ferreira, M.E., and Pistorius, P.C. 2017. Automated inclusion microanalysis in steel by computer-based scanning electron microscopy: Accelerating voltage, backscattered electron image quality, and analysis time. *Microscopy and Microanalysis*, vol. 23. pp. 1082–1090.

Todoroki, H., Mizuno, K., Noda, M., and Tohge, T. 2001. Formation mechanism of spinel type inclusion in 304 stainless steel deoxidized with ferrosilicon alloys. *Proceedings of the 2001 Steelmaking Conference*, Baltimore, MD, 25–28 March 2001. ISS-AIME, Warrendale, PA. pp. 331–341.

Turkdogan, E.T. 1983. Ladle deoxidation, desulphurisation and inclusions in steel – Part 1: fundamentals. *Archiv für das Eisenhüttenwesen*, vol. 54. pp. 1–52.

Verma, N., Pistorius, P.C., Fruehan, R.J., Potter, M.S., Oltmann, H.G., and Pretorius, E.B. 2012. Calcium modification of spinel inclusions in aluminum-killed steel: Reaction steps. *Metallurgical and Materials Transactions B*, vol. 43B. pp. 830–840.

Wang, H., Sun, L., Peng, B., and Jiang, M. 2013. Inclusions for ultra-pure ferritic stainless steels containing 21% chromium. *Journal of Iron and Steel Research, International*, vol. 20, no. 10. pp. 70–74.

Washko, S.D. and Aggen, G. 1990. Wrought stainless steels. *ASM Handbook, Volume 1: Properties and Selection: Irons, Steels, and High-Performance Alloys*. ASM International, Metals Park, OH. pp. 841–907. ◆

Mineral resource modelling using an unequal sampling pattern: An improved practice based on factorization techniques

D. Orynbassar[1] and N. Madani[1]

Affiliation:
[1]School of Mining and Geosciences, Nazarbayev University, Nur-Sultan city, Kazakhstan.

Correspondence to:
N. Madani

Email:
nasser.madani@nu.edu.kz

Dates:
Received: 29 Aug. 2020
Revised: 8 Feb. 2021
Accepted: 29 Apr. 2021
Published: August 2021

How to cite:
Orynbassar, D. and Madani, N. 2021
Mineral resource modelling on the question of unequal sampling pattern: An improved practice based on factorization techniques.
Journal of the Southern African Institute of Mining and Metallurgy, vol. 121, no. 8, pp. 385–396

DOI ID:
http://dx.doi.org/10.17159/2411-9717/1332/2021

ORCID:
N. Madani
https://orcid.org/0000-0002-5833-9758

Synopsis

This work addresses the problem of geostatistical simulation of cross-correlated variables by factorization approaches in the case when the sampling pattern is unequal. A solution is presented, based on a Co-Gibbs sampler algorithm, by which the missing values can be imputed. In this algorithm, a heterotopic simple cokriging approach is introduced to take into account the cross-dependency of the undersampled variable with the secondary variable that is more available over the entire region. A real gold deposit is employed to test the algorithm. The imputation results are compared with other Gibbs sampler techniques for which simple cokriging and simple kriging are used. The results show that heterotopic simple cokriging outperforms the other two techniques. The imputed values are then employed for the purpose of resource estimation by using principal component analysis (PCA) as a factorization technique, and the output compared with traditional factorization approaches where the heterotopic part of the data is removed. Comparison of the results of these two techniques shows that the latter leads to substantial losses of important information in the case of an unequal sampling pattern, while the former is capable of reproducing better recovery functions.

Keywords
Co-Gibbs sampler, variogram analysis, data imputation, principal component analysis.

Introduction

Multivariate geostatistical analysis of cross-correlated variables is of paramount importance in orebody evaluation, which directly impacts further stages in a mining project such as resource classification, mine planning, and geometallurgical design (Battalgazy and Madani, 2019a, 2019b; Abildin, Madani, and Topal, 2019; Maleki *et al.*, 2020; Adeli, Emery, and Dowd, 2018; Adeli and Emery, 2017, 2021). However, when the number of variables increases, the modelling process becomes cumbersome. This difficulty can be ascribed to two main factors. The first deals with establishing a linear model of coregionalization (Journel and Huijbregts, 1978) for the inference of the cospatial continuity (Leuangthong and Deutsch, 2003; Goovaerts, 1993). The second involves using a cokriging system for establishing and deriving the corresponding weights, which might be demanding in terms of computation time. This problem becomes more manifests when one is dealing with multivariate geostatistical simulation (Abildin, Madani, and Topal, 2019).

To overcome these impediments, several geostatistical avenues have been suggested in order to use factorization methods such as minimum/maximum autocorrelation factors (MAF) (Switzer and Green, 1985; Maleki and Madani, 2016), principal component analysis (Goovaerts, 1993), stepwise conditioning transformation (SCT) (Leuangthong and Deutsch, 2003), flow anamorphosis (Van den Boogaart, Mueller, and Tolosana-Delgado, 2017), and projection pursuit multivariate transform (Barnett, Manchuk, and Deutsch, 2016), to name a few. In these methods, the cross-correlated variables can be converted to uncorrelated factors where independent modelling can be implemented without the requirement to establish a cokriging system and infer a linear model of coregionalization. However, these approaches necessitate an equal sampling pattern of each variable, hence both variables should be accessible in all the sample observations. This, however, is problematic in the case of an unequal sampling pattern such as a partially heterotopic configuration (Wackernagel, 2003) of the data-set. One solution for using the factorization approach over such a data-set is to completely remove the incomplete part of the sample observations and continue the modelling process with the remaining isotopic portion of data. This could be problematic because one may lose a substantial part of the

information (Barnet and Deutsch, 2015). Another alternative is to impute the values at unsampled locations to quantify the uncertainty, and then use the multivariate relationship that exist between the variables.

Methods and tools have been developed in this study first for data imputation at unsampled location by using a Co-Gibbs sampler algorithm in a multivariate case study, and secondly to use PCA for factorization of variables with imputed values for the purpose of mineral resource modelling.

We first review the theory of data imputation techniques. We then analyse the proposed data-set, apply data imputation techniques to the heterotopic data-set, and compare the results. Finally, we perform the resource modelling by PCA on the imputed data-set and original heterotopic data-set, and compare the results.

Methodology

Rationale of missing data

First, we consider the theory of missing data and basic concepts in this problem of geostatistical modelling. Missing data or incomplete data-sets do not necessarily imply flaws in the data collection process. A good example is in oil reservoir modelling, where there is always more seismic information available than other data (Xu *et al.*, 1992). In this case, the abundance of secondary information can be used to improve the quality of estimation (modelling) using the scarce primary data alone. In ore deposits, it is also common to find a secondary variable that is abundantly available compared to the primary variable. The reasons for unequal sampling of the primary and secondary variables vary, but could be related to the costs of assaying some particular elements/minerals. In this sense, one may face three sampling patterns for the purpose of orebody evaluation in multi-element deposits (Wackernagel, 2003) (Table I):

- Isotopic (homotopic): primary and secondary variables are available at all sample locations
- Totally heterotopic: primary and secondary variables are available at different sample locations
- Partially heterotopic: some primary and secondary variables share the same locations.

Most geostatistical algorithms need data at all sample locations (isotopic sampling). The challenge in geostatistical factorization analysis, therefore, is how to deal with the missing data in partially and totally heterotopic sampling patterns. An imprecise yet immediate solution is to remove the incomplete data from the whole data-set. However, losing this important information will produce biased results (Barnett and Deutsch, 2015). Another solution is using a regression function to impute the values at missing locations (Little and Rubin, 2002). For instance, linear regression analysis aims to fit a function to the available data irrespective of geographical location (Enders, 2010). This method is impractical since it provides a unique single value for that location where it is unable to compute the uncertainty. Another difficulty is that this method may ignore the location of the variables, and fail to recognize the spatial continuity of the corresponding variables. An alternative for data imputation is to simulate the values at unsampled locations by some iterative geostatistical approach such as the Gibbs sampler.

Gibbs sampler

The Gibbs sampler algorithm is a practical approach to missing data analysis (Barnett and Deutsch, 2015). The rationale of this

Table I

Isotopic (a), partially heterotopic (b) and totally heterotopic (c) sampling pattern; (- indicates missing datum

Coordinates			Primary variable	Secondary variable
(a) ISOTOPIC (HOMOTOPIC) DATA-SET				
East	North	Elevation		
193.0	528.6	39.0	0.032	0.12
335.1	38.0	97.0	0.109	0.13
250.7	593.4	36.0	0.066	0.13
275.8	517.2	86.1	0.400	0.19
(b) PARTIALLY HETEROTOPIC DATA-SET				
East	North	Elevation		
193.0	528.6	39.0	-	0.12
335.1	38.0	97.0	0.109	0.13
250.7	593.4	36.0	-	0.13
275.8	517.2	86.1	0.400	0.19
c) TOTALLY HETEROTOPIC DATA-SET				
East	North	Elevation		
193.0	528.6	39.0	-	0.12
335.1	38.0	97.0	-	0.13
250.7	593.4	36.0	0.066	-
275.8	517.2	86.1	0.400	-

algorithm is built on the Markov chain theory, which implements sampling from a multivariate Gaussian distribution. By virtue of its iterative nature, the Gibbs sampler updates the simulated values several times, taking into account the conditioning of available data, until it reaches a target distribution (Casella and George, 1992). In a univariate case, wherever only one variable is considered for imputation of the value at an unsampled location, a univariate Gaussian random vector with missed m observations, $Z = (Z_1,\ldots,Z_m)_T$, with zero mean and variance-covariance matrix **C**, can be imputed in an iterative manner, by updating one selected observation based on conditioning to the other hard and previously imputed observations in the corresponding vector. This algorithm consists of the following steps (Barnett, Manchuk, and Deutsch, 2016; Madani and Bazarbekov, 2020):

- Initialization: Commence the imputation by an independent random vector $Z^{(0)}_{m\times1}$. This can be done by acceptance-rejection method.
- Iteration: for $i = 1,2,\ldots,I$
  - Choose an index $j \in \{1,\ldots,m\}$ either in regular or random order (Roberts and Sahu, 1997; Galli and Gao, 2001; Arroyo *et al.*, 2012).
  - Estimate Z_j conditionally to the other observations, $(Z_1,\ldots,Z(j\text{-}1), Z(j+1),\ldots Z_m)$ by employing simple kriging in a unique neighbourhood to return the kriging estimated value $Z_j^{SK(i)}$ and variance of estimation error $\sigma_j^{SK(i)}$. In this step, the conditioning data includes hard data and previously imputed values at missing m observations.
  - Impute a new random vector $Z_j^{(i)}$ using the conditional distribution, with mean equal to its simple kriging estimate and variance equal to its variance of estimation error.
  - Update the random vector by

$$\left(Z_1^{(i-1)},\ldots Z_{j-1}^{(i-1)}, Z_j^{(i)}, Z_{j+1}^{(i-1)},\ldots, Z_m^{(i-1)}\right) \quad [1]$$

- Go back to step 1 and loop I times.

One of the exceptional advantages of this sampling technique is the iterative process, *i.e.* it continues to simulate the values at undersampled points through a loop until it reaches the desired spatial continuity. The stated feature of the Gibbs sampler originates from the Markov chain that allows communicating of any states with positive probability distribution in a determined number of transitions, which accentuates the distinctive properties of this chain, namely aperiodicity and irreducibility (Lantuéjoul, 2002). Moreover, through promotion of the initial probability to a higher state, it aims at reaching the intended distribution (*e.g.* standard Gaussian distribution), which will entail the equilibrium or invariant distribution. These characteristics of the process encourage convergence of the global distribution to a Gaussian random vector with zero mean and the desired variance-covariance matrix $C(x)$ through an increasing number of iterations (I_α) (Tierney 1994; Lantuéjoul 2002).

In order to illustrate the notation of the Gibbs sampler mechanism in data imputation, a simple example is provided. A data-set is given with N number of observations, including some missing observation locations (Figure 1a, right). The variogram model is constructed using the known (isotopic) part of the data and is depicted in Figure 1a, left. After running the Gibbs sampler with setting for 100 iterations, a value is inferred for the missing point (consider only one missing point), and the corresponding variogram is computed (Figure 1b, left). Subsequently, the results are given after 1000 and 10000 iterations (Figures 1c and 1d). With an increasing number of iterations, the variogram of the data-set, including the imputed value, approaches the variogram model, until it matches it completely, at which point the final value is accepted and iterations cease.

However, the Gibbs sampler algorithm is not suitable for multivariate data imputation, because it ignores the dependency of the undersampled variable on other available data. We now show how data imputation is performed in a multivariate context.

Proposed algorithm

In a multivariate data-set, the data imputation may result in total or partial heterotopic sampling patterns. In this method, the imputed values at missing locations are subject to the cross-correlation structure that exists between the primary and secondary variable. In this study, we only show the methodology for imputation in a multivariate case with a partially heterotopic sampling pattern. This can be applied further for resource modelling using the factorization techniques where an isotopic sampling pattern is required. Therefore, the first step is to impute the values at unsampled locations of the data-set to make the sampling pattern isotopic. In this respect the secondary variable with more data accessibility boosts the quality of imputation of values for the primary variable at missing locations. To achieve this, Madani and Bazarbekov (2020) proposed a Co-Gibbs sampler algorithm, in which simple kriging in the conventional Gibbs sampler (as already explained) can be substituted for the simple cokriging system based on two neighborhood search strategies:

- *Isotopic searc*h: all sampling locations containing both the primary and secondary variables are selected (Table II, right).
- *Multiple search*: all sampling locations containing both the primary and secondary variables are selected, together with the secondary datum at target-undersampled location (Table II left).

These two neighbourhoods allow for two alternatives cokriging systems: (a) isotopic simple cokriging, and (b) heterotopic simple cokriging, in a unique neighbourhood. It is also possible to use moving neighbourhood; however, the rate of convergence may be slow and unconvincing (Arroyo, Emery, and Peláez, 2012). Readers are referred to Madani and Bazarbekov (2020) for more detail about the proposed Co-Gibbs sampler algorithm for data imputation.

Once both variables are available at sampling locations (*i.e.*, building an isotopic sampling pattern), the next step is to decorrelate the variables. This can be done by any decorrelation technique; however, in this study we propose PCA due to its simplicity and straightforwardness. Since one avails several realizations at imputed locations, one needs to implement the PCA over all these realizations. In this step, one variable is always fixed and another variable that conveys the imputed values changes with each run of PCA. After this step, the factors can be simulated independently subject to the variogram analysis of each factor. Each realization of conditioning data leads to one realization over the target grids. Therefore, $\boldsymbol{R}$ realizations of imputed values produce R maps over the simulated grid nodes. Then, simulated results are back-transformed to the original scale to restitute the original correlation coefficient. The final step is to use the simulated results for resource modelling.

The capability of the proposed algorithm, its validity, and the improved performance of either of these two alternatives compared to the Gibbs sampler for data imputation, are presented and the proposed searching strategies are compared in the following case study.

Case study

The data-set used in this work belongs to an undisclosed gold deposit located in Australia. It includes 2458 sample locations with availability of two elements: gold (Au) and silver (Ag). This data-set is partially heterotopic, in that Ag data is less available and is missing at some sample locations, whereas Au grades are available at all sample locations. The 614 (scarce) Ag data points are primary, with the 2458 (abundant) Au data points being secondary. Therefore, only 614 observations include both Au and Ag variables (the isotopic part of the data-set).

Exploratory data analysis

Exploratory data analysis establishes statistical parameters for the data-set aimed at detecting data errors and statistical inconsistencies which, if ignored, could lead to significant biases in the output results (Rossi and Deutsch, 2014). In this context, the presence of duplicates and outliers must be identified through diagrammatic statistical tools such as histograms and scatter plots, particularly in the case of s multivariate data-set (Rossi and Deutsch, 2014; Verly, 1993). Once identified, duplicate data and outliers are removed or capped from the data-set, respectively.

The original histograms for Au and Ag data are shown in Figure 2, and statistical parameters of the data-set are presented in Table III.

The linear correlation between the 614 isotopic silver and gold data-points, shown in the scattergram of Figure 3, has a correlation coefficient of 0.65, indicating a high dependency between Au and Ag in this deposit. The strength of the correlation coefficient suggests that data imputation by means of the proposed algorithm is acceptable, by first imputing values of Ag at locations missing this variable and secondly by apply PCA for Au resource modelling. The method is motivated because the Ag data will contribute to the modelling of Au in the deposit.

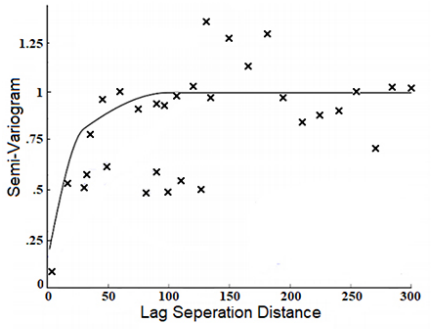

Primary Variable Grade (%)	Secondary Variable Grade (%)
0.48	2.3
0.35	3.2
1.15	7.8
0.78	5.5
⋮	⋮
-NaN-	4.8

a) Initialization – Partially heterotopic case: -NaN- implies missing data.

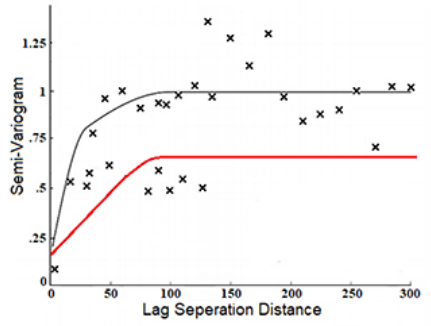

Primary Variable Grade (%)	Secondary Variable Grade (%)
0.48	2.3
0.35	3.2
1.15	7.8
0.78	5.5
⋮	⋮
0.29	4.8

b) Iteration 100.

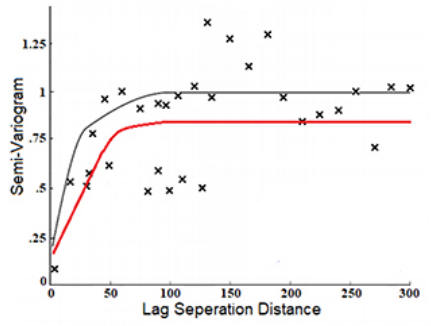

Primary Variable Grade (%)	Secondary Variable Grade (%)
0.48	2.3
0.35	3.2
1.15	7.8
0.78	5.5
⋮	⋮
0.58	4.8

c) Iteration 1000.

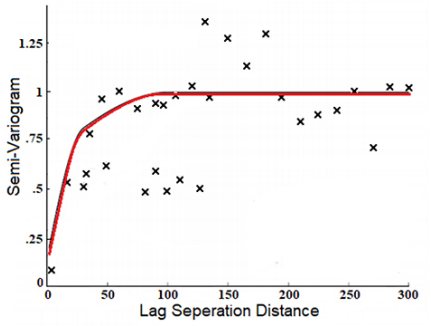

Primary Variable Grade (%)	Secondary Variable Grade (%)
0.48	2.3
0.35	3.2
1.15	7.8
0.78	5.5
⋮	⋮
0.73	4.8

d) Iteration 10,000.

Figure 1—Gibbs sampler algorithm example – left: variogram model, and right: portion of data-set; black solid line: desired variogram model; red: variogram model of imputed data-set

Table II

Two possible options for cokriging neighbourhood in partially heterotopic data-set (Wackernagel, 2003); (- indicates missing data)

Multiple Search		Isotopic Search	
Primary variable grade (%)	Secondary variable grade (%)	Primary variable grade (%)	Secondary variable grade (%)
0.032	0.12	0.032	0.12
0.109	0.13	0.109	0.13
0.066	0.13	0.066	0.13
-NaN-	0.19	-	0.19

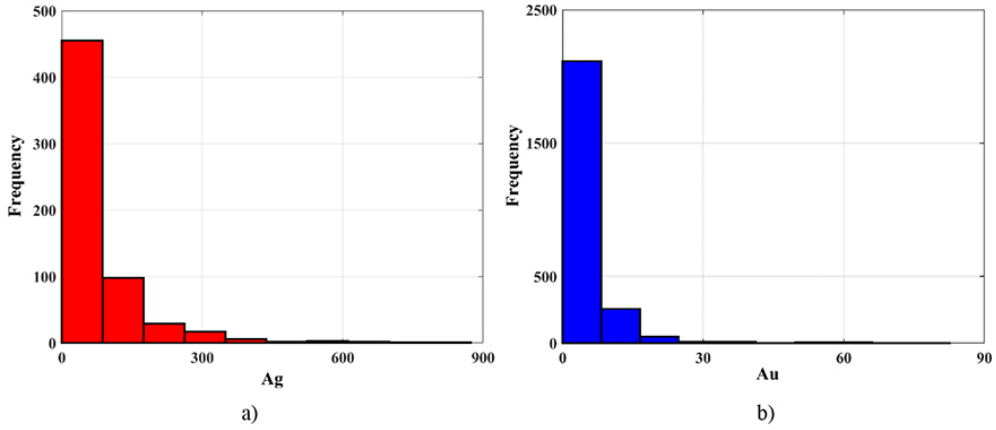

Figure 2—Original histograms of Ag (a) and Au (b) grade distributions (both in ppm)

Table III

Statistical parameters of original Ag and Au grades (ppm)

Variables	Number of Samples	Max	Min	Mean	Variance	Coefficient of variation
Ag	614	874.35	0.025	70.111	10627.53	1.471
Au	2458	82.60	0.015	4.221	47.04	1.625

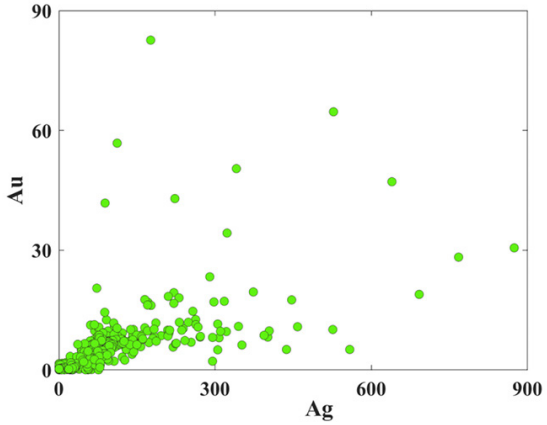

Figure 3—Scattergram of Au *versus* Ag (ppm) with a correlation coefficient of 0.65

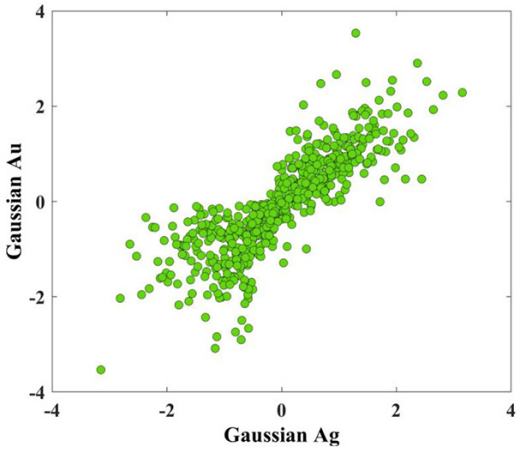

Figure 4—Scattergram of Gaussian Au and Ag

Generally, a high dependency between two variables and a heterotopic sampling pattern are two most important factors determining the suitability of the proposed algorithm in this study.

Normal score transformation and variogram analysis

The first step in implementing the Gibbs sampler is a transformation of original data to a normal score distribution with mean 0 and variance 1, using an independent quantile-based approach for each variable (Verly, 1993). A scattergram of normal score-transformed data, shown in Figure 4, indicates a linear bivariate distribution of points, suggesting that the multivariate relationship between normal scores for Au and Ag meets bivariate Gaussianity.

Next, the omnidirectional experimental direct and cross-variograms were calculated for the standard normal scores data-set. The cross-variogram is calculated for paired observations of silver and gold, *i.e.* the isotopic part of the data-set that involves only 25% of all the data. The variogram models were fitted by using the linear model of coregionalization, where a two-spherical structure, including the respective nugget effect, is fitted to these experimental variograms. The corresponding values of sill matrices, ranges, and models are as follow:

$$\begin{pmatrix} \gamma_{Au}(h) & \gamma_{\frac{Au}{Ag}}(h) \\ \gamma_{\frac{Au}{Ag}}(h) & \gamma_{Ag}(h) \end{pmatrix} = \begin{pmatrix} 0.0310 & -0.0554 \\ -0.0554 & 0.0995 \end{pmatrix} (nugget) + \begin{pmatrix} 0.6915 & 0.7317 \\ 0.7317 & 0.7742 \end{pmatrix} Spherical(9.64\,m, 9.64\,m, 9.64\,m) + \begin{pmatrix} 0.2433 & 0.1454 \\ 0.1454 & 0.1205 \end{pmatrix} Spherical(57.49\,m, 57.49\,m, 57.49\,m) \quad [2]$$

As can be seen in Figure 5, all depicted variogram models adequately reveal the spatial continuity of the data of interest. The sill variance for direct variograms has reached unity, entailing a stationary phenomenon. Lastly, the presence of a nugget effect (Equation [2]) also can be observed in all cases.

Results and validation

Once the linear models of coregionalization have been established, the Gibbs sampler algorithm can be implemented over the missing data locations to impute the Ag values. The

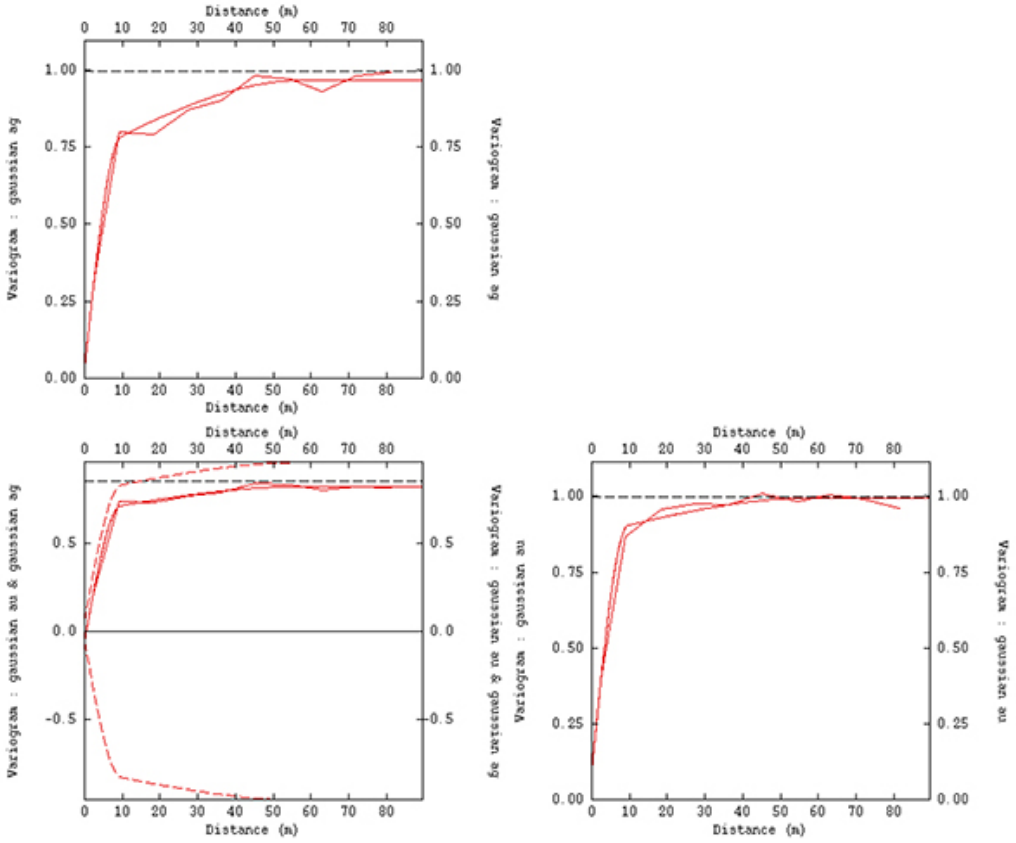

Figure 5—Experimental and theoretical direct and cross-variograms; the sawtooth line is the experimental variogram and the the straight line is the theoretical variogram obtained from the linear model of coregionalization

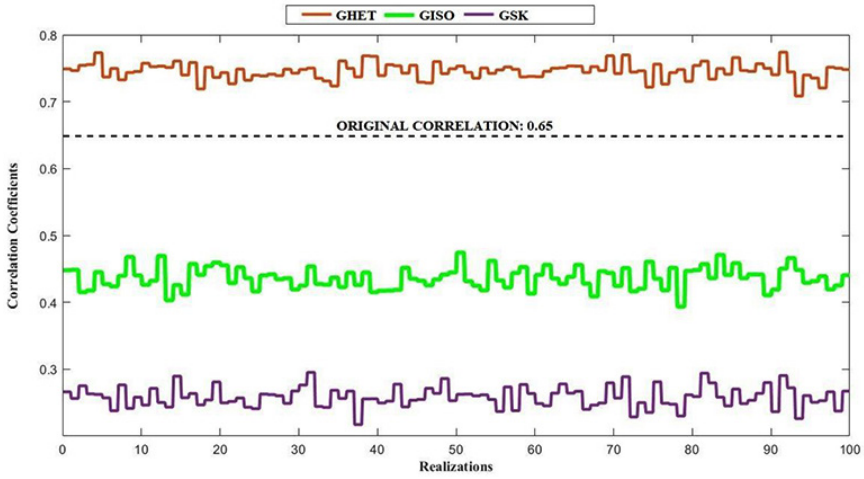

Figure 6—Correlation coefficient between Imputed Ag and Au over 100 realizations

number of iterations is set to 10 000, provided updates for inferred values can reasonably reach the target multivariate distribution.

Following the proposed algorithm, three alternatives of the proposed Gibbs sampler are mainly examined:

- *GISO*: Co-Gibbs sampler with isotopic simple cokriging.
- *GHET*: Co-Gibbs sampler with heterotopic simple cokriging
- *GSK*: Gibbs sampler with simple kriging

The results of two alternatives (GISO and GHET) are compared to the conventional Gibbs sampler where only simple kriging (GSK) is employed. Therefore, we consider this as the third alternative, where one ignores the existence of a secondary variable.

The derived results can be validated by examining the correlation coefficients between imputed Ag and Au values and comparing them with the original cross-correlation coefficient of 0.65. The distribution of correlation coefficients for 100 realizations is shown in Figure 6, with reference to the original correlation coefficient of 0.65. The average correlation coefficients for all three approaches, including GSK, are shown in Table IV. The overall outcome for the correlation between Au and imputed

Ag values (GHET) is reasonably close to the original correlation coefficient (0.65), whereas GISO and GSK yielded poor results, failing to reach desired value of cross-correlation.

The measure of correlation between the average correlation of imputed values of Ag and original Au is another statistical parameter for validating the reproduction of bivariate relationships. A comparison of Figure 7 and Figure 3 shows that GHET outperformed GISO and GSK, the reason being that GISO and GSK ignore the importance of secondary data at the target locations. The efficiency of the Gibbs sampler alternative can be compared based on the reproduction of the original shape of bivariate relation (Figure 7). As can be observed, GSK's bivariate pattern certainly failed to follow the initial scatter pattern showing same value of Ag for a portion of the respective Au values. Also, from the visual representation of GISO's case, the pattern is ambiguous and does not properly reproduce the original 'diagonal' pattern. However, in the case of GHET, the bivariate relationship is compatible with the original bivariate relationship between Au and Ag, as demonstrated in Figure 3.

Resource calculation

The overall results show that the Gibbs sampler with heterotopic simple cokriging (GHET) provides satisfactory results in term of reproduction of original correlation coefficient for imputation of Ag values at missing sample locations.

Furthermore, through using available 100 series of the data-set, inclusive of the imputed Ag values, one can proceed to the resource calculation for the deposit. In this study, we chose principal component analysis (PCA) (Wackernagel, 2003; Sarma *et al.*, 2007) for factorization of Au and Ag. The rationale/principle of this methodology is to transform a set of correlated variables into independent uncorrelated factors thorough solving the eigenvalue problem.

Table IV

Correlation Coefficient results between imputed Ag and Au

Original correlation	GHET	GISO	GSK
0.65	0.7459	0.4364	0.2583

The advantages of the proposed algorithm for resource modelling based on factorization by means of data imputation are considered in two cases:

- Case I: an isotopic sampling pattern for 614 sample locations where both Au and Ag are available
- Case II: an isotopic sampling pattern, where all 2458 sample locations are informed by existing Au data and imputed Ag values (100 realizations) obtained by heterotopic simple cokriging.

The first step after PCA factorization is to check the degree of correlation of derived factors at all lag distances. To achieve this, the cross-correlogram over the factors is calculated (Goovaerts, 1997) as illustrated for cases I and II in Figure 8, indicating the factors are uncorrelated over all lag distances. Therefore, one can use the independent simulation for modelling the factors since there is no dependency between these factors.

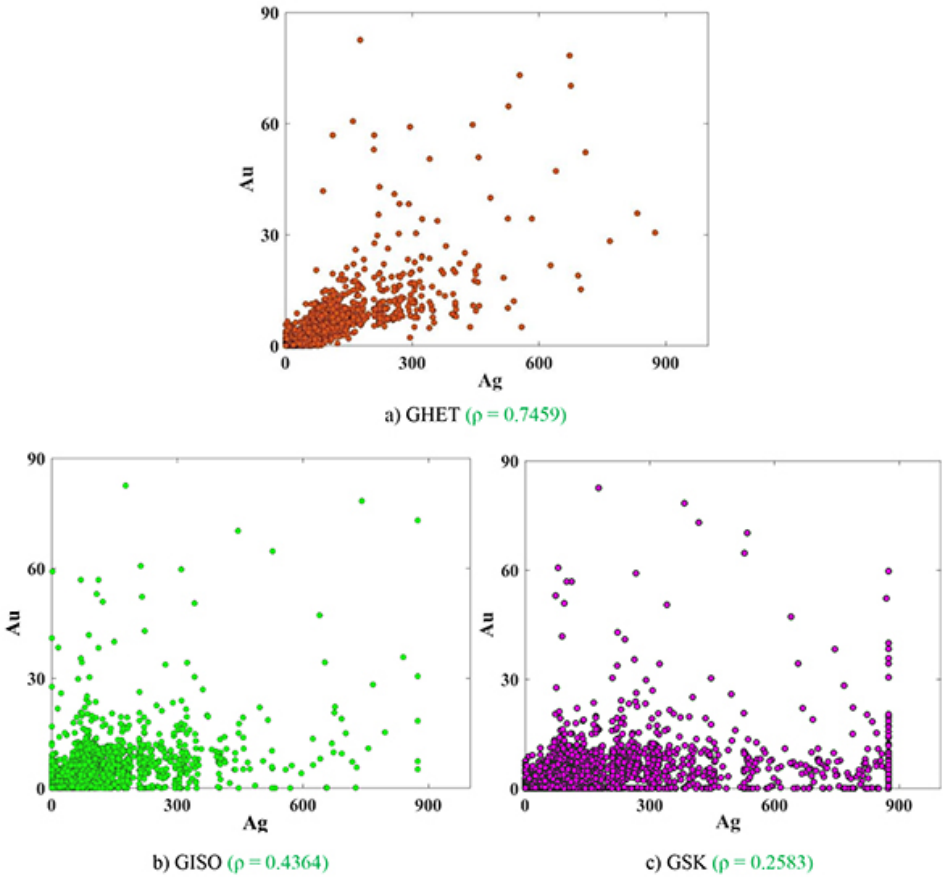

Figure 7—Scattergram between imputed Ag (ppm) and Au (ppm): GHET (a), GISO (b), and GSK (c)

Variograms for the decorrelated variables of interest are established as a necessary step towards simulation. The variograms for case I and case II are illustrated in Figure 9. The variogram analysis for case II is implemented over the uncorrelated factors that are obtained from 100 imputed realizations for Ag. The average experimental variogram is calculated and the theoretical model fitted. The variogram formulae are as follows:

Case I:

$$\gamma_{Factor\,1}(h) = 0.15\ Spherical\ (18.74\ m, 18.74\ m, 18.74\ m) \quad [3]$$

$$\gamma_{Factor\,2}(h) = 1.81\ Spherical\ (18.74\ m, 18.74\ m, 18.74\ m) \quad [4]$$

Case II:

$$\gamma_{Factor\,1}(h) = 0.124\ Spherical\ (16.76\ m, 16.76\ m, 16.76\ m) \quad [5]$$

$$\gamma_{Factor\,2}(h) = 1.77\ Spherical\ (62.13\ m, 62.13\ m, 62.13\ m) \quad [6]$$

For both case, the variogram models are quite simple, consisting of only one structure (spherical) and without any nugget effects. Furthermore, case II with 100 realizations (green variograms) with averaged variogram (red variogram), and so the respective variogram fitting in case II was done over the average of variograms for simplicity.

Once the variogram models are derived, a turning bands simulation algorithm (Emery and Lantuejoul, 2006) is used to simulate the factors independently. This technique of simulation is selected because of simplicity and straightforwardness and its ability to reproduce the statistical parameters of the original data (Paravarzar, Emery, and Madani, 2015). The E-type maps (average map of 100 realizations/maps) of each case are illustrated in Figure 10. As can be seen, there is a visible difference between the results obtained from two cases.

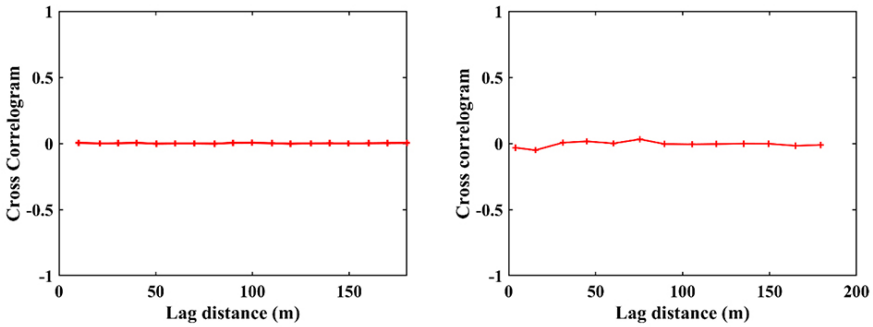

Figure 8—Cross-correlogram between the factors: left – case I, right – case II. The cross-correlogram for case II is obtained through averaging the cross-correlograms obtained from each single realization

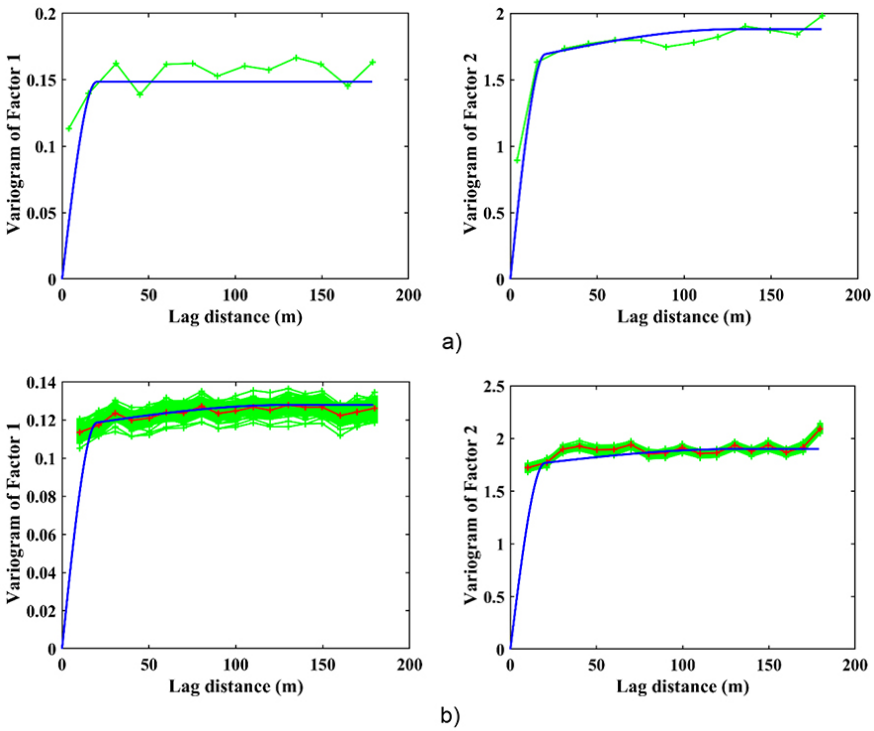

Figure 9—Variogram analysis. The direct variograms are obtained from decorrelated factors of original data as in case I (a), and case II (b). The green line is the experimental variogram of the factors and the blue line is the theoretical variogram model; the red line in case II is the average of realizations conveying the imputed data; the fitting variogram in case II is implemented over the red line (i.e., average of variograms)

For instance, eastern part of the maps in Case II shows more concentration of both variables (Au and Ag) comparing to the maps obtained from Case I. This difference also is very tangible in the north-eastern and south-eastern part of the deposit. In north-eastern, Case I shows a high concentration of Au and Ag, whereas in south-eastern part of the region almost lacks the high concentration. This can happen due to ignoring substantial part of important information of Au by removing 1,844 sample observations in this Case. The results obtained from Case II is more compatible with the geological information of the deposit.

It is of interest to check which of the simulation results could produce the outcome approximate to the original statistical parameters of the data-set. The direct and cross-variograms for the simulation results can be compared with the original theoretical model, as shown in Figure 11. Cases I and II were both able to reproduce the spatial statistical parameters. The cross-variogram for case II is slightly better than that for case I, but not significantly so, since the cross-variogram is informed by homotopic part of the data-set (614 sample points), which is the same in both cases.

The box or whisker plot of the derived correlation coefficient distribution was calculated and is illustrated in Figure 12. Once again the findings from the imputed data-set are distinguished by a higher median value and shorter interquartile range (IQR) in case II. Reproduction of the mean value for Au is also examined through the calculation of a mean value for each of the 100 realizations, and the distribution of means is shown in Figure 13. As can be observed, case II improves the reproduction of the original mean.

The recovery functions, including tonnage, mean grade, and metal quantity above cut-offs for Au, are computed over the simulated results. As it can be seen from Table V, the results of the imputed data-set for case II provide the highest values of the recovery functions for each cut-off grade.

This significant difference should be seriously considered in the case of conventional removal of the data-set that is common in factorization techniques. Furthermore, the application of these methods goes beyond resource estimation, also affecting the cash flow of the project, the net present value (NPV) calculation, and other decision-making procedures in further mine planning exercises. Due to the distinct results obtained above, the data imputation role in enhancing the outputs should be reconsidered in modern resource modelling.

Conclusions

An iterative algorithm based on the Gibbs sampler has been presented in this study for data imputation at unsampled locations. For this, a heterotopic simple cokriging is applied in the Gibbs sampler that considers the cross-dependency of the undersampled variable with another variable that is more available. This algorithm showed that the correlation coefficient after imputation corresponds more closely to the original

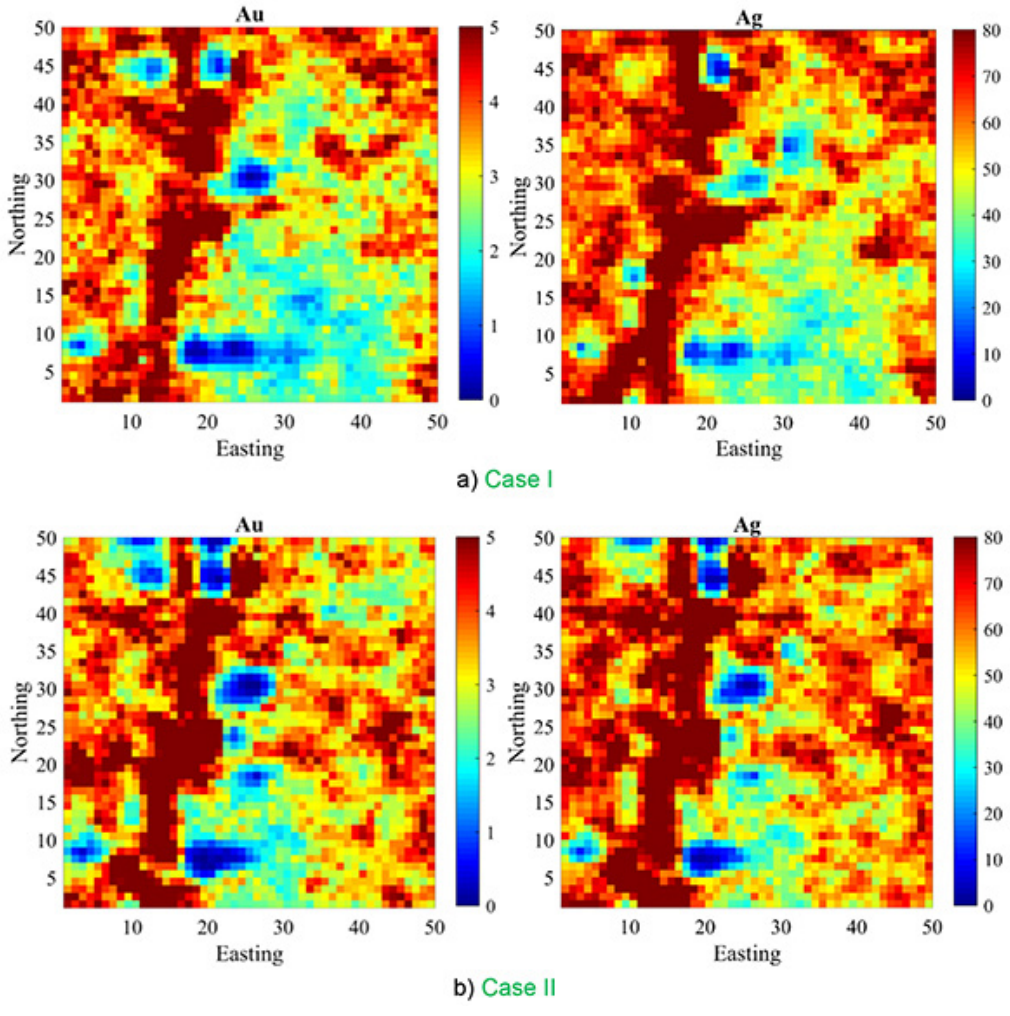

Figure 10—E-type maps obtained from case I (a) and case II (b)

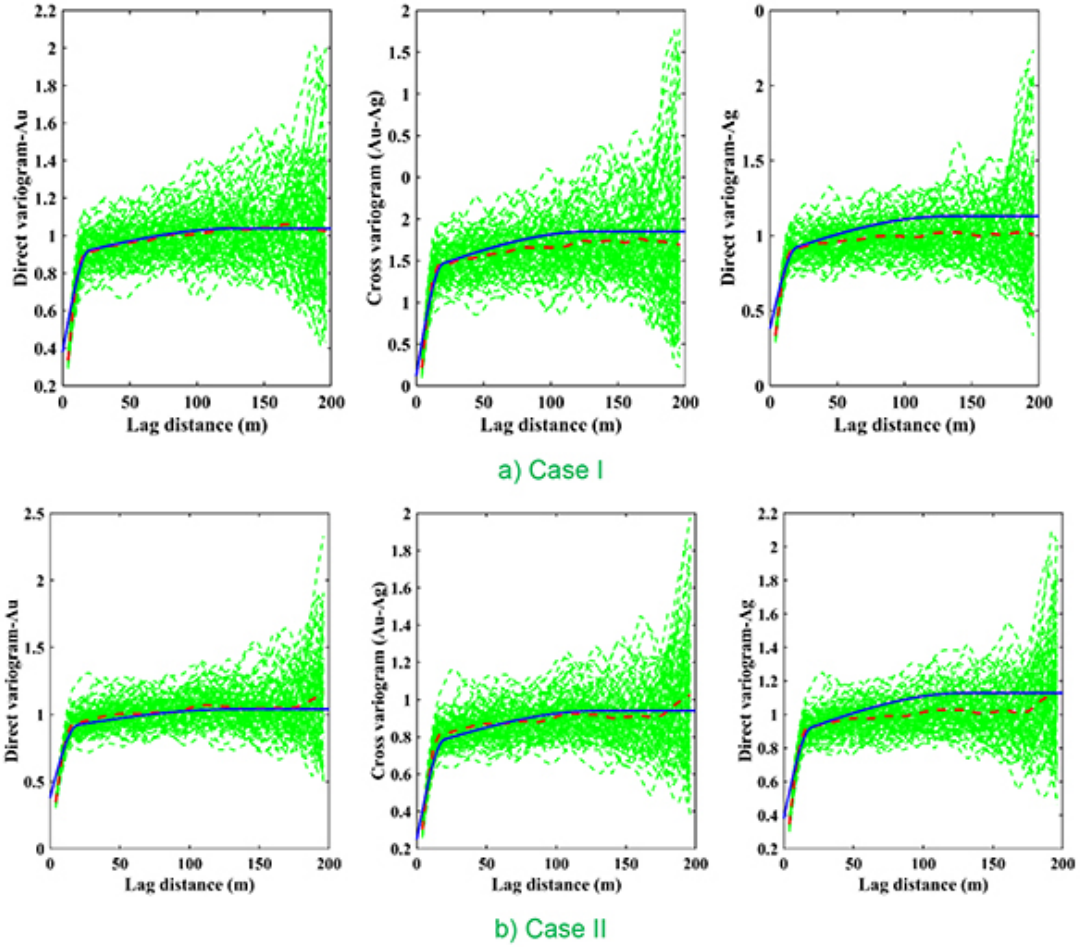

Figure 11—Variogram reproduction over 100 simulated realizations for case I (a) and case II (b). Green: individual realizations; blue: theoretical variogram model; red: average of individual realizations

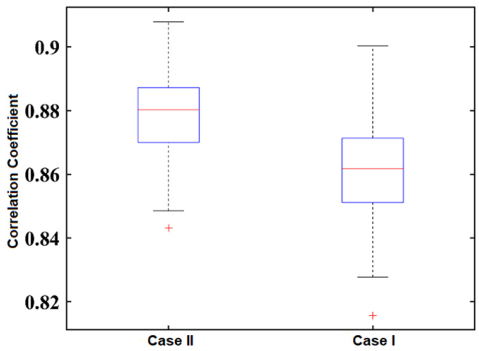

Figure 12—Box plots for case I and case II, original theoretical correlation coefficient 0.94

correlation coefficient. This shows that even using simple cokriging or simple kriging may not be an appropriate approach for such imputation. The results of employing a factorization approach also illustrate a good practice for resource modelling and calculation of recovery functions comparing to the traditional approaches, which only remove the incomplete part of the data-set, in terms of better computation of recovery functions. This work can also be expanded for modelling a data-set with more than two variables.

Acknowledgment

This research was funded by Nazarbayev University through the Faculty Development Competitive Research Grants for 2018 2020, grant number 090118FD5336. We are also grateful to the editorial team and two anonymous reviewers for their valuable comments, which substantially helped improving the final version of the manuscript. We also acknowledge Micromine Company for providing the data-set.

Computer code availability

The Co-Gibbs sampler executable file and the relevant source code files (Python-compatible) that are used in this study are freely available at https://github.com/btalgat/Co-Gibbs_Sampler/

References

Abildin, Y., Madani, N., and Topal, E. 2019. A hybrid approach for joint simulation of geometallurgical variables with inequality constraint. *Minerals*, vol. 9, no. 24. https://doi.org/10.3390/min9010024

Adeli, A. and Emery, X. 2017. A geostatistical approach to measure the consistency between geological logs and quantitative covariates. *Ore Geology Reviews*, vol. 82. pp.160–169.

Adeli, A. and Emery, X. 2021. Geostatistical simulation of rock physical and geochemical properties with spatial filtering and its application to predictive geological mapping. *Journal of Geochemical Exploration*, vol. 220. 106661.

Adeli, A., Emery, X., and Dowd, P. 2018. Geological modelling and validation of geological interpretations via simulation and classification of quantitative covariates. *Minerals*, vol. 8. 7 pp. https://doi.org/10.3390/min8010007

Arroyo, D., Emery, X., and Peláez, M. 2012. An enhanced Gibbs sampler algorithm for non-conditional simulation of Gaussian random vectors. *Computers & Geosciences*, vol 46. pp. 138–148.

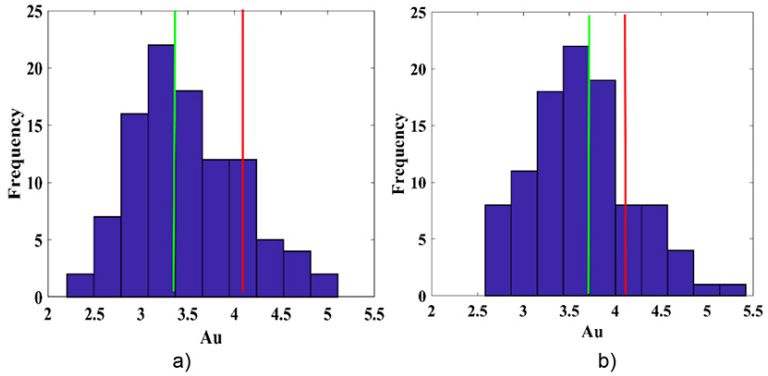

Figure 13—Mean reproduction of Au for Case I (a); and Case II (b). (green line: average of realizations; red line: original average of the variable)

Table V

Recovery function reports based on Cut-off for Au

Cut-off	Tonnage (t)		Mean grade (ppm)		Metal quantity (t, ppm)	
	Case II	Case I	Case II	Case I	Case II	Case I
0.021	466,390	458,142	1.5572	1.5222	72,721	69,919
0.040	436,934	428,118	1.6599	1.6265	72,687	69,883
0.046	423,632	413,310	1.7110	1.6834	72,665	69,859
0.057	407,482	398,294	1.7773	1.7454	72,632	69,828
0.0620	395,670	388,706	1.8293	1.7875	72,604	69,806
0.105	352,656	347,070	2.0471	1.9966	72,463	69,668
0.12	342,396	336,592	2.1069	2.0570	72,417	69,621
0.150	327,682	318,878	2.1988	2.1680	72,340	69,528
0.252	300,628	296,714	2.3891	2.3237	72,128	69,355
0.473	275,454	273,428	2.5940	2.5091	71,767	69,019
1.086	250,324	244,602	2.8264	2.7716	71,062	68,213

Barnett, R.M. and Deutsch, C. 2015. Multivariate imputation of unequally sampled geological variables. *Mathematical Geosciences*, vol. 47. pp. 791–817.

Barnett, R.M., Manchuk, J.G.m and Deutsch, C.V. 2016. The projection-pursuit multivariate transform for improved continuous variable modeling. *SPE Journal*, vol. 21. pp. 2010–2026.

Battalgazy, N. and Madani, N. 2019a. Categorization of mineral resources based on different geostatistical simulation algorithms: A case study from an iron ore deposit. *Natural Resources Research*, vol. 28. pp. 1329–1351.

Battalgazy, N. and Madani, N. 2019b. Stochastic modeling of chemical compounds in a limestone deposit by unlocking the complexity in bivariate relationships. *Minerals*, vol. 9. p. 683. https://doi.org/10.3390/min9110683

Casella, G. and George, E.I. 1992. Explaining the Gibbs sampler. *American Statistician*, vol. 46. pp. 167–174.

Emery, X. and Lantuéjoul, C. 2006. Tbsim: A computer program for conditional simulation of three-dimensional gaussian random fields via the turning bands method. *Computers & Geosciences*, vol. 32. pp. 1615–1628.

Enders, C.K. 2010. Applied Missing Data Analysis, Guilford Press, New York.

Galli, A. and Gao, H. 2001. Rate of convergence of the Gibbs sampler in the Gaussian case. *Mathematical Geology*, vol. 33. pp. 653–677.

Goovaerts, P. 1993. Spatial orthogonality of the principal components computed from coregionalized variables. *Mathematical Geology*, vol. 25. pp. 281–302.

Goovaerts, P. 1997. Geostatistics for Natural Resources Evaluation. Oxford University Press.

Journel, A.G. and Huijbregts, C.J. 1978. Mining Geostatistics, Academic Press, London.

Lantuéjoul, C. 2002. Conditional simulation of spatial stochastic models. *Proceedings of ISMM2002I*, Sydney, 3–5 April 2002. CSIRO Publishing, Clayton, Australia. pp. 327–335.

Lantuéjoul, C. 2013. Geostatistical simulation: models and algorithms. Springer Science & Business Media.

Leuangthong, O. and Deutsch, C.V. 2003. Stepwise conditional transformation for simulation of multiple variables. *Mathematical Geology*, vol. 35. pp. 155–173.

Little, R.J. and Rubin, D.B. 2002. Statistical analysis with missing data. Wiley. New York.

Madani, N. and Bazarbekov, T. 2020. An enhanced conditional Co-Gibbs sampler algorithm for data imputation. *Computers & Geosciences*, 104655.

Maleki, M. and Madani, N. 2022. Multivariate geostatistical analysis: An application to ore body evaluation. *Iranian Journal of Earth Sciences*, vol. 8, no. 2. pp. 173–184.

Maleki, Mohammad; Jélvez, Enrique; Emery, Xavier; Morales, Nelson. 2020. Stochastic open-pit mine production scheduling: A case study of an iron deposit. Minerals, 10, no. 7. https://doi.org/10.3390/min10070585

Paravarzar, S., Emery, X., and Madani, N. 2015. Comparing sequential Gaussian and turning bands algorithms for cosimulating grades in multi-element deposits. *Comptes Rendus Geoscience*, vol. 347. pp. 84–93.

Roberts, G.O. and Sahu, S.K. 1997. Updating schemes, correlation structure, blocking and parameterization for the Gibbs sampler. *Journal of the Royal Statistical Society: Series B (Statistical Methodology)*, vol. 59. pp. 291–317.

Rossi, M.E. and Deutsch, C.V. 2013. Mineral Resource Estimation, Springer Science & Business Media.

Sarma, P., Durlofsky, L.J., and Aziz, K. 2008. Kernel principal component analysis for efficient, differentiable parameterization of multipoint geostatistics. *Mathematical Geosciences*, vol. 40. pp. 3–32.

Sarma, P., Durlofsky, L.J., Aziz, K., and Chen, W.H. 2007. A new approach to automatic history matching using kernel PCA. *Proceedings of the SPE Reservoir Simulation Symposium*, 2007. Society of Petroleum Engineers, New York.

Switzer, P. and Green, A. 1984. Min/max autocorrelation factors for multivariate spatial imagery. *Tech. Rep*. 6. Department of Statistics, Stanford University.

Tierney, L. 1994. Markov chains for exploring posterior distributions. *Annals of Statistics*. pp. 1701–1728.

Van Den Boogaart, K.G., Mueller, U., and Tolosana-Delgado, R. 2017. An affine equivariant multivariate normal score transform for compositional data. *Mathematical Geosciences,* vol. 49. pp. 231–251.

Verly, G. 1993. Sequential Gaussian cosimulation: a simulation method integrating several types of information. *Proceedings of Geostatistics Troia'92*. Springer.

Wackernagel, H. 2013. Multivariate geostatistics: an introduction with applications, Springer Science & Business Media.

Xu, W., Tran, T., Srivastava, R., and Journel, A.G.1992. Integrating seismic data in reservoir modeling: The collocated cokriging alternative. *Proceedings of the SPE Annual Technical Conference and Exhibition*, 1992. Society of Petroleum Engineers, New York. ◆

ESG Inquisition findings

On 10-11 August, the Geological Society of South Africa (GSSA) held a virtual ESG Inquisition. The purpose of the Inquisition was three-fold:

- To highlight the importance of ESG issues internationally and locally; to showcase the latest developments in all aspects of ESG reporting from a global viewpoint; to highlight what ESG standards are accomplishing in the world of sustainability reporting, with specific relevance to the minerals industry; to highlight similarities and, especially, differences between Sustainability Reporting and Mineral Resource/Mineral Reserve reporting.
- To get an understanding of how investors, regulatory organizations, and other stakeholders view the importance of ESG in reporting Mineral Resources and Mineral Reserves.
- To gather industry views and input regarding the potential ESG reporting requirements when disclosing Mineral Resource and Mineral Reserve estimates in Competent Persons reports, and also in the Annual Mineral Resource and Mineral Reserve reports published by mineral companies. This is particularly important at this time since the SAMESG Guideline is being redrafted and this is seen as the occasion to obtain industry views on potential improvements.

The event comprised two half-days, with 14 speakers (five of whom were international), three panel discussions, and a keynote address by Roger Dixon. The results of the Inquisition will be presented to the various SAMCODE Committees to be used to inform the next series of updates.
The significant outcomes of the discussions are as follows.

- ESG is not going away and will need to be integrated into Public Reporting (i.e., Competent Persons Reports, Integrated Annual Reports, and Annual Mineral Resource and Mineral Reserve Statements.
- However, these documents are not Sustainability Reports – they are primarily technical reports, with ESG as one of the Modifying Factors which needs to be addressed to the extent that it may affect the MRMR estimate. The big question is how much ESG data/information is relevant – probably somewhat more than currently is the case.
- Authors of such reports must view ESG as adding value to the company and not just as a potentially expensive compliance (box-ticking) exercise.
- There will always be companies that are leaders in the field of ESG reporting, but the industry needs minimum reporting requirements that are clear, simple, and practicable. There needs to be a distinction between materiality and ‘data-dumping’, which simply leads to inflated and unwieldy documents. What needs to be included or summarized in the body of the report and what can be included simply by reference to external material?
- There needs to be convergence and alignment between all of the SAMCODES/Guidelines and CRIRSCO.
    - Does SAMESG need to be assimilated into SAMREC, SAMVAL, and SAMOG, in whole or in part?
    - Do we take our lead from CRIRSCO, or do we lead the way, knowing that other CRIRSCO organizations are also updating the ESG requirements of their Codes?
- The recognition that ’one size will not fit all’; that there needs to be different requirements for different sized companies and also different requirements across the various project stages.

It was also recommended that a Working Group be constituted of representatives from the SAMREC, SAMVAL, and SAMOG Committees, from large companies, junior companies, and consultants. The mandate of such a Working Group would be to assist the SAMESG Committee to update the SAMESG Guidelines and ensure integration and alignment with the SAMCODES in a manner that is both practicable and useful.

Predicting standard threshold shifts for occupational hearing loss among miners at a large-scale platinum mine in South Africa

L. Ntlhakana[1,2], G. Nelson[1], K. Khoza-Shangase[2], and I. Maposa[1]

Affiliation:
[1]School of Public Health, University of the Witwatersrand, Faculty of Health Sciences, South Africa.
[2]Department of Speech Pathology and Audiology, School of Human and Community Development, University of the Witwatersrand, Faculty of Humanities, South Africa.

Correspondence to:
L. Ntlhakana

Email:
liepollo.ntlhakana@wits.ac.za

Dates:
Received: 11 Aug. 2020
Revised: 15 Apr. 2021
Accepted: 22 Apr. 2021
Published: August 2021

How to cite:
Ntlhakana, L., Nelson, G., Khoza-Shangase, K., and Maposa, I. 2021
Predicting standard threshold shifts for occupational hearing loss among miners at a large-scale platinum mine in South Africa.
Journal of the Southern African Institute of Mining and Metallurgy, vol. 121, no. 8, pp. 397–404

DOI ID:
http://dx.doi.org/10.17159/2411-9717/1318/2021

ORCID:
L. Ntlhakana
https://orcid.org/0000-0002-8632-0616

G. Nelson
https://orcid.org/0000-0001-7815-3718

K. Khoza-Shangase
https://orcid.org/0000-0002-6220-9606

I. Maposa
https://orcid.org/0000-0002-3448-4096

Synopsis

Occupational noise-induced hearing loss (ONIHL) is associated with various risk factors in South African mines. We investigated the association between standard threshold shifts (STSs) and exposure to noise and platinum mine dust (PMD), using demographic data, five years of annual audiometry screening results, and noise and dust exposure data.

Miners' age, sex, percentage hearing loss (PLH), and dust and noise exposure data were gathered, and a linear mixed effects regression model used to predict STS. Average occupational exposure levels to noise and dust were calculated from recorded measurements. A total of 12 692 records were analysed. Most miners were male (89.6%) and more than 50% were younger than 41 years. More than 70% were exposed to > 85 dBA noise and 58% were exposed to 1.5–2.99 mg/m3 PMD. Changes in hearing levels ranged from 8.3 dBHL at baseline (2014/2015) to 10 dBHL in 2016 (STS), with no changes thereafter. The model showed that the estimated effect on STS for males was 27% and 21% higher than for females, for the left and right ear, respectively The estimated effect of age, PLH, noise exposure and years of exposure on STS was < 10% for each variable. There was no statistically significant association between PMD and STS.

The combined effects of age, sex, years of exposure to noise, and noise exposure levels, and strength of associations can be used to predict STS for this group of miners. Our findings may be used to measure the efficacy of the mine's hearing conservation programme.

Keywords
occupational noise-induced hearing loss, noise, platinum mine dust, standard threshold shift.

Introduction

In 2005, the most recent year for which data is available 16% of global disabling hearing impairment, which affects about four million adults, was due to occupational noise; with the burden ranging from 7% to 21% in different subregions.(Nelson *et al.*, 2005) The estimated prevalence in African countries was 18% (12–23%).(Nelson *et al.*, 2005) In the USA, the estimated prevalence of occupational noise-induced hearing loss (ONIHL) in the mining industry for the period 2006–2010 was reported to be 24% (Masterson *et al.*, 2015). For South African mines during the same period a prevalence of 30% was reported (Mine Health and Safety Inspectorate, 2017). ONIHL is common in South Africa across all mining commodities. The prevalence in the gold mining sector was estimated to be 17% in 2012 (Strauss *et al.*, 2012).

An improved understanding of risk factors for miners' hearing deterioration, in addition to those already established and considered in hearing conservation programmes (HCPs), is essential. Research on the associations of socio-demographic factors (age, sex, and race), genetic predisposition, recreational noise exposure, and occupational exposures (noise, platinum mine dust, and chemicals) (Pillay, 2020, Sepadi, Chadyiwa, and Nkosi, 2020) with ONIHL has been extensively conducted, globally (Khoza-Shangase, 2019; Campo, Morat, and Hong, 2013; 2019, Strauss *et al.*, 2012; Brits *et al.*, 2012; Grobler *et al.*, 2020). Research in South African mines has shown that age, sex (Strauss *et al.*, 2014), ototoxic drugs used for treatment of pulmonary tuberculosis (PTB) and human immunodeficiency virus (HIV) (Khoza-Shangase, 2019; Brits *et al.*, 2012), and noise exposure levels ≥ 85 dBA are associated with ONIHL (Edwards *et al.*, 2015; Strauss *et al.*, 2012; Balfour-Kaipa, 2014).

Although exposure to platinum mine dust (PMD), which contains below detectable levels of crystalline silica (Nelson and Murray, 2013; Biffi and Belle, 2003), is not directly associated with any occupational diseases, platinum miners exposed to PMD experience symptoms such as blocked nose, scratchy throat, itchy ears and eyes (Levene and Calnan, 1971; Fickl, 2007). All of these are allergic

reactions that are associated with conductive hearing loss (Signia, 2018), which occurs when there is an obstruction of sound waves from the outer ear (pinna to tympanic membrane) to the middle ear; also due to a build-up of ear wax or fluid (Katz *et al*., 2009). This type of hearing loss is treatable but causes temporary difficulty in hearing low-frequency sounds.

The prevalence of PTB in the South African mining industry is high (Mine Health and Safety Inspectorate, 2017), and has been associated with ONIHL in gold miners (Khoza-Shangase, 2019). PTB is also associated with exposure to silica dust in the gold mines (Nelson, 2013; Sepadi, Chadyiwa, and Nkosi, 2020). HIV is a also a risk factor for PTB (Ebonyi *et al*, 2016), and treatments for both PTB and HIV are ototoxic (Khoza-Shangase, 2019). Certain cancers are also treated with ototoxic drugs, *e.g.* cisplatin, which contains platinum salts (Lenntech, 2020). Although some research has been conducted on the association between NIHL and PTB in the South African mining industry (Khoza-Shangase, 2019), no investigation has examined the association of NIHL with exposure to PMD or ototoxic TB, HIV, and cancer treatments (Lenntech, 2020; Phanguphangu and Ramma, 2018). There is a dearth of knowledge among mine medical practitioners on the multifactorial effects of certain diseases and medical conditions, and their treatments, on the auditory system (Edwards, van Coller, and Badenhorst, 2010).

The South African HCP guideline states that programmes to prevent ONIHL should include seven pillars: noise measurement, engineering and administrative controls, hearing protection devices, risk-based medicals, medical surveillance, and audiometry (SANS, 2013). However, audiometry data and reports on miners' hearing conditions in the South African mines surveillance programmes are not integrated (Ntlhakana, Khoza-Shangase, and Nelson, 2020). Data regarding risk factors associated with miners' hearing loss, health data, and occupational hygiene data (including noise exposure measurements) is recorded in different data-sets (under the auspices of HCPs). Data on diseases such as cancer, TB, and HIV is recorded separately from audiometry data, and records are not linked for hearing conservation reporting (Khoza-Shangase, Moroe, and Edwards, 2020).

The identification of risk factors associated with hearing loss, coupled with pure-tone and distortion-product otoacoustic emissions (DPOAEs) audiometric tests, can assist in the early diagnosis of ONIHL (Moepeng, Soer, and Vinck, 2017). These two tests measure hearing thresholds across low (250 Hz) mid (1000 Hz), and high (2-8 kHz) frequencies (Feuerstein and Chasin, 2009). While both the DPOAE and pure tone tests are used in HCPs (Edwards, van Coller, and Badenhorst, 2010), it has been reported that DPOAE is more sensitive, feasible, and helpful for the early identification of ONIHL than pure-tone audiometry (Edwards and Kritzinger, 2012; Edwards, van Coller, and Badenhorst, 2010). Results from the two tests are recorded separately in the miners' audiometry records, and DPOAE results are not always available.

Workers exposed to high noise levels lose the ability to hear high-frequency sounds first (Edwards, van Coller, and Badenhorst, 2010; Grobler *et al*., 2020). Hearing loss, as a decline in hearing thresholds, is measured by percentage loss of hearing (PLH) (Department of Labour, 2001) and standard threshold shifts (STS) (Department of Mineral Resources, 2016). The PLH is calculated from measured hearing thresholds (0.5, 1, 2, 3, and 4 kHz), and a baseline audiogram is recorded based on this value.(Department of Labour, 2001) This is the method that was used by South African hearing conservation practitioners to define hearing loss for compensation purposes from 2001 to 2016 (Department of Labour, 2001).

The STS method is based on an International Organization for Standardization (ISO) standard (ISO1999:2013) which specifies that a decline of 8 dB in the STS indicates early ONIHL. The STS method has been used by South African mines since 2016 to benchmark miners' hearing and to track STS deterioration as a function of hearing loss (Strauss *et al*., 2012; Grobler *et al*., 2020). In 2008, the Department of Mineral Resources and Energy (DMRE) set NIHL milestones for the mining industry, stating that, after December 2008, the HCP implemented by the industry 'must ensure that there is no deterioration in hearing greater than ten per cent amongst occupationally exposed individuals' (Msiza, 2014; Department of Mineral Resources and Energy, 2008). However, hearing loss prevention efforts were not successful (Edwards and Kritzinger, 2012) and the DMRE revised the milestones in 2014 (Chamber of Mines, 2016), stating that, by December 2016 no employee's STS will exceed 10 dBHL from the baseline when averaged at 2000, 3000, and 4000 Hz in one or both ears (MHSC, 2015).

Thus, STS was prioritized in the measurement of hearing loss for miners. Normal hearing is recorded as 0 dBHL (Chamber of Mines, 2016). A STS is defined as an average shift in hearing threshold of 10 dBHL. Although there is no hearing loss at this stage, any shift > 10 dBHL should be reported, and warrants investigation and intervention (Chamber of Mines, 2016). A shift in the hearing threshold of ≥ 25 dBHL for one or both ears indicates hearing loss. Thus, diagnostic audiometry is required in order to confirm hearing loss (Department of Mineral Resources and Energy, 2016). Worldwide, STS has been used to describe the hearing function of workers exposed to excessive noise levels since the early 2000s (Masterson *et al*., 2016; Heyer *et al*., 2011). The South African mining industry's hearing loss prevention efforts, as per the NIHL 2016 milestones, are now aligned with first world countries such as the USA. However, the success of these interventions will only be assessed in 2024 (MHSC, 2015).

The purpose of our analysis was to examine the association of STS with exposure to noise and PMD, and to develop prediction model for STS for miners employed at one of South Africa's large platinum mines, using demographic data and five years of audiometry, noise, and dust data.

Methods

The results of individual miners' hearing screening tests and occupational hygiene data from 2014 to 2018 were analysed. Data on diseases was not available. We accessed 24 321 hearing screening records and 15 769 occupational hygiene records (noise exposure levels) from the mine's two available data-sets. The hearing screening data-set contained audiometry screening records from examinations conducted by a qualified audiometrist (occupational health nurse) according to the South African National Standard (SANS) 10083:2013.(SANS, 2013), bilateral audiometry results at frequencies of 0.5, 1, 2, 3, 4, 6, and 8 kHz, calculated PLH, and averaged bilateral STS. The occupational hygiene data-set contained information about occupation (job title), noise exposure levels (dBA), and total PMD exposure measurements (mg/m^3) for each miner, collected by a qualified occupational hygienist. Both data-sets included the miner's

employee number, age, and sex. These three variables were used to combine the data-sets using STATA (version 15.1). The data was further categorized using the mine's risk rankings as follows: PLH as low (0–2%), moderate (2.1–5%) and high (>5%); noise exposure levels as 0–81.99 dBA, 82–84.99 dBA, 85–104.99 dBA, and 105–160 dBA; dust exposure levels as 0–0.299 mg/m³, 0.3–1.499 mg/m³, 1.5–2.99 mg/m³, and 3–100mg/m³, as well as the standard hearing loss classifications of mild (26–45 dBHL), moderate (46–55 dBHL), moderately-severe (56–70 dBHL), severe (71–90 dBHL), and profound (>90 dBHL) (Katz *et al.*, 2009).

Permission to use the miners' data was granted by the mine management, and ethical clearance was obtained from the University of the Witwatersrand's Human Research Ethics Committee (clearance certificate no. M180273).

The combined data-set contained 17 304 electronic records (Figure 1). A total of 4 675 duplicate records, records with no employee numbers, records with no initial dates of employment, records with more than two baseline PHL values, and records with > 50% PLH (invalid calculations) were excluded. The number of records included in the analysis differed from year to year – 12 605 for 2014, 12 602 for 2015, 12 599 for 2016, 12 591 for 2017, and 12 592 for 2018.

Data analysis

Frequencies and percentages were used to describe miners' sex, age group, noise exposure and PMD levels, and PLH and STS categories. Medians and ranges were used to describe continuous PLH and STS scores. Differences in male and female miners' STS were graphically depicted by age group and PLH category.

A linear mixed effects model was used to estimate the effects of different exposure factors on the bilateral STS, using continuous data from all the variables with the exception of sex.

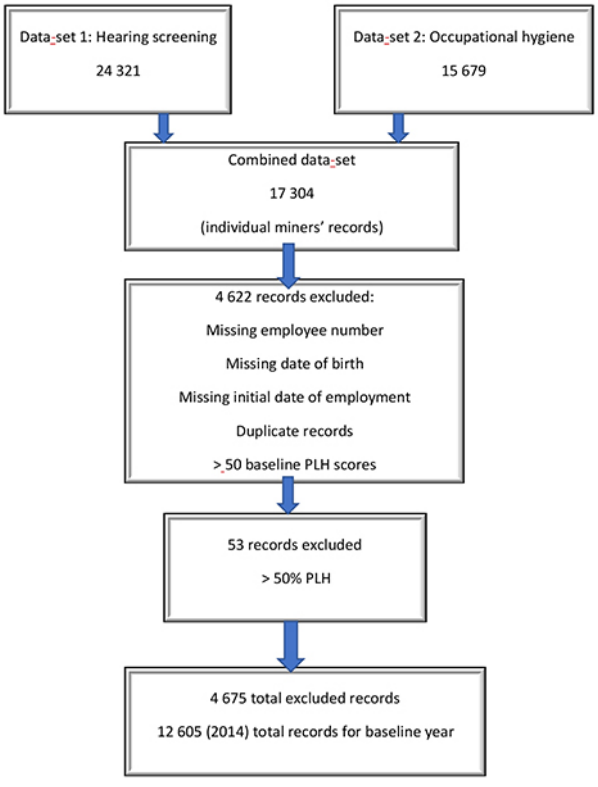

Figure 1—Individual miners' records excluded from merged data-set

Distributions of selected variables, including bilateral STS, were assessed to ascertain skewness before fitting the model. The bilateral STS (left and right) data were skewed and were therefore log-transformed before fitting the model. For the mixed effects model, when fitting the bilateral STS levels to predictor variables, a random intercept was assumed. The estimates are reported with 95% confidence intervals. Significance for two-sided tests was set at $P < 0.05$. Goodness of fit of the final prediction model was tested using the likelihood ratio test.

Results

The characteristics of the miners in the 2018 cohort are shown in Table I. There were more males (n = 11 283; 89.6%) than females (n = 1 309; 10.4%); most (53.4%) were younger than 41 years, most (76.4%) had low PLH; 72.4% were exposed to noise levels of 85 dBA or higher; and 57.9% were exposed to 1.5–2.99 mg/m³ PMD. Approximately 10% of the miners had high PLH (> 5%) and STS ≥ 26 dBHL.

Table I

Miners' demographic, exposure, and hearing function characteristics (N = 12 592*)

Variable	n	%
Sex		
Female	1 309	10.4
Male	11 283	89.6
Age (years)		
≤ 40	5 243	53.4
41–55	3 766	38.4
≥ 56	810	8.3
*Noise exposure level (dBA)***		
0–81.99	1 239	11.2
82–84.99	1 813	16.4
85–104.99	8 015	72.4
*PMD exposure level (mg/m³)***		
0–0.299	3 004	28.4
0.3–1.499	1 454	13.8
1.5–2.99	6 116	57.9
*PLH (%)***		
Low (0–2)	9 619	76.4
Moderate (2.1–5)	1 706	13.5
High (> 5)	1 274	10.1
*STS (dBHL)****		
–10–25	11 287	89.6
26–45	1 029	8.2
46–55	176	1.4
56–70	93	0.7
71–90	27	0.2
> 90	2	0.01

* Based on 2018 data; ** risk-ranking scales used by the participating mine;
***range of hearing function (Katz *et al.*, 2009)

Table II shows the medians and range used to describe the miners' hearing function measurements (PLH and STS). The median PLH did not change throughout the study period (1.2%); some miners had a maximum PLH range of up to 50%. The median STS was 8.3–10 dBHL, with a hearing deterioration (STS) of 1.7 dBHL from baseline to 2016 in the left ear, and to 2017 in the right ear. Some miners had a maximum STS range of up to 99 dBHL at baseline, which increased to 95 dBHL by 2018.

Figure 2 shows STS for the left ear for male and female miners of different age groups and PLH categories across the five

Table II

Median values for hearing function measurements (N = 12 592*)

Year	PLH (%)		STS left ear (dBHL)		STS right ear (dBHL)	
	Median	Range	Median	Range	Median	Range
2014	1.2	1.1–49.9	8.3	1.0–99.0	8.3	10.0–93.0
2015	1.2	1.1–49.7	8.3	–8.3–99.0	8.3	–6.6–97.6
2016	1.2	1.1–49.9	10.0	–10.0–93.3	8.3	–8.3–91.3
2017	1.2	1.1–50.0	10.0	–8.3–95.0	10.0	–8.3–93.3
2018	1.2	1.1–49.3	10.0	–10.0–95.0	10.0	–10.0–94.3

* Based on 2018 data

years of follow-up. There was a small increase in mean STS over the five years in the high PLH category for males > 41 years. Male miners in most PLH categories had higher mean STS levels than female miners in all years of exposure, across different age categories. The differences in mean STS between males and females were greatest in the high PLH and > 41 years age categories.

Figure 3 shows STS for the right ear for male and female miners of different age groups and PLH categories, across the five years of follow-up. There was a small increase in mean STS over the five years in the high PLH category for males > 41 years. Male miners in most PLH categories had higher mean STS levels than female miners in all years of exposure, across different

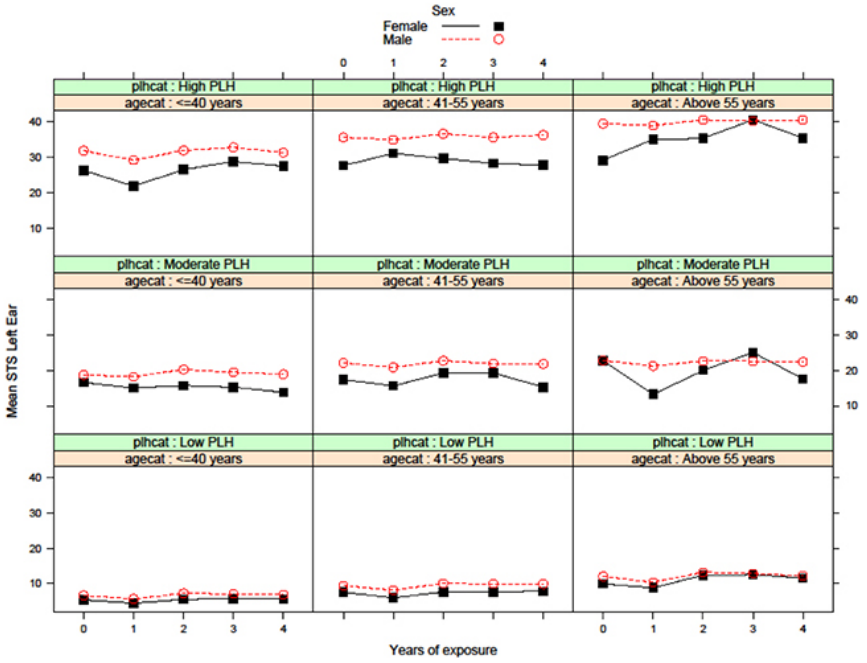

Figure 2—Mean STS for left ear by PLH level, age group, and sex for all years of follow-up

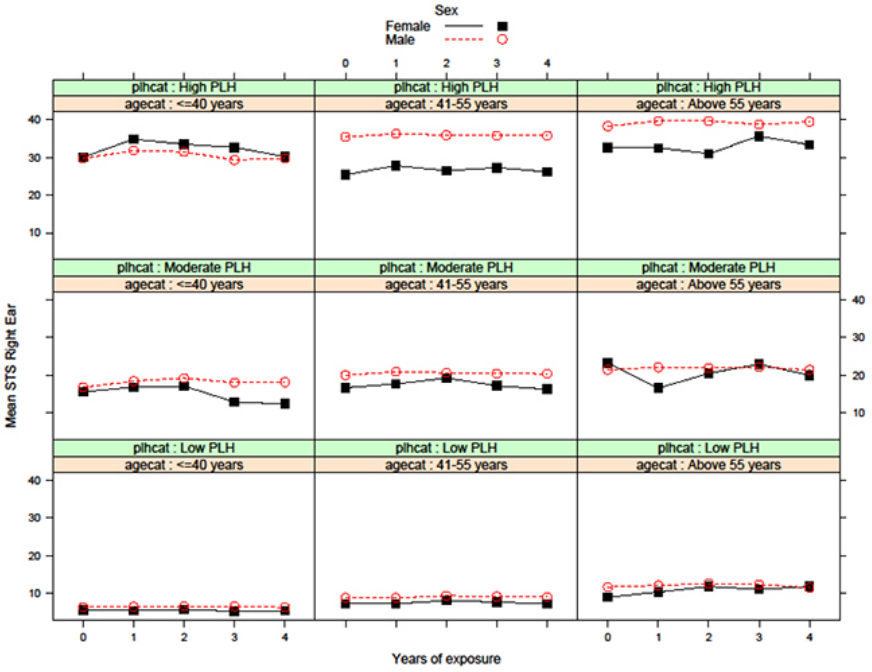

Figure 3—Mean STS for right ear by PLH level, age group, and sex for all years of follow-up

age categories. The differences in mean STS between males and females were greatest in the high PLH and > 41 years age categories.

Predicting standard threshold shifts for occupational hearing loss

The year 2014 was set as the baseline year; 2015, 2016, 2017, and 2018 represented cumulative years of noise and dust exposure. The log-transformed STS data was used in the mixed effects linear regression model as the outcome variable; the predictor variables were sex, age, PLH, noise exposure level, dust exposure level, and years of exposure (as described in Table III). The model showed that the estimated effect on STS for males was 27% and 21% higher than for females, for the left and right ear, respectively. The estimated effects on STS of a unit increase in PLH, age, duration of exposure, and noise exposure level were all < 10%, but nevertheless statistically significant. The effect of dust exposure on STS was not statistically significant. The likelihood ratio test showed that the predictive model was a good fit ($p < 0.001$).

Figure 4 shows an increasing effect of years of exposure on predicted STS for both male and female miners, controlling for age, PLH, and noise and dust levels. There was a steady increase in the predicted STS (and, therefore, a gradual hearing deterioration) for both the left and the right ears over time. Males start with a higher baseline STS and maintain higher STS levels across all years of exposure, compared to females.

Figure 5 shows the effect of increasing age on the predicted STS for males and females, when years of exposure, PLH, and noise and dust levels were controlled for. For males, the predicted STS increased steadily, and was higher than that for females for both the left and right ears. Again, males start with a higher baseline STS than females, which is consistent across all ages.

Discussion

Although the STS milestone (Regulation 839) was introduced by the DMRE and due to be updated in 2024 ('by December 2016, no employee's STS will exceed 10 dB from the baseline when averaged at 2000, 3000 and 4000 Hz in one or both ears') (Chamber of Mines, 2016), our study is the first to evaluate the progress made by this platinum mine. By analysing the mine's data we were able to benchmark miners' hearing, track STS deterioration, and identify miners at risk of developing hearing loss.

In this group of miners, both age and sex were associated with deterioration in hearing, measured by increases in STS in the high frequencies. This supports the findings of Grobler *et al.* (2020) that male gold miners older than 40 years and exposed to excessive occupational noise had hearing deterioration in the high frequencies. Bilateral loss of hearing, measured by STS (HFA234) was generally worse in male than female miners. This may be due to differences in genetic susceptibility (Sliwinska-Kowalska and Pawelczyk, 2013), recreational noise exposure (Gates *et al.*, 2000), previous occupational noise exposure (Grobler *et al.*, 2020), diagnosis of conductive hearing loss (Ntlhakana, Khoza-Shangase, and Nelson, 2020), or medical conditions such as TB and HIV, and treatments thereof (Khoza-

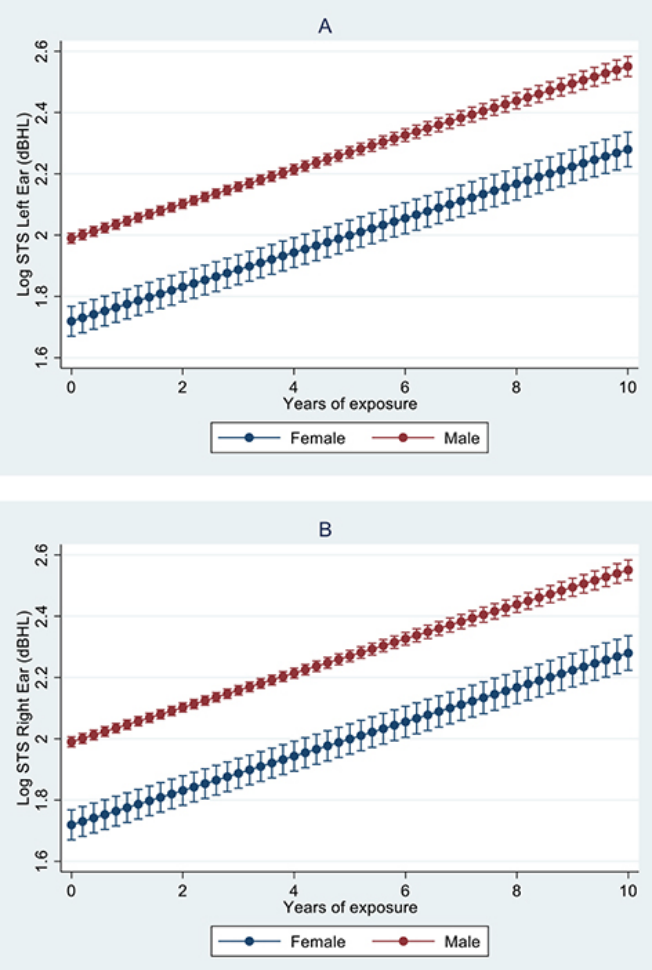

Figure 4—Prediction of STS for males and females, over 10 years (A and B) 95% CI predictive margins

Table III

Average predicted STS for miners from 2014 to 2018

	Standard threshold shifts (dBHL)					
	Left ear			Right ear		
Variable	Estimated effect (%)	95% CI	p value	Estimated effect (%)	95% CI	p value
Sex (male)	0.27	0.220–0.323	< 0.001	0.21	0.162–0.261	< 0.001
PLH	0.08	0.078–0.083	< 0.001	0.08	0.075–0.079	< 0.001
Age (years)	0.03	0.0367–0.040	< 0.001	0.04	0.038–0.041	< 0.001
Duration of exposure from 2014 (years)	0.03	0.0524–0.059	< 0.001	0.03	0.024–0.031	< 0.001
Noise level (dBA)	0.01	0.003–0.008	< 0.001	0. 00	0.002–0.007	0.002
Dust level (mg/m³)	0.02	–0.094–0.1538	0.270	–0.01	–0.132–0.109	0.850

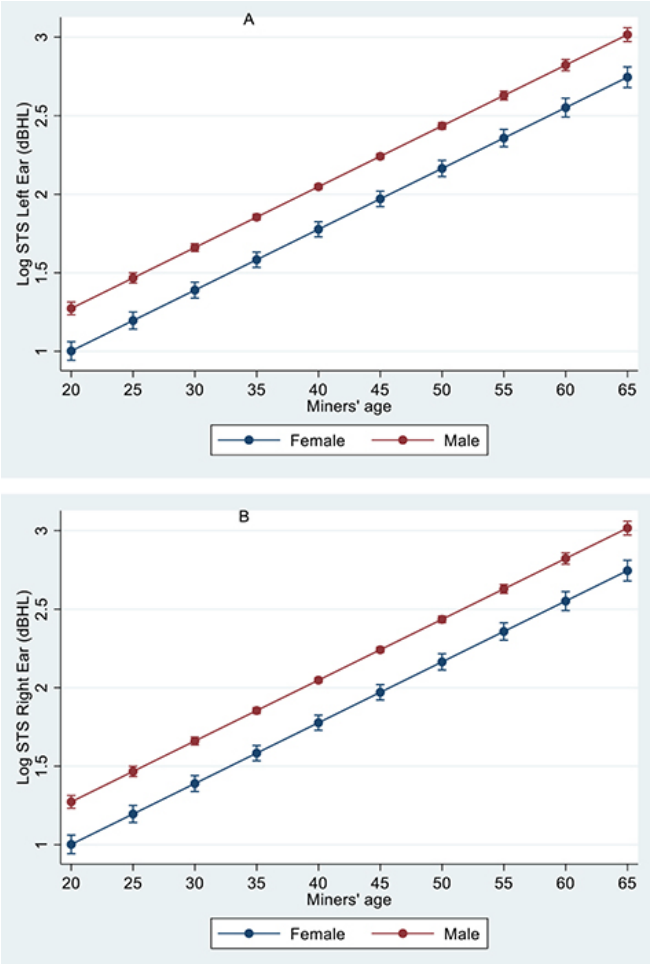

Figure 5—Prediction of STS for males and females over time, by age (A and B) 95% CI predictive margins (95% CI are too narrow to be depicted)

Shangase, 2019). Recently, coronavirus (COVID-19), associated with otitis media (Fidan, 2020) and otitis media, have been included among the risk factors that affect South African miners (Ntlhakana, Khoza-Shangase, and Nelson, 2020). Exclusion of this data from the audiometry records may lead to an under-estimation of the miners' hearing deterioration.

Hearing threshold changes and hearing deterioration that is due to a combination of various factors, including occupational noise exposure, are gradual and incremental. This has been reported previously in South African gold mines (Strauss *et al.*, 2014; Grobler *et al.*, 2020). Some miners had presented with hearing loss in 2018, ranging from 26 dBHL to 90 dBHL, which may prevent the mine from achieving the NIHL milestone target for 2024. Furthermore, some miners' pure-tone air conduction data was not available for every year, so the mine did not consistently follow audiometry requirements for individual miners who were at risk of developing ONIHL. Standard threshold shifts and hearing severity classification scales should be used together, from baseline, to measure miners' hearing deterioration and for early identification of at-risk miners. Our findings may be used by the participating mine to achieve the targets for the NIHL milestone for 2024.

Although the participating mine's noise exposure records showed a maximum noise exposure level (105 dBA) that was below the DMRE's targeted level of 107 dBA for 2024 (Chamber of Mines, 2016), more than 70% of the miners in the cohort were exposed to > 85 dBA over the five-year period. This is a concern as acoustic pressure at > 85 dBA damages the auditory system (Rodrigue, 2020; Grobler *et al.*, 2020). Cumulative exposure to high noise levels had a negative impact on miners' auditory systems, as some of the miners in our study presented with STS that ranged between 26 dBHL and >90 dBHL (Ntlhakana, Khoza-Shangase, and Nelson, 2020). High noise exposure levels will continue to increase the miners' risks of ONIHL.

There are no studies on the effects of dust exposure on hearing loss, which may be due to the fact that dust exposure levels in the South African platinum mines are lower than the regulated occupational exposure level (OEL) of 3 mg/m^3 (Belle and Stanton, 2007). Although more than half of the miners in the database were exposed to 1.5–2.99 mg/m^3 PMD, which is classified as 'significant' according to the mine's PMD risk ranking scale, we found no effect of PMD on hearing function. However, some platinum miners have reported irritation of the throat, nose, ears, and eyes (Levene and Calnan, 1971), which are allergic reactions to PMD that are associated with conductive hearing loss (Levene and Calnan, 1971). Therefore, other types of hearing loss such as conductive hearing loss should be considered to avoid an over-estimation of ONIHL as well as to account for different types of hearing loss that affect miners (Sebothoma, 2020). The findings of this analysis also have implications for preventive audiology in the form of early identification of hearing impairment in miners, and interventions to both reduce the risk of progressive hearing loss in those already affected and prevent hearing loss in miners who are not yet affected (Khoza-Shangase, Moroe, and Edwards, 2020).

Despite the fact that some studies have reported effects of PTB and HIV treatment on miners' hearing function (Khoza-Shangase, 2019), and that certain treatments for these diseases and cancer are ototoxic (Khoza-Shangase, 2019; Lenntech, 2020; Phanguphangu and Ramma, 2018), we were not able to access miners' medical records on PTB, HIV, and cancer treatment, as these records were in a database that was separate from the audiometry data. A lack of integration of the miners' PTB, HIV, and cancer data with audiometry data limits understanding of the miners' hearing function and deterioration.

Hearing changes due to occupational and individual characteristics occur gradually over time and reflect the mine's HCP efficiency. Our findings were similar to those of Strauss *et al.* (2014) and Grobler *et al.* (2020) in that hearing thresholds of males were more adversely affected than those of females. We predicted that the estimated effect on STS associated with being males was more than that of PLH, age, years of exposure, and noise exposure, although all were statistically significant. Our model showed that age had a small effect on STS compared to sex, which was surprising because studies on South African gold miners have reported age to be associated with ONIHL (Strauss *et al.*, 2014; Grobler *et al.*, 2020). There was also evidence that males started with higher STS than females, when years of exposure and age were controlled for, and thus were more susceptible to hearing loss from baseline than females. Furthermore, our model predicted a gradual STS deterioration over 10 years which, without intervention, will continue. Although we used five years (2014–2018) of data in our analysis, the mean duration of employment and noise exposure for platinum miners was more than five years (Ntlhakana,

Khoza-Shangase, and Nelson, 2020). The model showed that combined exposure variables produced an effect on the bilateral STS over a period of time. This presents an opportunity for the mines to use our prediction model and to include miners' exposure variables (age, sex, noise, dust exposure levels, and duration of exposure) to predict hearing deterioration, with the hope of identifying miners at risk of occupational hearing loss.

Most investigations of the prevalence of ONIHL among miners have used cross-sectional study designs (Khoza-Shangase, 2019; Moepeng, Soer, and VInck, 2017; Strauss *et al.*, 2012, 2014; Brits *et al.*, 2012; Campo, Morata, and Hong, 2013; Masterson *et al.*, 2016; Heyer *et al.*, 2011). These have provided limited evidence for synergistic risk factors in occupational hearing loss, and no time-specific information associated with the onset and development of ONIHL. We conducted a retrospective cohort analysis that used the miners' longitudinal data to understand risk factors associated with hearing function. However, prospective cohort longitudinal studies would improve our understand of the development of ONIHL and its associated risk factors over time (Seixas *et al.*, 2012; Worku and Ohaju, 2004).

Strength and limitations

A strength of our study was the use of large data-sets that included miners' occupational exposures and audiometry data to understand the mine's recording of occupational exposure and audiometry data to determine trends in the miners' hearing function.

The main limitation was the unavailability of the miners' medical surveillance records linked to the data-sets used in the study. We could therefore not include medical conditions that cause conductive hearing loss (*e.g.* allergies, COVID-19), chronic medical conditions such as PTB and HIV, and medications used to treat PTB and HIV, in the analysis and in the predictive model. This mine cited the POPI and Medical Ethics Acts as stumbling blocks to providing the miners' medical records, which are classified as confidential with limited rights of access. Thus, effects due to ototoxicity were not factored into our analysis. In addition, there was no information about other factors associated with NIHL, such as recreational noise exposure and previous occupational noise exposure. It is therefore possible that we overestimated the prevalence of ONIHL. This mine's HCP data was not integrated, and some miners' records omitted demographic and audiometry data, hence 2014 was used as the baseline year, which was not necessarily a true baseline for miners in this study.

Conclusion

This is the first study conducted at a South African mine that includes miners' audiometry and occupational exposure data to predict hearing changes over a period of time. We showed that demographic characteristics (age and sex) and occupational exposures (noise) can be used to predict occupational hearing deterioration and calculated the contribution of each variable over a period of time. We showed that miners' STS changes are gradual over time and are due to a combination of risk factors, not only noise exposure. These findings may be used to evaluate HCP efficacy at this and other mines.

The miners' demographic data and risk ranking categories for occupational and audiometry data may be useful for development of the HCP data repository for this and other South African mines. We have highlighted gaps in the literature on the potential association of exposure to PMD and conductive hearing loss in the South African platinum mines. Our results reinforce the need to shift the focus from ONIHL prevention only towards HCPs that will address different types of hearing loss.

Acknowledgements

The authors would like to thank the participating mine for permission to use their data in this study, and the hearing conservation medical and occupational hygiene practitioners for technical guidance. This study was funded by the University of the Witwatersrand Faculty of Humanities Research Committee. Grant sponsor: Faculty of Humanities Research Committee; ad hoc grant.

References

Balfour-Kaipa, T. 2014. Occupational Health Milestones and Chamber's response to key health issues. *Occupational Health Southern Africa*, vol. 20. pp. 26–27.

Belle, B.K. and Stanton, D.W. 2007. Inhalable and respirable dust. *Handbook on Mine Occupational Hygiene Measurements*. Stanton, D.W., Kielblock, J., and Schoeman, J.J. (eds). Mine Health and Safety Council (MHSC), Johannesburg.

Biffi, M. and Belle, B.K. 2003. Quantification of dust-generating sources in gold and platinum mines. *GAP 802*. Mine Health and Safety Council. Johannesburg.

Brits, J., Strauss, S., Eloff, Z., Becker, P.J. and De Swanepoel, W. 2012. Hearing profile of gold miners with and without tuberculosis. *Occupational and Environmental Medicine*, vol. 69. pp. 243–249.

Campo, P., Morata, T.C., and Hong, O. 2013. Chemical exposure and hearing loss. *Disease-a-Month*, vol. 59, no. 4. pp. 119–138. doi: 10.1016/j.disamonth.2013.01.003

Chamber of Mines. 2016. Noise Team on the Mine Health and Safety Milestones. Johannesburg.

Department of Labour. 2001. Circular instruction no. 171 – The determination of permanent disablement resulting from hearing loss caused by exposure to excessive noise and trauma. Pretoria.

Department of Mineral Resources. 2016. Guidance note for the implementation of standard threshold shift in the medical surveillance of noise induced hearing loss. Pretoria.

Department of Minerals and Energy. 2008. Presidential Mine Health and Safety Audit. Pretoria.

Ebonyi, A.O., Oguche, S., Ejeliogu, E.U., Agbaji, O.O., Shehu, N.Y., Abah, I.O., Sagay, A.S., Ugoagwu, P. O., Okonkwo, P.I., Idoko, J.A., and Kanki, P.J. 2016. Prevalence of and risk factors for pulmonary tuberculosis among newly diagnosed HIV-1 infected Nigerian children. *Germs*, vol. 6. pp. 21–8.

Edwards, A. and Kritzinger, D. 2012. Noise-induced hearing loss milestones: past and future. *Journal of the Southern African Institute of Mining and Metallurgy*, vol. 112. pp. 865–869.

Edwards, A., van Coller, P., and Badenhorst, C. 2010. Early identification of noise induced hearing loss: A pilot study on the use of distortion product otoacoustic emissions as an adjunct to screening audiometry in the mining industry. *Occupational Health Southern Africa*, vol. 6. http://www.occhealth.co.za/?/viewArticle/1164

Edwards, A.L., Malanzi, M., Khoza, N.N., and Zungu, L.I. 2015. Evaluation of the current practices of noise induced hearing loss awareness training in the South African mining industry. *Occupational Health Southern Africa*, vol. 21, no. 5. pp. 11–17.

Feuerstein, J. and Chasin, M. 2009. Noise exposure and issues in hearing conservation. *Handbook of Clinical Audiology*. 7th edn. Lippincott Williams & Wilkins, Baltimore, MD.

Fickl, H. 2007. Investigation of the pro-oxidative and pro-inflammatory interactions of cobalt, palladium, platinum and vanadium with human neutrophils *in vitro*. PhD thesis, University of Pretoria.

Fidan, V. 2020. New type of corona virus induced acute otitis media in adult. *American Journal of Otolaryngology*, vol. 41. https://www.ncbi.nlm.nih.gov/pmc/articles/PMC7161479/

Gates, G.A., Schmid, P., Kujawa, S G., Nam, B., and D'Agostino, R. 2000. Longitudinal threshold changes in older men with audiometric notches. *Hearing Research*, vol. 141. pp. 220–228.

Grobler, L.M. 2019. Occupational noise and age: A longitudinal study of hearing sensitivity. M. Pathology (Audiology) dissertation, University of Pretoria.

Grobler, L.M., Swanepoel, D.W., Strauss, S., and Eloff, P.B.Z. 2020. Occupational noise and age: A longitudinal study of hearing sensitivity as a function of noise exposure andage in South African gold mine workers. *South African Journal of Communication Disorders*, vol. 67, no. 2. https://sajcd.org.za/index.php/sajcd/article/view/687/1165

Heyer, N., Morata, T.C., Pinkerton, L., Brueck, S.E., Stancesc, D., Panaccio, M.P., Kim, H., Sinclair, S.J., Waters, M.A., Estill, C., and Franks, J.R. 2011. Use of historical data and a novel metric in the evaluation of the effectiveness of heairng conservation program components. *Occupational and Environmental Medicine*, vol. 68. pp. 510–517.

Mine Health and Safety Inspectorate. 2017. State of health in the South African mining industry. *Annual Report*. Department of Mineral Resources, Pretoria.

Katz, J., Medwetsky, L., Burkard, R., and Hood, L. 2009. Pure tone evaluation. *Handbook of Clinical Audiology*. Katz, J. (ed.). Lippincott Williams & Wilkins, Baltimore, MD.

Khoza-Shangase, K. 2019. Hearing function of gold miners with and without a history of tuberculosis treatment: A retrospective data review. *Brazilian Journal of Otorhinolaryngology*, vol. 86, no. 3. pp. 294–299.

Khoza-Shangase, K., Moroe, N.F., and Edwards, A. 2020. Occupational hearing loss in Africa: An interdisciplinary view of the current status. S*outh African Journal of Communication Disorders*, vol. 67, no. 2. doi: 10.4102/sajcd.v67i2.700

Lenntech, B.V. 2020. Platinum. https://www.lenntech.com/periodic/elements/pt.htm [accessed 7 May 2020].

Levene, G. and Calnan, C.D. 1971. Platinum sensitivity: treatment by specific hyposensitization. *Clinical Allergy*, vol. 1. pp. 75–82.

Masterson, A., Bushnell, P.T., Themann, C.L., and Morata, T.C. 2016. Hearing impairment among noise-exposed workers - United States, 2003-2012. *Morbidity and Mortality Weekly Report* (MMWR), vol. 65. pp. 389-94.

Masterson, A., Deddens, J., Themann, C., Bertke, S., and Calvert, G.M. 2015. Trends in worker hearing loss by industry sector, 1981-2010. *American Journal fo Industrial Medicine*, vol. 58. pp. 392–401.

MHSC. 2015. 'Every mine worker returning from work unharmed every day. Striving for zero harm' - 2014 Occupational Health and Safety Summit Milestones. *Journal of Occupational Health Southern Africa*, vol. 20, no. 2.

Moepeng, M., Soer, M., and Vinck, B.M. 2017. Distortion product otoacoustic emissions as a health surveillance technique for hearing screening in workers in the steel manufacturing industry. *Occupational Health Southern Africa*, vol. 22. pp. 8–13.

Msiza, D. 2014. The road to zero harm: new milestones. Mine Health and Safety Council, Johannesburg.

Nelson, D.I., Nelson, R.Y., Concha-Barrientos, M., and Fingerhut, M. 2005. The global burden of occupational noise-induced hearing loss. *American Journal of Industrial Medicine,* vol. 48. pp. 446–58.

Nelson, G. 2013. Occupational respiratory diseases in the South African mining industry. *Global Health Action*, vol. 6. pp. 89–98.

Nelson, G. and Murray, J. 2013. Silicosis at autopsy in platinum mine workers. *Occupational Medicine*, vol. 63. pp. 196–202.

Ntlhakana, L., Khoza-Shangase, K., and Nelson, G. 2020. Occupational noise-induced hearing loss in platinum miners: What do the data tell us? *Occupational Health Southern Africa*, vol. 26. pp. 8–14.

Phanguphangu, M. and Ramma, L. 2018. High incidence of cisplatin-induced ototoxicity in paediatric patients in the Western Cape, South Africa. *South African Journal of Oncology*, vol. 2. doi: https://doi.org/10.4102/sajo.v2i0.41

Pillay, M. 2020. Chemicals, noise and occupational hearing health in South Africa: A mapping study. *South African Journal of Communication Disorders*, vol. 67, no. 2. doi: https://doi.org/10.4102/sajcd.v67i2.693

Rodrigue, J. 2020. Transportation and the environment. *The Geography of Transport Systems*. Rodrigue, J. (ed.). 5th edn. Routledge, New York.

SANS. 2013. The measurement and assessment of occupational noise for hearing conservation purposes. South African National Standards, Pretoria.

Sebothoma, B. 2020. Middle ear pathologies in adults within the mining industry: A systematic review. *South African Journal of Communication Disorders*, vol. 67. https://sajcd.org.za/index.php/sajcd/article/view/679/1157

Seixas, N.S., Neitzel, R., Stover, B., Sheppard, L., Feeney, P., Mills, D., and Kujawa, S. 2012. 10-Year prospective study of noise exposure and hearing damage among construction workers. *Occupational and Environmental Medicine*,vol. 69. pp. 643–650.

Sepadi, M.M., Chadyiwa, M., and Nkosi, V. 2020. Platinum mine workers' exposure to dust particles emitted at mine waste rock ,crusher plants in Limpopo, South Africa. *International Journal of Environmental Research and Public Health*, vol. 17. doi: 10.3390/ijerph17020655

SIGNIA. 2018. Allergy or sudden hearing loss—Can you tell the difference? [accessed 29 May 2020]. https://assets.signia-hearing.com/blog/allergy-sudden-hearing-loss-can-tell-difference/[accessed 29 May 2020].

Sliwinska-Kowalska, M. and Pawelczyk, M. 2013. Contribution of genetic factors to noise-induced hearing loss: A human studies review. *Mutation Research/Reviews in Mutation Research*, vol. 752. pp. 61-65.

Strauss, S., Swanepoel, D., Becker, P., Eloff, Z., and Hall, J.W. 2012. Prevalence and degree of noise induced hearing loss in South African gold miners. *Occupational Health Southern Africa*, vol. 18, no. 6. pp. 20–25. shttps://journals.co.za/doi/10.10520/EJC128495

Strauss, S., Swanepoel, D.W., Becker, P., Eloff, Z., and Hall, J.W. 3RD 2014. Noise and age-related hearing loss: a study of 40 123 gold miners in South Africa. *International Journal of Audiology*, vol. 53, suppl. 2. pp. S66–575.

Worku, Z. and Ohaju, M. 2004. A statistical analysis of common occupational diseases among South African miners from 2000 to 2003. *Occupational Health Southern Africa*, vol. 10, no. 5. pp. 16–21. ◆

A semi-empirical solution for estimating the elastic stresses around inclined mine stopes for the Mathews-Potvin stability analysis

P. Pagé[1], P. Yang[1], L. Li[1], and R. Simon[1]

Affiliation:
[1]Research Institute on Mines and Environment, Department of Civil, Geological and Mining Engineering, École. Polytechnique de Montréal, Canada.

Correspondence to:
P. Yang

Email:
pengyu.yang@polymtl.ca

Dates:
Received: 27 Mar. 2019
Revised: 13 May 2021
Accepted: 30 Jun. 2021
Published: August 2021

How to cite:
Pagé, P., Yang, P., Li, L., and Simon, R. 2021
A semi-empirical solution for estimating the elastic stresses around inclined mine stopes for the Mathews-Potvin stability analysis.
Journal of the Southern African Institute of Mining and Metallurgy, vol. 121, no. 8, pp. 405–414

DOI ID:
http://dx.doi.org/10.17159/2411-9717/690/2021

ORCID:
L. Li
https://orcid.org/0000-0002-3900-5234

Synopsis

The Mathews-Potvin stability method is widely used in the Canadian mining industry as a starting point to determine the maximum dimensions of mine stopes. However, it cannot be applied to inclined (more frequently encountered) mine stopes without conducting numerical modelling to obtain the stress factor *A*, defined as a function of the ratio of unconfined compressive strength of intact rock to the induced principal stress on the exposed stope walls. The need to conduct numerical modelling significantly limits the application of the Mathews-Potvin method. In addition, given its empirical nature and main application for preliminary design, it is deemed undesirable to conduct numerical modelling, especially elaborate modelling. Alternatively, theoretical methods can provide a much simpler and quicker way to estimate stresses around stopes and the corresponding stress factors. Over the years, a large number of studies have been conducted to estimate stresses around openings excavated with various cross-sections. However, theoretical or graphical solutions remain unavailable for mine stopes that typically consist of horizontal floor and roof, and two parallel inclined walls (hangingwall and footwall). To remedy this situation, a series of numerical simulations is first performed for openings with vertical and inclined walls, including typical stopes commonly encountered in underground mines. A group of empirical solutions is then formulated to estimate the induced principal stresses at the roof centre and mid-height of the stope walls. The validity and predictability of the proposed solution have been verified using additional numerical simulations. The proposed solution can thus be used to calculate stresses and the resultant stress factors *A* around typical mine stopes with any inclination angle and height to width ratio, under any *in-situ* stress state, without conducting numerical modelling.

Keywords
Mathews-Potvin, inclined stope, simulation, semi-empirical solution.

Introduction

Ground stability is a challenging issue frequently faced by rock engineers. The trend towards larger and more powerful equipment to improve productivity requires larger underground openings. However, the dimensions of stable underground excavations are finite, limited by field stresses and rock mass conditions. The correct design of underground openings is thus of paramount importance.

The Mathews-Potvin method is a simple and useful tool for mining engineers. It is commonly used as a starting point to determine the dimensions of stopes or design the required support (*e.g.*, Mathews *et al.* 1981; Potvin 1988; Hutchinson and Diederichs 1996; Li and Ouellet 2009). The Mathews-Potvin method is also used to estimate the unplanned dilution due to the slough that can take place around the hangingwall and footwall during blasting or muck-out of blasted ore (Scoble and Moss 1994; Clark and Pakalnis 1997; Kaiser *et al.* 1997; Diederichs and Kaiser 1999, Diederichs, Kaiser, and Eberhardt, 2004; Papaioanou and Suorineni 2016). Another application of the Mathews-Potvin method is to estimate the minimum span exposures to ensure the cavability (self-collapse) of ore in caving mining methods (Sunwoo, Jung, and Karanam, 2006).

Over the years, the Mathews-Potvin method has received extensive modifications (*e.g.*, Mathews *et al.*, 1981; Potvin, Hudyma, and Miller, 1989; Potvin and Milne 1992; Nickson 1992; Hadjigeorgiou, Leclair, and Potvin, 1995; Stewart and Forsyth 1995; Milne, Pakalnis, and Felderer, 1996; Clark and Pakalnis 1997; Germain and Hadjigeorgiou 1998; Suorineni 1998; Diederichs and Kaiser 1999; Trueman, Mikula, and Mawdesley, 2000; Mawdesley, Trueman, and Whiten, 2001; Suorineni, 1998; Suorineni, Tannant, and Kaiser, 1999a, 1999b; Stewart and Trueman, 2001; Suorineni, Henning, and

Kaiser, 2001, Suorineni, Tannant, and Kaiser, 2001; Suorineni *et al.*, 2001; Trueman and Mawdesley, 2003; Wang, 2004; Bewick and Kaiser, 2009; Capes, 2009; Li and Ouellet, 2009; Zhang, Hughes, and Mitri, 2011; Suorineni, 2012; Papaioanou and Suorineni, 2016; Madenova and Suorineni, 2020). An extensive review of various versions of this method was reported by Suorineni (2010).

For mine stope design, a major limitation associated with the Mathews-Potvin method is the need to conduct numerical simulations to obtain a key parameter, called the stress factor (*A*), which depends on the ratio of the unconfined compressive strength of intact rock to the induced principal stress (σ_1) on the walls of the opening. When the geometry of the openings is simple, such as a circular cross-section, analytical solutions exist for estimating the stress around such openings (Kirsch, 1898; Hiramatsu, 1962; Logie and van, Tonder 1967; Hiramatsu and Oka, 1968; Li, 1997). More sophisticated analytical solutions are equally available for estimating the elastic stresses around tunnels with a vertical axis of symmetry, including openings with elliptical, rectangular, and arched walls (Logie and van Tonder 1967; Hoek and Brown 1980; Gerçek 1997; Exadaktylos and Stavropoulou 2002; Brady and Brown 2013).

For vertical mine stopes, graphical solutions used to estimate the induced stresses have been elaborated in two dimensions (2D plane strain; Potvin 1988; Stewart and Forsythe 1995) and three dimensions (Mawdesley, Trueman, and Whiten, 2001; Vallejos, Delonca, and Perez, 2017). In practice, however, orebodies are always inclined to a greater or lesser degree. Few theoretical or graphical solutions are available to assess the induced stresses around inclined stopes with one horizontal floor, one horizontal roof, and two parallel and inclined walls (hangingwall and footwall). Numerical modelling has to be performed to obtain the induced stresses for each specific mining project (Li and Ouellet, 2009). This requires not only the availability of pertinent software and hardware, but also qualified numerical modellers who have a good understanding of field conditions and the behaviour of the rock mass, and know in particular how to obtain reliable numerical outcomes. It is thus desirable to have theoretical solutions that can be used to estimate the stresses around inclined stopes.

In this paper, the Mathews-Potvin method is first briefly recalled for the sake of completeness. Numerical simulation results are then presented by considering inclined mine stopes surrounded by a homogenous, isotropic and linearly elastic rock mass. A large range of wall inclination angles, height to width ratios, and *in-situ* stresses are considered. Semi-empirical solutions are proposed to estimate the induced principal stresses on stope walls by applying the principle of superposition of linearly elasticity theory through a curve-fitting technique applied to the numerical results. The prediction capability of the proposed semi-empirical solutions is verified with additional numerical simulations. A typical example is also given to illustrate the application of the proposed solution.

The Mathews-Potvin method

The Mathews-Potvin method is an empirical method based on numerous field observations. This method relates the stability of an exposed wall to two factors – the hydraulic radius (*HR*) and the stability number (*N'*). The former is defined as (Potvin 1988):

$$HR = \frac{\text{Area of an exposed face}}{\text{Perimeter of the exposed face}} \quad [1]$$

The stability number (*N'*) of the exposed wall is defined by the following equation:

$$N' = Q' * A * B * C \quad [2]$$

where *Q'* is a modified rock tunnelling quality index, *A* is the rock stress factor, *B* is the joint orientation adjustment factor, and *C* is the gravity adjustment factor.

The parameter *Q'* resulted from a modification on the Rock Tunnelling Index (*Q*) of Barton, Lien, and Lunde (1974), is defined as follows:

$$Q' = \frac{RQD}{J_n} \times \frac{J_r}{J_a} \quad [3]$$

where *RQD* is the rock quality designation, J_n is the joint set number, J_r is the joint roughness number, and J_a is the joint alteration number.

The rock stress factor *A* is a function of the ratio between the unconfined compressive strength of the intact rock (σ_c) and the induced major principal stress (σ_1) on the exposed walls of a stope. The stress factor *A* can be expressed as follows (Potvin, 1988), which is further illustrated in Figure 1a:

$$A = \begin{cases} 0.1 & \text{for} \quad \sigma_c/\sigma_1 < 2 \\ 0.1125(\sigma_c/\sigma_1) - 0.125 & \text{for} \; 10 > \sigma_c/\sigma_1 > 2 \\ 1.0 & \text{for} \quad \sigma_c/\sigma_1 > 10 \end{cases} \quad [4]$$

Factor *B* considers the influence of joints on the stability of the studied exposed wall (Potvin 1988). It represents the effect of the angle between the most critical joints and the wall, as shown in Figure 1b. The gravity factor *C* depends on the individual influence of the inclination of the exposed wall and the inclination of the critical joints, as illustrated in Figure 1c. Once the stability number *N'* and hydraulic radius *HR* are determined, the stability of the exposed wall can be evaluated using the chart of Mathews-Potvin, as shown in Figure 1d.

From Equation [4], one notes that the rock stress factor *A* proposed by Potvin (1988) has some limitations when the rock is submitted to a tensional stress. In this case, the induced principal stress σ_1 is zero (for a 2D model) or non-zero in the third dimension (for a 3D model). Factor *A* can thus reach its maximum value of 1.0 independent of the tensile stress and tensile strength of the rock, which is unrealistic. Therefore, Equation [4] is not entirely adequate to describe the stability or failure of rock by tension. To overcome this limitation, Li and Ouellet (2009) proposed two approaches. The first is to neglect the tensile strength of the rock, and to fix $A = 0.1$ for $\sigma_3 \leq 0$ (where σ_3 is the induced tensile stress around the excavation). The second approach is to compare the tensile stress with the tensile strength of the rock, so that $A = 0.1125|^{\sigma t}/_{\sigma 3}|-0.125$ (same form as Equation [4]; where σ_t is the tensile strength of the intact rock). Zhang, Hughes, and Mitri (2011) adopted a similar approach to that of Li and Ouellet (2009) when the rock is submitted to tension. Suorineni (2012) concluded that the stress factor for tension (and other factors) needs to be calibrated. Further discussion on the definition of this factor is beyond the scope of the paper, but it is seen that the determination of factor *A* depends on knowledge of the induced principal stresses on the exposed stope walls.

Numerical modelling of the elastic stresses around inclined stope walls

Figure 2 shows a typical mine stope consisting of a horizontal

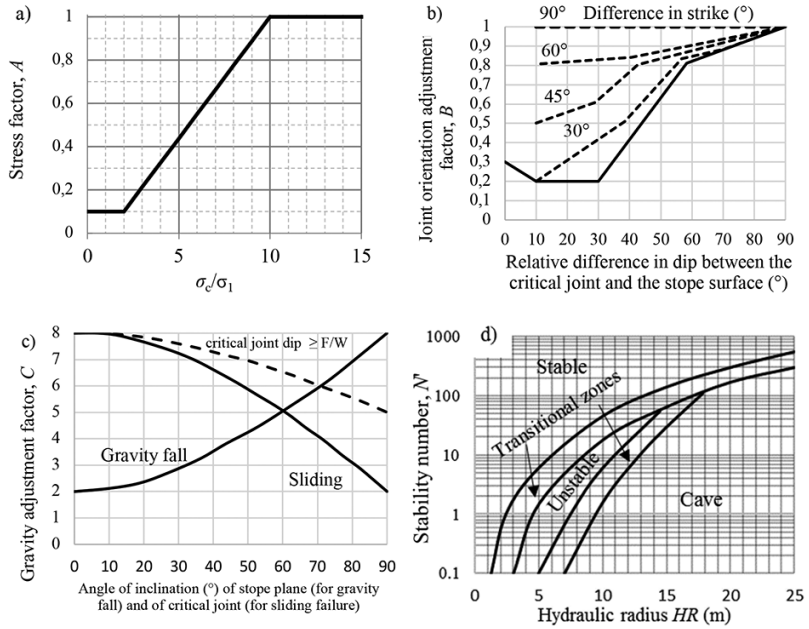

Figure 1—Mathews-Potvin method: (a) determination of the rock stress factor, *A* (after Potvin 1988); (b) determination of the orientation factor, *B* (after Potvin 1988); (c) determination of the gravity factor, *C* (after Potvin and Hadjigeorgiou 2001); and (d) standard stability graph (after Suorineni 2010)

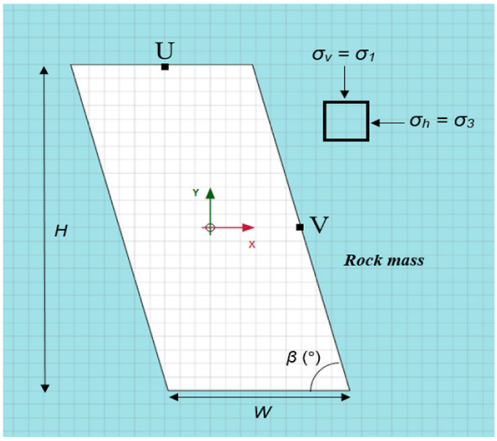

Figure 2—Schematic representation of a typical mine stope; points U and V indicate the mid-points of the roof and sidewall respectively

roof, a horizontal base and two parallel and inclined walls. In the figure, *W* and *H* are the width and height of the stope, respectively; β is the inclination angle of the stope walls; σ_v and σ_h on the stress block represent the vertical and horizontal natural *in-situ* principal stresses, respectively; the out-of-plane stress is another *in-situ* principal stress. The mid-points have been denoted as U and V on the surfaces of roof and sidewall respectively.

The numerical code Plaxis 2D (Brinkgreve and Vermeer 1999), based on the finite element method and commonly adapted for rock mechanics and geotechnical engineering, is used here to evaluate the stresses around mine stopes. The sign convention used by Plaxis 2D considers compression negative (–) and tension positive (+). However, the results presented in this study follow the sign convention commonly used in rock mechanics analysis, where compression is positive (+) and tension is negative (–).

The linearly elastic model of Plaxis 2D was first validated by comparing the simulated stresses against the analytical solutions for a circular opening (Kirsch, 1898; Hiramatsu, 1962; Hiramatsu and Oka, 1968; Li, 1997). Additional validations were made against the graphical and analytical solutions of Hoek and Brown (1980) in the cases of elliptical and square openings. More details are presented in Pagé (2018).

Table I presents the program of numerical simulations. Forty-eight stope geometries were considered by combining the stope width (*W*), height (*H*), and wall inclination angle (β). Two regimes of natural *in-situ* stresses were considered: Case 1 with σ_v = 30 MPa and σ_h = 0; Case 2 with σ_v = 0 and σ_h = 30 MPa. It should be noted that the consideration of a zero horizontal *in-situ* stress σ_h in Case 1 and a zero vertical *in-situ* stress σ_v in Case 2 is necessary for applying the principle of superposition. This does not mean that the numerical models only correspond to zero vertical or horizontal *in-situ* stress, although the models remain valid for such extreme cases. The principal stresses tangential to the exposed faces at points U and V (on the wall surfaces) are calculated (see Figure 2).

Figure 3 shows a numerical model constructed with Plaxis 2D. An enlarged view of the stope with refined meshes around the stope before excavation is presented. The natural *in-situ* stresses were first initiated over the entire model. The four outer boundaries were then fixed in all directions. Finally, the excavation of the stope was simulated. For each numerical model with a new stope geometry, domain and meshes sensitivity analyses have been done to ensure that the outer boundaries are far enough from the stope and the meshes around the stope are fine enough. A sufficiently large domain is necessary to avoid the boundary effect, while finer meshes around the stope are required to ensure stable numerical results (see more details presented in Pagé, 2018).

Figure 4 presents the minor (σ_3, Figure 4a) and major (σ_1, Figure 4b) principal stresses contours around a stope with *H*/W = 2 and β = 75°, obtained from numerical modelling using an *in-situ* stress state of σ_v = 30 MPa and σ_h = 0 MPa (with σ_v = –30 MPa and σ_h = 0 MPa as inputs to Plaxis 2D). Note that the major and minor in-plane principal stresses in Plaxis 2D are represented by σ_1 and σ_3 respectively, while the out-of-plane

Table I

Program of numerical simulations conducted to calculate critical tangential stresses around mine stopes

In-situ stress	Stope inclination β	*W* x *H* (m)	*H*/*W*
Case 1:			
σ_v = 30 MPa		120x12	0.1
σ_h = 0		48x12	0.25
		36x12	0.33
		24x12	0.5
		16x12	0.75
		12x12	1
	90°, 75°, 60° and 45°	12x24	2
Case 2:			
σ_v = 0		12x36	3
σ_h = 30 MPa		12x48	4
		12x72	6
		12x96	8
		12x120	10

principal stress is denoted by σ_2. Figure 4a shows that the critical tangential stresses on the roof are under tension (positive in Plaxis 2D), while Figure 4b indicates that the critical tangential stresses on the walls undergo compression (negative in Plaxis 2D). The minor principal stress at the roof centre is –26.8 MPa (in tension), while the major principal stress at the mid-height of the hangingwall and footwall is 37.4 MPa (in compression).

Figure 5 shows the major (σ_1, Figure 5a) and minor (σ_3, Figure 5b) principal stress contours around the stope with *H*/*W* = 2 and β = 75°, obtained by numerical modelling with a natural *in-situ* stress state of σ_v = 0 MPa and σ_h = 30 MPa (with σ_v = 0 MPa and σ_h = –30 MPa as inputs to Plaxis 2D). In this case, the critical tangential stress on the roof is under compression (negative in Plaxis 2D) based on the major principal stress (σ_1, Figure 5a), while the critical tangential stresses on the walls are under tension (positive in Plaxis 2D) based on the minor principal stress (σ_3, Figure 5b). The major principal (compressive) stress at the roof centre is 61.1 MPa, while the minor principal (tensile) stress at the mid-height of the hangingwall and footwall is –23.6 MPa.

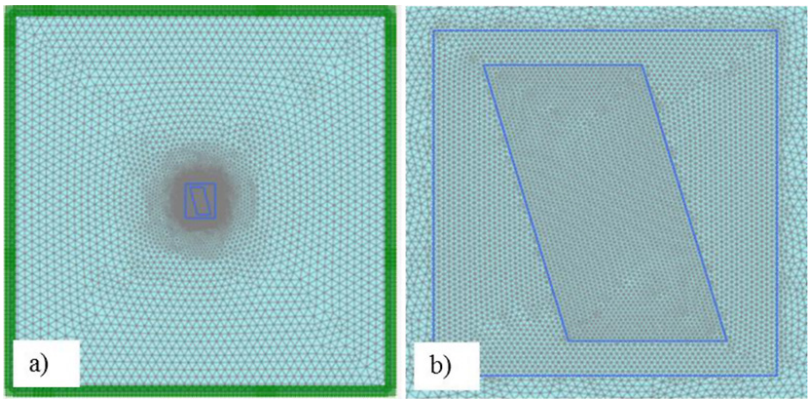

Figure 3—(a) A numerical model constructed with Plaxis 2D for a typical mine stope; and (b) an enlarged view of the stope with finer meshes

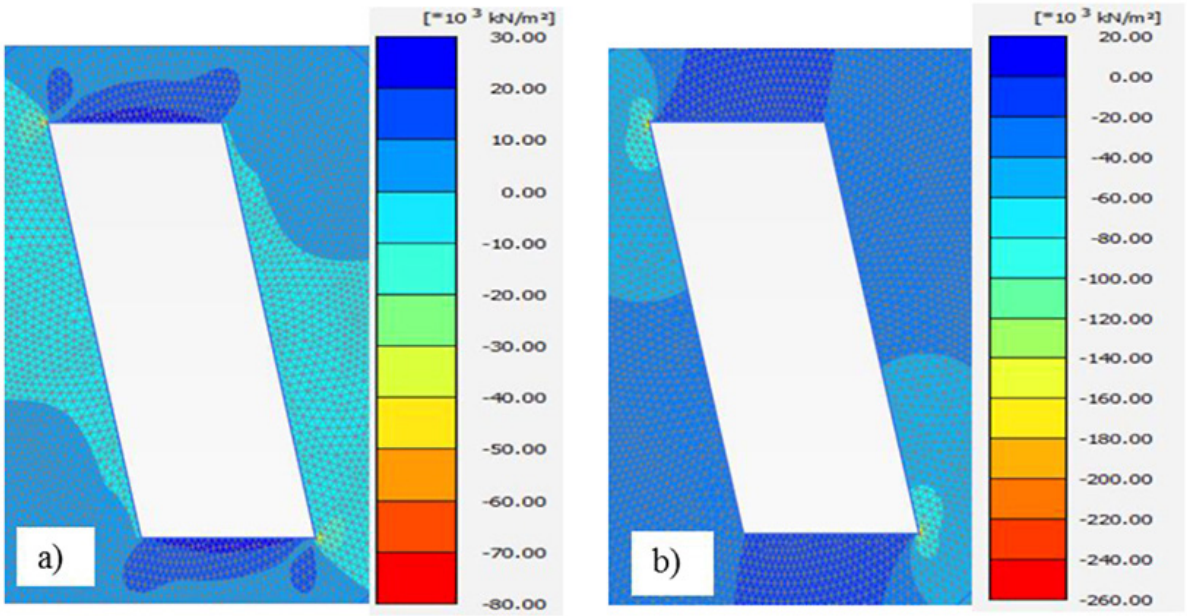

Figure 4—Iso-contours of the (a) minor (σ_3) and (b) major (σ_1) principal stresses around a stope with *H*/*W* = 2 and β = 75°, calculated by applying a natural *in-situ* stress state of σ_v = 30 MPa and σ_h = 0 MPa in Plaxis 2D (with σ_v = –30 MPa and σ_h = 0 MPa as inputs to Plaxis 2D)

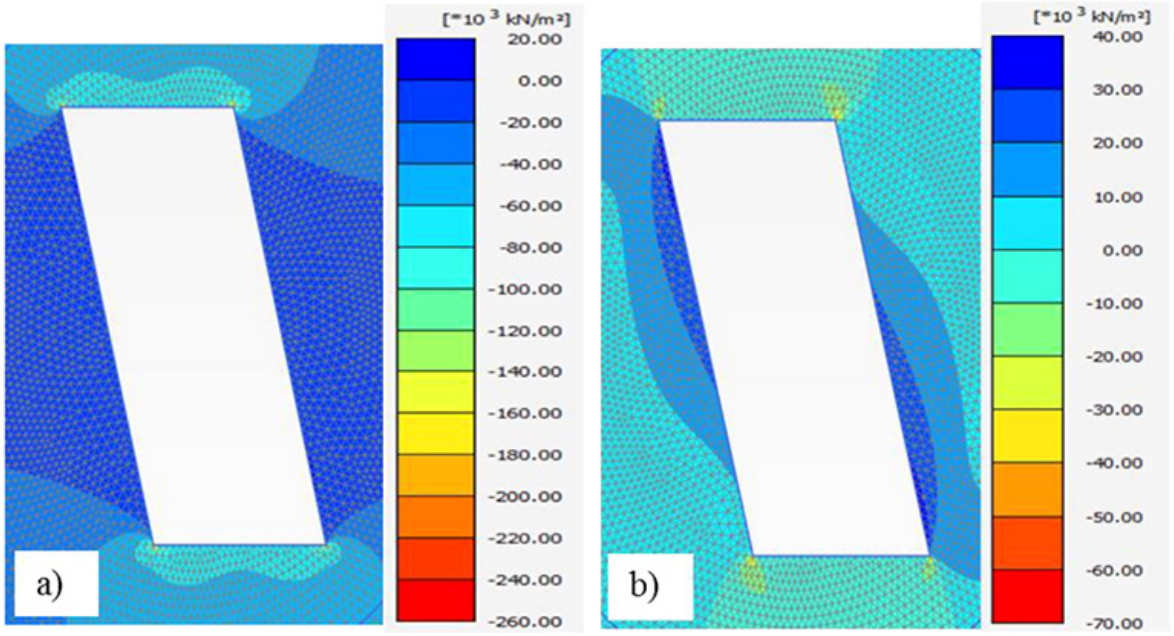

Figure 5—Isocontours of σ_1 (a) and σ_3 (b) principal stresses around the stope with *H*/*W* = 2 and β = 75°, calculated by applying a natural *in-situ* stress state of σ_v = 0 MPa and σ_h = 30 MPa in Plaxis 2D (with σ_v = 0 MPa and σ_h = –30 MPa as inputs tp Plaxis 2D)

Proposed semi-empirical solution

Formulation

To formulate a semi-empirical solution for evaluating the elastic stresses around mine stopes, one uses the principle of superposition valid in elasticity theory for homogenous, isotropic, and linearly elastic material. For a given stope geometry, the stresses around the opening are investigated by applying a horizontal natural *in-situ* stress. The induced stresses at the point of interest on the stope wall are then normalized by the applied horizontal natural *in-situ* stress. By changing the stope height to width ratio (*H*/*W*) and wall inclination angle (β), a relationship based on curve fitting can then be established between the studied stresses at the point of interest on the stope wall and the horizontal natural *in-situ* stress, stope width to height ratio, and stope wall inclination angle.

The same process is repeated for the vertical natural *in-situ* stress with different stope width to height ratios and stope wall inclination angles. Applying the curve-fitting technique leads to another equation, which describes the induced stress around the stope opening as a function of the vertical natural *in-situ* stress, stope width to height ratio, and stope wall inclination angle.

By adding the two equations, one obtains an equation that describes the studied stresses at the point of interest on the wall or roof as a function of the horizontal and vertical natural *in-situ* stresses, stope geometry, and wall inclination. The procedure can be summarized as follows:

$$\sigma_{roof} = \sigma_v \times f_1\left(\frac{H}{W}, sin\beta\right) + \sigma_h \times f_2\left(\frac{H}{W}, sin\beta\right) \quad [5]$$

$$\sigma_{wall} = \sigma_v \times g_1\left(\frac{H}{W}, sin\beta\right) + \sigma_h \times g_2\left(\frac{H}{W}, sin\beta\right) \quad [6]$$

where f_1 and f_2 are the geometric functions on the critical tangential stress at the roof centre, associated with the vertical and horizontal natural *in-situ* stresses, respectively; g_1 and g_2 are the geometric functions on the critical tangential stress at the mid-height of the hangingwall and footwall, associated with the vertical and horizontal natural *in-situ* stresses, respectively.

To obtain the four geometric functions f_1, f_2, g_1, and g_2, a second-degree polynomial regression fit (for both f_1 and f_2), and a combination of a power regression fit and a second-degree polynomial regression fit (for g_1 and g_2 respectively) were applied to the numerical results of the critical induced stresses at the roof centre and at the mid-height of the wall as a function of the *H*/*W* ratio, separately for β = 90°, 75°, 60°, and 45°. Figure 6 shows the four geometric functions (tendency curves in dotted lines) as a function of *H*/*W* for β = 90° (Figure 6a), 75° (Figure 6b), 60° (Figure 6c), and 45° (Figure 6d).

A second calibration of these four geometric functions by considering the wall inclination angle leads to the following equations: Equations [5] to [10] constitute the proposed solution for estimating the elastic stresses at the roof centre and mid-height of the hangingwall and footwall around typical mine stopes. These equations are independent of the stope depth and rock mass strength.

$$f_1\left(\frac{H}{W}, sin\beta\right) = -1.34\left(\frac{H}{W}\right)^{1.01} + (-0.92sin^2\beta + 1.74sin\beta + 0.52)\left(\frac{H}{W}\right) + 4.02sin^2\beta - 6.32sin\beta + 1.52 \quad [7]$$

$$f_2\left(\frac{H}{W}, sin\beta\right) = -8.9\left(\frac{H}{W}\right)^{1.016} + (1.17sin^2\beta - 1.9sin\beta + 10.28)\left(\frac{H}{W}\right) - 4.09sin^2\beta + 6.43sin\beta - 1.47 \quad [8]$$

$$g_1\left(\frac{H}{W}, sin\beta\right) = (4.64sin\beta - 2.9) \times \left(\frac{H}{W}\right)^{(-3.46sin^2\beta + 6.83sin\beta - 3.7)} \quad [9]$$

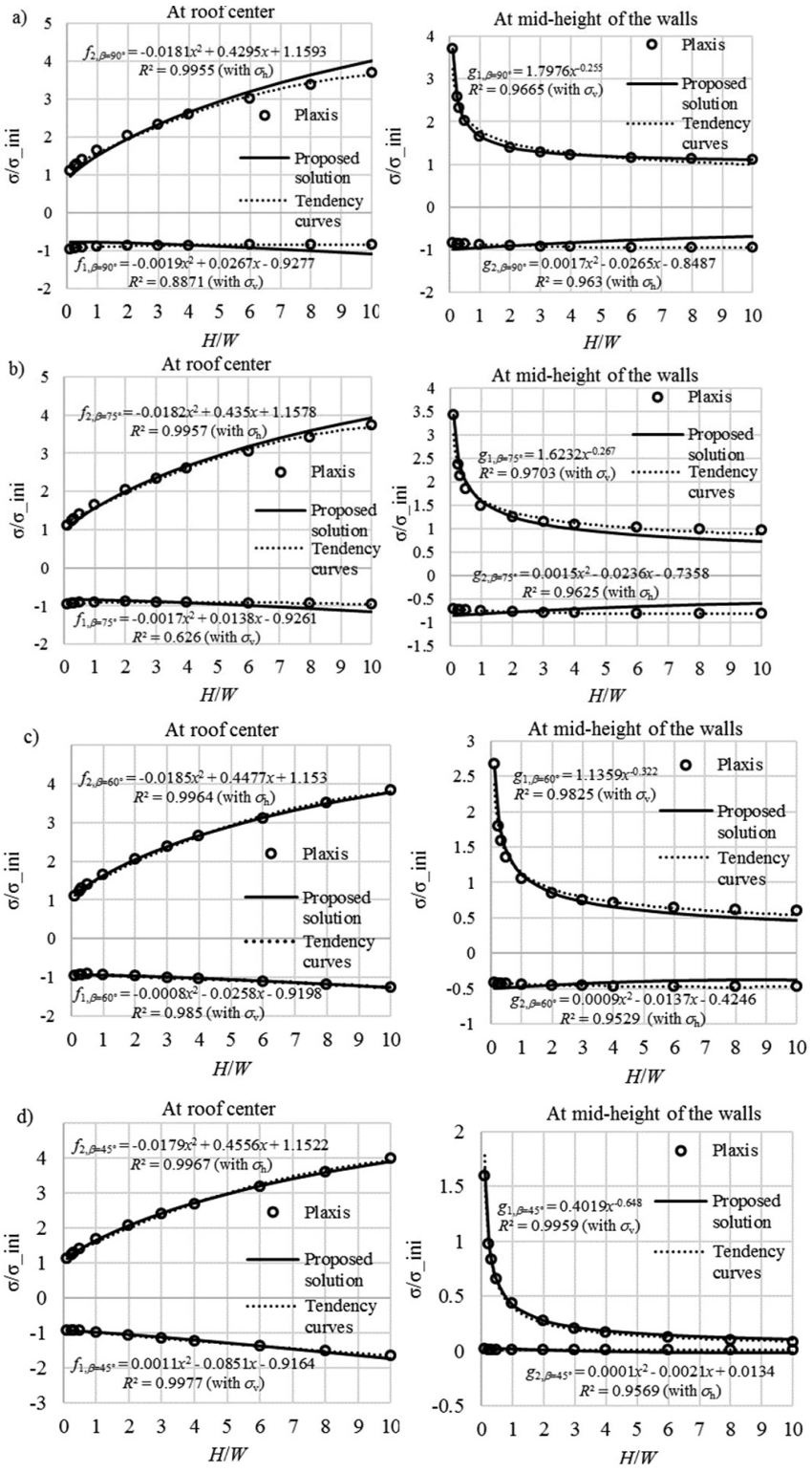

Figure 6—Variation of the critical induced tangential stresses at the roof centre and mid-height of wall, respectively normalized by the applied horizontal (σ_h) and vertical (σ_v) *in-situ* stresses as a function of the *H/W* ratio for stope inclination angles (β) of (a) 90°; (b) 75°; (c) 60°; and (d) 45°

$$g_2\left(\frac{H}{W}, sin\beta\right) = (0.051sin^2\beta - 0.094sin\beta + 0.042)\left(\frac{H}{W}\right)^2 \quad [10]$$

$$-(0.41sin^2\beta - 0.89sin\beta + 0.44)\left(\frac{H}{W}\right) - 3.47sin\beta + 2.49$$

When the natural *in-situ* stress state is $\sigma_v > 0$ (in compression) and $\sigma_h = 0$, the solution predicts tension ($\sigma_{roof} < 0$) acting on the roof and compression ($\sigma_{wall} > 0$) on the mid-height of the walls. Conversely, when the natural *in-situ* stress state is $\sigma_v = 0$ and $\sigma_h > 0$ (in compression), the solution leads to compression ($\sigma_{roof} > 0$) on the roof and tension ($\sigma_{wall} < 0$) on the mid-height of the walls.

Figure 6 shows that the critical induced stresses at the roof centre and at the mid-height of the hangingwall and footwall

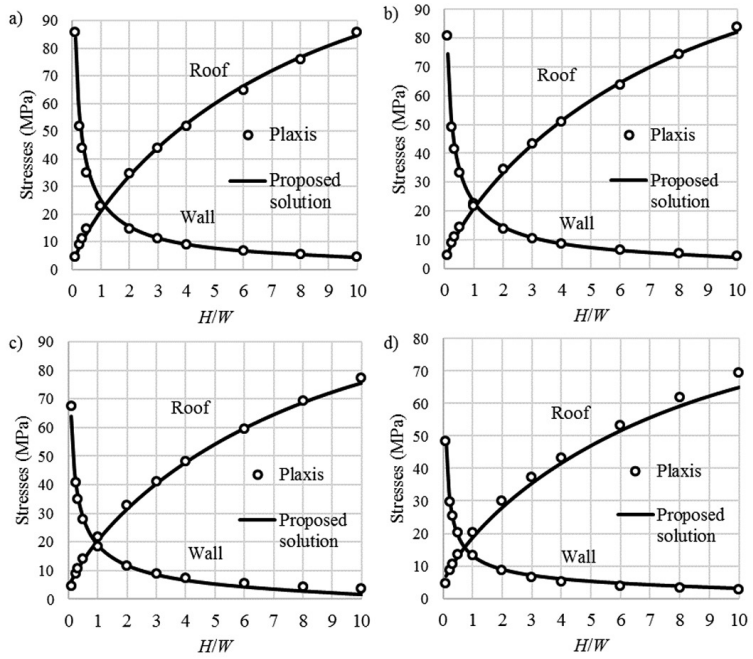

Figure 7—Variation of the induced tangential stresses, obtained by numerical modelling with Plaxis 2D and predicted by the proposed semi-empirical solution (Equations [5] to [10]) around the stopes as a function of the *H/W* ratio, submitted to an isotropic natural *in-situ* stress of 30 MPa (compression) with stope wall inclination angles (β) of (a) 90°; (b) 75°; (c) 60°; and (d) 45°

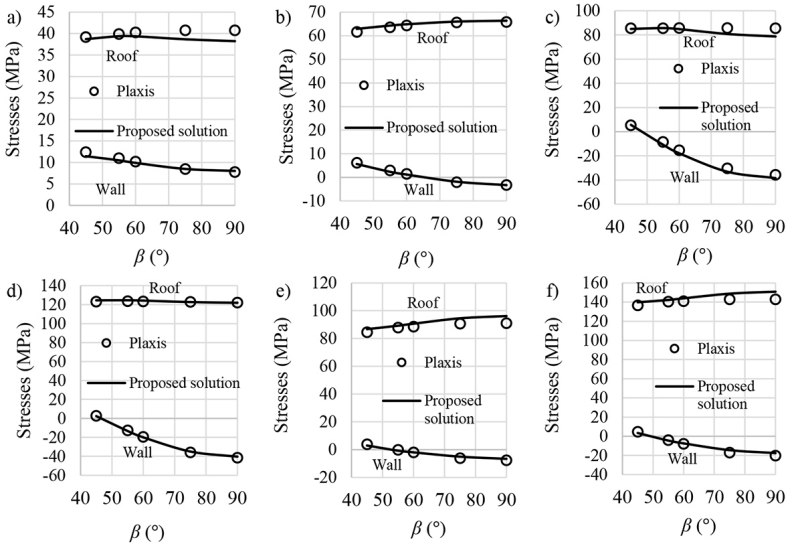

Figure 8—Variation of the induced tangential stresses around the stopes opening as a function of the stope wall inclination angle β, obtained by numerical modelling and predicted by the proposed semi-empirical solution by considering: (a) σ_v = 25 MPa (compression), σ_h = 40 MPa (compression), *H/W* = 0.85; (b) σ_v = 25 MPa, σ_h = 40 MPa, *H/W* = 2.5; (c) σ_v = 10 MPa, σ_h = 60 MPa, *H/W* = 0.85; (d) σ_v = 10 MPa, σ_h = 60 MPa, *H/W* = 2.5; (e) σ_v = 25 MPa, σ_h = 40 MPa, *H/W* = 5; and (f) σ_v = 30 MPa, σ_h = 60 MPa, *H/W* = 5

calculated by the proposed solution (Equations [5] to [10]), and represented by the full lines, correspond well to those obtained by the numerical modelling. This type of comparison between a proposed solution and numerical (or experimental) results, which is used in the calibration or curve fitting to obtain the required parameters, is usually considered as validation or prediction. This is, however, not true. The validity and predictability of the calibrated model (obtained by calibration or curve filling) should be tested against additional and different numerical (or experimental) results.

Validation and predictability

To test the validity and predictability of the proposed solution, additional numerical simulations were performed by considering more stope geometries and virgin *in-situ* stress states.

Figure 7 shows the variation of the induced tangential stresses, obtained by numerical modelling and predicted by the proposed semi-empirical solution, at the roof centre and at mid-height of the walls, for an isotropic natural *in-situ* stress state of 30 MPa (compression) and stopes having wall inclination angles β = 90°, 75°, 60°, and 45° and *H/W* ratio varying from 0.1 to 10. It is seen that the agreement between these two different approaches is excellent.

Figure 8 presents another validation and test of predictability of the proposed semi-empirical solution using additional numerical simulations conducted with anisotropic *in-situ* stresses

as the stope wall inclination angle β varies from 90° to 45°. Once again, good agreement is obtained between the numerical and theoretical results for the case of σ_v = 25 MPa (compression), σ_h = 40 MPa (compression), H/W = 0.85 (Figure 8a), σ_v = 25 MPa, σ_h = 40 MPa, H/W = 2.5 (Figure 8b), σ_v = 10 MPa, σ_h = 60 MPa, H/W = 0.85 (Figure 8c), σ_v = 10 MPa, σ_h = 60 MPa, H/W = 2.5 (Figure 8d), σ_v = 25 MPa, σ_h = 40 MPa, H/W = 5 (Figure 8e), and σ_v = 30 MPa, σ_h = 60 MPa, H/W = 5 (Figure 8f).

The proposed solution can thus be considered as validated. It can then be used to calculate the stresses and the stress factor A for the case of typical mine stopes with any inclination angle and height to width ratio under any *in-situ* stress state.

Sample application

In the following, a sample calculation is presented to further illustrate the application of the proposed solution (Equations [5] to [10]).

It is planned to mine out a 6 m (W) wide ore vein inclined at 67° (β), with a 30 m (H) high stope located 500 m below the ground surface. The vertical *in-situ* stress can be estimated based on the overburden depth, while the horizontal *in-situ* stress is 1.67 times the vertical *in-situ* stress. These parameters give the following *in-situ* stress state and stope geometry:

σ_v = 500 m × 0.027 MN/m^3 = 13.5 MPa, $\sigma_h = 1.67\sigma_v$ = 22.5 MPa, β = 67°, H/W = 30 m/6 m = 5.

Applying Equations [7] to [10] leads to:

$$f_1\left(\frac{H}{W}, sin\beta\right) = -1.34 \times 5^{1.01} + (-0.92sin^2 67° + 1.74sin67° + 0.52) \times 5 + 4.02sin^2 67° - 6.32sin67° + 1.52 = -0.9894$$

$$f_2\left(\frac{H}{W}, sin\beta\right) = -8.9 \times 5^{1.016} + (1.17sin^2 67° - 1.9sin67° + 10.28) \times 5 - 4.09sin^2 67° + 6.43sin67° - 1.47 = 2.9345$$

$$g_1\left(\frac{H}{W}, sin\beta\right) = (4.64sin67° - 2.9) \times 5^{(-3.46sin^2 67° + 6.83sin67° - 3.7)} = 0.7873$$

$$g_2\left(\frac{H}{W}, sin\beta\right) = (0.051sin^2 67° - 0.094sin67° + 0.042) \times 5^2 - (0.41sin^2 67° - 0.89sin67° + 0.44) \times 5 - 3.47sin67° + 2.49 = -0.5778$$

By applying Equations [5] and [6], the principal stresses induced on the roof and wall of the stope can be obtained as follows:

σ_{roof} = 13.5 MPa × (–0.9894) + 22.5 MPa × 2.9345 = 52.7 MPa

σ_{wall} = 13.5 MPa × 0.7873 + 22.5 MPa × (–0.5778) = –2.4 MPa

Discussion

Numerical modelling requires the availability of pertinent software and hardware and qualified modellers who know how to correctly conduct numerical modelling. Currently, the availability of computation resources in terms of hardware and software is no longer an issue, and numerical modelling has become a common practice for various research and design projects. However, knowing how to use a numerical code is often considered equivalent of knowing how to correctly perform numerical modelling. This can partly explain the crisis of confidence in numerical modelling and why many modellers do not believe in even their own numerical results. In fact, knowing how to use a numerical code is totally different from knowing how to conduct numerical modelling. The former needs only short training (a couple of hours) while the latter requires much more advanced training and rich experience in order to obtain stable and reliable numerical outcomes (Chapuis *et al.*, 2001; Barbour and Krahn 2004; Cheng, Lansivaara, and Wei, 2007; Diederichs *et al.*, 2007; Krahn 2007; Chapuis, 2012a, 2012b; Duncan 2013).

This work is partly motivated by a perception that the Mathews-Potvin method was considered useless for stope analysis, and that the stability and the maximum dimensions of the stopes can be directly analysed using numerical models, instead of determining the stress factor A and applying the Mathews-Potvin method. It should be recalled that the empirical Mathews-Potvin method was based on many case study observations. The numerical models performed to determine the stress factor A are very simple, considering only an isolated opening around a homogenous, isotropic, and linearly elastic rock. The effectiveness of the method has been proven, especially when it is used as a starting point for the determination of stope dimensions in the preliminary stage of mining projects. When numerical modelling is conducted for stope stability analysis, the models are usually much more complex in terms of stope geometry, mining sequence, and material parameters. Calibrations using field data/observations can be necessary to find the required (but unknown) parameters. In the preliminary stage of a mining project, little field data and information are available to allow the construction and calibration of such sophisticated numerical models.

All of these considerations indicate that the Mathews-Potvin method is very useful at the beginning of a mining project, where it can provide a quick and preliminary estimation of the dimensions of stopes. The necessity for more sophisticated numerical modelling at the advanced stage of a mining project does not invalidate the Mathews-Potvin method. Rather, the Mathews-Potvin method can be more appealing if theoretical or graphical solutions are available for estimating the induced stresses around inclined mine stopes. To this end, a semi-empirical solution has been proposed in which curve-fitting techniques are applied against numerical modelling and the principle of superposition of linearly elasticity theory. The results show that the proposed semi-empirical solution can be used to evaluate the induced principal stresses at the roof centre and mid-height of the wall around typical mine stopes. However, one should keep in mind that the numerical models presented in this study contain several assumptions.

First, a limitation of the numerical models is associated with the 2D plane strain conditions. The numerical results and the proposed semi-empirical solution are valid only when the stope is very long in one horizontal direction. In an actual mine, this is not always the case. Graphical solutions have been presented by Mawdesley, Treman, and Whiten (2001) and Vallejos, Delonca, and Perex (2017) for 3D vertical stopes. Further work is necessary to consider three-dimensional inclined stopes.

The assumption of a linearly elastic rock mass can be held true at relatively shallow depths. At greater depths (deep mines), the behaviour of rocks and rock masses may change to a nonlinear and non-elastic behaviour. Consequently, the validity of the empirical relationships proposed here may be limited to a certain depth. Additional studies could be conducted to formulate similar empirical relationships in nonlinear rock masses.

Another limitation of the proposed semi-empirical relationships is related to the stope geometry. The stopes considered here have a parallel hangingwall and footwall as well as parallel roof and floor. In practice, stopes with nonparallel walls are commonly encountered. More work is needed to propose solutions for estimating the stresses around stopes with nonparallel walls.

In this study, the vertical and horizontal *in-situ* stresses were considered to be two principal stresses, implicitly assuming that the out-plane *in-situ* stress is another principal stress. In practice, the vertical *in-situ* stress and the two horizontal *in-situ* stresses could form three normal stresses. Further work is thus necessary to develop a more general solution.

Finally, it is very important to point out that the stress factor A defined in the Mathews-Potvin method corresponds to the maximum induced principal stresses on the exposed faces. However, as shown in Figures 4 and 5, the maximum compressive stresses are close to the four corners rather than at the roof centre. We believe that an accurate estimation of the maximum principal compressive stress at stope corners is difficult and unnecessary due to stress concentration – therefore the critical locations in terms of compression should be at the centre, not the stope corners. For tension, as Figure 5b shows, the largest tensile stresses are located near (but somehow distant from) the stope corners, which correspond to the critical locations (rather than the roof or wall centre). In this study, the maximum tensile stress is not considered as its location varies when the stope geometry or natural *in-situ* stresses change. This renders the formulation very difficult. More work is needed on this aspect. Nonetheless, given the empirical nature of the Mathews-Potvin method and the still limited considerations of the tensile stresses in applying the method, the proposed solutions can provide useful estimation of stresses for application of the Mathews-Potvin method.

Conclusions

The well-known Mathews-Potvin method is an important design tool for mining engineers. However, the application of this method requires the determination of the induced stresses (and stress factor A) around inclined mine stopes using numerical modelling, as few graphical or theoretical solutions are available for such purposes. To overcome this limitation, a semi-empirical solution has been proposed to estimate the induced principal stresses at the roof centre and mid-height of the walls around mine stopes, by applying the superposition principle of linearly elasticity theory and curve-fitting techniques to numerical results. The validity and the predictive capability of the proposed solution have been verified by additional numerical simulations. The proposed semi-empirical solution can thus be used to evaluate the induced tangential stresses at the roof centre and mid-height of the walls around mine stopes with any inclination angles, height to width ratios, and *in-situ* stress states, as long as the values of H/W are in the range from 0.1 to 10 and β in the range from 45° to 90°. With these empirical expressions, the stress factor A, a key parameter used in the Mathews-Potvin method, can be determined without conducting numerical modelling.

Acknowledgments

The authors acknowledge the financial support from the Natural Sciences and Engineering Research Council of Canada (NSERC 402318), Fonds de recherche du Québec - Nature et Technologies (FRQNT 2015-MI-191676), Mitacs Elevate Postdoctoral Fellowship (IT08484), and the partners of the Research Institute on Mines and Environment (RIME UQAT-Polytechnique; http://rime-irme.ca/).

References

Barbour, S.L. and Krahn, J. 2004. Numerical modelling – Prediction or process. *Geotechnical News*, vol. 22, no. 4. pp. 44–52.

Barton, N., Lien, R., and Lunde, J. 1974. Engineering classification of rock masses for the design of tunnel support. *Rock Mechanics*, vol. 6, no. 4. pp. 189–236.

Bewick, R. and Kaiser, P.K. 2009. Numerical assessment of factor B in Mathews' method for open stope design. *Proceedings of the 3rd Canada-US Rock Mechanics Symposium*, May 2009, Toronto, Canada. Diederichs, M. and Grasselli, G. (eds). pp. 89–90.

Brady, B.H. and Brown, E.T. 2013. Rock Mechanics for Underground Mining. Springer Science and Business Media, Berlin.

Brinkgreve, R.B.J. and Vermeer, P.A. 1999. Plaxis Finite Element Code for Soil and Rock Analysis. Plaxis BV, Delft, The Netherlands.

Capes, G.W. 2009. Open stope hangingwall design based on general and detailed data collection in unfavourable hangingwall conditions. PhD thesis, University of Saskatchewan, Canada.

Chapuis, R.P. 2012a. Influence of element size in numerical studies of seepage: small-scale details. *Geotechnical News*, vol. 30, no. 1. pp. 32–35.

Chapuis, R.P. 2012b. Influence of element size in numerical studies of seepage: unsaturated zones, steady-state. *Geotechnical News*, vol. 30, no. 3. pp. 27–30.

Chapuis, R.P., Chenaf, D., Bussière, B., Aubertin, M., and Crespo, R. 2001. A user's approach to assess numerical codes for saturated and unsaturated seepage conditions. *Canadian Geotechnical Journal*, vol. 38, no. 5. pp. 1113–1126.

Cheng, Y.M., Lansivaara, T., and Wei, W.B. 2007. Two-dimensional slope stability analysis by limit equilibrium and strength reduction methods. *Computers and Geotechnics*, vol. 34, no. 3. pp. 137–150.

Clark, L.M. AND Pakalnis, R.C. 1997. An empirical design approach for estimating unplanned dilution from open stope hangingwalls and footwalls. *Proceedings of the 99th Annual General Meeting*. Canadian Institute of Mining, Metallurgy and Petroleum, Vancouver, Canada.

Diederichs, M.S. and Kaiser, P.K. 1999. Tensile strength and abutment relaxation as failure control mechanisms in underground excavations. *International Journal of Rock Mechanics and Mining Sciences*, vol. 36, no. 1, pp. 69–96.

Diederichs, M.S., Kaiser, P.K., and Eberhardt, E. 2004. Damage initiation and propagation in hard rock during tunnelling and the influence of near-face stress rotation. *International Journal of Rock Mechanics and Mining Sciences*, vol. 41, no. 5. pp. 785–812.

Diederichs, M.S., Lato, M., Hammah, R., and Quinn, P. 2007. Shear strength reduction SSR approach for slope stability analyses. *Proceedings of the 1st Canada–US Rock Mechanics Symposium*, Vancouver, Canada. Eberhardt, E., Stead D., and Morrison T. (eds).Taylor & Francis, London. pp. 319–327.

Duncan, J.M. 2013. Slope stability then and now. *Proceedings of Geo-Congress 2013*, San Diego, California, 3-7 March 2013 Vol. 3. Stability and Performance of Slopes and Embankments., Geo-Institute of ASCE, Reston, VA. pp. 2184–2203.

Exadaktylos, G.E. and Stavropoulou, M.C. 2002. A closed-form elastic solution for stresses and displacements around tunnels. *International Journal of Rock Mechanics and Mining Sciences*, vol. 39, no. 7. pp. 905–916.

Gerçek, H. 1997. An elastic solution for stresses around tunnels with conventional shapes. *International Journal of Rock Mechanics and Mining Sciences*, vol. 34, no. 3–4. pp. 96–e1.

Germain, P, and Hadjigeorgiou, J. 1998. Influence of stope geometry on mining performance. *Proceedings of the CIM AGM*, Montreal, Canada. [CD-ROM]

Hadjigeorgiou, J., Leclair, J., and Potvin, Y. 1995. An update of the stability graph method for open stope design. *Proceedings of the CIM Rock Mechanics and Strata Control Session*, Halifax, Nova Scotia, Canada. Canadian Institute of Mining, Metallurgy, and Petroleum, Montreal. pp. 14–18.

Hiramatsu, Y. 1962. Stress around a shaft or level excavated in ground with a three-dimensional stress state. *Memoirs of the Faculty of Engineering*, Kyoto University, vol. 24, no. 1.

Hiramatsu, Y. and Oka, Y. 1968. Determination of the stress in rock unaffected by boreholes or drifts, from measured strains or deformations. *International Journal of Rock Mechanics and Mining Sciences and Geomechanics Abstracts*, vol. 5, no. 4. pp. 337–353.

Hoek, E., and Brown, E.T. 1980. Underground Excavations in Rock. Institution of Mining and Metallurgy, London.

Hutchinson, D.J. and Diederichs, M.S. 1996. Cablebolting in Underground Mines. BiTech Publishers, Richmond, BC.

Kaiser, P.K., Falmagne, V., Suorineni, F.T., Diederichs, M.S., and Tannant, D.D. 1997. Incorporation of rock mass relaxation and degradation into empirical stope design. *Proceedings of the 99th CIM Annual General Meeting*, Vancouver, Canada, vol. 15. Canadian Intsitute of Mining, Metallurgy, and Petrolerum, Montreal.

Kirsch, C. 1898. Die theorie der elastizitat und die bedurfnisse der festigkeitslehre. *Zeitschrift des Vereines Deutscher Ingenieure*, vol. 42. pp. 797–807.

Krahn, J. 2007, May. Limit equilibrium, strength summation and strength reduction methods for assessing slope stability. *Proceedings of Rock Mechanics: Meeting Society's Challenges and Demands*, Eberhardt, E., Stead D., and Morrison T. (eds). Taylor & Francis, London pp. 311–318.

Li, L. 1997. Étude expérimentale du comportement hydromécanique d'une fracture. PhD thesis, Université Paris 7, France.

Li, L. and Ouellet, S. 2009. Analyse préliminaire pour le dimensionnement des travaux souterrains. *Projet Bracemac-McLeod*, Report submitted to Xstrata Zinc.

Logie, C.V. and van Tonder, C.P.G. 1967. Stress distribution and potential fracture zone around rectangular, elliptical and circular opening in biaxial stress fields. *Report MEG* 575, Rock Mechanics Division, National Mechanical Engineering Research Institute, CSIR, Pretoria.

Madenova, Y and Suorineni, F.T. 2020. On the question of original versus modified stability graph factors – A critical evaluation. *Mining Technology*, vol. 129, no. 1. pp. 40–52.

Mathews, K.E., Hoek, E., Wyllie, D.C., and Stewart, S. 1981. Prediction of stable excavation spans for mining at depths below 1000 m in hard rock. *CANMET DSS* Serial No: 0sQ80-00081. Ottawa.

Mawdesley, C., Trueman, R., and Whiten, W.J. 2001. Extending the Mathews stability graph for open–stope design. *Mining Technology*, vol. 110, no. 1. pp. 27–39.

Milne, D., Pakalnis, R.C., and Felderer, M. 1996. Surface geometry assessment for open stope design. *Rock Mechanics: Proceedings of the 2nd North American Rock Mechanics Symposium*, Montreal, Quebec 19-21 June 1996. Vol. 1. American Rocck Mechanics Association, Alexandria, VA. pp. 315–322.

Nickson, S.D. 1992. Cable support guidelines for underground hard rock mine operations. PhD thesis, University of British Columbia, Canada.

Pagé, P. 2018. Évaluation numérique de la stabilité des chantiers: Contraintes élastiques autour des chantiers et résistance nécessaire des semelles en remblai cimenté. MS thesis, École Polytechnique Montréal, Canada

Papaioanou, A. and Suorineni, F.T. 2016. Development of a generalised dilution-based stability graph for open stope design. *Mining Technology*, vol. 125, no. 2. pp. 121–128.

Potvin, Y. 1988. Empirical open stope design in Canada. PhD thesis, University of British Columbia, Canada.

Potvin, Y., Hudyma, M., and Miller, H.D.S. 1989. Design guidelines for open stope support. CIM Bulletin, vol. 82, no. 926. pp. 53–62.

Potvin, Y., and Milne, D. 1992. Empirical cable bolt support design. *Rock Support in Mining and Underground Construction: Proceedings of the International Symposium on Rock Support*. Balkema, Rotterdam. pp. 269–275.

Scoble, M.J., and Moss, A. 1994. Dilution in underground bulk mining: implications for production management. *Geological Society, Special Publications*, London, vol. 79, no. 1. pp. 95–108.

Stewart, S.B.V. and Forsyth, W.W. 1995. The Mathew's method for open stope design. *CIM Bulletin*, vol. 88, no. 992. pp. 45–53.

Stewart, P.C. and Trueman, R. 2001. The extended Mathews stability graph: Quantifying case history requirements and site-specific effects. *Proceedings of the International Symposium on Mining Techniques*, Val d-Or, Quebec, Canada. Canadian Institute of Mining, Metallurgy, and Petroleum, Montreal. pp. 84–92.

Sunwoo, C., Jung, Y.B., and Karanam, U.R. 2006. Stability assessment in wide underground mine openings by Mathews' stability graph method. *Tunnelling and Underground Space Technology*, vol. 21, no. 3. pp. 246.

Suorineni, F.T. 1998. Effects of faults and stress on open stope design. PhD thesis, University of Waterloo, Canada.

Suorineni, F.T. 2010. The stability graph after three decades in use: experiences and the way forward. *International Journal of Mining, Reclamation and Environment*, vol. 24, no. 4. pp. 307–339.

Suorineni, F.T. 2012. A critical review of the stability graph method for open stope design. *MassMin 2012: Proceedings of the 6th International Conference & Exhibition on Mass Mining*, Sudbury, Ontario, 10-14 June 2012. Canadian Institute of Mining, Metallurgy, and Petrolerum, Montreal. pp. 10–14.

Suorineni, F.T., Tannant, D.D., and Kaiser, P.K. 1999a. Determination of fault-related sloughage in open stopes. *International Journal of Rock Mechanics and Mining Sciences*, vol. 36, no. 7. pp. 891–906.

Suorineni, F.T., Tannant, D.D., and Kaiser, P.K. 1999b. Fault factor for the stability graph method of open-stope design. *Transactions of the Institution of Mining and Metallurgy Section A: Mining Industry*, vol. 108. pp. A92–A104.

Suorineni, F.T., Henning, J.G., and Kaiser, P.K. 2001a. Narrow-vein mining experiences at Ashanti: case study. *Proceedings of the International Symposium on Mining techniques of Narrow-vein Deposits*, Val-dOr, QC, Canada. pp. 57–62. Canadian Institute of Mining, Metallurgy, and Petroleum, Montreal.

Suorineni, F.T., Tannant, D.D., and Kaiser, P.K. 2001b. Likelihood statistic for interpretation of the stability graph for open stope design. *International Journal of Rock Mechanics and Mining Sciences*, vol. 38, no. 5. pp. 735–744.

Suorineni, F.T., Tannant, D.D., Kaiser, P.K., and Dusseault, M.B. 2001. Incorporation of a fault factor into the stability graph method: Kidd mine case studies. *Mineral Resources Engineering*, vol. 10, no. 1. pp. 3–37.

Trueman, R., Mikula, P., Mawdesley, C., and Harries, N. 2000. Experience in Australia with the application of the Mathews' method for open stope design. *CIM Bulletin*, vol. 93, no. 1036. pp. 162–167.

Trueman, R. and Mawdesley, C. 2003. Predicting cave initiation and propagation. *CIM Bulletin*, vol. 96, no. 1071. pp. 54–59.

Vallejos, J.A., Delonca, A., and Perez, E. 2017. Three-dimensional effect of stresses in open stope mine design. *International Journal of Mining, Reclamation and Environment*, vol. 32, no. 5. pp. 355–374.

Wang, J. 2004. Influence of stress, undercutting, blasting and time on open stope stability and dilution. PhD thesis, University of Saskatchewan, Canada.

Zhang, Y., Hughes, R., and Mitri, H.S. 2011. Modified stability graph method with a new rock stress factor. *Proceedings of the 45th US Rock Mechanics/ Geomechanics Symposium*. San Francisco, California, 26-29 June 2011. American Rock Mechanics Association, Alexandria, VA. ◆

Stemming and best practice in the mining industry: A literature review

T.E. Oates[1] and W. Spiteri[1]

Affiliation:
[1]Mining Engineering Department, University of Pretoria, South Africa.

Correspondence to:
T. Oates

Email:
thomasxxoates@gmail.com
william.spiteri@up.ac.za

Dates:
Received: 21 Apr. 2021
Revised: 24 Jun. 2021
Accepted: 7 Jul. 2021
Published: August 2021

How to cite:
Oates, T.E. and Spiteri, W. 2021 Stemming and best practice in the mining industry: A literature review.
Journal of the Southern African Institute of Mining and Metallurgy, vol. 121, no. 8, pp. 415–426

DOI ID:
http://dx.doi.org/10.17159/2411-9717/1606/2021

ORCID:
T. Oates
https://orcid.org/0000-0001-9037-0627

Synopsis

In 2015, after amendments to the explosives regulations, stemming became a mandatory activity for all South African mining operations. There are, however, circumstances in which it is thought stemming has an adverse impact on the blasting outcome. Some of these circumstances include blasting in hot holes, in reactive ground, or when blasting a pre-split. In order to determine when stemming is necessary, its role in the control of adverse blasting phenomena and impact on explosive performance were reviewed. Stemming was found to play a significant role in the fragmentation process and burden movement. Additionally, stemming significantly influences the control of flyrock, air-blast, and toxic fume generation. The review of the literature indicates some motivation for not using stemming for pre-split, trim, hot hole, and reactive ground blasting, provided the benefits associated with not stemming the holes outweigh the risks of stemming them. Best practice for stemming from the literature indicates a stemming length of 0.7 × burden is best for larger hole diameters, and 20 to 30 × Ø for smaller hole diameters. Crushed aggregate appears to be the most effective stemming material. The South African explosives regulations pertaining to stemming were found to be consistent with those of Australia and the USA.

Keywords
stemming, explosive performance, pre-split, hot hole, reactive ground.

Introduction

The practice surrounding the use of stemming has in recent years become topical and, in some cases, a controversial subject. Generally, legislation and regulations pertaining to the use of stemming are vague. Literature on stemming and best practices for stemming is also difficult to find. This leaves explosive engineers and blasters on mines divided on what stemming material is best and what quantities of material to use. Additionally, some question the need to use stemming entirely. Particularly for underground mining operations, the use of stemming poses logistical and production challenges. Zhang *et al.* (2020) state 'Unfortunately, up till now stemming has not been widely used in underground blasts, such as production blasts in underground mining, blasts in tunnelling and drifting, and blasts in other types of underground space construction using explosives'. They attribute this to the lack of quantitative studies demonstrating the necessity and importance of stemming in rock fragmentation.

In 2006 the South African regulations' only requirement for stemming was that underground coal mines use clay, sand, or non-flammable material to stem holes. However, the 2015 amendments essentially required all shot-holes on any surface or underground mine to be stemmed and tamped. Furthermore, the regulations gave guidelines as to the length of stemming required, as well as some forethought regarding the material that should be used. In 2018, more detail was added to the requirements for stemming. The length requirements were replaced by a risk assessment that needs to be conducted with the stemming supplier, explosive supplier, and the competent person conducting the blasting. The risk assessment also needs to include various considerations stipulated in Section 4.14(2) of the GG41904, a Government Gazetted amendment to Chapter 4 of the Mine Health and Safety Act in 2018. Additionally, the stemming material now must comply with the SANS120:2009 code as stipulated in 4.14(3) of the GG41904. The South African regulations stipulate that the purpose of stemming is to reduce the hazards associated with unconfined explosives, blowouts, flyrock, and harmful gases escaping the shot-hole.

While the requirement to stem holes is apparent to the government, some blasters still question the need to stem blast-holes (Zhang, *et al.*, 2020). This is further complicated by the fact that the use of stemming when performing pre-split blasting or blasting in hot holes is believed to have adverse safety impacts. In the case of pre-split blasting, it is believed that stemming the shot-holes will result in overbreak into the final pit walls, potentially affecting highwall stability. When blasting in hot holes or reactive ground it is believed that stemming may promote the premature detonation of the explosive due to heating under confined conditions. In both these situations, failure to use stemming constitutes a contravention of the explosive regulations, which stipulate that all shot-holes be stemmed. Mines are therefore required to apply for exemption from the Inspector of Mines to enable them to omit stemming under these circumstances. However, very little scientific literature in the public domain exists to substantiate an exemption.

This study aimed at investigating the necessity of stemming through a literature review on the effect of stemming on explosive performance, blast safety, and the use of stemming in pre-split, trim, hot holes, and reactive ground.

The study also reviewed best practice for the selection of stemming length and type. A comparison of international explosive regulations pertaining to stemming in comparable countries was done to determine international regulatory practice relating to stemming.

Literature review

Effect of stemming on explosive performance

Stemming has a significant effect on explosive performance. Stemming retains useful explosive gas energy that is wasted in the case of unstemmed holes. This affects the explosive utilization and fragmentation results. An improvement in explosive energy utilization would enable the use of smaller quantities of explosives to achieve the same blasting results. Improvements in fragmentation will result in lower downstream handling costs. While these improvements do not directly indicate the need for stemming, they do reduce costs and improve the productivity and profitability of a mining operation.

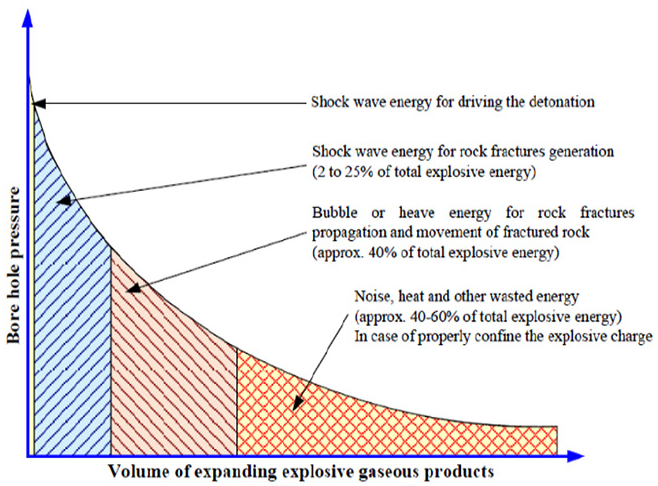

Figure 1—Partition of explosive energy during rock blasting (Sazid, Saharan, and Singh, 2016)

Effect on explosive energy distribution

When explosives detonate in a shot-hole both shock and gas energy are generated (Tobin, 2013). Generally, the contribution of each of these energies to useful work is as shown in Figure 1. The shock energy is the lesser of the two energies and it drives the detonation process forward in the explosive column as well as generating cracks the surrounding rock mass. The total shock energy component accounts for approximately 2–25% of the total explosive energy. The useful gas energy accounts for 40% of the total explosive energy in the case of an adequately confined hole. The gas energy extends the cracks made in the rock mass by the shock energy and heaves the material. The remaining 40–60% of the total explosive energy manifests as waste energy. (Saharan, Saharan, and Singh, 2016). Dhekne (2015) states that 'the waste energy appears in the form of seismic energy, noise, heat and light'.

The contributions of shock and gas energy differ based on the hardness of the rock. As shown in Figure 2, the gas energy plays a more significant role in soft rock. This is particularly true for lower-order detonations. When a higher-order detonation occurs in hard rock the contributions of shock and gas energy to fracturing the rock are more evenly distributed.

The significance of gas energy in the fragmentation process was highlighted by Mchugh (1981) in a series of tests conducted on lined and unlined explosive charges in a plexiglass cylinder. It was concluded that the gas energy increases the length of the cracks generated by the shock energy by a factor of five to ten. Similarly, Dally *et al.* (1975) found that 'containing the charge produced cracks which were larger by a factor of seven than those produced with the vented charge'. Sharama and Rai (2015) state that 'the blasthole pressure plays over 80% of role in fragmenting the rock mass'. Armstrong (1994) states that 'approximately 80 percent of the explosive energy is manifested as gas energy to perform the final fragmentation and movement of the burden material'. This process is driven by the gas energy penetrating fractures generated by the shock energy and lengthening them (McHugh, 1983). Zang (2016) found that stemming seems to affect the size and duration of the dilational wave that fractures the rock mass. Zhang (2016) performed two experiments, one with a vented charge (no stemming) and another with a contained charge (with stemming). It was found that the P-wave leading the compression pulse was 20% longer and the tailing tension pulse was 50% higher for the stemmed charge. Additionally, the duration of the tailing pulse was increased by 30%. Zhang (2016) also found that stemming improved the maximum crack radius at crack arrest by a factor of five in comparison to an unstemmed charge. It is thought that each millisecond of increased retention time will increase the work done on the rock mass and reduce waste energy (Eloranta, 1994).

Considering the significance of the gas energy's contribution to successful rock breaking, it is logical to confine this energy in the shot-hole. However, there is a belief, recorded as early as 1912 among miners, that higher velocity of detonation (VOD) explosives do not require stemming as it is thought that the shock energy will break the ground, rather than the gas energy (Snelling and Hall, 1912; Saffy, 1961). This is held to be particularly true by underground miners (Zhang, 2016). However, the literature indicates that explosives with a higher VOD exhibit the greatest improvement in efficiency with the addition of stemming material (Snelling and Hall, 1912).

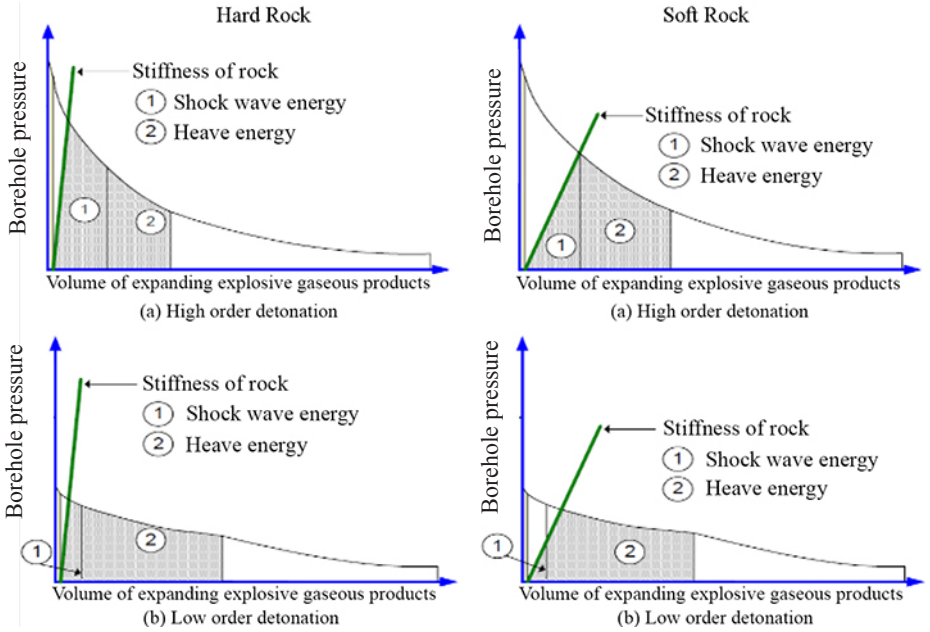

Figure 2—Schematic energy utilization (Sazid, 2014) after (Brinkmann, 1990; Lownds and Du Plessis 1983)

Explosives with a higher VOD generate significantly greater borehole pressures and, in the absence of stemming, the reaction gases would be rapidly ejected (Pearton, 2014). Snelling and Hall (1912) confirmed this in a series of Trauzl lead-block tests, and found that even a small quantity of stemming significantly improved the efficiency of fast-acting explosives.

Brinkman (1994) found that up to 50% of the explosive energy (released in the blast-hole) was carried away by gases venting from the collar when no stemming material was used. Brinkman (1994) further found that the use of a single clay tamping plug reduced the energy vented from the blast-hole to as little as 15% of that of an unconfined hole. Snelling and Hall (1912) found that the use of even the least efficient stemming materials may increase the useful energy of a shot by 60%, and by up to 93% for the most efficient stemming materials. Konya and Konya (2018) state that proper stemming has been shown to improve explosive efficiency by over 41%.

Based on the available literature it is evident that stemming has a significant impact on the utilization of the explosive energy in a shot-hole. Additionally, the literature indicates the importance of gas energy in the fragmentation process. The view that stemming is unnecessary because the shock energy will fragment the rock is not erroneous. However, the use of a small amount of stemming will significantly improve the rock-breaking efficiency of explosives in a shot-hole (Armstrong, 1994).

Effect on fragmentation.

Fragmentation is the fundamental goal of explosive rock-breaking. Good fragmentation results in significant benefits down the value chain, particularly in the loading and hauling operations and the crushing circuit of a mining operation (Phamotse and Nhleko, 2019). The use of chemical energy, in the form of explosives instead of mechanical energy to break the rock is widely accepted as cheaper and more efficient.

Stemming plays a significant role in the fragmentation process, improving the total amount of useful explosive energy as well as the distribution of that energy in the blast-hole. Literature on the impact of stemming on fragmentation deals with two issues – the stemming length and the stemming material. Both factors have a significant impact on downstream processes.

When no stemming is used there is a significant impact on the fragmentation. Armstrong (1994) found that a stemmed hole decreases the K_{50}, the quadratic mesh size that 50% of the material of a certain dimension will pass, by 50% in comparison to an unstemmed hole. Additionally, it was found that the burden velocity increased by 25% for stemmed holes in comparison to unstemmed holes (Armstrong, 1994).

Zhang *et al.* (2020) conducted a series of tests using molecular RDX explosives, an energetic and brisant military high explosive, on granite blocks using various stemming materials. From the study, it was concluded that stemmed blasts yield much better fragmentation than unstemmed holes. Zhang *et al.* (2020) state 'stemmed blasts produce higher mass percentile than unstemmed ones at a given particle size'. They conclude that 'Stemming must be used in all blasts aimed at good rock fragmentation'. Without more quantitative studies to benchmark unstemmed holes against stemmed holes, only the benefits derived from good stemming practices can be used to motivate the necessity of stemming shot-holes.

Effect of stemming length on fragmentation

There is no generic stemming length rule or ratio that offers the optimum fragmentation. There are guidelines for making initial estimates of the blasting parameter, but the best stemming length is found through trial-and-error iterations.

When the stemming length is too short the holes tend to crater, resulting in the premature venting of explosive energy and reduced fragmentation efficiency along the entire shot-hole. When the stemming is too long it leads to improved gas retention and finer fragmentation in the bottom and middle part of the hole. However, the increased length of stemming reduces the energy in the top of the hole, leading to coarser fragmentation on the top layer of the muckpile (Lachamp, Grannas, and Chavez, 2020).

Trivedi, Singh, and Gupta (2015) mention that the stemming to burden ratio becomes more relevant when blasting hard rock

near the collar zone. They also noted that rock with natural fractures in the burden region should be stemmed with longer stemming. Lamchap, Grannas, and Chavez (2020) conducted a series of tests based on this idea at a gold mine in northern Sweden, in which stemming lengths were adjusted based on the fractured rock in the collar region of the drill-hole. Stemming lenghts between 2.5 and 3 m were used, depending on the penetration rate of the drills. Longer stemming was used when the drill logs indicated fractures in the top of the hole. This was done as less energy is required at the top of the hole if the rock is already fractured. Shorter stemming was used when holes did not show significant fracturing, in order to ensure sufficient energy was available in the collar region to fragment the rock. Lamchap, Grannas, and Chavez (2020) found that varying the stemming lengths resulted in fewer stemming blowouts and smaller horizontal movement, which is desirable when trying to limit dilution. A reduction in stemming blowouts is significant as it is associated with reduced flyrock, improved dilution control, and better fragmentation.

Effect of stemming material on fragmentation

Whereas the literature on the effect of stemming length on fragmentation is somewhat limited, that on the effect of stemming contrivances and different stemming materials is well documented. The length of stemming that is required is somewhat dependent on the type of material used. The more efficient a stemming material at containing explosive energy, the shorter the stemming length required. Konya and Konya (2018) state 'the use of a proper stemming material can reduce the total amount of stemming needed by over 40%'. A reduction in stemming length while maintaining the same confining effect allows additional explosives to be used in the hole and significantly improves the fragmentation in the collar (Konya and Konya, 2028). Three types of stemming material are mentioned consistently in stemming literature dealing with fragmentation, namely drill chippings, crushed aggregate, and stemming contrivances. Drill chippings are often the benchmark material as they are widely used due to their availability during the charging operation.

Significant improvements in fragmentation have been observed when crushed aggregate is used to replace drill chippings. Authors generally agree that the use of crushed aggregate in the place of drill chippings results in improved fragmentation (Armstrong, 1994; Kojovic, 2005; Richards, 2013;, Sharma and Rai, 2015; Konya and Konya, 2018). Sharma and Rai (2015) found that holes stemmed with drill chippings had K_{50} values higher than those stemmed with crushed aggregate. Where crushed aggregate was used in the place of drill chippings a reduction in the size distribution from 0.58–0.77 m to 0.45–0.59 m was achieved. Additionally, the holes stemmed with crushed aggregate had a 21.2% better muckpile throw, and the productivity of loading and hauling improved by 18%. Kojovic (2005) measured the impact of changing from drill chippings to crushed aggregate stemming at Red Dog mine in Alaska. The blasts stemmed with crushed aggregate significantly improved the uniformity of the ROM (run of mine), with a 36% reduction in semi-autogenous grinding (SAG) mill feed variability. When the ROM feed to the crushers is more uniform the settings on the crushers can be adjusted to reduce the energy required. With a 3% increase in <25 mm material and 3% decrease in the F_{80} size, a 5% reduction in the power input for the mill was recorded. Additionally, the improved fragmentation as a result of the use of crushed aggregate reduced the wear on the crusher, resulting in a 20% longer period between crusher relines (Kojovic, 2005).

Investgations in which stemming contrivances have been used also indicate a strong relationship between the stemming material and the resulting fragmentation. The use of stemming contrivances tends to improve the blast fragmentation (Karakus *et al.*, 2003; Correa and Navarrete, 2004; Tobin, 2013; Sazid, 2014; Konya and Konya, 2018). A comprehensive review of commercially available stemming contrivances is beyond the scope of this work and would entail a separate dedicated investigation. Suffice to point out that the devices do, to a lesser or greater extent, improve blasting results. An example of this is the Stemming Plug Augmenting Resistance to Stemming Holes (SPARSH), shown in Figure 3. Sazid (2014) conducted several experiments on four different mines comparing the SPARSH to conventional stemming. The introduction of the SPARSH eliminated the occurrence of boulders at all four mines and reduced the mean fragment size by over 30%. The reduction in boulders was achieved by reducing the length of stemming, as seen in Figure 4. Additionally, a 30% reduction in explosives was achieved while improving the fragmentation. Two of the four mines showed a 50% improvement in loading and hauling times.

Effect of stemming on adverse blasting phenomena

The legislative requirement for stemming is rooted in the control of adverse blasting phenomena, as noted in Section 4.14(1) of GG41904 which stipulates stemming is required 'to reduce the hazards of unconfined explosives, blowouts, flyrocks and harmful explosive gases from escaping the shot hole.' This section of the paper will cover the impact of stemming on the following adverse blasting phenomena:

- Flyrock
- Air-blast
- Blasting fumes
- Ground vibrations.

Effect of stemming on flyrock

Flyrock is an undesirable phenomenon that accounts for approximately 40–60% of opencast blasting accidents (Dhekne, 2015). Flyrock is a result of a mismatch of the explosive energy, confinement, and the geomechanical strength of the rock mass. Flyrock typically originates from the bench top or the vertical highwall face (Bajpayee *et al.*, 2001).

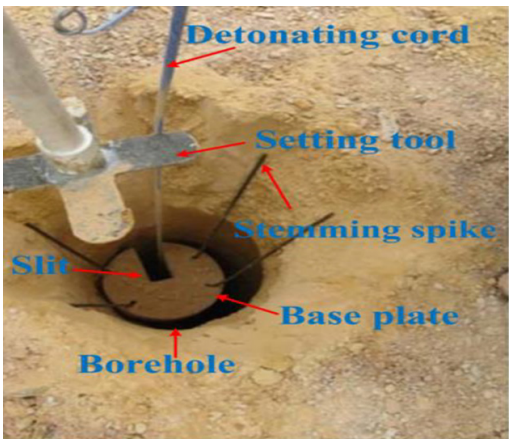

Figure 3—A schematic of a SPARSH (Sazid,2014)

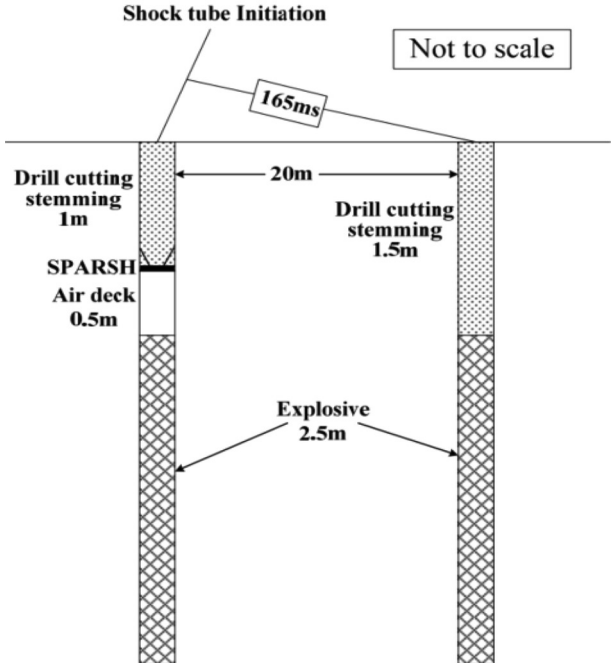

Figure 4—A comparison between the stemming arrangement with SPARSH and conventional stemming (Sazid, 2014)

Flyrock is typically managed by establishment of a blast clearance zone, which is a calculated variable that predicts the maximum travel of flyrock. This clearance zone is calculated using a prediction model such as the Terrock flyrock prediction model.

Flyrock is not well understood. Models are site-specific and non-transferrable (van der Walt and Spiteri, 2020). This is likely why the models at times fail to accurately predict the maximum throw of the flyrock. An event of this nature occurred at a coal mine in Central Queensland where a dwelling 1230 m from the blast was struck by flyrock with a 1000 m exclusion zone being set (Downs, 2012). Although the prediction models do mitigate the risk of injury or damage as a result of flyrock, they do not treat the root cause of the flyrock.

Significance of stemming in the control of flyrock.

While stemming may not be the only factor that contributes to successful flyrock management, it has been identified as a significant control variable. Dhekne (2015) identified stemming material and length as significant influences on the generation of flyrock. Similarly, Ghasemi, Sari, and Ataei (2012) identified stemming, as well as powder factor and burden, as significant control factors of flyrock in an analysis of flyrock prediction models. It can therefore be concluded that stemming (or the lack thereof) plays a causative role in the generation of flyrock (Otuonye, 1981; Armstrong, 1994; Adhikari, 1999; S&T Projects, 2001; Bajpayee, *et al.*, 2002; Radomsky and kecojevic, 2005; US Department of the Interior, n.d.; Australian Explosives Industry and Safety Group, 2007; Armaghani *et al.*, 2015; Trivedi, Singh, and Gupta, 2015; University of Pretoria, 2016; BME, 2018; Konya and Konya, 2018).

Impact of stemming length on flyrock

In a study conducted on flyrock at limestone quarries, Adhikari (1999) found that stemming length was one of the most neglected blast design parameters. Stemming length is a significant variable in many flyrock prediction models. The Scale Depth of Burial (SDOB) flyrock prediction model employs an exponential relationship between the stemming length and the calculated clearance distance (ISEE, 2011). However, no model was encountered that included the type of stemming material in flyrock throw prediction. Adhikari (1999) found that the maximum flyrock distance decreases with an increase in stemming length and does not exceed 100 m when the ratio of stemming length to hole diameter is less than or equal to 20. It was concluded that flyrock at the limestone quarries would be reduced by ensuring a ratio of stemming length to hole diameter greater than, or equal to 20, and using a suitable stemming material such as angular gravel (Adhikari, 1999). In a sensitivity analysis by Trivedi, Singh, and Gupta (2015) on an adaptive neuro-fuzzy inference system (ANFIS), the influence of stemming length on the reduction in flyrock distance was found to be more significant for large hole diameters.

Effect of stemming material on flyrock

There is only limited literature on the influence of the type of stemming material on flyrock. Sharma and Ria (2015) compared the effect of drill chippings to crushed aggregate, and found that flyrock from holes stemmed with crushed aggregate did not leave the bench floor, whereas holes stemmed with drill chippings generated flyrock that reached other benches. The use of stemming plugs in conjunction with stemming materials such as drill chippings is said to reduce stemming ejection, and in turn flyrock (Adhikari, 1999; Karakus *et al.*, 2003; Sazid, 2014).

Effect of stemming on the control of air-blast.

Air-blast is an inevitable outcome of blasting in the surface mining industry and is typically managed by ensuring that air-blast generated is below a threshold limit. The US Office of Surface Mining and Reclamation Enforcement specifies a safe overpressure level of 133 dB for impulse air-blast in a frequency range of at least 2–-200Hz (Singh, Klemenz, and Niemaan-Delius, 2005).

It is well established that stemming is effective at minimizing air-blast in surface blasting activities (Otuonye, 1981; Armstrong, 1994;, Adhikari, 1999; S&T Projects, 2001; Cunningham *et al.*, 2002, Karakus *et al.*, 2003; Rorke, 2011; Richards, 2013; Bansah *et al.*, 2016; BME, 2018; Konya and Konya, 2018; US Department of the Interior, n.d.). A reduction in air-blast increases the total useful work done by the explosion on the fragmentation and movement (Armstrong, 1994).

Effect of unstemmed holes on air-blast

Just (1979) reported that unstemmed holes can produce a maximum air blast of 140 dB, while holes stemmed with crushed rock produced 134 dB. Unfortunately, no details of the blasting parameters could be found (Just, 1979). Konya and Konya (2017) state that 'the community impact of proper stemming design is often seen in a reduction of up to 6 dB of air overpressure', which coincides with the findings of Just (1979). Konya and Konya (2018) similarly mention that air-blast can be reduced by 98% by the use of adequate stemming. The reduction in air-blast derived by the use of adequate stemming, both in quantity and quality, necessitates the use of stemming in surface blasting.

Effect of stemming on blast-induced vibration

Ground vibration is an unwanted blasting phenomenon that

can induce cracking and damage the integrity of structures in the vicinity of the blasting operation (Bansah, *et al.*, 2016). Opinion is divided on the role of stemming in the generation or mitigation of blast-induced ground vibrations. Dhekne (2015) rated stemming length and material as insignificant variables in the reduction of blast-induced ground vibration. Standards Australian (2006) also found stemming quantity and type to be insignificant contributors to ground vibrations. However, some literature indicates a correlation between stemming length and the generation of blast-induced ground vibration. When the stemming is excessive, blast-induced ground vibrations are produced (Sazid, 2014; Konya and Konya, 2018). This is likely the result of the increased SDOB of the explosive charge. Elevli and Arpaz (2010) assessed the relationship of blasting parameters in predictive models and found stemming to account for 13.1% of the estimated peak particle velocity (PPV). This is likely due to the reduction in powder factor due to the addition of stemming material.

No studies could be found in which the blast-induced ground vibrations were compared for stemmed and unstemmed holes. Therefore, based on the available information, only over-stemming holes can be associated with increased blast-induced ground vibrations.

Effect of stemming on the generation of blasting fumes

Blasting operations produce both toxic and nontoxic gases. The toxic gases are predominately oxides of nitrogen (NOx) and carbon monoxide (CO). The quantity of these gases is a function of the following factors (Maniero, Harris, and Rowland, 2007):

- Formulation of the explosives
- Confinement and age of the explosives
- Contamination of the explosive with water or drill cuttings
- Other.

For this study, the focus was on the confinement of the explosive and the role that it plays in the reduction of toxic explosive-related fumes. Surface mines are typically not as concerned with blasting fumes as underground operations as it is believed that the toxic fumes are dispersed into the open air. However, Maniero, Harris, and Rowland (2007) mention that little work has been done to prove that the orange clouds that are seen after a blast do not contain toxic levels of NO_2. Furthermore, they mention that the danger with carbon monoxide is that it remains in the ground after the blast. This occurred in an incident in Kittanning, Pennsylvania, where blast fumes travelled 137 m from a strip coal mine to a home, poisoning a couple and their baby. The fumes migrate through the ground and collect in confined spaces. Toxic fumes are of greater concern in the underground mining environment as all the air at the working faces needs to be cleared with forced ventilation to decontaminate the air to breathable levels.

In order to minimize the quantity of toxic fumes produced, incomplete detonation needs to be prevented through the use of adequate stemming (*Otuonye et al., 1983*; US Department of the Interior, n.d.). Additionally, Maniero, Harris, and Rowland (2007) state that 'stemming plugs can be used at the top and bottom of blastholes to prevent the mixture of the blasting agent with drill cuttings or rocks.' Mixing of drill chippings with the blasting agent results in contamination of the explosive, causing increased toxic fume emmissions, reduced explosive performance, and deviation from the designed density of the explosive.

Use of stemming in relation to specialized blasting techniques

Although the effects of stemming are generally beneficial, there are special conditions where additional confinement of the explosive charge is undesirable. The first of these circumstances is where overbreak control is important in blasting techniques such as pre-splitting. The other is when blasting in reactive ground or in hot holes. The additional confinement of the holes is thought to increase the likelihood of a shot-hole detonating instead of deflagrating.

Use of stemming for pre-split blasting

Tose (2006) states that 'in many circumstances the confined gas energy from explosives can significantly reduce the structural strength of the rock behind and to the sides of the blasted volume'. This is the result of explosive energy creating weaknesses and fractures that reduce the rock mass stability (Tose, 2006). The goal of a pre-split blast is to protect the highwall from explosive-induced fracturing. The addition of stemming improves the rock fracturing action of explosives, thus it would seem intuitive not to stem pre-split blasts. However, firing unstemmed charge-holes is a contravention of the South African explosive regulations. The original legislated requirement for stemming arises from 'to reduce the hazards associated with unconfined explosives, blowouts, fly rocks and harmful explosive gases escaping the shot hole'. All these hazards are still present during a pre-split blast. The decision to stem the holes therefore involves a trade-off between highwall stability and the risks associated with firing unstemmed charges in the case of pre-splits. Alternatively, new methods of firing pre-split blasts are required to mitigate both risks.

Tose (2006) mentions that pre-split holes should be stemmed if blasting unstemmed holes is likely to cause an annoyance to the neighbours. He further states that stemmed pre-split holes will tend to crater and cause some damage in the crest of the new face. Rorke (2011) recommends the use of a stemming plug, approximately 11 hole diameters in length, at the top of a pre-split hole should excessive air-blast be a concern. The Bulk Mining Explosives (BME) blasting guide stipulates that stemming should not be used in pre-split blasting. However, if necessary, stemming with a length of 10 to 12 hole diameters should be used for noise reduction or rock control (BME, 2018). In an optimization study on the effectiveness of pre-split blasting, Dindarloo (2015) found that leaving pre-split holes unstemmed yielded the best results. While most authors caution against the anticipated air-blast, Rorke (2011) mentions that the factors that cause high air-blast levels are the same as those that create dangerous flyrock and excessive dust. It is reasonable to assume that the firing of unstemmed pre-split holes will be accompanied not only by air-blast but also flyrock and dust.

Not all authors agree with leaving pre-splits unstemmed, though. Konya and Walter (1991) state that 'the upper portion of all pre-split holes, from the top of the charge to the hole collar shall be stemmed'. Bender (n.d.) recommends that the tops of pre-split holes be stemmed, but that a plug should be used to prevent stemming material from packing around the explosive. This is to reduce the coupling ratio of the pre-split charge. Konya and Konya (2018) state that 'stemming is also of extreme importance in overbreak control, with proper stemming leading to a 200% increase in the performance of pre-split holes versus unstemmed pre-split holes'. Konya and Konya cite personal

correspondence with Matthews (1978) as the source regarding the 200% increase in performance; however, the methods used to obtain this data could not be verified, nor the definition of performance concerning pre-split blasting clarified.

Based on the available literature, the consensus appears to be that pre-split blasts should be left unstemmed unless air-blast is a concern. However, what is not clear is when air-blast should be a concern. Air-blast accompanied by dust generation and flyrock should not be tolerated. The choice to stem pre-splits will lie in the tolerance for air-blast, flyrock, and dust generation on the mine. The South African Explosive Regulations (2018) stipulate in Section 4.7 that 'the employer at any mine must take reasonable measures to ensure that when blasting takes place, air and ground vibrations, shock waves and fly material are limited to such an extent and at such a distance from any building, public thoroughfare, railway, powerline or any other place where persons congregate to ensure that there is no significant risk to health or safety of persons'.

Therefore, it would be reasonable to assume that should the mine not experience any air-blast, flyrock, shock waves, or ground vibrations that impact the stipulated infrastructure or places of congregation, the pre-splits can be fired without stemming, provided that exemption is granted by the regulatory authority.

Should adverse consequences associated with firing unstemmed charges be an issue, stemming plugs can be used. Konya and Walter (1991) mention that drill chippings are an effective stemming material for pre-splits as the stemming momentarily confines the gases and reduces some of the air-blast. Air decking is a controlled blasting technique that has been successfully used in pre-split blasting. An air space is intentionally left above the explosive charge to allow gases generated during detonation to fill the void instead of being forced into the adjacent rock Mass. Eades and Perry (2019) state that 'it is generally accepted that air decking will produce results that are comparable to, but not quite as good as, pre-splitting', particularly for small borehole diameters. Pre-splits can further be improved by decreasing the coupling ratio between the charge and the borehole. The space between the charge and the borehole constitutes an additional void for the charge to dissipate gas energy into before it can permeate the crack network in the surrounding rock mass Eades and Perry (2019). Additionally, the decoupling of the charge results in less localized crushing in the borehole and ultimately less overbreak (Etchells, Sellers, and Furtney, 2013).

Etchells, Sellers, and Furtney (2013) state that overbreak caused by pre-split blasts can be reduced by selecting the correct spacing, decoupling ratio, and split factor. Should a mine require the use of stemming plugs, the efficiency of these can be maximized by using an air deck as well as small-diameter boreholes with the appropriate spacing and a highly decoupled charge with the correct split factor.

Therefore, it is recommended that stemming should be used during pre-splitting to reduce the adverse effects such as flyrock and air-blast associated with firing unstemmed charge holes, unless the mine can present a good case for exemption, *e.g.* due to the mine's remoteness, where flyrock and air-blast will not influence the areas of concern addressed in the regulations.

Trim blasting

Trim blasting is another specialized blasting technique in which stemming holes is undesirable. As with pre-split blasting, trim blasting is used to control overbreak by pre-fracturing the rock mass. Trim blasting, in contrast to pre-splitting, involves multiple rows of modified blast-holes instead of the single line used when blasting a pre-split. Owing to the similar mechanisms used in pre-split and trim blasting the same conclusions can be made for trim blasting. Stemming should be used unless the mine can motivate the need for exemption.

Use of stemming in hot hole blasting

Another circumstance where stemming holes is undesirable is in hot hole blasting. A hot hole, as defined by the South African explosives regulations, is any hole in a coal mine that after being drilled has an in-hole ambient temperature of 40°C or an increase of 3°C (Department of Mineral Resources, 2018). The use stemming is not desirable on hot holes as confining an explosive that is undergoing heating is more likely to result premature detonation (BHP Billiton, 2008). However, hot holes charged with explosives can detonate with or without stemming. In 2006 a shot-hole detonated prematurely during deep hole blasting of pillars on a mechanized coal mine in India. After 2.5 hours a hole charged with a site-mixed system explosive, a cast booster, and a down-the-hole shock tube detonator detonated without stemming. It was later found that the temperature of the strata within a radius of 20 m from the event was 1010°C (Government of India, 2006). In 2003, BHP Billiton experienced an uncontrolled detonation of a shot-hole in hot ground. The shot-hole was charged with heavy ANFO and primed with a 400 g cast booster and a non-electric detonator used in conjunction with detonating cord. The hole was stemmed with 4 m of drill chippings, and detonated approximately 15 minutes after the hole showed visible signs of heating (BHP Billiton, 2008). These two incidents indicate that detonation can occur with or without stemming.

While it is commonly thought that not stemming hot holes is beneficial, this is not mentioned specifically in the literature. The South African legislation deals with hot holes only briefly. The regulations stipulate that a written procedure is to be prepared and implemented after consultation with the explosive manufacturer. The procedure must include temperature measurement in the hole by the competent person and recording of the hole temperatures before charging up (DMR, 2018). The guidelines do not mention any specific actions that need to be taken when blasting in hot holes. The literature tends to focus on the following actions when dealing with hot holes (Sharma, 2010):

- Minimum explosive sleep times
- Hole temperature monitoring
- Hole loading sequence (on the pattern)
- Delineation of the blast zone
- Selection of the explosives and initiating system
- Minimizing spillage
- Harmful gas exposure
- Training and procedures
- Flushing holes with quenching agents.

Procedures at mines with hot holes generally stipulate that holes should not be stemmed to avoid a pressure build-up in the hole (BHP Billiton, 2008; Vale, 2019). However, Sharma (2010) states that 'it is good practice sufficient non-combustible stemming material such as sand, crushed stone chips or drill cuttings should be available near the collar of

each hole prior to commencing the charging operation, in order to fast accomplishing stemming and charging operation'. No other significant literature could be found in the public domain regarding stemming hot holes. Based on the available information it is difficult to conclude as to the necessity of stemming hot holes.

Stemming is necessary to reduce adverse blasting phenomena such as flyrock, air-blast, and toxic fume generation. However, the addition of stemming material may limit visible signs that a hole is undergoing heating and may increase the likelihood of detonation. Further research is needed to clearly identify the role stemming plays in hot hole blasting. Information in this regard will greatly assist mines in motivating for exemption from Section 14.1 of the GG41904 of 2018. If stemming is necessary when blasting in hot holes due to environmental concerns, it should be done as quickly as possible and be the last activity to occur on the bench before blasting to prevent pressure build-up in the hole.

Use of stemming in reactive ground

Reactive ground is the term applied to a rock type that exothermically reacts with explosives, potentially resulting in premature detonation (Bellairs and Sen, 2004). Reactive ground is not common in South African mines, although there are some mines that blast in these conditions. Reactive ground is another circumstance in which stemming holes is thought to be undesirable. As the exothermic reaction perpetuates in the explosive column the explosives heat up, much like in hot holes. The primary difference being that reactive ground will not show any signs of heating prior to the explosive being charged into the hole.

Slightly more formal literature exists for the management of reactive ground than that for hot holes. Most of the publications tend to deal with specialized explosives that inhibit the reaction between the ammonium nitrate and the sulphides from the rock, such as the work of Djerdjev *et al.* (2018). Reactive ground is particularly dangerous as the explosives heat rapidly in the intermediate stage where an increase of more than 100°C can occur in a few minutes (Botha, 2014). Botha (2014) states that even without the detonator and booster in the hole, the explosives can detonate. However, should the conditions not be ideal the explosives will deflagrate. Botha (2014) mentions the following methods of controlling self-detonation in reactive ground:

- Temperature logging
- Load and shoot
- Specialized stemming material
- Physical separation
- Inhibited explosives
- Integrated risk management.

Only limited information concerning stemming reactive ground was found in the literature, although two recommendations were observed. The first being that should stemming be carried out in reactive ground it should be done with an inert material. A specific concern was raised regarding the use of drill chippings, which may contain sulphides that could react with the explosives (Australian Explosives Industry and Safety Group, 2007; Botha, 2014). The second observation is that stemming in reactive ground should be done as quickly as possible. Botha (2014) found that stemming a 280-hole blast at Goedgevonden mine took 3.2 days, resulting in excessive sleep times for the explosives. As with hot holes, time is of the essence for safe blasting in reactive ground. The longer the explosives remain in contact with reactive ground, the higher the risk of a reaction between the ammonium nitrate and sulphides in the hole. Botha (2014) concluded that 'if the environmental factors allow, confirmed reactive ground blasts should be initiated without stemming the holes to reduce the preparation time'. Rorke (2010) similarly stated, 'whenever the environmental considerations allow an increase in flyrock and air-blast the holes may need to be left unstemmed'. This is because unstemmed holes are less confined and the hole is likely to deflagrate rather than detonate if the temperature exceeds 300°C (Rorke, 2011).

There is limited literature pertaining to the effect stemming has on the confinement of explosives in reactive ground. Based on the available information, the decision whether to stem holes in reactive ground depends on the tolerability of flyrock and air-blast for a given blast. Additionally, should stemming be necessary to limit flyrock and air-blast in a reactive ground blast, an inert material that can be quickly loaded into the holes should be used.

Stemming effectiveness metric

Before the recommendations for stemming lengths and materials can be discussed it is important to note that there is currently no universal metric for evaluating the effectiveness of stemming. Laboratory testing on stemming typically involves the measurement of pressure differences or explosive performance variables. The problem with laboratory testing is that test charge diameters are typically too small and the detonator takes up too much of the charge. Most modern investigations on stemming performance are done through field experiments. High-speed photography and post-blast metrics such as fragmentation are used to evaluate the stemming performance or impact that stemming had on the blast outcomes. Unfortunately, field testing on stemming performance requires an accurate benchmark for comparison. Many studies found in the literature derive relationships on stemming effectiveness from as little as one blast.

Figure 5 shows the metrics used in the literature to evaluate stemming performance. Stemming ejection velocity is commonly used as a metric for stemming effectiveness. However, reduced stemming ejection velocity often goes hand in hand with poor blast performance (Eloranta, 1994). An effective test for stemming should as far as practically possible include elements of both the laboratory and field metrics over a wide data-set in order to accurately measure the effectiveness of a stemming material. Additionally, all other blasting parameters should remain as constant as possible to reduce the influence of external variables on the results.

Stemming material recommendations

The choice of stemming material plays a significant role in the effectiveness of the stemming. The use of appropriate stemming material is said to reduce the required length of stemming by 40% (Konya and Davis, 1978). A reduction in stemming length means that more explosives could be added to the shot-hole if neccessary. Additionally, a shorter stemming length results in better explosive energy distribution in the shot-hole. This will assist with fragmentation, and specifically the fragmentation of the collar region of the shot-hole.

The choice of stemming material will likely be driven by availability and cost. As a result, the use of drill chippings is

common practice, yet it is one of the most inefficient forms of stemming (Konya amd Konya, 2018). The use of drill chippings as stemming material will likely require longer stemming lengths to achieve an adequate level of retention. In order to determine what stemming material is best, recommendations in the literature were compiled in Figure 6. Crushed aggregate of uniform particle size is the most common stemming recommendation. Although only a limited number of studies has been done to validate its effectiveness as a stemming material, it has the most quantitative literature substantiating its use.

No studies could be found where stemming plugs are benchmarked against a crushed aggregate. However, there is sufficient evidence validating the enhancement of nonideal stemming materials such as drill chippings using stemming plugs. (Konya and Konya, 2018).

Stemming length recommendations

There is no optimal length of stemming that provides the ideal blasting outcome. The determination of stemming length is based on a set of rules of thumb that do not constitute a scientific analysis of the estimation (Sazid, 2014). Stemming length recommendations have largely remained the same since the work of Sir John Fox Burgoyne (1895), who recommended that one-third of the blast-hole should be stemmed.

To date, a stemming length estimation of 0.7 × burden is common practice. Konya and Walter (1991) attempted to trace the origin of the empirically obtained 0.7 × burden rule and found it to be a standardized blasting parameter dating back to 1903, when blasting powder was still used. The recommendations for stemming length found in the literature are compiled in Figure 7. It was found that stemming relationships to burden are most effective for larger hole diameters, and stemming lengths based on the hole diameter for smaller hole diameters. For large boreholes, stemming 0.7 × burden is best when an effective stemming material is used, such as crushed aggregate, and 1.0 × burden for stemming material such as drill chippings. For smaller hole diameters a range of 20–30 × Ø is best. In order to determine which end of the range the following variables should be considered (Tobin, 2013):

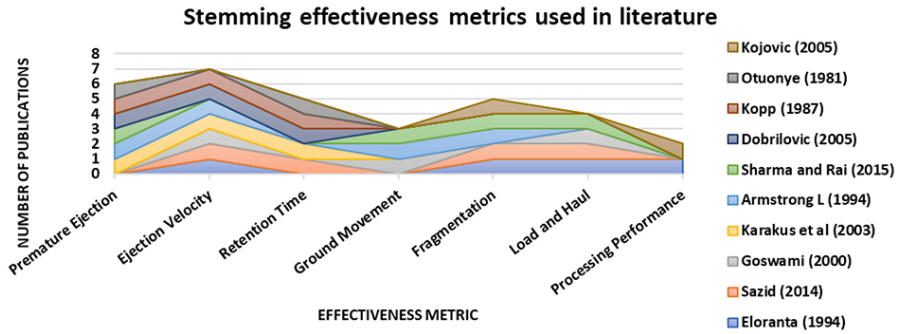

Figure 5—Stemming effectiveness metrics found in the literature

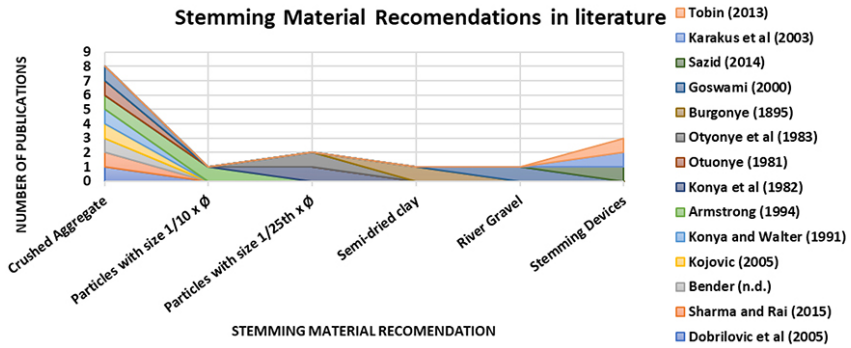

Figure 6—Stemming material recommendations in the literature

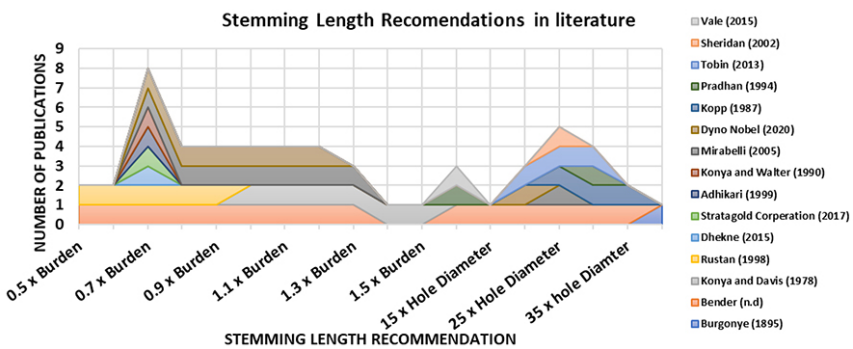

Figure 7—Stemming legnth recommendations in literature

- Rock strength
- Charge energy
- Burden size and strength
- Water in the blast-hole
- Portion of loose material such as drill chippings in the stemming material.

Regulatory requirements for stemming.

The South African regulations pertaining to stemming are among the best that can be found globally. While no specific mention of stemming lengths or materials were found in the Canadian and Indian explosive regulations, the South African, Australian, and American regulations do contain such information. The current South African regulations take a consultative and risk-adjusted approach to the selection of stemming material and quantity. The considerations mentioned in the risk-adjusted approach are salient and comprehensive, making the South African regulations pertaining to stemming a world leader.

Conclusion

This research aimed to determine the necessity of stemming through a literature review. Based on the findings, it is recommended that shot-holes be always stemmed. The control of adverse blasting phenomena such as flyrock, air-blast, and blasting fumes, as well as the significant explosive performance benefits derived from the use of adequate stemming, necessitate its use.

Without an appropriate metric by which to evaluate the effectiveness of stemming it is difficult to determine what quantity and type of stemming material is best. The literature generally recommends the use of a crushed aggregate and a stemming length of 20–30 × Ø for small hole diameters and a length of 0.7 × burden for larger hole diameters.

There are scientific reasons not to stem holes in the case of pre-split, hot hole, and reactive ground blasting. However, there is limited quantitative information in the public domain to substantiate this. Additionally, leaving holes unstemmed results in increased flyrock and air-blast generation, which is undesirable. A risk-adjusted trade-off is therefore required to balance the risks associated with firing unstemmed holes versus stemmed holes in these circumstances.

The South African explosive regulations relating to stemming are world-leading. The risk-adjusted approach is the most flexible regulatory approach found in this study. The correct use of stemming offers significant improvements to blast performance and safety. Stemming should therefore always be used unless the risk of using stemming outweight the benefits.

References

Adhikari, G.R. 1999. Studies on Flyrock at Limestone Quarries. *Rock Mechanics and Rock Engineering*, vol. 32, no. 4. pp. 29–1301.

Armaghani, D.J. *et al.*, 2015. Application of two intelligent systems in predicting environmental impacts of quarry blasting. *Saudi Society for Geosciences*, vol. 8, pp. 9647–9665.

Armstrong, L.W. 1994. *The quality of Stemming in Assessing Blazsting Efficiency*, New South Wales: The University of New South Wales.

Australian Explosives Industry and Safety Group. 2007. *Code of Practice- Elevated Temperature and Reactive Ground,* s.l.: AEISG.

Bajpayee, T.S. *et al.*, 2001. *Fatal accidents due to flyrock and lack of blast area security and working practices in mining*, Pennsylvania: National Institute for Occupational Safety and Health Pittsburgh.

Bajpayee, T.S., Verakis, H.C., and Lobb, T.E. 2002. *An Analysis and Prevention of Flyrock Accidents in Surface Blasting Operations*, s.l.: s.n.

Bansah, K.J., Arko-Gyimah, K., Kansake, B.A, and Dumakor-Dupey, N.K. 2016. Mitigating Blast Vibration Impact. *UMat Biennial International Mining and Mineral Conference*, vol. 4, pp. 30–36.

Bellairs, P. and Sen, G.,2004. *Blasting safely and efficently in reactive ground and efficently in reactive ground and/or hot gorund or in sulphide dust explosion generating rock*, s.l.: Mines Angnic Egal Itee.

Bender, W.L., n.d. Back to Basics - *The fundamentals of blast design*. Golden West, International Society of Explosive Engineers.

BHP Billiton. 2008. *Guidelines to hot drilling and blasting*. [Online] Available at: https://www.slideserve.com/santo/guidelines-to-hot-hole-drilling-and-blasting [Accessed 18 January 2020].

BME. 2018. *Surface mining blasting guide*. 13 ed. s.l.:Omina Group (Pty) Ltd.

Botha, G.L. 2014. *Management of Reactive Ground at the Goedgevonden Opencast Coal Mine in the Witbank Coalfields of South Africa*, Johannesburg: University of Witwatersrand.

Burgonye, S.J.F. 1895. *A Treatise on the Blasting and Quarrying of Stone for Building and Other Purposes: With the Constituents and Analyses of Granite, Slate, Limestone, and Sandstone. To which is Added Some Remarks on the Blowing Up of Bridges*. London: Crosby Lockwood and Son.

Correa, C.E. and Navarrete, M.F. 2004. Assesment of Stemming Plug Plastic Elements to Improve Blasting Gases Confinement in Escondida. *EXPLO*, pp. 95–100.

Cunningham, C.V., Zaniewski, T., and kernahan, N.,2002. Threshold Blasting: The Renaissance of Explosives in narrow reef mining. *The Journal of The South African Institute of Mining and Metallurgy,* pp. 25–31.

Dally, J.W., Fourney, W.L., and Holloway, D.C. 1975. Influence of Containment of the Bore Hole pressures on Explosive Induced Fracture. *International Journal of Rock Mechanics, Mineral Science and Geomechanics*, vol. 12, pp. 5–12.

Department of Mineral Resources. 2018. *Regulations Relating to Explosives - Mine Health and Safety Act, 1996 (Act No 29 of 1996)*, Pretoria: Government Gazette.

Dhekne, P.Y. 2015. Environmental Impacts of Rock Blasting and Their Mitigation. *International Journal of Chemical, Environmental & Biological Sciences*, vol. 3, no. 1. pp. 46–50.

Dindarloo, S. R., Askarnejad, N. A., and Ataei, M. 2015. Design of controlled blasting (pre-splitting) in Golegohar iron ore mine, Iran. *Institute of Materials, Minerals and Mining Science and Technology*, vol. 124, no. 1. pp. 64–68.

Djerdjev, A.M. *et al.*, 2018. The mechanism of spontaneous detonation of ammonium nitrate in reactive grounds. *Journal of Environmental Chemical Engineering*, vol. 6. pp. 281–288.

Dobrilovic, M., Ester, Z., and Jankovic, B. 2005. Measurement in blast hole stem and influence of steming material on blasting quality. *The Mining-Geological-Petroleum Engineering Bullitin*, vol. 17. pp. 47–53.

Downs, G. 2012. *Flyrock damage outside the blast-exclusion zone*. [Online] Available at: https://www.dnrme.qld.gov.au/business/mining/safety-and-health/alerts-and-bulletins/explosives/flyrock-damage-outside-the-blast-exclusion-zone [Accessed 25 October 2020].

Dyno Nobel. 2020. *Explosives Engineers' Guide*. [Online] Available at: https://www.dynonobel.com/apac/~/media/Files/Dyno/ResourceHub/Brochures/APAC/Explosives%20Engineers%20Guide.pdf [Accessed 02 November 2020].

Eades, R.Q. and Perry, K. 2019. Understanding the Connection Between Blasting and Highwall Stability. *International Journal of Mining Science and Technology*, vol. 29. pp. 99–103.

Elevli, B. and Arpaz, E. 2010. Evaluation of Parameters Affected on the Blast Induced Ground Vibration (BIGV) by Using Relatioin Diagram Method. *Acta Montanistica Slovaca*, vol. 4. pp. 261–268.

Eloranta, J. 1994. *Stemming Selection for Large-Diamter Blastholes*, s.l.: Minntac Mine.

Etchells, S. ., Sellers, E.J., and Furtney, J. 2013. Understanding the Blast Damage Mechanisms in Slopes Using Observations and Numerical Modelling, Perth: Australian Centre for Geomechanics.

Ghasemi, E., Sari, M., and Ataei, M., 2012. Development of an emperical model for predicting the effects of controlable blasting parameters on flyrock distance in surface mines. *International Jouranla of Rock Mechanics & Mining Sciences*, vol. 52. pp. 163–170.

Goswami, T. 2000. *Assessment of the Relative Efficiency of Two Stemming Materials*. s.l., s.n., pp. 171–182.

Government of India. 2006. *Notice: Firing of Shots in Fire Areas/ in Vicinity of Hot Strata in Opencast Coal Mine*, s.l.: Ministry of Labour & Employment, Directorate-General of Mines Safety.

ISEE. 2011. *Blasters' Handbook*. 18th ed. Cleavland, Ohio USA 441392295: Initernational Society of Explosives Engineers.

Just, J.D. 1979. Stemming of Blastholes in Mining Excavations. *Australian institute of minerals and metallurgy*, pp. 7–15.

Karakus, D., Onur, A.H., Konak, G., and Kose, H. 2003. A*pplication of Stemming Plugs and A Case Study in A Limestone Quarry*. Turkey, International Mining Congress and Exhibition of Turkey.

Kojovic, T. 2005. Influence of Aggregate Stemming in Blasting on the SAG Mill Performance. *Minerals Engineering*, vol. 18. pp. 1398–1404.

Konya , C.J. and Davis, J. 1978. *The Effects of Stemming Consist on Retention in Blast Holes*. s.l., ISEE, pp. 102-112.

Konya, A. and Konya, C.J. 2017. *Pit & QUarry*. [Online] Available at: https://www.pitandquarry.com/resolving-explosives-inefficiency/[Accessed 03 May 2020].

Konya, C.J. and Konya, A. 2018. Effect of Hole Stemming Practices on Energy Efficiecy of Comminution. In: K. Awuah-Offei, ed. *Energy Efficiency in the Minerals Industry*. Cham: Springer, pp. 31–53.

Konya, C.J. and Walter, E.J. 1991. *Rock Blasting and Overbreak Control*, Virginia: U. S. Depatment of Transportation.

Lachamp, M., Grannas, S., AND Chavez, R. 2020. *Influence of Stemming Length and Initiation Sequence on Rock Movement and Dilution During a Blast*, s.l.: EFEE.

Maniero, R.J., Harris, M.L., and Rowland, J.H. 2007. *Dangers of Toxic Fumes from Blasting*. Nashville, International Society of Explosives Engineers.

McHugh, S. 1983. Crack Extension Caused by Internal Gas Pressure Compared with Extension Caused by Tensile Stress. *International Jouranal of Fracture*, vol. 21, pp. 163–176.

Mirabelli, L. 2005. *Blast Management - National Quarry Academy*, s.l.: Quarry Academy 2005.

Otuonye, F.O. 1981. *PHD, Effective blasthole stemming*, Ohio: The Ohio State University.

Otuonye, F.O., Skidmore, D.R., and Konya, C.J. 1983. *Measurements and Predicitons of Borehole Pressure Variations in Model Blasitng Systems*. Lulea, Sweden, First International Symposium on Rock Fragmentation by Blasting.

Pardhan, G.K. 1994. *Explosives and Blasting Techniques*. Bhubaneswar, India: Mintech.

Pearton, S. 2014. *Evaluatinig the Viability of Pumpable Emulsion Explosives for use in Narrow Reef Mining Operations*, Johannesburg: University of Witwatersrand.

Phamotse, K.M. and Nhleko, A.S. 2019. Determination of optimal fragmentation curves for a surface diamond mine. *Journal of the Southern African Institute of Mining and Metallurgy*, vol. 119, pp. 613–619.

Radomsky, M. and Kecojevic, V. 2005. Flyrock Phenomena and Area Security in Blasting-Related Accidents. *Safety Science*, vol. 43. pp. 739–750.

Ratcliff, J., Sheehan, E., and Carte, K. 2011. *Predictability of Airblast at Surface Coal Mines in West Virginia*, West Virginia: Office of Explosives and Blasting (OEB).

Richards, A.B. 2013. Predictive Modelling of Airblast Overpressure. *Institute of Materials, Minerals and Mining and the AusIMM*, vol. 122, no. 4, pp. 215–220.

Richards, A. B. & Moore, A. J., 2005. Golden pike cut-back flyrock control and calibration of a predictive model, s.l.: Terrock Consulting Engineers.

Rorke, A.J. 2011. *Blasting Impact Assessment for the proposed New Largo Colliery*, s.l.: AJ Rorke.

Rustan, A. 1998. *Rock Blasting Terms and Symbols - A Dictionary of Symbols and Terminology in Rock Blasting*. 1 ed. London: AA Balkema.

S&T Projects. 2001. *Evaluation of Explosives Performance Through In-The-Hole Detonation Velocity Measurement*, Karnataka: National Institute of Rock Mechanics.

Saffy, A.A. 1961. *An experimental investigation of the factors influencing the efficent use of explosives in short drill holes*, s.l.: University of the Witwatersrand.

Sazid, M. 2014. *Investigating the role of effective stemming in engineering blasting operations for open-pit mines*, s.l.: Department of Earth Sciences, Indian Institute of technology bombay.

Sazid, M., Saharan, M.R., and Singh, T.N. 2016. Enhancement of the Explosive Energy Utilization with the Application of New Stemming Contrivance. *International Journal of Innovative Science and Modern Engineering*, vol. 4, no. 2. pp. 2319–6386.

Sharma, P. D. 2010. *Charging and Blasting in Hot Strata Condition in Opencast Coal Mines Most Crucial aspect is implementaion of Effective Safety Management*, s.l.: s.n.

Sharma, S.K. and Rai, P. 2015. Investigation of Crushed Aggregate as Stemming Material in Bench Blasting: A Case Study. *Geotech Geol Eng*, vol. 33. pp. 1449–1463.

Sheridan, R.A. 2002. *Explosives Information Bulletin - Precautions Agaisnt Flyrock*, Queensland: Explosives Inspectorate - Safety and Health Administration.

Singh, P.K., Klemenz, M., and Niemaan-Delius, C. 2005. *Air Overpressure*. [Online] Available at: https://www.agg-net.com/resources/articles/drilling-blasting/air-overpressure [Accessed 26 October 2020].

Snelling, W.O. and Hall, C. 1912. *The effect of stemming on the efficiency of explosives*, Washington: United States Government Printing Office.

Standards Australia. 2006. *Explosives-Storage and use*, Sydney: Standards Austalia.

StrataGold Corperation. 2017. *Eagle Gold Project, Explosives Management Plan*, s.l.: StrataGold Corperation.

Tobin, G. 2013. *The Importance of Energy Containment to the Blsat Outcome & Justification for use of Stemming Plugs in Over Burden Removal*, Australia: Oresome Products Pty Ltd.

Tose, S.S.J. 2006. A Review of the Design Criteria and Practical Aspects of Developing a Successful Pre-Split. *The South African Institute of Mining and Metallurgy*, pp. 525–546.

Trivedi, R., Singh, T.N., and Gupta, N. 2015. Prediction of Blast-Induced Flyrock in Opencast Mines Using ANN and ANFIS. *Geotech Geol Eng*, vol. 33. pp. 875–891.

U.S. Department of the Interior, n.d. *Office of Surface Mining Reclamation and Enforcement*. [Online] Available at: https://www.osmre.gov/resources/blasting/docs/WYBlasterCertModules/8AdverseEffectsBlasting.pdf [Accessed 17 01 2020].

University of Pretoria. 2016. *UP Research Summary*, s.l.: Univeristy of Pretoria.

Vale, 2015. *Blast Managment Plan*, Singleton, Hunter Valley: Integra Coal Operations.

Vale. 2019. *Hot Hole Charging Procedur*e, s.l.: Vale.

van der Walt, J. and Spiteri, W. 2020. A critical analysis of recent research into the prediction of flyrock and related issues resulting from surface blasting activites. *SAIMM*. pp. 701–714.

Zhang, Z.-X., De-Feng , H., Guo, Z., and He, Z. 2020. Labratory experiment of stemming impact on rock fragmentation by a high explosive. *Tunnelling and Underground Space Technology*, vol. 97, no. 1. pp. 1–10.

Zhang, Z.X.,2016. Stemming and Charge Length. In: M. K. Leme, ed. *Rock Fracture and Blasting*. s.l.:Joe Hayton, pp. 271-281. ◆

We strive to offer you the lowest cost of ownership

Weir Minerals is a leading designer and manufacturer of mine dewatering solutions, slurry pumps, hydrocyclones, valves, screens, centrifuges, crushers, feeders, washers, conveyers, rubber lining, hoses and wear-resistant linings for the global mining and minerals processing, sand and aggregate, and power and general industrial sectors.

For more information contact us on +27 11 9292600

WEIR

Minerals
www.global.weir
www.weirafricastore.com

Optimization of shift cycles in the South African mining sector

J. Pelders[1], F. Magweregwede[1], and S.M. Rupprecht[2]

Affiliation:
[1]CSIR Mining Cluster, South Africa.
[2]University of Johannesburg, South Africa.

Correspondence to:
J.L. Pelders

Email:
JHodgskiss@csir.co.za

Dates:
Received: 19 Nov. 2020
Revised: 1 Jul. 2021
Accepted: 8 Jul. 2021
Published: August 2021

How to cite:
Pelders, J.L., Magweregwede, F., and Rupprecht, S.M. 2021 Optimization of shift cycles in the South African mining sector. Journal of the Southern African Institute of Mining and Metallurgy, vol. 121, no. 8, pp. 427–436

DOI ID:
http://dx.doi.org/10.17159/2411-9717/1428/2021

ORCID:
J.L. Pelders
http://orcid.org/0000-0003-4671-1951

F. Magweregwede
https://orcid.org/0000-0002-4824-2266

S.M. Rupprecht
https://orcid.org/0000-0003-2462-2819

Synopsis

Increased depths of conventional gold and platinum mines, longer travelling times as working places move further from the shaft, and ancillary activities taking place in the mining cycle reduce the useable time spent at the workface. Current shift lengths of 8 hours 20 minutes may no longer be adequate to complete required mining activities.The impact of mineworker commuting times on shift work is also not well understood. The aim of this research was to draft a framework to optimize shift cycles in order to maximize productivity, health, safety, and wellness in the South African mining sector. The framework was informed by a review of the literature, case studies at a local gold mine and platinum mine, and a workshop with industry experts. The findings indicate potential advantages of extended shift lengths and continuous operations, such as improved productivity, asset utilization, and employee morale. However, concerns included fatigue and the associated safety hazards, particularly when working longer shifts, night shifts, and numerous consecutive shifts. Job demands, personal factors, and commuting times are further considerations when scheduling shifts. The ideal shift system for the mining sector should holistically consider and balance operational requirements, health and safety, and employees' and their families' requirements, and suit the unique needs of each operation. Changes in shift cycles will require a structured change management process, which involves all stakeholders, and could help to enhance the viability of the South African mining sector.

Keywords
ancillary activities, continuous operations, fatigue, occupational health and safety (OHS), productivity, travelling time.

Introduction

The productivity of most conventional South African underground gold and platinum mines is declining, operational costs are increasing, and profit margins are shrinking, while health, safety, social, and environmental challenges are present (Neingo and Tholana, 2016; Singh, 2017). Many narrow-reef gold and platinum mines in the country are increasing in depth to reach new deposits, resulting in longer travelling times, rising costs, reduced profits, and heightened risks (Deloitte, 2014; Jacobs and Webber-Youngman, 2017; Minerals Council South Africa, 2018; Rupprecht, 2018a; Singh, 2017). The increased travelling times, along with additional ancillary activities taking place in the mining cycle, reduce time spent at the workface, and might hinder the attainment of a daily conformant blast (Gumbie, 2018). Previous research has indicated that mandatory shift lengths of 8 hours 20 minutes may no longer be adequate to complete the required mining activities (Rupprecht, 2018b). Increased shift lengths and the adoption of close-to-continuous operations (CONOPs) could help to address these challenges (Lazare, 2013). Factors affecting occupational health and safety (OHS) and worker wellbeing also need to be considered in relation to shift work. For example, the effects of worker travelling times from home to the stope face and the impacts of working conditions on worker fatigue are not well understood (Gumbie, 2018).

The purpose of the project was to draft a framework to assist mines to optimize shift cycles in order to maximize productivity, OHS performance, and employee wellness. The research assessed potential challenges in different activities in relation to on available face time, and feasible alternative shift cycles in the South African mining industry. Additionally, we examined the effects of commuting times, particularly regarding fatigue. The project was informed by a review of the literature, two case studies conducted in the South African mining industry, and a workshop with technical experts. The

project was commissioned by the South African Mining Research, Development and Innovation (SAMERDI) strategy's Longevity of Current Mines (LoCM) programme of the Mandela Mining Precinct (Pelders *et al.*, 2019).

Literature review

Shift work

Shift work is required in many industries, including mining, and allows for longer hours of operation (Baulk *et al.*, 2009). Shift work refers to 'an organisation of work where workers succeed each other at the same workplace while performing similar operations at different times of the day thus allowing longer hours of operation than feasible for a single worker' (Department of Mineral Resources, 2014, p. 36). Continuous shift work refers to operations that run 24 hours per day, seven days per week, throughout the year (Department of Labour, 1998). For this research, the terms 'continuous operations' (CONOPS) and 'full calendar operations' (FULCO) are used interchangeably. Numerous shift cycles are used in industry, and typically involve three 8-hour shifts or two 12-hour shifts, while some mines in South Africa operate two 10-, 10.5-, or 11-hour shifts (Baulk *et al.*, 2009; Theron, 2014).

Conflicting findings regarding the pros and cons of different shift lengths are evident in the literature and are likely context-dependent. However, potential advantages of extended (*e.g.* 12-hour) shift lengths might include improved productivity, better asset utilization, improved communication at shift changeovers, reduced sick leave, and improved employee morale (Baker, Heiler, and Ferguson, 2003; Stenzel, 2002). The use of 12-hour shifts results in compressed working weeks, which allows for longer periods of time off for social and domestic interaction and leisure, and a reduction in total commuting time (Baulk *et al.*, 2009). Meanwhile, disadvantages of extended shifts could include fatigue, impaired performance, and increased rate of incidents (Baker, Heiler, and Ferguson, 2003; Bates, 2009; Baulk *et al.*, 2009; Spencer, Robertson, and Folkard, 2006). As such, shift cycles should be designed to minimize fatigue, optimize productivity and OHS performance, and improve mine viability (Ngobese, 2017; Pickering, du Plessis, and Annandale, 2010; Smith *et al.*, 1998; Stenzel, 2002).

Legal requirements and guidelines

Shift work and working hours are subject to regulations. Key pieces of legislation covering shift rostering at mining operations in South Africa include the following.

- Occupational Health and Safety Act (OHSA, Act No. 85 of 1993) (Department of Labour, 1993)
- Mine Health and Safety Act (MHSA, Act No. 29 of 1996) (Department of Mineral Resources, 1996)
- Basic Conditions of Employment Act (BCEA, Act No. 75 of 1997) (Department of Labour, 1997)
- Code of Good Practice on the Arrangement of Working Time (Department of Labour, 2017);
- Guideline for Mandatory Code of Practice (COP) for Risk-Based Fatigue Management at Mines (Department of Mineral Resources, 2014).

Employers are required to evaluate work schedules to ensure that the health and safety of employees will not be at risk. The MHSA No. 29 of 1996 and OHSA No. 85 of 1993 require employers to conduct a risk assessment, implement measures to eliminate or control identified hazards, conduct medical surveillance concerning those hazards for employees, and train and inform employees about the risks and controls. The BCEA No. 75 of 1997 considers factors such as ordinary hours of work, overtime, compressed working weeks, averaging the hours of work, meal intervals, daily and weekly rest periods, and pay for work on Sundays, night work and public holidays. Exemptions in terms of collective agreements can be provided, subject to provisions.

The Code of Good Practice on the Arrangement of Working Time relates to shift work, night work, and rest periods during working time, and provides information about the impact of working time arrangements on the health, safety, and family responsibilities of employees (Department of Labour, 1997, 1998). The Guideline for a Mandatory COP for Risk-Based Fatigue Management at Mines assists employers to prepare a risk-based COP on fatigue management (Department of Mineral Resources, 2014).

Fatigue and other impacts of shift cycles on people

Shift work is associated with disturbed sleep, fatigue, reduced alertness and performance, occupational accidents and incidents, health problems, negative effects on social and domestic activities, and impaired mood (Baulk *et al.*, 2009; Greubel *et al.*, 2016; Härmä *et al.*, 2018; Kalmbach *et al.*, 2018). These risks could lead to economic losses resulting from increased sick leave and staff turnover rates (Greubel *et al.*, 2016; Jacobsen and Fjeldbraaten, 2018). Absenteeism has been attributed to lengthy work hours, fatigue resulting from shift length and/or environmental conditions in the stope, and commuting to and from home (Rupprecht, 2018b).

Shift work, or work performed at unusual times, results in misalignment of the circadian rhythm (or 'body clock') with activities and sleep schedules, which contributes to fatigue or sleepiness at work (Department of Mineral Resources, 2014; Greubel *et al.*, 2016; Kalmbach *et al.*, 2018; Schutte, 2010a). Shift cycle characteristics that are associated with the risk of fatigue and incidents include the time of day, direction and speed of shift rotation, consecutive hours on duty, number of consecutive shifts, breaks between work periods, and rest breaks during work. In particular, factors associated with higher risk of fatigue and accidents include early morning or night shift work, backward rotating shifts, long shift durations (*e.g.* 12-hour shifts), too many consecutive shifts, a lack of rest breaks, and excessive overtime and on-call work (Bates, 2009; Department of Mineral Resources, 2014; Greubel *et al.*, 2016; Härmä *et al.*, 2018; Kalmbach *et al.*, 2018; Spencer, Robertson, and Folkard, 2006; Theron, 2014).

As a result of these circadian and sleep disruptions, fatigue is an inherent hazard in shift work and is a causal or contributing factor in many occupational incidents in the mining industry (Hodgskiss *et al.*, 2015; Pelders and Nelson, 2019; Schutte, 2010a; Theron, 2014). Fatigue results in reduced performance and productivity, impaired alertness, increased error rates, and can also result in medical and psychological problems such as heart disease, hypertension, diabetes, digestive problems, anxiety and depression (Bates, 2009; Department of Mineral Resources, 2014; Pelders and Nelson, 2019; Pfeifer, 2017; Schutte, 2010a; Theron, 2014). Numerous factors can contribute to fatigue in addition to shift work, including the job demands (*e.g.* stress), work environment (*e.g.* lighting, heat, and humidity), medical

conditions, psychological factors, lifestyle and activities outside of work, nutrition, demographics, socio-economic status, living conditions, and commuting times (Department of Mineral Resources, 2014; Pelders and Nelson, 2019; Schutte, 2010a; Theron, 2014).

Work factors associated with high risk of fatigue and accidents during shift work include heavy physical work, sustained effort, complex tasks, critical monitoring tasks, or repetitive and monotonous tasks (Baulk *et al*., 2009; Department of Labour, 1997; Department of Mineral Resources, 2014). Temperature extremes, excessive noise, work stress, poor ergonomic design of workstations and equipment, and long walking distances in underground workplaces can also contribute to fatigue (Department of Mineral Resources, 2014; Hodgskiss *et al*., 2015; Neingo and Tholana, 2016).

Lifestyle factors, such as activities outside of work and family commitments, poor diet or nutrition, a lack of exercise, as well as drug and alcohol abuse, can also contribute to fatigue (Hodgskiss *et al*., 2015; Pelders and Nelson, 2019; Department of Mineral Resources, 2014; Theron, 2014). Shift work can prevent workers from completing personal chores and can result in desynchronization with social participation and increased risk of poor work-life balance (Brown *et al*., 2010; Greubel *et al.*, 2016; Rupprecht, 2018b). Additionally, factors such as sleep routines, maintaining healthy diets, and exercise and recreational activities can affect how employees adapt to shift work (Department of Labour, 1998; Department of Mineral Resources, 2014).

Commuting times, including time to travel from home to the mine and back again, and month-end travelling to and from labour-sending areas, can have an impact on health, safety, absenteeism, and fatigue outcomes (Brovko *et al*., 2018; Pfeifer, 2017; Rupprecht, 2018b; Sanqu, 2016). Workers with longer commutes have been shown to obtain less sleep during the work week, report higher levels of sleepiness, be less productive at work, and have significantly higher absenteeism rates (Hodgskiss *et al*, 2015; Pfeifer, 2017; van Ommeren and Gutierrez-i-Puigarnau, 2009). Theron (2014), for example, noted that mine employees' days commonly start at 3 am to catch public transport in order to start work at 6 am, and that they might only return home around 5 pm. These commutes limit the time available for workers to attend to household responsibilities and to sleep (Hodgskiss *et al*., 2015; Pelders and Nelson, 2019; Theron, 2014). Previous research conducted across eight operations in the South African mining industry revealed that over half of the sample of 875 participating mineworkers usually obtained less than 6 hours of sleep in the 24 hours before a work shift, and 31% reported having occasionally fallen asleep at work (Hodgskiss *et al*., 2015). Although this sample was not fully representative of the South African mining industry, it incorporated participants from the gold, platinum, coal, diamond, and manganese sectors and was considered to provide a basic indication of the levels of sleep obtained and fatigue among mineworkers in South Africa.

Productivity and operational requirements

Over the past few years, productivity in narrow-reef hard-rock underground gold and platinum group metal (PGM) mines has been declining due to a number of reasons, including additional safety requirements (*e.g.* nets), labour unrest, greater mining depth, and increasing working distance from the shaft. Most narrow-reef hard-rock underground gold and PGM mines utilize labour-intensive conventional drill-and-blast mining methods, requiring a re-entry period of between one and four hours after blasting prior to commencement of the subsequent shift (Brake, 2015). The literature study revealed that the standard current shift length of 8 hours 20 minutes is no longer adequate to complete most of the mining tasks in a single shift at most conventional underground mines (Lazare, 2013; Rupprecht, 2018b). The available face time is increasingly becoming marginal due to a number of factors such as increasing travelling times as mines are getting deeper and working faces are progressing further from existing shafts, unauthorized breaks due to lack of discipline, early work stoppages and late shift starts due to activities such as meetings, safety talks, early entry examinations, and risk assessments (Neingo and Tholana, 2016). Other factors that affect labour productivity include prevailing working environmental conditions (such as temperature, humidity, and stoping width), equipment availability, competence and skills of the workforce, workforce efficiency, workforce availability and work ethic within the workforce (Aljuhani, 2002; Neingo and Tholana, 2016; Roussos, 1996).

Productivity in conventional underground gold and PGM mines could be improved through optimization of shift cycles, ensuring the availability of the right-sized workforce to complete all the required tasks within the allotted time (Lazare, 2013; Neingo and Cawood, 2014; Rupprecht, 2016 and 2018b). In order to attain all planned conformant blasts, sufficient time should be allowed for travelling, execution and completion of work, and other ancillary tasks (Rupprecht *et al*., 2001). Time-motion studies conducted during the Sindisa project were used to identify major ancillary activities that caused delays in the mine production system (Table I). In order to attain an optimal mine production system, a systems thinking approach, aiming to optimize the shift cycles together with other components of system, should be adopted. The majority of the identified delays could be mitigated through good practices such as proper planning, good work organization, efficient communication strategies, and sound maintenance practices. Interventions that could be put in place to improve available face time include reduction of travelling times through efficient personnel transportation systems, longer shifts, and technology solutions to expedite completion of ancillary activities such as early entry examination, barring, support, and risk assessments (Rupprecht, 2016).

The Sindisa Gold project was initiated in 2011 by the Minerals Council South Africa (MCSA) in collaboration with mining companies and organized labour, to explore opportunities for optimizing utilization of mine assets. For the purpose of this article, mine assets include ore reserves, plant, equipment, and machinery. The Sindisa Gold project envisaged optimizing asset utilization through practices such as increasing the number of production days per annum, attaining more planned conformant blasts, and ensuring the availability of mineable ground (including a contingency) all the time (Lazare, 2013). Optimum utilization of labour was to be achieved by increasing the number of production days per annum through adoption of close-to-CONOPs, with shift lengths not exceeding 12 hours crush-to-crush (Lazare, 2013). Critical enablers of the process include co-creation of the shift cycles with all stakeholders (including the workforce), sufficient consultation and engagement witj all key stakeholders, and ensuring that the new shift schedules do not violate any legal requirements (Lazare, 2013).

Table I

Examples of delays in ancillary activities in the mining cycle (Lazare, 2013)

Category of activity	Examples of delays
Cleaning cycle-related tasks	• Locomotive and hopper derailments • Waiting for the crew at the face (late arrivals) • Repairing mechanical loader hoses • Waiting for loco to fetch hopper • Congestion at the tip • Loader derailment • Air coupling came loose • Fixing fishplate • No compressed air • Waiting for support crew • Work stopped due to temperature and ventilation challenges
Drilling and supporting cycle-related tasks	• Ventilation interruptions in all the operations • Waiting for equipment • Repairs on water pipe • Replacement of hydraulic pipes • Briefing on safety • Waiting for methanometer • Barring rock from face • Waiting for previous crew to finish • Waiting for drill rigs • Drill bit stuck / replaced • Power outage • Miner and shift boss talks with the team • Waiting for miner • Drill rig with only one boom • Adjusting motors

Methods

Two case studies were conducted at mine sites in South Africa. Data was collected at one platinum mine and one gold mine in April and August 2019, respectively. These mines are not representative of the South African mining sector, but provide examples of aspects that are impacted by the design of shift schedules in the industry, in the local context. Convenience sampling was used to identify potential mine sites, with input and understanding from experts in the field, and the sites were selected based on permissions received to collect data. Data was collected from individuals at each mine who had an in-depth knowledge of the operation and access to required information, including human resources (HR), mine planning, and production personnel.

This was a mixed methods study, as both qualitative and quantitative data was gathered. Qualitative data was obtained in interviews and focus group discussions held with the participants. The discussion guides included open-ended questions relating to shift cycles, ancillary activities, face time, travelling times, work conditions, resources, and fatigue. Quantitative data was provided by the mines. This data included the shift rosters and shaft schedules, planned versus actual bank-to-bank times, productivity, health, and safety data, and shift activity durations, where available. The data was captured into an electronic format for analysis. Thematic analysis was used to analyse the qualitative data, and themes from the data were coded and summarized. Basic statistical analyses were conducted on quantitative data. Selected shift cycles were analysed using the Health and Safety Executive (HSE) Fatigue and Risk Index calculator. A framework for optimizing shift cycles in the South African mining industry was drafted, based on the results.

A workshop was held following data collection and analysis to present and discuss the findings from this project, and to gain technical input into the draft framework. The workshop was held at the Mandela Mining Precinct on 25 October 2019. The participants included representatives from mining companies, research partners, and the SAMERDI programme. Feedback received from the stakeholders was used to update and refine the draft framework, and to identify future research topics. Engagement with further stakeholders, including labour representatives, will be required before finalization of the shift cycle guidelines for industry.

Ethics approval for the project was granted by the CSIR Research Ethics Committee (reference number: 239/2017).

Results

Case study 1

The participating platinum mine is located in the Bushveld Complex in Mpumalanga Province, South Africa. It operates underground at depths of between 50 m and 850 m, using low-profile mechanized board-and-pillar mining. The mine was classified as a 'hot' mine (wet bulb temperature: ≥27.5°C) (Schutte, 2010b), while the work performed was not considered labour-intensive. The mine operated continuously and, in general, the implementation of CONOPs at this mine was considered successful.

The mine operated seven days per week, throughout the year, except for certain public holidays and over the Christmas period. Two 10-hour production shifts operated each day, using a 5D 5N 5O roster (where D = day shift, N = night shift, and O = day off). The start and end times for the day and night shifts were 07h00 to 17h00 and 20h00 to 06h00, respectively. However, different documents from the mine showed discrepancies in the official shift start and end times. Other shift cycles that were used at the mine were 4D 4O 4N 4O shifts (*e.g.* for essential services and at the plant), and straight shifts, which operated from Monday to

Friday, and only during the day. The mine had 341 production days per year. Employees on CONOPs worked an average of 243 shifts each per year. Maintenance took place in each level every two weeks during day shifts.

During the 10-hour shifts worked by CONOPs employees, approximately 7 hours were spent at the workface. The average travelling time to the face was 30 to 40 minutes, but reached up to 2 hours depending on location in the operation. The longest travelling distance was approximately 2.5 km. The drilling time was approximately 2.5 hours per face. Two spare panels were available to allow for redundancy. Drilling, supporting, and cleaning could extend throughout the shift, as work could continue at another panel once one was completed. Two blasts per day were planned, and the re-entry period was approximately 1 hour. The overall rate of lost blasts for the year to date was 20%, with breakdowns, labour shortages, and service days among the causes.

An analysis was conducted of the number of hours that mining crews spent underground during the previous seven days. The average number of underground hours worked ranged from 6 hours 35 minutes to 8 hours 23 minutes. In general, the night shift underground hours were longer than the day shift hours. Results of face time studies conducted at the mine in 2011 were also assessed, for which average face times of around 7.5 hours were reported. In levels with the longest horizontal travel distances, differences between collar-to-collar and face times ranged from 49 to 98 minutes. Ancillary activities that workers conducted upon arriving at the mine included the collection of lamps and gas detection instruments; queuing for and travelling on chairlifts; walking to (and from) the waiting place; safety and waiting place meetings; and travelling to and from the workface.

The commuting distances for workers ranged from approximately 4 km to 70 km. Mine buses were available to transport workers to and from the surrounding communities. From an analysis of the pick-up and drop-off times of the mine buses, it was estimated that an employee with a commuting time of 1 hour between home and work, who works 10-hour shifts, had 11 hours available for personal activities and sleep during each workday. This time allowed for the additional half hour between transport arrival/departure and working times, but excluded the time between leaving home and arriving at the transport pick-up point and waiting for the transport to arrive.

The fatality frequency rate at the time of the assessment was 0.00 and the lost-time injury frequency rate was 0.5 (per 200 000 shifts worked). The average turnover rate at the mine was 0.5%, and a large portion of the workforce had been at the mine since the operation commenced. The absenteeism rate was considered by the mine management to be relatively low compared to other mines. The average rate of sick leave ranged from 3.5% to 4.5%, and the average annual and other leave ranged from 7% to 13.5% for the previous three months.

Case study 2

The second case study site was a fully mechanized gold mine in Gauteng Province, South Africa. The mine operated underground at depths of 3000 m. The average wet bulb temperature in the workplaces was 27.5°C. The mine used CONOPs arrangements. Changes to the shift systems at the mine had been made to improve productivity and to better suit current conditions. The changes involved extension of the shifts and reducing the number of consecutive shifts worked. Improvements in production, maintenance, and safety were reported as a result of the shift changes. However, the cited disadvantages were higher absenteeism and fatigue.

The mining production teams, and some engineering personnel, operated using 4×3 (or 4×4) shifts (4D 4O 4N 4O) that were 11.5 hours long. A maintenance shift was incorporated into this roster, such that three production shifts and one maintenance shift took place in the cycle. The reported clock-in and clock-out times for the day shift were 05h45 and 17h35, and 17h40 and 05h35 for the night shift. As with the other case study, slight discrepancies between shift times from different sources were evident, and it was not clear when employees were required to arrive at work versus when they clocked in at the shaft. Production could take place 351 days per year. An agreement was negotiated whereby workers would work for six of the 12 national public holidays and be off for the other six public holidays and over the Christmas break. It was noted that an increase in the number of non-production days could assist with maintenance at the mine. Mining employees each worked approximately 180 shifts per year, including training and leave, and around 107 days excluding training and leave days.

During the 11.5-hour shift, time spent at the face ranged from 8 to 11.5 hours, and incorporated at least two of the following activities: drilling (approx. 4.2 hours); charging and blasting (aprox. 2.5 hours); support (approx. 5.2 hours); and loading (approx. 3.4 hours). Two blasts were planned per day, but sometimes only one blast was possible. The re-entry period was around 1 hour and was relatively short because of the long travelling times and as the working place was not confined. The time taken for workers to travel from the lamp room to the workplace was approximately 1 hour. The horizontal travelling distances to the workplaces were up to 2 km, and the workers either walked or used trains to travel underground. Problems booked at the mine for the year to date were assessed, the majority of which related to support, and also included those relating to services and breakdowns. Contingency plans were in place in terms of labour, equipment, and power at the mine. Additional labour was planned for certain occupations in production. The planned contingency was around 15% per section, and an extra roving crew was available.

Most of the workers were reported to live within a 15 km radius of the mine. Workers used a range of transport modes to commute, including public transport, private vehicles, and mine buses (for those living in the mine hostel). The working hours were adjusted to accommodate for public transport availability. It was estimated that workers could spend approximately 10 hours at home on workdays, when accounting for working hours and commuting times. It was reported that some of the workers lived in informal housing (shacks), and the poor living conditions associated with this housing could contribute to fatigue. In addition to the long shifts worked, commuting times, and living conditions the high temperatures in the mine were a potential contributor to fatigue. Fatigue management programmes, processes, and training, wellness programmes, and mid-shift meal breaks were in place.

The fatality frequency rate was 0.00 and the lost-time injury rate was 1.20 for 2019 (at the time of the data collation), compared the rates from the previous year of 0.05 and 0.98, respectively. The absenteeism rate at the mine for all causes was 16% for the year to date, and was considered by mine management to be reasonable, compared to other mines. Absenteeism comprised approximately 43% annual leave, 24% training, 14% sick leave, 3% 'absent', and 16% 'other'.

Fatigue and risk indices

The HSE fatigue calculator was used to estimate and compare fatigue and incident/accident risk for different shift rosters. Three shift rosters were chosen as examples, and the results are shown in Figures 1 to 3. Fatigue and risk scores are provided for each shift within a schedule. The fatigue and risk indices are similar in many respects, but differences include time-of-day effects (*e.g.* accident risk tends to be higher close to midnight, while fatigue tends to peak in the early morning). The fatigue scores range from zero to 100 and indicate the percentage chance of experiencing high levels of sleepiness, such that the workers might struggle to stay awake during that shift. Meanwhile, the risk scores refer to the relative risk of an accident or incident, with a baseline value of 1.0.

The default scores of the index can be adjusted according to commuting times, job types, and job breaks components. For this analysis, the default scores were kept consistent, and were set at 1 hour commuting time, a moderately demanding workload, mostly continuous attention requirement, and rest breaks taken for 30 minutes after every 5.5 hours, and for 5 minutes every 2 hours. Changes in these components, and in shift start and end times, have significant impacts on the fatigue and incident risk scores. The tool is useful for assessing risks of fatigue and injury, but should not be relied on as the primary means of assessing these risks, and does not account for factors such as specific work-related issues, individual differences, or social factors that might affect workers' tolerance to shift work (HSE, 2019).

It is evident that the scores, particularly for fatigue, are higher during night shifts than during day shifts. Additionally,

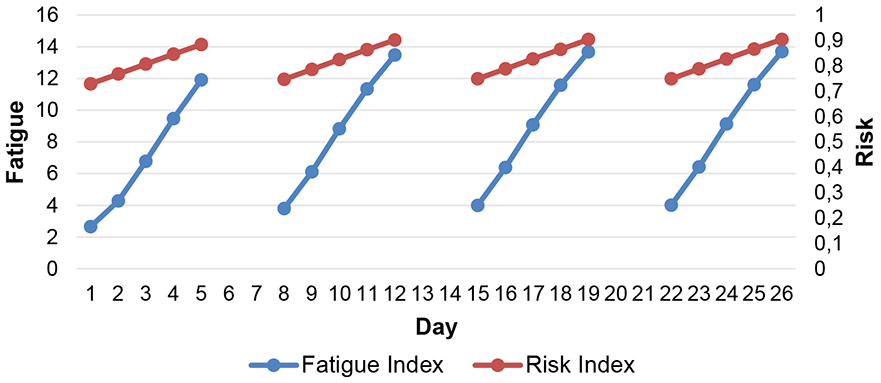

Figure 1—Fatigue and accident risk of a 5D 2O (day shift only) cycle with 8-hour 40-minute shifts (starting at 07h00 and ending at 15h40)

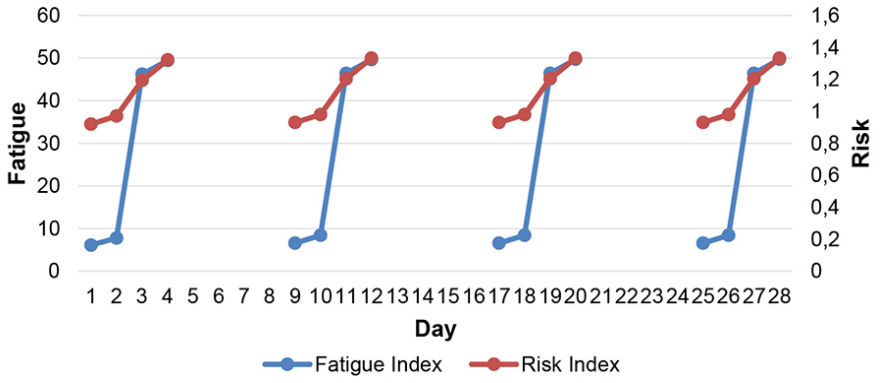

Figure 2—Fatigue and accident risk of 2D 2N 4O CONOPs cycle with 12-hour shifts, starting and ending at 07h00 and 19h00 (day shift) and 19h00 and 07h00 (night shift)

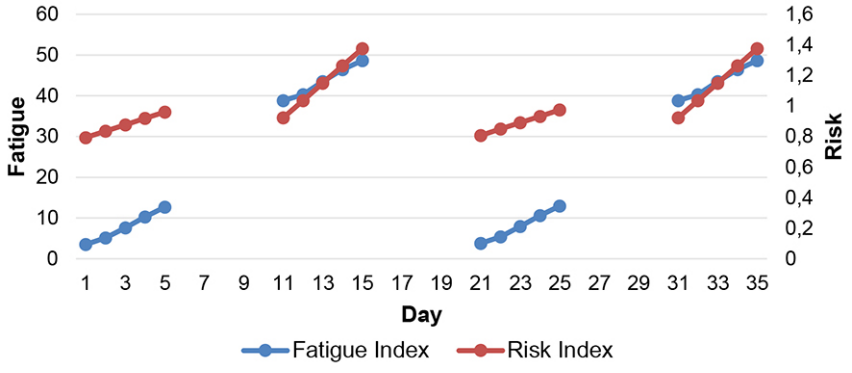

Figure 3—Fatigue and accident risk of a 5D 5N 5O CONOPs cycle with 10-hour shifts, starting and ending at 07h00 and 15h00 (day shift) and 20h00 and 06h00 (night shifts)

the fatigue and accident risks increase with the number of consecutive shifts worked. Meanwhile, the days off provide an opportunity for recovery in between shifts worked. If fatigue and accident risk scores do not return to the original values when the shift cycle is repeated, it indicates that workers do not have the opportunity to fully recover within the shift cycle. Higher fatigue and accident scores were evident for the rosters with longer shift lengths, while lowest risk scores were evident in the rosters that only incorporated day shifts.

Discussion and recommendations

The case studies provide examples of the successful implementation of CONOPs at mines in South Africa. The main benefit of CONOPs that was indicated was improved productivity (in terms of the number of tons produced per month), as the longer shifts helped to increase face times in relation to the total number of hours worked. This finding is in support of the literature on the topic; for example, Stenzel (2002) reported that the productivity of a certain mine increased by 21% after implementation of CONOPs with a 12-hour shift roster. Additionally, maintenance was improved, as service shifts were incorporated into the rosters. The use of contingency measures such as availability of spare panels and extra roving crews further aided continued production. However, potential challenges associated with longer shifts included increased fatigue and absenteeism. Other factors that were associated with fatigue and OHS outcomes during shift work included commuting times, living conditions, the provision of meal breaks and mid-shift meals, the workplace environmental conditions (*e.g.* heat), and job demands. Analysis of the fatigue and accident risks associated with selected rosters revealed that the risks were higher with longer shifts, during night shifts, and when numerous consecutive shifts were worked. The implementation of CONOPs might differ between the case study sites and conventional mining operations in some respects; however, the basic principles relating to the use of CONOPs could be applied to different types of mining operations.

A draft framework was compiled based on the findings from the literature review and research conducted, and was discussed and amended based on feedback received from the technical workshop. The draft framework serves as a basis for further industry engagement and recommended research for the optimization of shift cycles in the South African mining industry. The framework includes numerous considerations and recommendations relating to shift cycle design, which are summarized in Table II.

It is evident that the ideal shift rostering system for the mining sector must holistically consider and balance operational requirements, employee needs, and OHS requirements. The assessment of shift cycles and fatigue should consider a number of factors, and be developed to suit the unique needs of each operation. Consultation between stakeholders, including mining companies and worker representatives, is important for the successful implementation of changes to shift cycles.

The development and implementation of new shift schedules will require a structured change management process and effective stakeholder engagement. For example, the Plan-Do-Check-Act (PDCA) model can be used to plan, develop, implement, and continually improve the new shift roster. This project links to work conducted in the Successful Application of Technology Centred Around People (SATCAP) programme, which aimed to identify appropriate change management and stakeholder engagement processes for shift cycles appropriate for mine modernization. The Mining Industry Occupational Safety and Health (MOSH) adoption process for leading practices could be used to facilitate the implementation of new shift schedules.

Recommendations for future research needs were identified during the project. Primarily, the need for involvement of further stakeholders, including representatives from a range of mines, labour representatives from each union, and government and community representatives, was emphasised for the finalization of guidelines for shift cycle optimization in the South African mining sector. Qualitative research involving mineworkers was recommended. In addition, participation from members involved with the Sindisa Gold Project was suggested to build on this work. Further research could involve additional analyses of the processes that have been used by mines when successfully implementing changes to shift cycles. Additional input relating to occupational medicine impacts of different shifts would be helpful to refine the shift cycle framework. An assessment of best and worst practices relating to shift cycles, and available monitoring systems and tools, would be valuable, along with the development of a toolbox for monitoring and evaluation of performance. Research involving the use of real-time information management and monitoring systems, such as smart watches, was also recommended. Further suggested work relates to reward systems or remuneration practices, the ageing workforce, resistance to change, and workplace culture in the modernizing South African mining industry. In addition, a systems approach, integrating work conducted within the LoCM and broader SAMERDI projects, is suggested, as many of the findings could be related for appropriate implementation in the mining sector.

Conclusion

Changes to shift cycles could help to enhance the viability of the South African mining sector. These changes could help to address challenges relating to increased travelling times, reduced face times, and impaired productivity, while addressing the impact of commuting times, personal factors, and worker fatigue in relation to shift work. This paper outlined several factors to consider when assessing shift cycle options. Operational and productivity requirements, OHS matters, and employee preferences need to be taken into account. Furthermore, stakeholder engagement and change processes need to be effectively managed. Additional research, involving a broader range of stakeholders, will assist in the completion of guidelines for shift cycle optimization in the South African mining sector.

Acknowledgements

This project was funded by the Minerals Council South Africa (MCSA) and commissioned by the Mandela Mining Precinct. The Mandela Mining Precinct is a public-private partnership between the Department of Science and Innovation and the MCSA. The Precinct is co-hosted by the CSIR and the MCSA. We would like to acknowledge Martin Pretorius in the role of LoCM Programme Manager. We also thank Sophi Hlatshwayo, Zintle Nontso, and Refiloe Maponya for their contributions. Finally, we are grateful to the mines and individuals who participated in this research.

References

Aljuhani, M. 2002. Labour's utilisation and labour's productivity of a gold mine in Saudi Arabia. *Journal of the Southern African Institute of Mining and Metallurgy*, vol. 102, no. 5. pp 307–310.

Table II

Shift cycle design element considerations

Shift roster element	Category	Description	Recommendation
Understanding shift rosters	Shift cycles	• Assess various shift rosters, taking into consideration all the key shift roster design parameters	• Do a cost benefit analysis of different shift lengths and schedules
Operational requirements	Legal requirements and company standards	• Ensure compliance of the selected shift roster to all applicable legislation	• If the shift roster does not comply to certain provisions of the legislation consider the following: ▪ Aligning the shift roster to legislation ▪ Selecting alternative shift rosters ▪ Blasting time considerations (including regional requirements) ▪ Requesting for exemptions from the responsible authorities
	Understand the gaps of the current shift roster	• Understand major constraints within the current shift roster	• Do a detailed analysis of major constraints and suggest suitable interventions
	Define the goals and key performance indicators (KPIs)	• From the identified constraints, define goals and KPIs which will be achieved by changing the shift roster	• Develop specific, measurable, attainable, relevant, and time-bound (SMART) goals and KPIs
	Determine the labour requirements	• Determine the human resource requirements of the shift roster options	• Labour requirements should be informed by the workload and practical evidence from time motion studies • Ensure the availability of the right expertise at the right work place and right time • Avail at least one supervisor with the necessary expertise, to oversee all operational activities on every shift
	Enhancing effectiveness and utilisation of labour	• Put in place measures to maximise the effectiveness and utilisation of labour on all shifts	• Effective supervision ▪ Avail at least one supervisor with the necessary expertise, to oversee all operational activities on every shift ▪ Use real-time information management systems (RTIMS) to improve the effectiveness of supervision, utilisation of labour and expedite decision-making • Effective training to improve the competency and skills of the workforce • Focus on improving team morale and cultivating a high performance work culture • Promote team works and use of self-directed work teams (SDWT) • Ensure effective communication at all levels within the organisation
	Shift length	• Determine the correct shift length	• Shift length should be determined taking cognisance of factors such as work requirements, travelling time, OHS requirements and workplace conditions
	Support services	• Provide sufficient support services to ensure asset integrity and optimum utilisation of equipment	• Having maintenance crews operating on all mining shifts • Use of cross-trained operator-maintenance artisans • Scheduling most of the maintenance tasks during day shift • Ensure underground facilities and infrastructure have capacity to support the proposed shift roster and work arrangements
	Optimise the utilisation of equipment	• Ensure optimum utilisation of mine equipment	• Mines must strive to operate continuously (i.e., 365 days a year, 7 days a week and 24 hours a day)
	Ore reserve availability	• Ensure availability of ground to mine all the time	• Maintain a minimum of 18 months ore availability period (Sebutsoe and Musingwini, 2017). • Investigate the use of accelerated ore reserve development technologies
	Logistics and inventory control	• Ensure an efficient logistics and inventory control system	• Use of underground buffer stores utilising scanning technologies for controlling inventory levels • Use of asset tracking • Proper planning and scheduling • Investigate alternative efficient transportation systems
OHS requirements and employee needs	Fatigue	• Design shift schedule optimally to reduce the risk of fatigue	• Overtime and on-call work should be limited • Avoid backward rotating shifts (e.g. night to afternoon to morning) • Avoid shift rosters with irregular or unpredictable patterns • Avoid working more than four consecutive 12-hour night shifts • Provide at least 36 hours off following a period of night shift work • Fatigue management programmes should address the unique conditions of each operation • Implement systems or technology to monitor performance of workers in safety-critical positions
	Occupational health and wellness	• Manage the health and occupational exposures of workers	• Occupational exposures are affected by shift lengths and should be managed accordingly, such as for radiation, silicosis, diesel particulate matter, and thermal strain. • Medical conditions and psychological issues are associated with fatigue, and should be managed in the context of shift work • Workers should be able to eat properly, participate in recreational exercise, and be educated about lifestyle factors that can affect their health (e.g. smoking and substance abuse)
	Working conditions	• Assess working conditions to minimise health, safety and fatigue risks	• Safety critical tasks should not be undertaken when employees are likely to be fatigued (e.g. during night shifts, 12-hour shifts, or when performing work with high physical or mental demands, or repetitive or monotonous work) • Ensure appropriate rest breaks within each shift • Poor nutrition contributes to fatigue, therefore consider the supply of meals or supplements for workers; the impact of restrictions due to illegal mining should also be considered • Ensure availability of drinking water • Work environment factors such as lighting, noise, vibration, and temperature should be appropriate for worker health, safety, and comfort • Appropriate management services should be available to those working outside of ordinary hours • Ensure availability of appropriate resources e.g. staffing and equipment
	Socioeconomic factors	• Consider workers' financial and living conditions	• Consider the living conditions of workers, as aspects such as exposure to noise and temperature extremes contributes to a lack of sleep and fatigue • Financial wellness of workers should be considered
	Commuting times	• Assess the length of time it takes for workers to commute to and home from work	• The total amount of time from when workers leave home before a work shift until returning home afterwards should allow for continuous sleep of seven to eight hours in each 24-hour period • Consider the availability or provision of transport for workers • Consider travel times of migrant workers to avoid high risk when travelling from or returning to work
	Social and domestic responsibilities	• Ensure that workers have sufficient time between shifts to attend to personal activities	• Workers should have sufficient time each day to attend to daily responsibilities • Workers should have time within their shift schedule to attend to family and social commitments, including shopping or going to the bank • Workers should have at least one weekend off per month
	Worker preferences	• Consider worker preferences in shift schedule design	• Consider employee preferences and needs in shift schedule design • Provide workers with information or training about shift work, and strategies to cope with irregular working hours • Consult with workers before changes to shift cycles are made
	Stakeholder engagement and change processes	• Follow a structured change management process, which includes and involves all stakeholders	• The following approach has been considered best practice for change management: ▪ Identify what will be changed/improved ▪ Use an inclusive process to arrive at a solid business case ▪ Plan for the change ▪ Provide resources and use data for evaluation ▪ Ensure effective communication ▪ Monitor and manage resistance, dependencies, and budgeting risks ▪ Celebrate success ▪ Review, revise and continuously improve

Baker, A., Heiler, K., and Ferguson, S.A. 2003. The impact of roster changes on absenteeism and incident frequency in an Australian coal mine. *Journal of Occupational and Environmental Medicine*, vol. 60. pp. 43–49.

Bates, D.W. 2009. Fatigue, resident work hours, and safety. *Medical Care*, vol. 47, no. 7, pp. 711–713.

Baulk, S.D., Fletcher, A., Kandelaars, K.J., Dawson, D., and Roach, G.D. 2009. A field study of sleep and fatigue in a regular rotating 12-h shift system. *Applied Ergonomics*, vol. 40, no. 4. pp. 694–698.

Brake, D.J. 2015. A review of good practice standards and re-entry procedures after blasting and gas detection generally in underground hardrock mines. *Proceedings of the 15th North American Mine Ventilation Symposium*, Backsburg, VA. Virginia Tech.

Brovko, F., Kgarume, T., Maseka, C., Sereme, B., and Ngobese, S. 2018. Work package 1: Detailed gap analysis and recommendation for process improvement of mining cycle elements of conventional gold and platinum operations in order to design a system to enable a blast per day that confirms to mine standard (Appendix A). 2018. *Technical LoCM Close-Out Report for the Period – 2017/2018*. Gumbie, A. (ed.). Longevity of Current Mines Programme. Mandela Mining Precinct, Johannesburg. Unpublished report.

Brown, M., Tucker, P., Rapport, F., Hutchings, H., Dahlgren, A., Davies, G., and Ebden, P. 2010. The impact of shift patterns on junior doctors' perceptions of fatigue, training, work/life balance and the role of social support. *Quality Safety Health Care*, vol. 19, no. 6. pp. 1–4.

Deloitte. 2014. The future of mining in South Africa: Innovation imperative. https://www2.deloitte.com/content/dam/Deloitte/za/Documents/energy-resources/ZA_Mine_of_the_Future_06022015.pdf [accessed 18 July 2018].

Department of Labour. 1993. Occupational Health and Safety Act. Act No. 85 of 1993. Republic of South Africa.

Department of Labour. 1997. Basic Conditions of Employment Act. Act No. 75 of 1997. Republic of South Africa.

Department of Labour. 1998. Code of Good Practice on the Arrangement of Working Time. Republic of South Africa.

Department of Mineral Resources. 1996. Mine Health and Safety Act. Act No. 29 of 1996. Republic of South Africa.

Department of Mineral Resources. 2014. Guideline for a Mandatory Code of Practice for Risk-Based Fatigue Management at Mines. Republic of South Africa.

Greubel, J., Arlinghaus, A., Nachreiner, F., and Lombardi, D.A. 2016. Higher risks when working unusual times? A cross-validation of the effects on safety, health, and work-life balance. *International Archives of Occupational and Environmental Health*, vol. 89, no. 8. pp. 1205–1214.

Gumbie, A. 2018. Technical LoCM Close-Out Report for the Period – 2017/2018. *Longevity of Current Mines Programme*. Mandela Mining Precinct, Johannesburg. Unpublished report.

Härmä, M., Karhula, K., Ropponen, A., Puttonen, S., Koskinen, A., Ojajärvi, A., Hakola, T., Pentti, J., Oksanen, T., Vahtera, J., and Kivimäki, M. 2018. Association of changes in work shifts and shift intensity with change in fatigue and disturbed sleep: a within-subject study. *Scandinavian Journal of Work, Environment and Health*, vol. 44, no. 4. pp. 394–402.

Health and Safety Executive (HSE). 2019. The development of a fatigue / risk index for shiftworkers. https://www.hse.gov.uk/research/rrhtm/rr446.htm# [accessed 13 September 2019].

Hodgskiss, J., Letsoalo, S., April, Y., and Schutte, S. 2015. Health and safety impacts of socioeconomic conditions and other matters relating to living conditions in the South African mining industry. *Project no*. SIM 13-09-01. Mine Health and Safety Council.

Jacobs, J. and Webber-Youngman, R.C.W. 2017. A technology map to facilitate the process of mine modernization throughout the mining cycle. *Journal of the Southern African Institute of Mining and Metallurgy*, vol. 117, no. 7. pp. 637–648.

Jacobsen, D.I. and Fjelldbraaten, E.M. 2018. Shift work and sickness absence-the mediating roles of work-home conflict and perceived health. *Human Resources Management*, vol. 57, no. 5. pp. 1145–1157.

Kalmbach, D.A., Fang, Y., Arnedt, T., Cochran, A.L., Deldin, P.J., Kaplin, A.I., and Sen, S. 2018. Effects of sleep, physical activity, and shift work on daily mood: a prospective mobile monitoring study of medical interns. *Journal of General Internal Medicine*, vol. 33, no. 6. pp. 914–920.

Lazare, R. 2013. SA Region Shift Optimisation-SVP Review. Unpublished report.

Minerals Council South Africa. 2018. Modernization: Towards the mine of tomorrow. Fact Sheet. http://www.mineralscouncil.org.za/industry-news/publications/fact-sheets/send/3-fact-sheets/378-modernisation-towards-the-mine-of-tomorrow [accessed 18 July 2018].

Neingo, P.N. and Cawood, F.T. 2014. Correlation of productivity trends with market factors at three selected platinum mines. *Proceedings of the 6th International Platinum Conference, 'Platinum – Metal for the Future'*, Sun City, South Africa, 20–22 October 2014. Southern African Institute of Mining and Metallurgy, Johannesburg. pp. 181–188.

Neingo, P.N. and Tholana, T. 2016. Trends in productivity in the South African gold mining industry. *Proceedings of the 23rd Internal Symposium on Mine Planning and Equipment Selection (MPES)* 2016, Sandton Convention Centre, Johannesburg, 8-11 November 2016. Southern African Institute of Mining and Metallurgy, Johannesburg.

Ngobese, S. 2017. Comparison of different shift rosters. CSIR, Pretoria. Unpublished report.

Pelders, J. and Nelson, G. 2019. Contributors to fatigue at a platinum smelter in South Africa. *Journal of the Southern African Institute for Mining and Metallurgy*, vol. 119, no. 3. pp. 313–319.

Pelders (Hodgskiss), J., Magweregwede, F., Maponya, R., Rupprecht, S.M., Hlatshwayo (Letsoalo), S., Nontso, Z., and Brovko, F. 2019. Shift cycles and productivity. Milestone 8: Final Report. *Longevity of Current Mines Programme*. Mandela Mining Precinct, Johannesburg. Unpublished report.

Pfeifer, C. 2017. An empirical note on commuting distance and sleep during workweek and weekend. *Bulletin of Economic Research*, vol. 70, no. 1. pp. 97–102.

Pickering, R., du Plessis, A., and Annandale, G. 2010. Hard-rock room and pillar mining best practice industry workshop. *Report no*. 01010-01. Centre for Mechanised Mining Systems, University of the Witwatersrand.

Roussos, M. 1996. Productivity barriers in the mining industry. MBA thesis, School of Business Administration, University of the Witwatersrand.

Rupprecht, S.M., Wilson, R.B., Lombard, H.E. and Peake, A.V. 2001. Transportation summary. DEEPMINE Collaborative Research Programme. March 2001.

Rupprecht, S.M. 2016. The need for material change in the South African mining industry. *New technology and innovation in the Minerals Industry Colloquium*, Emperor's Palace, 9-10 June 2016. Southern African Institute of Mining and Metallurgy, Johannesburg.

Rupprecht, S.M. 2018a. A move to a 12-hour working shift – The benefits and concerns. *Proceedings of the 27th International Symposium on Mine Planning and Equipment Selection*, Santiago, Chile. 20-22 November 2018. Springer. pp. 545–552.

Rupprecht, S.M. 2018b. Work Package 4: Ranking production related best practices based on current mining process and equipment available (Appendix E). Technical LoCM Close-Out Report for the Period – 2017/2018. Gumbie, A. (ed.). *Longevity of Current Mines Programme*. Mandela Mining Precinct, Johannesburg. Unpublished report.

Sanqu, A. 2016. An address on industry productivity: How bad (or good) are we really? *Joburg Indaba*, 5 October 2016. Chamber of Mines of South Africa.

Schutte, P.C. 2010a. Fatigue risk management: Charting a path to a safer workplace. *Journal of the Southern African Institute of Mining and Metallurgy*, vol. 110, pp. 53–55.

Schutte, P. 2010b. Heat stress management in hot mines. *Extracting the Science: A Century of Mining Research*. Brune, J.F. (ed.). Society for Mining, Metallurgy, and Exploration, Inc., Littleton, CO. pp. 30–34.

Sebutsoe, T. and Musingwini, C. 2017. Characterizing a mining production system for decision-making purposes in a platinum mine. *Journal of the Southern African Institute of Mining and Metallurgy*, vol. 112, no. 2. pp.199–206.

Singh, N. 2017. Weathering the 'perfect storm' facing the mining sector. *The Journal of the Southern African Institute of Mining and Metallurgy*, vol. 117, no. 3. pp. 223–229.

Smith, L., Folkard, S., Tucker, P., and Macdonald, I. 1998. Work shift duration: a review comparing eight hour and 12 hour shift systems. *Journal of Occupational Environmental Medicine*, vol. 55, no. 4. pp. 217–229.

Spencer, M.B., Robertson, K.A., and Folkard, S. 2006. The development of a fatigue / risk index for shiftworkers. *Research report no*. 446. Mine Health and Safety Executive.

Stenzel, G.G. 2002. Introduction of 12 hour shift and 4x4 roster working 24/7 at New Vaal Colliery. Colliery SACMA Meeting. Presentation at Goedehoop South African Colliery Managers Association.

Theron, W.J. 2014. Fatigue knowledge – A safety management imperative. AMMSA Safety General Meeting. Association of Mine Managers South Africa.

Van Ommeren, J. and Gutierrez-i-Puigarnau, E. 2009. Are workers with a long commute less productive? An empirical analysis of absenteeism. *Tinbergen Institute Discussion Paper.* no. 09-014/3. Tinbergen Institute, Amsterdam. ◆

Exxaro partners with the University of Pretoria in cutting-edge technology research programme to drive safer and sustainable mining

2 September 2021 — Pretoria

As part of its commitment to enhancing South Africa's educational and technological spheres, Exxaro Resources today announced a partnership with the University of Pretoria to establish the first ever Exxaro Chair in Extended Reality (XR) Technology.

Extended reality technology refers to all real-and-virtual combined environments and human-machine interactions generated by computer technology, including augmented reality (AR), mixed reality (MR), and virtual reality (VR).

Through this partnership, the Exxaro Chair in XR Technology will offer a framework firstly on how the XR technology can be used to address mining industry challenges, and secondly on identifying the best available technologies for the solutions. This investment in technological advancement will allow for constant research towards a safer, economical, and more environmentally sensitive form of mining.

'We are proud to have such a strategic partnership with the University of Pretoria and to be among the mining companies to explore the potential benefits of XR technology as a strategic intervention across its operations' says Exxaro CEO Mxolisi Mgojo. 'Together, we are expanding upon the practical capabilities of XR in the South African context while supporting our need for industry to embrace the opportunities of the 4th Industrial Revolution. The possibilities of what we could develop are really exciting.'

Exxaro will work with the Virtual Reality and Interaction (VRI) Laboratory, an initiative of the Department of Information Science at the University of Pretoria, as well as the Department of Mining Engineering. The VRI Laboratory applies XR technologies to create interactive user experiences for various applications.

The Exxaro Chair in XR Technology programme will assist in selecting the most effective XR technology for specific applications, and then design methods that can enable intuitive interaction with the virtual environment. It will also offer extensive user testing of proposed solutions to ensure that the solutions address and solve as many of the challenges as possible.

Among the solutions that will be explored are the application of individual and shared VR; mobile, tethered, and cave setup VR; communication VR; tracked and untracked VR space; as well as hand tracking and full body tracking.

Professor Ina Fourie, the Head of the Department of Information Science and the inaugural Exxaro Chair in XR Technology said 'Exxaro opens new opportunities for us to excel in industry-related XR research. They offer us an opportunity to become international leaders in the use of XR technology in the mining industry and mining safety. Many other applications and opportunities can follow'.

'The EBIT Faculty is honoured to work with an industry leading company such as Exxaro in taking the UN Sustainable Development Goals (SDGs), especially SDG 9 – Industry, Innovation, and Infrastructure, and also to strengthen SDG 8, which is Decent Work and Economic Growth, both being what South Africa desperately needs' says Professor Sunil Maharaj, Dean of the University of Pretoria's Faculty of Engineering, Built & Information Technology.

Mgojo concludes, 'We are extremely excited for this partnership as part of our drive to support research that overcomes the obstacles associated with the 4th Industrial Revolution. We believe that XR technology has immense applications for dealing with mining-related challenges and that can optimize the resources of companies like Exxaro.'

PlatMine pillar strength formula for the UG2 Reef

B.P. Watson[1], R.A. Lamos[2], and D.P. Roberts[3]

Affiliation:
[1]University of Witwatersrand, South Africa.
[2]Mine Support Consultants, South Africa.
[3]Sibanyestillwater, South Africa.

Correspondence to:
B.P. Watson

Email:
Bryan.Watson@wits.ac.za

Dates:
Received: 22 Sep. 2020
Revised: 17 Mar. 2021
Accepted: 6 Jun. 2021
Published: August 2021

How to cite:
Watson, B.P., Lamos, R.A. and Roberts, D.P. 2021
PlatMine pillar strength formula for the UG2 Reef.
Journal of the Southern African Institute of Mining and Metallurgy, vol. 121, no. 8, pp. 437–448

DOI ID:
http://dx.doi.org/10.17159/2411-9717/1387/2021

ORCID:
B.P. Watson
https://orcid.org/0000-0003-0787-8767
D.P. Roberts
https://orcid.org/0000-0002-7517-4836

Synopsis

The Upper Group 2 (UG2) chromitite reef is a shallow-dipping stratiform tabular orebody in the South African Bushveld Complex, which strikes for hundreds of kilometres. Mining is extensive, with depths ranging from close-to-surface to 2 500 m. Pillars are widely used to support the open stopes and bords. Little work has been done in the past to determine the strength of pillars on the UG2 Reef and design was done using formulae developed for other hard-rock mines. This has led to oversized pillars with consequent sterilization of ore. In this paper we describe a back-analysis of stable and failed UG2 pillars on the Bushveld platinum mines, and provides a strength formula for UG2 pillars. The formula may be used cautiously on all Bushveld platinum mines with similar geotechnical, geometrical, and geomechanical conditions to the pillars in the database.

Keywords
UG2, pillar strength formula, chromitite, back-analysis.

Introduction

The Bushveld Complex in the northern part of South Africa is a large layered igneous intrusion, which spans about 350 km from east to west (Figure 1). The platinum group metals are concentrated in two planar, shallow-dipping orebodies (reefs):

- The Upper Group 2 (UG2), chromitite seams
- The Merensky Reef, a mineralized pegmatoidal pyroxenite.

The Merensky Reef overlies the UG2 Reef, and the width of both ranges between 0.7 m and 1.5 m.

The strata generally dip at 8° to 15° toward the centre of the Complex, with a horizontal to vertical stress ratio (*k*-ratio) ranging from about 0.5 to over 2.5. The depth of mining ranges from outcrop to 2 500 m. Generally, the lower *k*-ratios are a feature of deeper level reefs.

In the depth range from surface to about 1 400 m, the vertical tensile zone often extends high into the hangingwall (roof). If the mining span is sufficiently large, or the stope abuts a geological feature, a large volume of hangingwall rock can become unstable, resulting in a stope collapse, or colloquially, a 'backbreak' (Roberts *et al.*, 1997). In order to prevent these backbreaks, a high-resistance support system is required. This is universally achieved using in-stope pillars. Conventional mining makes use of crush or yielding chain-pillars between 30 m wide panels. These pillars are oriented either on strike for breast mining (Figure 2) or on dip for up- and down-dip mining.

The in-panel pillars shown in Figure 2 are for a breast mining configuration, meaning that the faces are advanced on strike. These in-panel pillars are often located 1.5 m to 2.0 m below a gully (Figure 3) used to assist with ore removal to the boxholes or local orepasses. The zone between the gully and the pillar is termed a siding (Figure 3). Some mines do not make use of sidings (Figure 3), so that the in-panel pillar is higher on the gully side than on the panel side. Gully heights vary between 1.8 m and 2.5 m. Thus, typical pillars under these conditions could have a height of 2.3 m on the up-dip side and 1.5 m on the down-dip side.

Mechanization of the platinum mines has resulted in an increase in bord-and-pillar mining, particularly in the newer, shallow-depth mines on the eastern side of the Bushveld Complex. The Hedley and Grant formula (Hedley and Grant, 1972), developed for Canadian uranium mines, has become the industry accepted method for designing hard-rock pillars in shallow hard-rock mines in South Africa (Malan and Napier, 2011). This equation has been employed to design pillars on the UG2 Reef for many

PlatMine pillar strength formula for the UG2 Reef

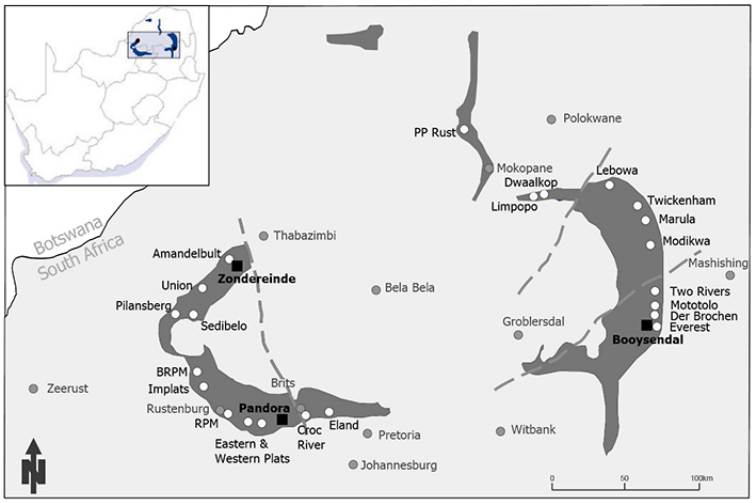

Figure 1—The extent of the Bushveld platinum exposure in South Africa, shown in relation to major towns (Northam Platinum Limited, 2018)

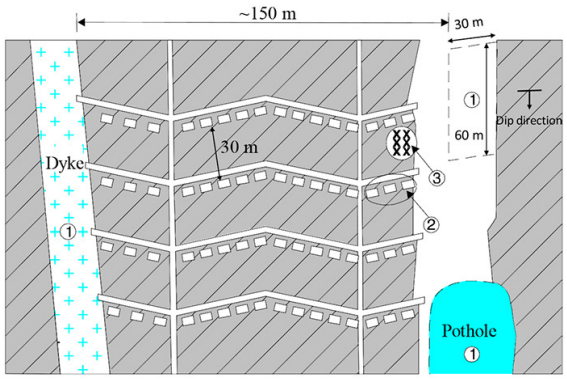

Figure 2—Plan view of a typical conventional mining layout with (1) regional stability pillars, often entailing loss of ground, (2) in-panel (crush) pillars; (3) local timber support (Jager and Ryder, 1999)

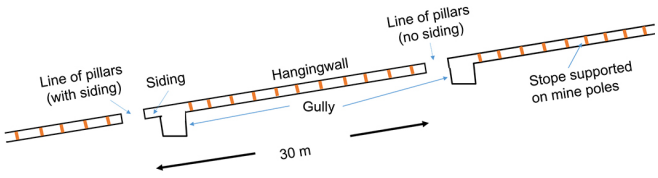

Figure 3—Section through typical conventional stopes showing gullies with and without sidings

years, using a downrated *k*-value of 35 MPa, which is about a third of the uniaxial compressive strength (UCS) of the pillar material (Malan and Napier, 2011). However, the formulation of the equation is based on a large number of unproven assumptions, and its application to the design of pillars in the Bushveld Complex is questionable (Malan and Napier, 2011). A potential consequence of using this uncertain methodology is to cut oversized pillars, which lowers the extraction ratio.

In order to remedy the lack of certainty in pillar design on the UG2 Reef, research was carried out to determine a pillar formula particularly suited to the reef. A maximum likelihood (ML) back-analysis study was conducted on failed and stable pillars, and a strength formula was developed for the UG2 Reef on the western side of the Bushveld Complex.

With the exception of pillars affected by thrust structures or weakened due to weathering, no failed pillars were available in the UG2 bord-and-pillar workings for the database. It was therefore necessary to assess pillars mined in the conventional stopes, where much larger spans were mined on either side of the pillars. In many instances, sidings were not left adjacent to the pillars, therefore pillar heights needed to be adjusted in the database to account for these gullies.

The CSIR in South Africa was sponsored by platinum mining companies and the government to conduct research that would improve mining conditions on the platinum mines. The reports that were produced by the PlatMine research collaborative belong to the sponsors, and there was a restriction (now expired) on publications for a period of five years. The back-analyses work described in this report was done under PlatMine 1.2 (Watson *et al.*, 2007) and completed in 2007.

Data collection procedures

Site observations

The *in-situ* dimensions of the evaluated pillars were measured directly and the presence/absence of sidings adjacent to pillars was evaluated in the same way as described in Watson *et al.* (2008). Pillar conditions were documented according to the following scale of condition codes (CC):

- 5: Pillar heavily damaged, date/geometry at failure not accurately known
- 4: Pillar presumed failed, date/geometry at failure not accurately known
- 3: Pillar definitely failed (or burst), date/geometry at failure known
- 2: Pillar sidewalls visibly fractured/scaled, date/geometry known
- 1: Pillar sidewall scaling barely visible, date/geometry known
- 0: Pillar with no visible damage, date/geometry known.

Pillars with CC 3 were the most directly relevant for back-analysing strength parameters, but no pillar bursts occurred that could be used to determine the date (and therefore the mining configuration) on which failure took place. Therefore, no CC 3 pillars are in the database. The evaluations relied heavily on visual observations, and therefore CC 0 to CC 2 (unfailed) and CC 4 to CC 5 (failed) pillars were lumped together in the strength analysis, *i.e.*, pillars were either unfailed or failed. The pillars

classified as CC 4 and CC 5 had failed at face positions that were different to when the observations were made, hence the face positions used in the numerical models would have resulted in an over-estimation of the stress condition at failure.

Pillar load estimation

Pillar loads were estimated using pseudo-3D, elastic, boundary displacement-discontinuity element modelling software, MinSim (COMRO, 1981) and MINF (Spottiswoode and Milev, 2002). Mine plans were digitized, capturing – in each instance – an area large enough to provide realistic stress conditions. Usually, these conditions were inferred by direct modelling and subsequent elimination of superfluous abutting mining windows. In many cases, it was necessary to estimate a correction factor (CF), based on a comparison of coarse-grid average pillar stress (APS) values on large pillars near the areas of interest, with and without a large flanking area of mining. Such factors were generally less than 1.2 (20% correction), and were, where feasible, checked using Equation [1] (Ryder *et al.*, 2005). This equation may be used if there is a large area of mining with roughly uniform convergence S over a sector bounded by radii R_1 and R_2 (Figure 4).

$$\left(\frac{\sigma_{zz}}{q}\right) \approx \underline{S}\left(\frac{\theta}{2\pi}\right)\left(\frac{1}{R_1}-\frac{1}{R_2}\right) \qquad [1]$$

where σ_{zz} is the stress resulting from a large area of mining, $S = (E^*S/q)$ is the normalized average convergence in this region, where S is the convergence and q is the virgin vertical stress. $E^* = E/4(1-\nu^2)$ where E is the Young's modulus and ν is the Poisson's ratio.

If, for example, the right-hand side of Equation [1] evaluates to 0.2, then the driving stress on the area of interest (and all calculated convergence or APS values) need to be increased by 20%.

A grid size of 0.5 m was used in order to adequately capture true pillar dimensions in the area of interest (Napier and Malan, 2011). The modelling results were validated, where possible, by analytic solutions and by comparing MinSim and MINF results. Discrepancies of less than 10% in APS values were determined from the comparisons. An average rock density of 3000 kg/m^3 was assumed in all cases, and pillar stresses were calculated based on depth of cover, extent of mining around the pillar, and the size of the pillar. The effects of adjacent pillars and abutments were also considered in the models.

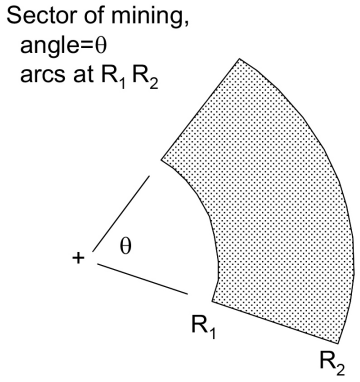

Figure 4—Areas of remote mining, well outside the centre (+) of the area of interest (Watson *et al.*, 2008)

Generally, a series of modelling runs was carried out. In the first run, all small pillars were modelled as intact structures. In the second run, any pillars carrying more load and being smaller than observed failed pillars in an area of interest were deemed to have failed, assigned a CC of 4 or 5, and allocated a residual stress of 20 MPa as suggested by Watson *et al.* (2007) and Roberts *et al.* (2005). This procedure was repeated until no further pillars fulfilled the failure criterion. The limit equilibrium model suggested by Napier and Malan (2012) has a number of parameters to calibrate, but for the purposes of the back-analysis it was more efficient to simply reduce the pillar strengths to 20 MPa, so that the stress could be appropriately redistributed to the intact pillars.

In the analysis, where necessary, an 'effective height' (h_e) was calculated to allow for the presence of gullies unprotected by sidings (Figure 3) using Equation [2]. The correction is based on numerical modelling by Roberts *et al.* (2002).

$$h_e \approx \left[1 + 0.2692\left(w/h_g\right)^{0.08}\right] \qquad [2]$$

where w and h are the pillar width and mining height respectively, and h_g is the gully vertical height. As a typical example: the effective height (in terms of expected strength) of a siding-less pillar with a gully vertical height of 2.3 m increases from 1.5 m to about 1.9 m.

The effective pillar width (w_e) accounts for rectangular pillars, taking cognisance of pillar length (L), according to the widely used 'perimeter rule', described by Wagner (1974):

$$w_e \approx 2wL/(w+L) \qquad [3]$$

Note that this rule leads to considerable increases in pillar w_e, ranging up to near doubling of effective width for very long rectangular pillars.

Strength parameter estimation

The strength of a pillar may be assumed to be a function of its known *physical* characteristics (including width, height, length), and certain unknown parameters (*e.g.*, Salamon and Munro, 1967: K, α, β values). An ML analysis was used to estimate a best fit for these parameters. This type of statistical back-analysis accounts for the many variables that contribute to pillar strength without necessarily needing to understand the failure mechanisms. The process involved the evaluation of a database of APS values calculated by MinSim (COMRO, 1981) where the 'condition', *i.e.*, 'intact' or 'failed', was known.

Following the approach of Salamon and Munro (1967), the SF of each pillar was defined by:

$$SF = Strength/APS \qquad [4]$$

A probabilistic *distribution* of SFs governs the condition of pillars, in the sense that a pillar with SF>1 is likely to be intact, while one with SF<1 is likely to have failed. A lognormal distribution was assumed for the SFs, having a log-mean of zero and standard deviation of S. With this formulation, physically meaningless negative SFs are disbarred, and reciprocal symmetry pertains, *e.g.*, a pillar having SF = 0.5 is about as likely to have failed as one with SF = 2 is to have not failed. The logarithmic standard deviation was assumed to account for all uncertainties in the system of pillars, *e.g.*, mismeasurement of widths, mis-estimating of pillar APS values, real geotechnical variations in pillar properties, *etc.* For historical reasons, logarithms to base 10

are used in the lognormal distribution of SFs, and to interpret S, $10^{\pm S}$ needs to be evaluated in relation to unity. The value of S is a parameter that the ML analysis must estimate along with the unknown parameters governing the strength of the pillars in a given data-set.

A 'likelihood function' (L_i) of the probability of the pillars exhibiting their stipulated condition ('intact' or 'failed') was set up. The logarithm (base e) of Li was used so that the function F was defined as:

$$F = \ln L_i = \sum \ln(\text{prob. of intact cases}) + \sum \ln(\text{prob. of failed cases}) \quad [5]$$

The probability of an intact case (condition codes CC = 0, 1, or 2 in this study) was given by ϕ(log SF) where ϕ is the cumulative normal distribution of SFs. Such cases biased the derived best parameter fits so that their SFs were as large as possible.

The probability of a failed case in which the APS value was the estimated load at which failure occurred (the situation in Salamon and Munro's (1967) back-analysis, and CC=3 in the present study) was not used as there were no pillars where the actual stress at failure could be determined. The function ϕ(log SF)/SF, where ϕ is the normal probability density function of SFs, would have been used in these instances.

The probability of a failed case where the APS was merely an upper bound and failure probably took place earlier at some lower APS value (the situation in many of the back-analysis scenarios where CC = 4 or 5) was expressed by the function 1 – ϕ(log SF). This is analogous to the treatment of intact cases and biased the best-fit parameters so that the SFs were as small as possible. Thus, the ML analyses included the presence of stable cases having low SFs and the failed cases. Equation [5] could thus be rewritten as follows:

$$F = \ln L_i = \sum \ln\left(\phi(\log SF)\right) + \sum \ln\left((1-\phi(\log SF))\right) \quad [6]$$

Validation of the numerical models used to estimate pillar loads (APS)

A system of regularly spaced, stable, Merensky Reef rib pillars at a mine on the western side of the Bushveld (western limb) provided an unusual quasi-2D situation where the numerical models could be validated against an analytic solution. Figure 5 depicts the geometry of this control site.

A 7 m wide by 1.4 m high dip pillar, with 28 m mined-out panels on either side, was observed *in situ* to be just beginning to scale (CC=1). The APS provided by the MinSim model was 80.8 MPa. This result compared favourably with an analytic estimate of 82 MPa using tributary area theory.

Data collection sites

Data on failed and unfailed pillars was collected from a total of four sites at three separate mines near the town of Thabazimbi (see Figure 1) for ML regression analyses. The pillars were composite, consisting mainly of chromitite with one or two narrow pyroxenite bands of variable width above the pillar centre (Figure 6). The immediate hangingwall and footwall (floor) materials were pyroxenite and anorthosite, respectively.

Mine A – Stope 1

Except for the mining of one panel at the bottom of the stope on the south-west side (Figure 7), all mining activities in this area were completed some years prior to the investigation. Time-dependent rock mass deformation may have resulted in pillar failures occurring at loads lower than the original strength of the pillars. Substantial remnants were left on the previously mined Merensky horizon above the UG2 workings, both to the southwestern and northern limits of the investigation site (middling 20 m), and these remnants are shown as dashed lines in Figure 7. The dip of the orebody is 18°.

During the investigations, it was apparent that seismic events had caused minor damage to the south-west side of the stope. The events may have resulted in premature pillar failure and excessive slabbing on the sides of pillars. Two pillars had obviously failed, and were therefore included in the model with a residual strength of 20 MPa.

Pillar 1 (Figure 7) was wedge-shaped, and the south-west side of the pillar was crushed. However, the wider end had caused hangingwall damage, and was obviously carrying a significant load. In addition, Pillar 2 caused hangingwall damage from about its mid-point towards the south-west (Figure 7). Pillar 8, on the west side of the stope and close to the overlying Merensky abutment (Figure 7), suffered a strain-burst after mining and ore removal had been completed in the stope (Figure 8). It was assumed that the peak strength of this pillar was almost reached when the stope reached its mining limits.

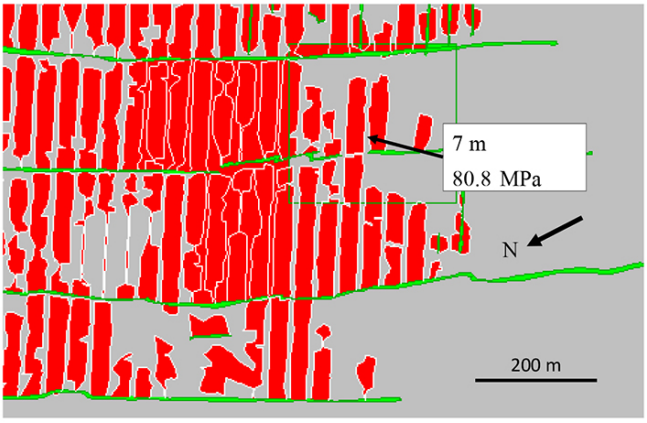

Figure 5—Dip pillar geometry: mined area in red, solid area grey (grid size 0.5 m, depth 660 m, dip 9°, stope width 1.4 m, k = 1)

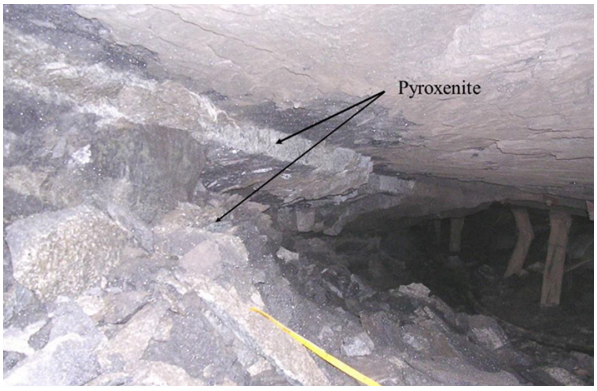

Figure 6—A typical composite pillar used in the statistical evaluations

PlatMine pillar strength formula for the UG2 Reef

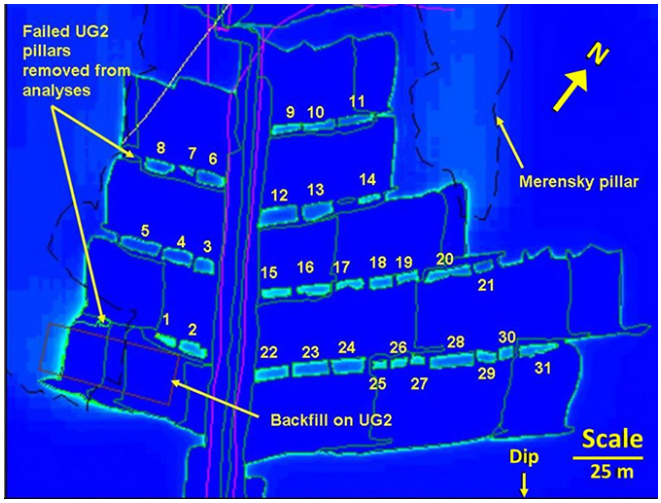

Figure 7—Mine plan showing the Mine A UG2 workings (the Merensky remnants shown by black dashed lines). The various shades of blue indicate stress conditions on the UG2. The dark colour represents de-stressed conditions and the lighter colours show the stress effects of Merensky Reef pillars on the UG2 pillars and stope faces (depth 1 670 m below surface)

Figure 8—Down-dip side of Pillar 8. View away from panel face

Blast-hole sockets in the access excavations suggested a *k*-ratio of 0.5 (Watson *et al.*, 2006). The depth of the workings was 1 670 m below surface, and the standard average rock density of 3000 kg/m^3 was assumed in the model. The results of the modelling and underground investigations are shown in Table I. Note that corrections for gullies and pillar length were applied to the width and height calculations. The low stresses on some pillars shown in Table I were due to the de-stressing effects of the pre-mined Merensky Reef.

Mine A – Stope 2

The stope shown in Figure 9 had been mined out several years before the investigation and no mining was being done in the area at the time of the evaluation. Both the 4E and 5E panels were backfilled and sidings were left adjacent to most of the pillars. A large remnant on the previously mined Merensky horizon was situated over the area of interest (dashed line in Figure 9). Pillars on the UG2 horizon were in various stages of failure and poor hangingwall conditions persisted above the 5E advanced strike gully (ASG), immediately below the Merensky remnant. A large UG2 pillar was left below the Merensky remnant, because of poor mining conditions experienced in the 4E panel (Figure 9). The middling between the two reefs was 20 m.

Pillars 2, 3, 6, 7, and 8 (Figure 9) were highly fractured (Figure 10) and between 70 mm and 200 mm of closure was estimated from adjacent mine poles. These pillars were obviously in an advanced stage of crushing. Pillar 1 and 4 (Figure 9) were also heavily fractured but fracturing in the hangingwall adjacent to the pillars suggested that the cores were still intact.

The effects of Merensky Reef remote mining could not be directly established in a single model with a grid size of 0.5 m.

Table I

Results of the stress modelling and underground investigations – Mine A Stope 1

Pillar no.	*L* (m)	h_e (m)	w_e (m)	APS	CC
2	10.9	1.9	5.2	191	2
3	6.4	1.9	5.1	89	2
4	10.4	1.9	6.2	106	2
5	12.8	1.9	5.9	153	2
6	9.8	1.9	5.5	82	2
8	9.4	1.9	5.4	200	2
9	12.6	1.9	4.2	57	2
10	10.2	1.9	5.2	69	2
12	14.0	1.9	8.2	25	1
13	11.4	1.9	6.6	43	1
15	9.8	1.9	4.4	33	1
16	11.4	1.9	5.7	20	1
17	10.0	1.9	4.6	36	1
18	8.4	1.9	5.4	51	1
19	8.2	1.9	4.9	97	2
20	14.8	1.9	5.8	120	2
21	6.2	1.9	5.1	109	2
22	12.2	1.9	6.9	27	1
23	12.9	1.9	7.0	8	0
24	14.2	1.9	7.2	5	0
25	5.6	1.9	4.5	9	0
26	5.6	1.9	4.5	14	0
27	5.2	1.9	4.1	20	0
28	14.8	1.9	5.5	16	1
29	5.0	1.9	4.0	23	1
30	5.0	1.9	4.4	29	2
31	14.0	1.9	4.9	26	1

L pillar length, w_e effective pillar width, h_e effective pillar height, APS average pillar strength, CC condition code (0 = no damage, 2 = pillar sidewalls visibly spalled/scaled)

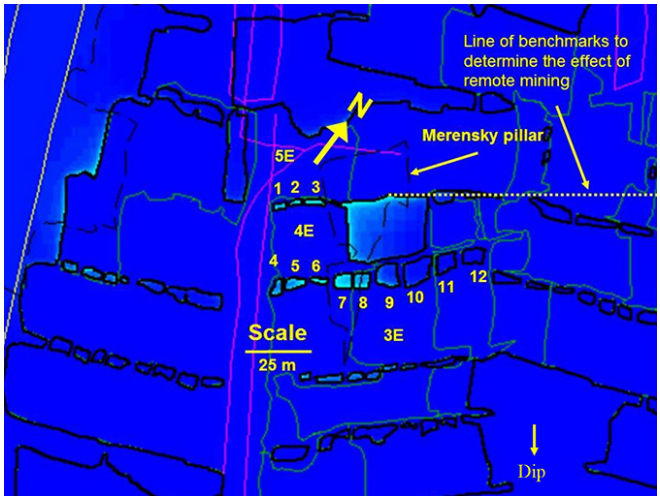

Figure 9—Plan showing Mine A UG2 stope 2 and the Merensky remnant (dashed) (depth 1 500 m, dip 18°). The various shades of blue indicate stress conditions on the UG2. The dark colour represents de-stressed conditions and the lighter colours show the stress effects of Merensky Reef pillars on the UG2 pillars and stope faces

Figure 10—Down-dip side of pillar 3

The final model was corrected for external mining (outside the model window) by means of a factor, which was determined from secondary MinSim modelling using a larger grid size. The correction factor was established on the assumption of no mining having occurred on the UG2 horizon. Two 1 m grid models were run, covering the whole mine and the area of interest, respectively. A line of benchmarks located on the UG2 horizon in the area of interest (Figure 9) was used to interrogate the effects of the Merensky abutment in both models. The results from the benchmark points showed that the remote Merensky mining provided an additional 20% load to the area of interest (CF = 1.20). The contribution of the limited UG2 mining outside the area of interest was not included in the analyses, but the effects are expected to be less than 5%, due to the de-stressing effects of the extensive mining on the Merensky Reef above. The results of the investigation are provided in Table II. None of the pillars had burst subsequent to sweeping operations. The date at which these pillars failed is therefore unknown and no CC3 pillars are recorded.

Mine B declines

The stope shown in Figure 11 was mined out several years before the investigation. The overlying Merensky Reef was mined out prior to the UG2 workings. A collapse occurred on the UG2 horizon in the two panels, shown in the figure (green outline), when the up-dip panel reached a position about halfway under the Merensky pillar (grey outline). In the down-dip panel, the collapse was bounded by a shear plane (black line). The middling between the two reefs was 34 m. The direction of mining in the lower panel is shown by the arrow.

Referring to Figure 11, a progression of pillar failure was observed:

- No fracturing on pillar 1
- Minor fracturing on the corners of pillars 2 and 3
- Significant fracturing to a depth of about 100 mm, from the original sidewall, on Pillar 4
- Large-scale slabbing and minor hangingwall damage on pillar 5
- A high degree of damage on pillars 6 and 7.

Figure 12 shows the condition of pillar 5, suggesting that the pillar was highly stressed.

The results of the numerical modelling and underground investigations are shown in Table III. No sidings were left, so corrections to the height and width were made to account for the additional height on the one side of the pillar and the pillar length, respectively.

Table II

Results of the Mine A stope 2 UG2 site

Pillar no.	*L* (m)	h_e (m)	w_e (m)	APS	CC
1	4.0	1.5	2.7	85	2
2	2.5	1.5	1.8	109	4
3	7.0	1.5	2.7	178	4
4	3.5	1.9	3.7	89	2
5	7.0	1.5	4.5	140	2
6	6.0	1.5	3.0	212	4
7	5.6	1.5	5.3	305	4
8	5.7	1.5	5.3	223	4
9	7.6	2.0	7.4	155	2
10	9.2	2.0	8.0	61	1
11	6.7	1.9	6.0	4	0
12	7.2	1.9	5.6	61	1

L pillar length, w_e effective pillar width, h_e effective pillar height, APS average pillar stress, CC condition code (0 = no damage, 2 = pillar sidewalls visibly spalled/scaled, 4 = pillar presumed failed)

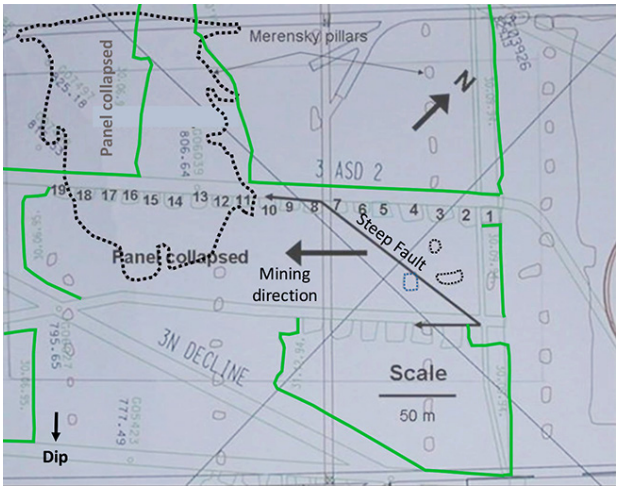

Figure 11—Plan showing the Mine B UG2 declines investigation site (depth 150 m, dip 18°)

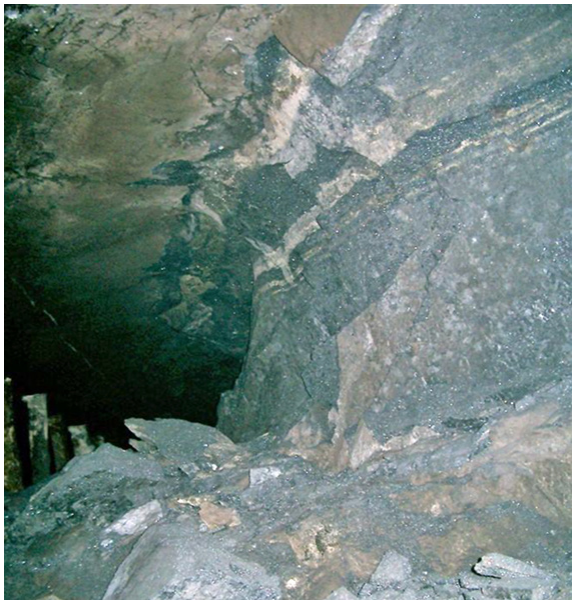

Figure 12—Significant damage to pillar 5 and adjacent hangingwall

Table III

MinSim results of the Mine B UG2 declines

Pillar no.	L (m)	h_e (m)	w_e (m)	APS	CC
1	6.0	1.9	5.5	27	0
2	5.0	1.9	5.0	45	1
3	9.0	1.9	6.4	55	1
4	8.0	1.9	6.2	66	2
5	5.5	1.9	3.9	77	2
6	6.0	1.9	4.8	63	2
7	6.0	1.9	4.8	53	2
8	6.0	1.9	4.0	55	2
9	5.0	1.9	3.8	66	2
10	5.0	1.9	3.8	73	2
11	7.0	1.9	5.1	77	2
12	5.0	1.9	4.4	90	2
13	6.0	1.9	5.5	88	2
14	5.0	1.9	4.1	91	2
15	6.0	1.9	4.8	101	2
17	7.0	1.9	4.2	102	2
18	5.0	1.9	3.8	81	2

L pllar length, w_e effective pillar width, h_e effective pillar height, APS average pillar strength, CC condition code

Mine C

The Merensky Reef was mined many years before the UG2, and some remnant pillars were left on the Merensky horizon. The middling between the two reefs is about 30 m. Subsequent mining of the UG2 Reef occurred under some of these remnants, providing, in some cases, both solid and crush pillars in a single panel. The condition of the recorded UG2 pillars was determined from visual observations. Thirty of these pillars were very heavily damaged and presumed failed. Modelled elastic stresses on the UG2 pillars ranged up to several hundred MPa due to the presence of extensive Merensky over-mining and scattered stress-concentrating remnants. The modelled geometry is shown in Figure 13. Each square represents a separate model.

Pillar size measurements were not made underground at this site. Scaled measurements were determined from plans. Some degree of uncertainty regarding the accuracy of the pillar dimensions on the plans necessitated a preliminary ML back-analysis to determine the value of the data. The analysis provided a good separation between failed and stable pillars (Figure 14), and the data was considered useful with only a few outliers. Although the effective pillar height was limited to about 1.9 m there was a significant range in width and length, providing a variety in $(w/h)_e$ contribution of between 1.2 and 4.7. The database of pillars from Mine C is provided in Appendix A.

The site was re-modelled using larger (and therefore fewer) MinSim windows, and a larger Merensky area (to account for remote mining), and the failed pillars on the UG2 elevation were replaced with a 20 MPa material. 111 pillars were added to the investigations.

Maximum likelihood evaluation

Database description

The total database consisted of 167 pillars, 134 of which represented modelled stresses at some value below the best-fit strengths, and 33 provided stresses somewhat higher than the strengths. Most of the pillar $(w/h)_e$ ratios ranged between 1.5 and 4, with the largest proportion being between 2.0 and 3.0 (Figure 15). No data was available below 1.1 or greater than 4.7.

The data-set included a wide range of pillar lengths (Figure 16) and w_e (Figure 17), but h_e fell into the limited range between 1.5 m and 2 m (Figure 18).

The value of K (the *in-situ* strength of a pillar of unit width and height) and exponents for the power formula were back-fitted, using an ML evaluation.

Pillar peak strength formula

Table IV shows the results of the standard power formula backfit (Equation 7). The length-strengthening effects are implicit in the use of the perimeter-rule (Equation 3), *i.e.*, effective width, w_e.

$$Strength = Kw_e^{\alpha}h_e^{\beta} \quad [7]$$

These α and β values differ significantly from the values back-fitted for the Hedley and Grant (1972) formula ($\alpha = 0.50$, $\beta = -0.75$) for quartzite. However, they are much closer to the

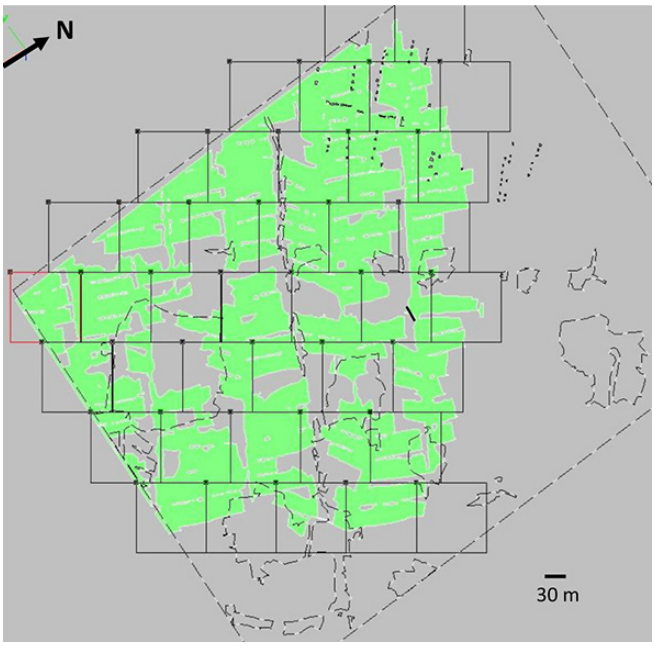

Figure 13—Mine C UG2 mining, modelled with 0.5 m grid size. Overlying Merensky Reef mining (5 m grid size) is shown by dashed lines and the UG2 mining is shown in green (depth 350 m – 650 m, dip 20°, middling 30 m)

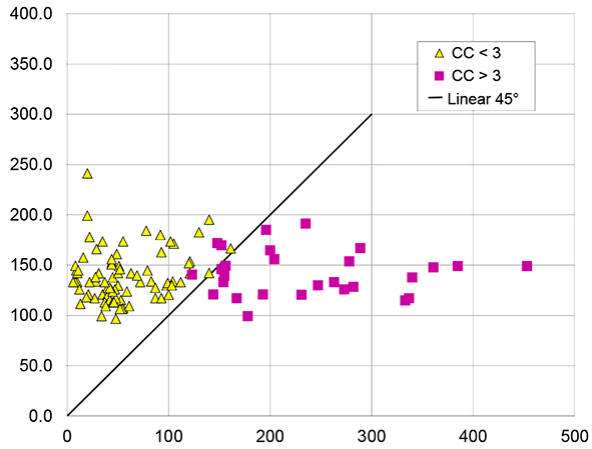

Figure 14—Back-analysis of Mine C UG2 pillars. Failed pillars are all 'condition 4' – exact date/geometry at failure not known. Triangles represent unfailed pillars, and squares failed

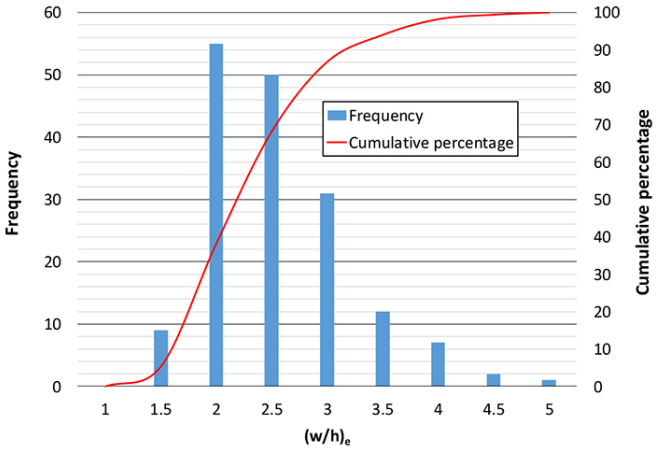

Figure 15—Distribution of pillar w_e/h_e in the database

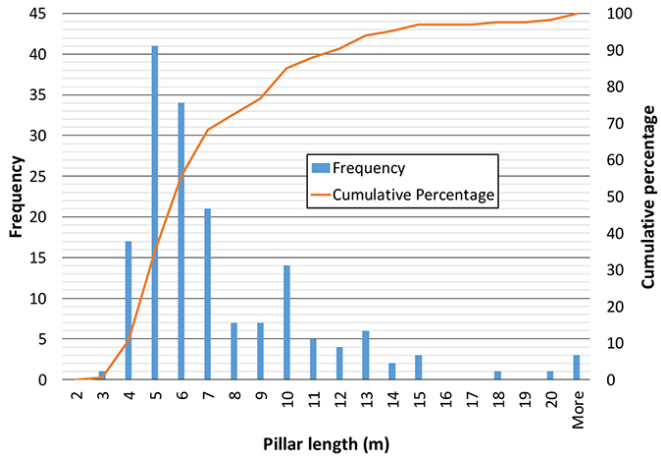

Figure 16—Distribution of pillar lengths in the database

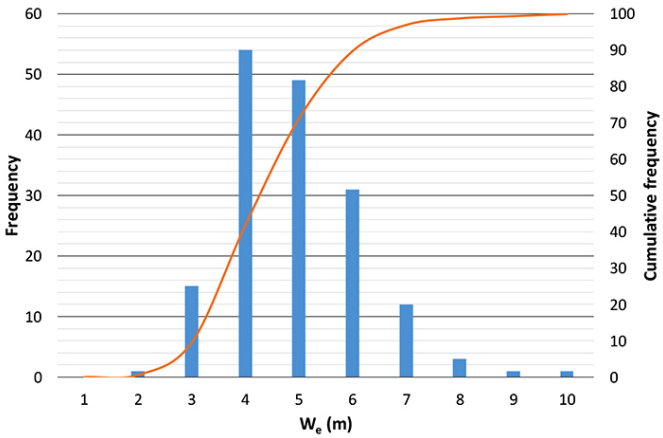

Figure 17—Distribution of pillar w_e in the database

Merensky formula (Watson *et al.*, 2008) where a = 0.76 and β = -0.36. Jager and Ryder (1999) suggest that chromitite has a slightly higher average angle of internal friction than quartzite, which could explain the greater strengthening effects of the α value. In addition, the material brittleness (rate of cohesion softening) has a major influence on the pillar strength (Watson *et al.*, 2008). The results of the three hard-rock formulae are compared in Figure 19. Note that the commonly used K = 35 MPa (Fernandes, 2020) was assumed in the Hedley and Grant formula

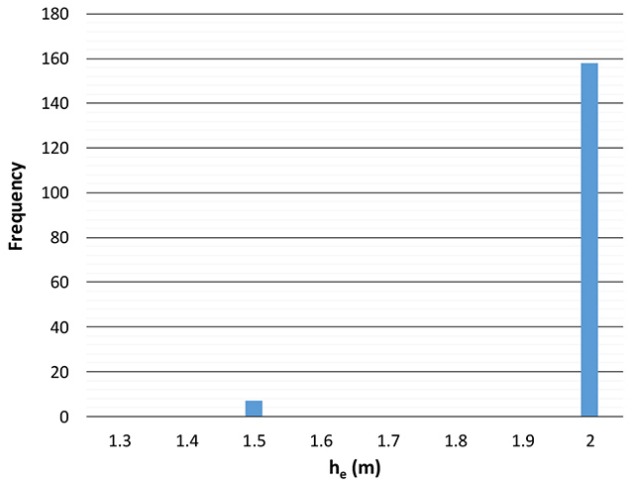

Figure 18—Distribution of pillar h_e in the database

Table IV

Back-fit values for Equation [7]

Parameter	Value
K	67
α (Effective width exponent)	0.67
β (Effective height exponent)	–0.32
S	0.068

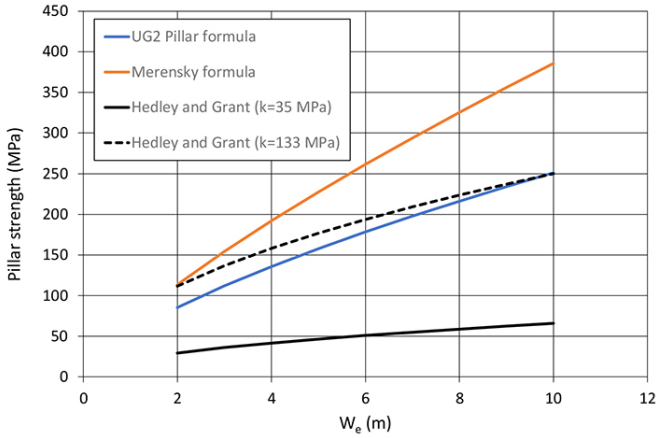

Figure 19—Comparison between the UG2 formula (Table IV), Merensky formula (Watson *et al.*, 2008) and Hedley and Grant formula (1972) for square pillars of 2 m height

(1972). For completeness, the Hedley and Grant formula with k = 133 MPa (Martin and Maybee, 2000) is included in the figure.

Figure 20 compares the modelled and calculated APS values. The investigations suggest a good correlation between calculated and actual strengths. The small standard deviation (S in Table IV) also confirms that the formula provides a reliable relationship between strength and $(w/h)_e$ ratio for the range of pillar we and he in the database. The green coloured triangles and squares in Figure 20 show the distribution of 1.5 m high pillars in the database.

The value of S (Table IV) was used to determine a range of safety factors, which are plotted as a function of probability of stability in Figure 21. The analyses include the presence of stable

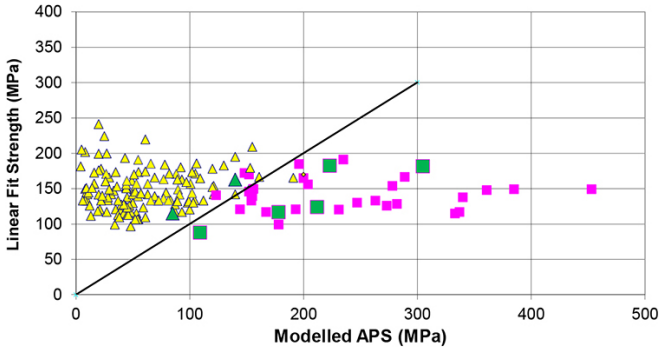

Figure 20—Back-fit strengths, using the power pillar-strength formula. Triangles represent unfailed pillars, and squares failed. Green symbols are distribution of h_e = 1.5 m pillars in the database

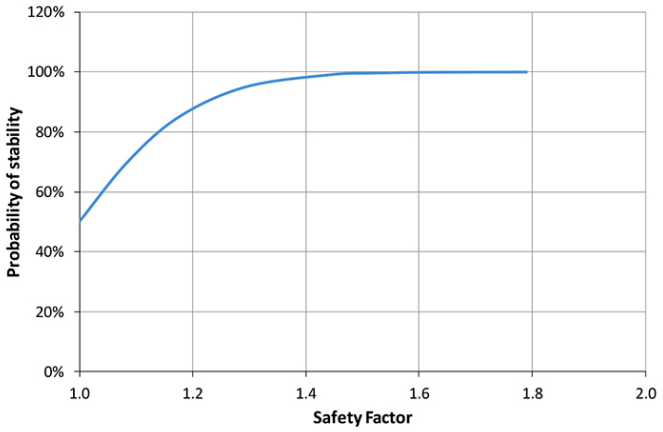

Figure 21—FOS for the pillars in the database as a function of probability of stability, based on the power formula back-fit analysis (log S = 0.068)

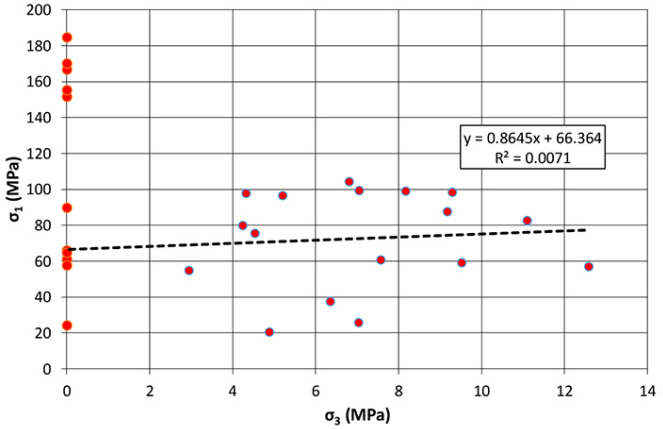

Figure 22—Uniaxial and triaxial UG2 chromitite strength test results from Impala Platinum (Gardner and Bosman, 2014)

cases (low SFs) and the failed cases. This graph may be used when designing stable UG2 pillars with dimensions within the range of the database. The analysis suggests that a SF of 1.62 will provide a probability of stability of 99.9%, based on the limited data in the database.

The β value in Table IV was determined from a relatively small range of heights (Figure 18) and may therefore not be applicable outside of the range of the database. The *K*-value in the power formula represents the rock mass strength (van der Merwe, 2003). The Impala database (Gardner and Bosman, 2014) shows a significant variation in strength (Figure 22), with a mean UCS of 71 MPa and a standard deviation of 14.2 MPa. Kersten (2016) also observed a significant variation in chromitite strength (Figure 23), with a much higher mean value than that provided in Figure 22. Observations indicate that such a variation in strength could exist within a single pillar. If the mean strength of 138 MPa in Figure 23 (Kersten, 2016) is representative of the pillar materials in the pillar strength database (as described in this paper), then the *K*-value in Table IV (67 MPa) is about 50% of the UCS. York and Canbulat (1998) suggested a critical rock mass strength for Merensky Reef at about 64% of a typical 50 mm diameter cylindrical sample.

Discussion

The very small standard deviation in pillar strength estimated by the statistical back-analysis (*S* in Table IV) is evidence of a good-quality database. However, the database consisted of a mixture of pillars with and without sidings, and the siding depths and the heights of gullies also varied. The effect of these parameters on pillar strength was determined using unproven theory and needs to be investigated further. It was therefore considered necessary to conduct an experiment in a UG2 bord-and-pillar working, where no gullies were cut. Such an experiment was carried out at Booysendal Platinum Mine, and is discussed in a separate paper (Watson *et al.*, 2021)

The variation of height in the database was limited due to the thickness of the UG2 Reef in the area where the data was collected. It is therefore recommended that a sensitivity analysis be done on the effects of height using a suitable nonlinear modelling code such as FLAC3D (Itasca Consulting Group, 2018). Input parameters could be determined from laboratory tests with post-failure behaviour, and the model calibrated against the underground measurements. Note that the 1.5 m high pillar results generally clustered around the line dividing failed and unfailed pillars in Figure 20, hence the estimated strengths in the database were generally highly weighted in the ML analyses. Thus the 1.5 m high pillars (though less numerous) played a significant role in the formulation of the final strength equation. A comparison between the strengths of 1.5 m and 2.0 m high pillars with the same *w*/*h* ratio, was computed using the PlatMine formula (Figure 24). The results show a slight drop in the strength of the 1.5 m high pillars compared to the 2 m high pillars at the same *w*/*h* ratio. The formula therefore yields a possible underestimation of pillar strength at lower pillar heights if the 2 m high pillars are assumed to be the dominating pillar height in the database.

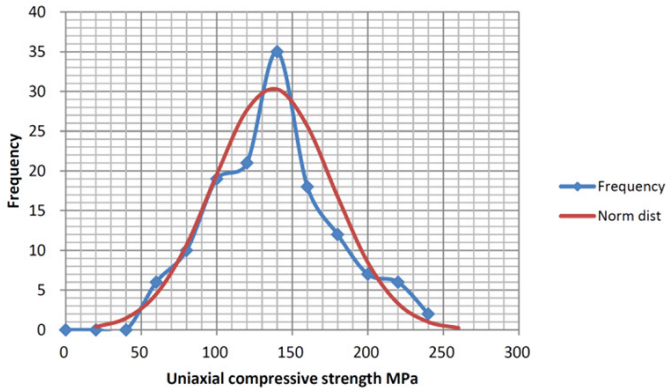

Figure 23—Distribution of UCS values for chromitite (Kersten, 2016)

PlatMine pillar strength formula for the UG2 Reef

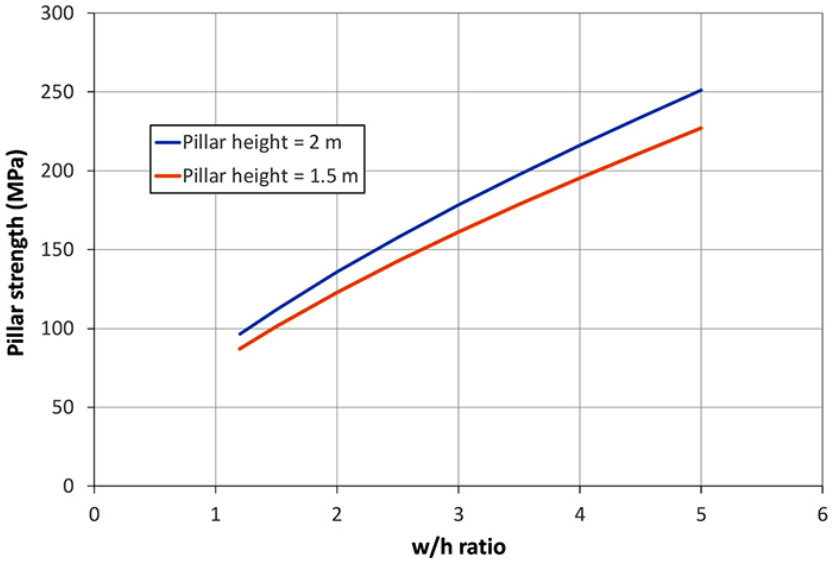

Figure 24—Comparison of pillar strength for pillars of 1.5 m and 2.0 m height, using the 'new' formula

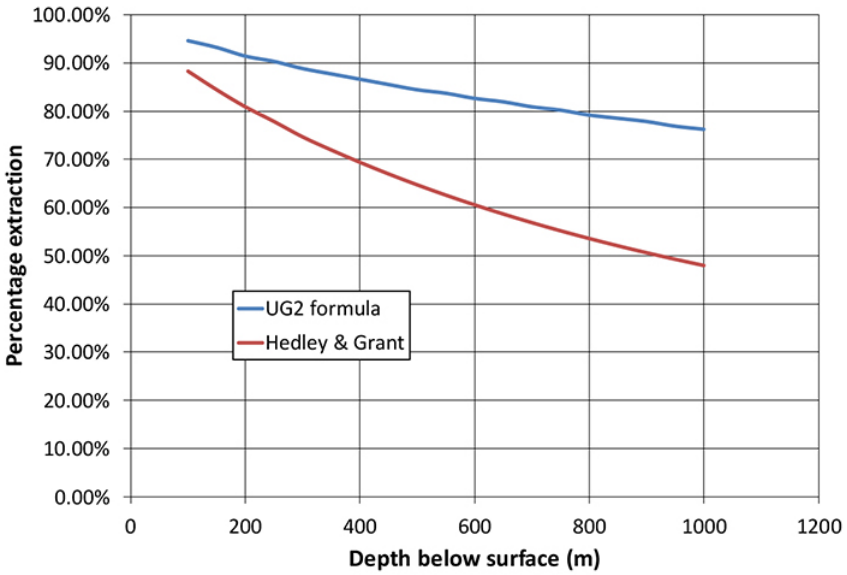

Figure 25—Extraction ratios with depth for pillars designed using the 'new' and currently used Hedley and Grant (1972) formulae (k = 35 MPa), assuming square pillars of 2 m height, bord widths of 8 m and SF of 1.6

The effects of gullies adjacent to pillars and the horizontal width of sidings (see Figure 3) have not been properly investigated, and better w/h ratio estimates may be possible if the equations to account for these factors are validated. The suggested pillar strength formula should not be used in areas where the strength of pillars is compromised by an adversely oriented thrust structure, or where pillars have been weakened due to weathering.

Previous numerical modelling performed on Merensky pillars (Watson *et al.*, 2008) suggests that the $(w/h)_e$ strength relationship is affected by foundation strength. Since the contribution of the foundations to UG2 pillar behaviour is unknown, it is recommended that the formula be used for pillars with conditions similar to those in the database (Esterhuizen, 2014). These conditions are:

- The immediate foundation materials are pyroxenite and anorthosite
- The pillars should not be weakened by thrust structures or weathering
- The height should be restricted to between 1.5 m and about 2 m
- The w/h ratio should be between 1.2 and 4.7.

The PlatMine formula for pillar strength calculation will allow for significantly greater extraction ratios on the UG2 than the currently accepted Hedley and Grant (1972) formula, which assumes a very low k-value of 35 MPa. A comparison of extraction percentages with depth below surface is shown in Figure 25. The analysis of both formulae assumed standard bord widths of 8 m and a SF of 1.6.

Conclusions

The database used in the paper to back-analyse underground pillar strengths is shown to be of high quality. It included a wide

range of widths (2–9 m) and lengths (4–49 m), but a small range of h_e (1.5–2 m). The analyses suggest that Equation [7] together with the exponents in Table IV provides reasonable strength results for the range of pillar sizes in the database. Caution should, however, be exercised when applying this formula to *w*/*h* ratios and pillar heights outside the range of the database and in areas with different geotechnical and geomechanical characteristics.

Recommendations

The database was restricted in height variation due to the uniform thickness of the UG2 Reef in the area where the data was collected. It is recommended that sensitivity analyses be done on the effects of height using a suitable nonlinear modelling code such as FLAC3D (Itasca Consulting Group, 2018). Input parameters could be obtained from suitably conducted laboratory tests, and calibrated from underground measurements.

Acknowledgements

PlatMine and the CSIR are acknowledged for facilitating the success of the project. Dr John Ryder is thanked for his assistance in developing statistical software to evaluate the database.

References

COMRO. 1981. MINSIM-D User's Manual. Chamber of Mines of South Africa (Minerals Council South Africa), Johannesburg.

Esterhuizen, G.S. 2014. Extending empirical evidence through numerical modelling in rock engineering design. *Proceedings of the 6th South African Rock Engineering Symposium. Southern African Institute of Mining and Metallurgy*, Johannesburg. pp 251–267.

Fernandes, N. 2020. Personal communication. Johannesburg.

Gardner, L.J. and Bosman J.D. 2014. Correlation of point load index with uniaxial compressive strength for Bushveld Complex rocks. South African National Institute of Rock Engineering, Johannesburg,

Hedley, D.G.F. and Grant, F. 1972. Stope pillar design for the Elliot Lake uranium mines. *Bulletin of the Canadian Institute of Mining and Metallurgy*, vol. 65. pp. 37–44.

Itasca Consulting Group, Inc. 2018. Fast Lagrangian Analysis of Continua (FLAC), v. 5.0. Minneapolis, MN.

Jager, A.J. and Ryder, J.A. 1999. A Handbook on Rock Engineering Practice for Tabular Hard Rock Mines. Safety in Mines Research Advisory Committee, Johannesburg.

Kersten, R.W.O. 2016. A probabilistic structural design process for bord and pillar workings in chrome and platinum mines in South Africa, *i*, School of Mining Engineering, University of the Witwatersrand, Johannesburg.

Malan, D.F. and Napier, J.A.L. 2011. The design of stable pillars in the Bushveld Complex mines: A problem solved? *Journal of the South African Institute of Mining and Metallurgy*, vol. 111. pp. 821–836.

Martin, C.D. and Maybee, W.G. 2000. The strength of hard rock pillars. *International Journal of Rock Mechanics and Mining Sciences*, vol. 37. pp. 1239–1246.

Napier, J.A.L. and Malan, D.F. 2011. Numerical computation of average pillar stress and implications for pillar design. *Journal of the South African Institute of Mining and Metallurgy*, vol. 111. pp. 837–846.

Napier, J.A.L. and Malan, D.F. 2012. Simulation of time-dependent crush pillar behaviour in tabular platinum mines. *Journal of the South African Institute of Mining and Metallurgy*, vol. 112. pp. 711–719.

Northam Platinum Limited. 2018. Annual Integrated Report 2018. https://www.northam.co.za/procurement/127-investors-and-media/publications/719-annual-report [accessed: 7 February 2020].

Roberts, D.P., Canbulat, I., and Ryder, J.A. 2002. Design parameters for mine pillars: strength of pillars adjacent to gullies; design of stable pillars with w/h ratio greater than 6; optimum depth for crush pillars. SIMRAC GAP617 Final Report. Safety in Mines Research Advisory Committee. Johannesburg.

Roberts, D.P., Roberts, M.K.C., Jager, A.J., and Coetzer, S. 2005. The determination of the residual strength of hard rock crush pillars with a width to height ratio of 2:1. *Journal of the South African Institute of Mining and Metallurgy*, vol 105. pp. 401–408.

Roberts, M.K.C., Grave, D.M.H., Jager, A.J., and Klokow, J. 1997. Rock mass behaviour of the Merensky Reef at Northam Platinum Mine. Safety in Mines Research Advisory Committee, Johannesburg,

Ryder, J.A., Watson, B.P. and Kataka, M.O. 2005. Pillar strength back-analyses. PlatMine 1.2, Johannesburg.

Salamon, M.D.G. and Munro, A.H. 1967. A study of the strength of coal pillars. *Journal of the South African Institute of Mining and Metallurgy*, vol.68. no. 2. pp. 55–67.

Spottiswoode, S.M. and Milev, A.M. 2002. A methodology and computer program for applying improved, inelastic ERR for the design of mine layouts on planar reefs. SIMRAC GAP722 Final Report. Safety in Mines Research Advisory Committee, Johannesburg. 85 pp

Van der Merwe, J.N. 2003. New pillar strength formula for South African coal. *Journal of the South African Institute of Mining and Metallurgy*, vol. 97. pp. 281–291.

Wagner, H. 1974. Determination of the complete load-deformation characteristics of coal pillars. *Proceedings of the 3rd International Congress on Rock Mechanics*, Denver, CO. Vol. 2B. ISRM, Lisbon. pp 1076-1082.

Watson, B.P., Kataka, M.O., Leteane, F.P., and Kuijpers, J.S. 2007. Merensky and UG2 pillar strength back analyses. PlatMine 1.2, Johannesburg.

Watson, B.P., Ryder, J.A., Kataka, M.O., Kuijpers, J.S. and Leteane, F.P. 2008. Merensky pillar strength formulae based on back-analysis of pillar failures at Impala Platinum. *Journal of the South African Institute of Mining and Metallurgy*, vol. 108. pp. 449–461.

Watson, B.P., Sellers, E.J., Kuijpers, J.S., Grave, D.M.H., Roberts, M.K.C., and Coetzer, S.J. 2006. Alternative cost-effective ways of determining the state of stress in mines. PlatMine 3.8, Johannesburg.

Watson, B.P., Theron W., Fernandes, N., Kekana, W.O. Mahlangu, M.P., Betz, G., and Carpedea, A. 2021. UG2 pillar strength: Verification of the PlatMine formula. *Journal of the Southern Afrıcn Institute of Mining and Metallurgy*, vol. 121, no. 8. pp. 449–456.

York G. and Canbulat I. 1998. The scale effect, critical rock mass strength and pillar system design. *Journal of the South African Institute of Mining and Metallurgy*, vol.98, no.1. pp. 27–37. ◆

PlatMine pillar strength formula for the UG2 Reef

Appendix A

The results of the investigations at Mine C are provided in Table A I. The full database consists of all the pillars at each site recorded in the report

Table A I

Results from the Mine C UG2 database

Pillar no.	*L* (m)	h_e (m)	w_e (m)	APS	CC	Pillar no.	*L* (m)	h_e (m)	w_e (m)	APS	CC
1	11.1	1.9	5.9	92	1	57	26.2	1.9	4.6	44	1
2	6.0	1.9	5.5	105	1	58	6.5	1.9	4.1	63	1
3	4.5	1.9	3.6	98	1	59	4.0	1.9	3.8	72	1
4	4.5	1.9	4.3	79	1	60	4.5	1.9	2.8	61	1
5	5.0	1.9	3.8	83	1	61	3.5	1.9	2.9	37	1
6	5.5	1.9	5.3	161	1	62	10.1	1.9	5.2	29	1
7	7.5	1.9	6.0	130	1	63	8.6	1.9	5.0	49	1
8	12.6	1.9	6.1	78	1	64	3.0	1.9	2.4	34	1
9	5.0	1.9	3.8	104	1	65	4.0	1.9	3.1	27	1
10	7.0	1.9	3.7	99	1	66	3.0	1.9	3.9	83	2
11	4.0	1.9	3.8	112	1	67	4.5	1.9	3.2	100	1
12	4.0	1.9	3.1	87	1	68	9.1	1.9	3.9	45	1
13	9.1	1.9	5.6	55	1	69	4.0	1.9	3.4	47	1
14	17.1	1.9	3.6	50	1	70	4.0	1.9	2.7	54	1
15	48.8	1.9	9.1	20	1	71	3.0	2.0	4.0	99	2
16	5.0	1.9	3.8	28	1	72	4.5	1.9	3.6	103	1
17	3.5	1.9	3.2	35	1	73	6.5	1.9	4.1	31	1
18	8.0	1.9	3.2	40	1	74	3.5	1.9	3.5	40	1
19	5.0	1.9	2.3	48	1	75	5.5	1.9	3.5	43	1
20	6.0	1.9	3.0	53	1	76	5.0	1.9	3.4	59	1
21	12.6	1.9	2.7	55	1	77	6.0	1.9	4.0	69	1
22	5.5	1.9	4.7	121	1	78	3.5	1.9	3.5	87	1
23	9.1	1.9	5.1	93	1	79	4.0	1.9	3.8	22	1
24	5.5	1.9	4.3	152	4	80	3.5	1.9	3.2	21	1
25	3.5	1.9	3.3	193	4	81	8.0	1.9	5.8	22	1
26	5.0	1.9	4.8	204	4	82	6.0	1.9	3.0	42	1
27	4.0	1.9	3.4	273	4	83	3.5	1.9	2.9	45	1
28	4.0	1.9	3.1	337	4	84	4.0	1.9	3.1	48	1
29	8.0	1.9	4.4	361	4	85	3.5	1.9	2.9	46	1
30	6.0	1.9	4.4	453	4	86	4.0	1.9	2.7	52	1
31	6.0	1.9	4.4	385	4	87	5.0	1.9	3.4	45	1
32	4.0	1.9	3.8	263	4	88	9.1	1.9	5.6	35	1
33	4.5	1.9	3.6	247	4	89	6.0	1.9	4.4	51	1
34	5.0	1.9	4.1	140	1	90	5.0	1.9	4.1	50	1
35	9.1	1.9	5.6	102	1	91	4.5	1.9	4.5	44	1
36	6.5	1.9	4.1	121	1	92	5.0	1.9	4.8	44	1
37	6.5	1.9	4.6	120	1	93	5.5	1.9	4.3	52	1
38	9.1	1.9	3.9	340	4	94	19.1	1.9	6.6	140	1
39	3.0	1.9	3.0	333	4	95	5.0	1.9	4.5	152	1
40	9.1	1.9	6.5	235	4	96	5.0	1.9	2.9	13	1
41	9.6	1.9	6.1	196	4	97	4.0	1.9	3.8	10	1
42	4.0	1.9	3.8	154	4	98	5.0	1.9	4.1	10	1
43	6.0	1.9	3.6	282	4	99	4.5	1.9	4.3	9	1
44	6.0	1.9	5.2	200	4	100	5.0	1.9	4.5	8	1
45	5.5	1.9	4.7	278	4	101	4.0	1.9	3.8	8	1
46	20.1	1.9	5.2	289	4	102	4.0	1.9	3.8	6	1
47	4.5	1.9	3.2	231	4	103	7.0	1.9	3.1	19	1
48	3.5	1.9	3.2	144	4	104	4.0	1.9	3.4	12	1
49	10.6	1.9	4.1	123	4	105	4.5	1.9	4.3	11	1
50	3.0	1.9	2.4	178	4	106	3.5	1.9	3.5	42	1
51	4.0	1.9	3.1	167	4	107	4.0	1.9	3.8	37	1
52	4.0	1.9	4.0	155	4	108	4.5	1.9	2.8	38	1
53	11.6	1.9	5.4	152	4	109	4.5	1.9	4.0	28	1
54	5.0	1.9	4.5	156	4	110	9.1	1.9	6.9	20	1
55	7.0	1.9	5.5	148	4	111	6.0	1.9	4.8	16	1
56	4.0	1.9	3.1	93	1						

L pillar length, w_e effective pillar width, h_e effective pillar height, APS average pillar stress, CC condition code (0 no damage, 2 pillar sidewalls visibly spalled/scaled, 4 pillar presumed failed)

UG2 pillar strength: Verification of the PlatMine formula

B.P. Watson[1], W. Theron[2], N. Fernandes[2], W.O. Kekana[2], M.P. Mahlangu[2], G. Betz[2], and A. Carpede[1]

Affiliation:
[1]University of Witwatersrand, South Africa.
[2]Northam Platinum, South Africa.

Correspondence to:
B.P. Watson

Email:
Bryan.Watson@wits.ac.za

Dates:
Received: 19 Jan. 2021
Published: August 2021

How to cite:
Watson, B.P., Theron, W., Fernandes, N., Kekana, W.O., Mahlangu, M.P., Betz, G., and Carpede, A. 2021
UG2 pillar strength: Verification of the PlatMine formula.
Journal of the Southern African Institute of Mining and Metallurgy, vol. 121, no. 8, pp. 449–456

DOI ID:
http://dx.doi.org/10.17159/2411-9717/1491/2021

ORCID:
B.P. Watson
https://orcid.org/0000-0003-0787-8767

Synopsis

The research described in this paper was done to confirm the Upper Group 2 (UG2) PlatMine peak pillar strength formula (Watson *et al.*, 2007), which was determined from a back-analysis of failed and unfailed pillars. Underground measurements were made on a stable pillar that was loaded by firstly reducing it's length and then by mining the surrounding pillars until pillar failure took place. The pillar was instrumented with suitably positioned strain cells and closure meters, which allowed both the average pillar stress and strain to be determined. The paper describes the methodology applied to identify a suitable position for the instrumentation, as well as the results. A stress/strain curve is presented for a UG2 pillar with a w/h ratio of 2.0, at Booysendal Platinum Mine. The measured pillar strength was similar to the predicted strength using the PlatMine pillar strength formula for UG2 pillars. The PlatMine formula has been successfully implemented on Booysendal Platinum Mine, and about 3 670 pillars have been cut without a single failure. An additional revenue of US$1.3 billion was calculated for the 25-year life of the mine as a direct result of the improved pillar design, given the January 2020 platinum group metals basket price. An extended life of mine and better mining efficiencies will also be realized.

Keywords
Pillar strength, UG2, PlatMine formula, chromitite, stress measurements, *in-situ* pillar behaviour, mining-efficiency, socio-economic benefit.

Introduction

Mechanization of the Bushveld Comlpex platinum mines has resulted in an increase in bord-and-pillar mining, particularly in the newer, shallow-depth mines on the eastern side of the Complex. The Upper Group 2 (UG2) chromitite pillars have been designed for many years using the Hedley and Grant (1972) formula to determine peak pillar strength. Generally the *k*-value in the formula (Equation [1]) is reduced to 35 MPa for these mines (Fernandes, 2020), which is about a third of the uniaxial compressive strength (UCS) of the pillar material (Malan and Napier, 2011).

$$Strength = k\frac{w_e^{0.5}}{h^{0.75}}\text{MPa} \quad [1]$$

where k = rock mass strength (35 MPa), w = pillar width, and h = pillar height.

However, the formulation of the equation is based on a large number of unproven assumptions, and its application to the design of pillars in the Bushveld Complex is questionable (Malan and Napier, 2011). A potential consequence of using this uncertain methodology is the cutting of oversized pillars, which lowers the extraction ratio. There is a need, therefore, to optimize pillar sizes, based on an understanding of UG2 pillar behaviour. The PlatMine pillar strength formula (Watson *et al.*, 2007) is based on a back-analysis of failed and unfailed pillars on the UG2 Reef. It suggests that pillar strengths are greater than predicted by Hedley and Grant (1972), if a downrated *k*-value of 35 MPa is assumed in the Hedley and Grant (1972) formula. The PlatMine formula is as follows (Watson *et al.*, 2007):

$$Strength = 67\frac{w_e^{0.67}}{h^{0.32}}\text{MPa} \quad [2]$$

The derivation of this formula is described in a separate paper (Watson, Lamos, and Roberts, 2021). In summary, it was based purely on a regression analysis of failed and unfailed pillars, where

elastic modelling was used to determine the pillar stresses. In the analysis, failed and unfailed pillar stresses over- and under-estimated pillar strength, respectively. A maximum likelihood regression was used to bias the failed and unfailed pillars to the lowest and highest values, respectively. Although the formula has been available for some time there was scepticism as regards its use because there were no pillars in the database for which the actual stress at failure was known. Therefore, none of the UG2 platinum mines used the PlatMine formula (Watson *et al.*, 2007). Booysendal (Pty) Limited wanted to use it because of the better extraction ratios it offered compared to the method according to Equation [1] (k = 35 MPa), which was being used at the time. In addition to the general scepticism, the pillar heights at Booysendal (2.5 m to 2.8 m) were slightly greater than the range in the database (1.5 m to 2.0 m). It was therefore considered necessary to instrument and monitor a pillar and load it to failure. The results of this investigation are described in the paper. To the best of the authors' knowledge, no other such investigations have been successfully completed on UG2 pillars.

Instrumentation was installed to determine the:

- Pillar stress at the start of the project
- Stress change during mining
- Deformation of the pillar.

The instrumentation results were used to construct a stress/strain curve for the pillar.

Instrumentation site

A site was set up on a bord-and-pillar working at Booysendal Platinum Mine, on the eastern side of the Bushveld Complex southwest of the town of Mashishing (Figure 1).

The instrumentation site was about 290 m below surface and is shown in context with the rest of the mine in Figure 2. The figure shows the mining face positions at the start of the project. Little effect of face advance was measured on the pillar stress during the monitoring period. The stress was increased by firstly mining the pillar smaller and subsequently mining out the surrounding pillars until pillar failure occurred. A comparison between Equation [2] and the stress determined by an elastic model was used to define the size of the final pillar and the amount of mining required on the surrounding pillars to cause the instrumented pillar (IP) to fail. The size and shape of IP and the surrounding pillars at the start of the project are shown in Figure 3. The reef dip was about 8°.

Pillar loading

Initially the IP was gradually reduced in size until the final size and shape shown in Figure 4. Subsequently, the surrounding pillars (first row of pillars) were progressively mined to the sizes shown in Figure 4. Some of the surrounding pillars did not fail, and failure had to be induced using low-energy deflagrating explosives (Figure 5). Finally, the pillars in the second row were mined to about half their original size (Figure 6), at which point failure occurred on the instrumented pillar. The schedule of mining activities at the instrumentation site is summarized in Table I.

Elastic numerical modelling

The surface profile at the site was mountainous and the effects

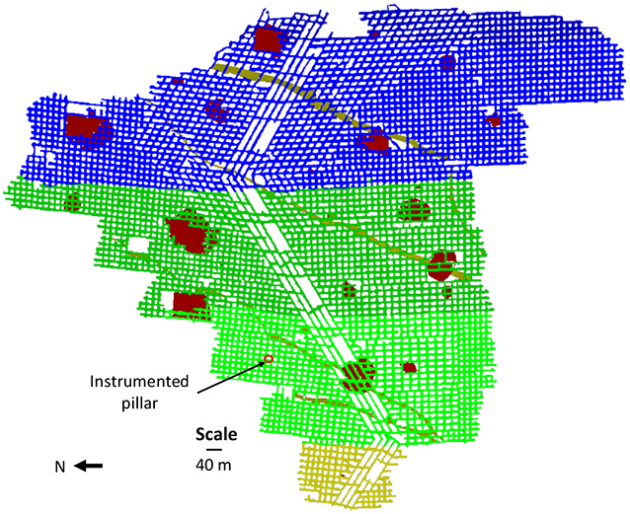

Figure 2—Mine plan showing the location of the instrumented pillar (reef dips at 8° towards bottom of figure). The instrumentation site is about 290 m below surface. The blue, green, and brown colours show the various sections on the mine according to depth. Potholes and dykes are shown in red and yellow, respectively

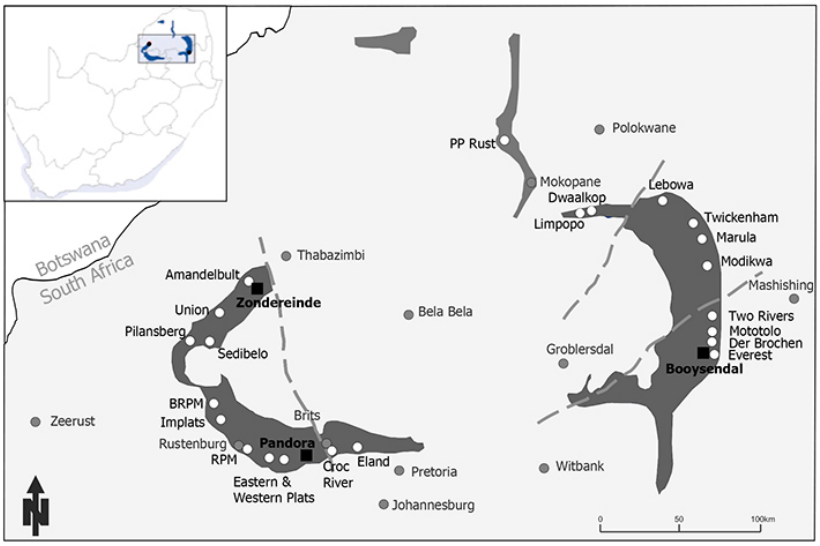

Figure 1—The extent of the Bushveld platinum exposure in South Africa (Northam Platinum Limited, 2018)

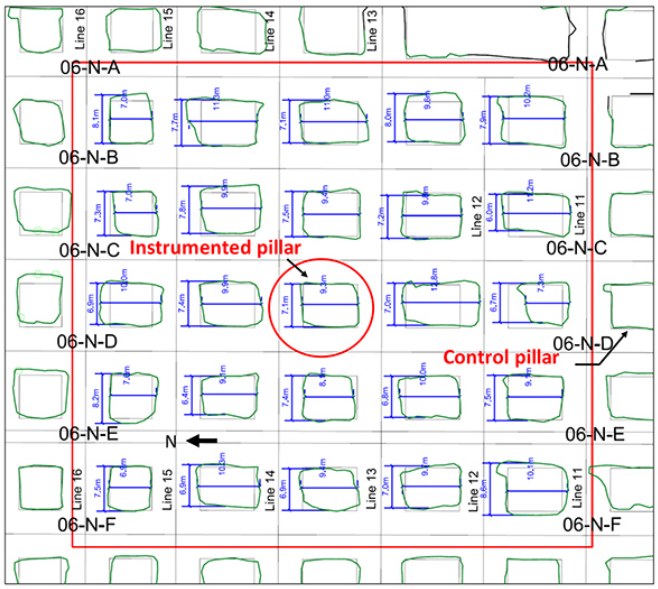

Figure 3—Plan view of the instrumented pillar (reef dips towards bottom of figure at about 8°)

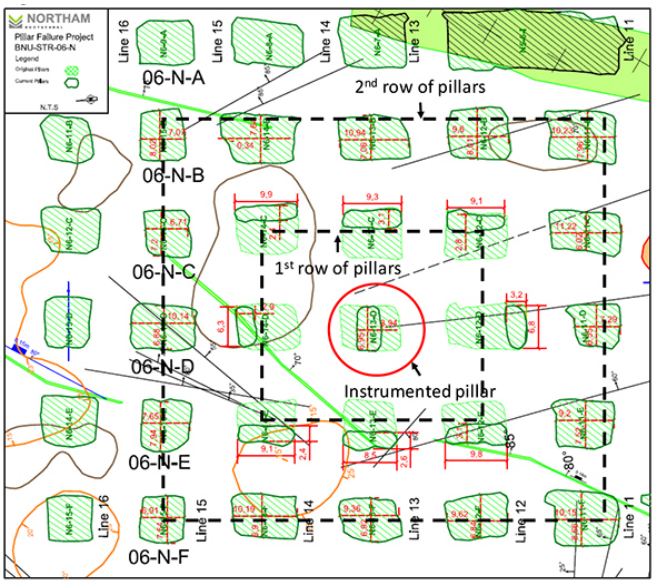

Figure 4—Mine plan showing the original and final boundaries of the instrumented pillar (reef dips towards bottom of figure)

of this topography were included in the MAP3D elastic boundary element modelling (Wiles, 2017). An average rock density of 3 000 kg/m^3, a *k*-ratio of unity, Young's Modulus of 85 GPa, and Poisson's ratio of 0.33 were used as input parameters to the model. The elastic constants were determined by uniaxial laboratory tests. In the model, the top of the highest mountain was used as the initial level of surface. A surface length of five times the mining length (in plan) was used all around the mining area and a grid size of 10 m × 10 m was used to evaluate the surface effects. As a first step, the surface was mined out using fictitious force elements to produce the actual topography profile and the virgin stress condition of the reef. The second mining step involved the mining of the reef using displacement discontinuity elements. A grid size of 0.5 m was used to adequately determine the pillar stresses. Subsequently, a second, smaller model was run covering sufficient area around the

Figure 5—First row of pillars surrounding the IP after using deflagrating explosives

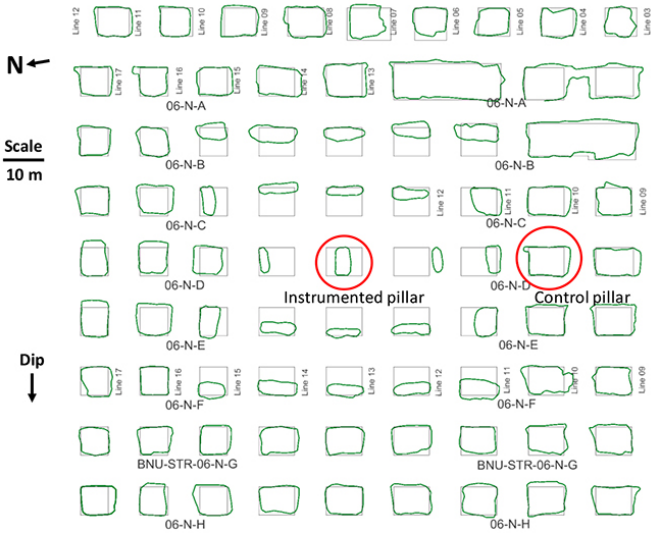

Figure 6—Mine plan showing the final pillar configuration (green) at pillar failure

Table I

Schedule of mining activities at the instrumentation site

Activity	From	To
Reducing IP by mining each side evenly	30/05/2018	16/08/2018
Mining the first row of pillars surrounding IP (Figure 4)	01/11/2018	28/03/2019
Preconditioning the pillars surrounding IP	04/09/2019	12/09/2019
Mining of second row of pillars around IP (Figure 6)	13/05/2019	07/10/2019

instrumentation site on a 0.25 m grid. The depth and horizontal stress inputs on the second model were modified to provide the same levels of stress as shown by the first model. An initial horizontal to vertical stress ratio (*k*-ratio) of unity was assumed, and as a result of mining the surface topography the *k*-ratio increased to about two.

The second model was used to determine the stress changes that occurred on the IP as it was mined smaller and the surrounding pillars were reduced in size. Benchmark lines were constructed in the model to simulate the measurement boreholes that were drilled over the instrumented pillars. Factors relating the average pillar stress (APS) to point stresses were determined at the positions where the stress measurements were made. Several stages of mining were evaluated.

Geology surrounding the pillar site

The geology at the site needed to be considered when determining the optimum position of the strain cells to determine

the APS and stress change during mining. Of particular interest was the abrupt parting between the pyroxenite and leuconorite about 3 m above the hangingwall (Figure 7), as this interface is often the location of parting in the bords. This parting plane is locally known as the Upper Pyroxenite Contact (UPC). The composition of the IP and the surrounding pillars (all about 2.55 m high) is also shown in the figure.

The 2.55 m high pillars extended from the norite footwall up to the triplets, and included several layers of pyroxenite. The immediate pillar hanging- and footwall materials were pyroxenite and norite, respectively (Figure 7).

Geomechanical properties

In 2009, a geomechanical testing programme was conducted at the mine on rock samples from the UG2 reef and the immediate UG2 hangingwall and footwall (Spencer 2009). Some 700 point-load samples were selected from 61 boreholes and 40 UCS samples from seven boreholes across the mine. The UCS tests were done by Rocklab in Pretoria in accordance with ISRM standards. The average results are shown in Table II. It should be noted that half of the 16 laboratory UCS samples from the UG2 chromitite reef failed on discontinuities, which would have resulted in an underestimation of UG2 strength (81 MPa). The UCS provided by the point load results is therefore probably more accurate (102 MPa). The UCS values for the immediate foundation to the pillars at the instrumentation site were about

Table II

Average UCS results from the geomechanical testing programme (Spencer 2009)

UG2 geotechnical domain	Laboratory tests (MPa)	Point-load tests (MPa)
Immediate hangingwall	147	151
UG2 Reef	81	102
Immediate footwall	145	126

147 MPa and 145 MPa for the hangingwall and footwall, respectively. Typical stress-strain curves from the three rock types at the instrumentation site are shown in Figure 8. The elastic constants for these tests are provided in Table III.

Design of stress measurements

The aim of the stress measurements was to determine the APS of the instrumented pillar from a stress measured at a point in a borehole somewhere above the pillar. It was important that this point should be high enough to determine the APS accurately, whether the stress profile was for a failed or unfailed pillar. Wagner's *in-situ* tests on coal pillars (1980) showed that stress concentrations change during pillar loading (Figure 9). A matrix of Boussinesq equations (Poulos and Davis, 1974) was set up, using Equation [3] and the grid provided in Figure 10,

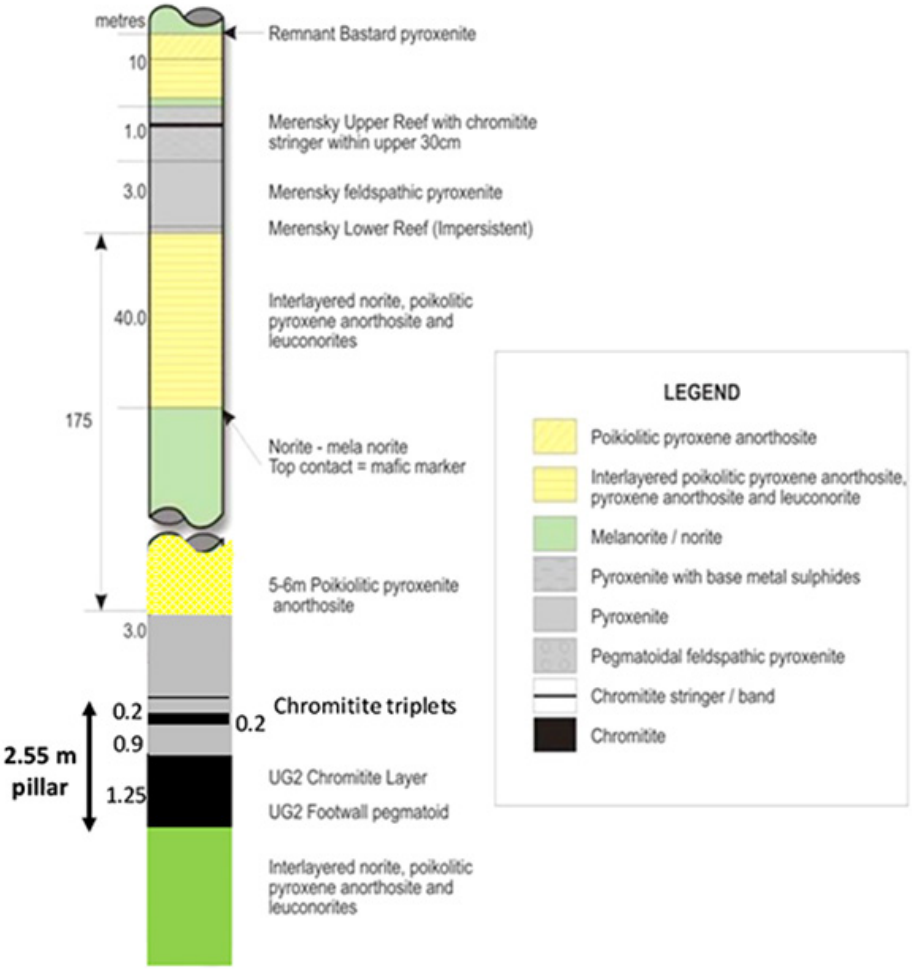

Figure 7—Stratigraphic column showing the rock types surrounding the UG2 Reef at Booysendal (after Mahlangu 2020)

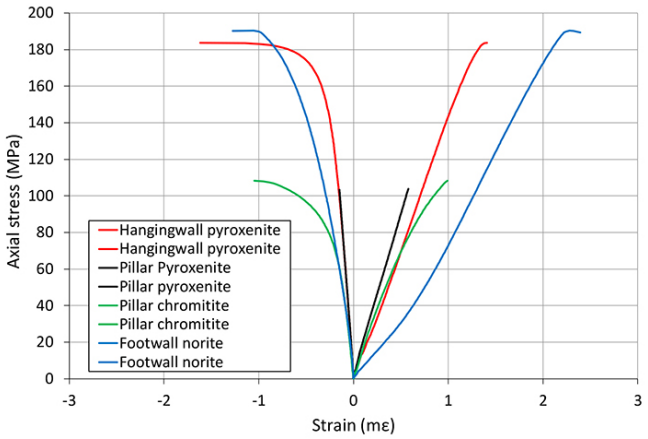

Figure 8—Typical stress-strain curves for the UG2 Reef and immediate hangingwall (H/W) and footwall (F/W) materials

Table III

Results of geomechanical tests on rock samples from the site

	UCS (MPa)	Young's modulus (GPa)	Poisson's ratio
Immediate hangingwall pyroxenite	161	71	0.23
Pillar pyroxenite	184	83	0.26
Pillar chromitite	108	85	0.33
Immediate footwall norite	190	51	0.39

to determine the effects of failed and unfailed stress profiles on the measurements. For the purposes of the calculations, the reef and measurements were rotated by eight degrees so that the top surface of the pillar could be considered horizontal. A plan view of the Boussinesq coordinate system used across the top boundary of the pillar is shown in Figure 10.

$$\sigma_{zz} = \sum_{i=1}^{n}\left[\frac{3A_i}{2\pi} \times \frac{z_i^3}{(x_i^2 \times y_i^2 \times z_i^2)^{5/2}} \times P_{zi}\right] \quad [3]$$

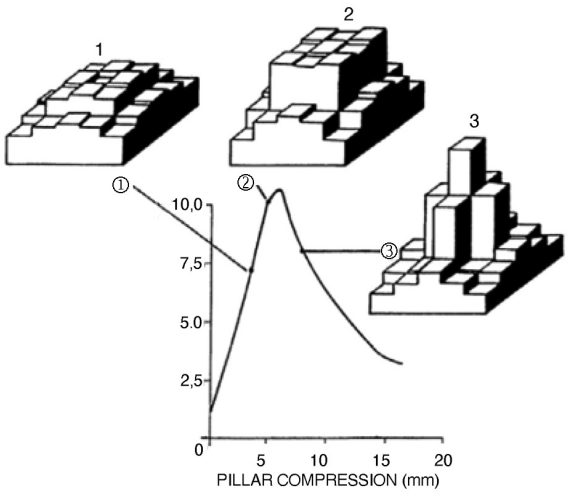

Figure 9—Wagner's *in-situ* tests on coal pillars (1980), showing the stress profile across a pillar for three APS levels (1 = elastic, 2 = yield. and 3 = post failure)

where: σ_{zz} = stress at a point in space; A_i = area of the grid '*i*'; and p_{zi} = vertical stress carried by the grid '*i*'.

Typical profiles of failed and unfailed pillars were determined from the results of measurements made on the Merensky Reef (Watson, Kuijpers, and Miovsky, 2008) and an elastic model, respectively. The profiles were normalized to their respective APS values as shown in Figure 11, and applied across the width of the grid in Figure 10. A series of heights above the centre of the grid were evaluated using Equation [3]. The resulting stresses of failed and unfailed pillars at each of the investigation points were normalized against APS and expressed as a percentage (Figure 12). The percentage difference between the failed and unfailed pillar values at an investigation point was considered to be an indication of the accuracy of the measurement.

Figure 12 shows a trade-off between the accuracy and percentage of the APS measured with height above the pillar. For example, a measurement height of 1.2 times the pillar width will allow only about 40% of the APS level to be measured. Thus at a peak strength of 160 MPa, the strain cell would measure

1 X=-3.25 Y=-1.75	2 X=-2.75 Y=-1.75	3 X=-2.25 Y=-1.75	4 X=-1.75 Y=-1.75	5 X=-1.25 Y=-1.75	6 X=-0.75 Y=-1.75	7 X=-0.25 Y=-1.75	8 X=0.25 Y=-1.75	9 X=0.75 Y=-1.75	10 X=1.25 Y=-1.75	11 X=1.75 Y=-1.75	12 X=2.25 Y=-1.75	13 X=2.75 Y=-1.75	14 X=3.25 Y=-1.75
15 X=-3.25 Y=-1.25	16 X=-2.75 Y=-1.25	17 X=-2.25 Y=-1.25	18 X=-1.75 Y=-1.25	19 X=-1.25 Y=-1.25	20 X=-0.75 Y=-1.25	21 X=-0.25 Y=-1.25	22 X=0.25 Y=-1.25	23 X=0.75 Y=-1.25	24 X=1.25 Y=-1.25	25 X=1.75 Y=-1.25	26 X=2.25 Y=-1.25	27 X=2.75 Y=-1.25	28 X=3.25 Y=-1.25
29 X=-3.25 Y=-0.75	30 X=-2.75 Y=-0.75	31 X=-2.25 Y=-0.75	32 X=-1.75 Y=-0.75	33 X=-1.25 Y=-0.75	34 X=-0.75 Y=-0.75	35 X=-0.25 Y=-0.75	36 X=0.25 Y=-0.75	37 X=0.75 Y=-0.75	38 X=1.25 Y=-0.75	39 X=1.75 Y=-0.75	40 X=2.25 Y=-0.75	41 X=2.75 Y=-0.75	42 X=3.25 Y=-0.75
43 X=-3.25 Y=-0.25	44 X=-2.75 Y=-0.25	45 X=-2.25 Y=-0.25	46 X=-1.75 Y=-0.25	47 X=-1.25 Y=-0.25	48 X=-0.75 Y=-0.25	49 X=-0.25 Y=-0.25	50 X=0.25 Y=-0.25	51 X=0.75 Y=-0.25	52 X=1.25 Y=-0.25	53 X=1.75 Y=-0.25	54 X=2.25 Y=-0.25	55 X=2.75 Y=-0.25	56 X=3.25 Y=-0.25
57 X=-3.25 Y=0.25	58 X=-2.75 Y=0.25	59 X=-2.25 Y=0.25	60 X=-1.75 Y=0.25	61 X=-1.25 Y=0.25	62 X=-0.75 Y=0.25	63 X=-0.25 Y=0.25	64 X=0.25 Y=0.25	65 X=0.75 Y=0.25	66 X=1.25 Y=0.25	67 X=1.75 Y=0.25	68 X=2.25 Y=0.25	69 X=2.75 Y=0.25	70 X=3.25 Y=0.25
71 X=-3.25 Y=0.75	72 X=-2.75 Y=0.75	73 X=-2.25 Y=0.75	74 X=-1.75 Y=0.75	75 X=-1.25 Y=0.75	76 X=-0.75 Y=0.75	77 X=-0.25 Y=0.75	78 X=0.25 Y=0.75	79 X=0.75 Y=0.75	80 X=1.25 Y=0.75	81 X=1.75 Y=0.75	82 X=2.25 Y=0.75	83 X=2.75 Y=0.75	84 X=3.25 Y=0.75
85 X=-3.25 Y=1.25	86 X=-2.75 Y=1.25	87 X=-2.25 Y=1.25	88 X=-1.75 Y=1.25	89 X=-1.25 Y=1.25	90 X=-0.75 Y=1.25	91 X=-0.25 Y=1.25	92 X=0.25 Y=1.25	93 X=0.75 Y=1.25	94 X=1.25 Y=1.25	95 X=1.75 Y=1.25	96 X=2.25 Y=1.25	97 X=2.75 Y=1.25	98 X=3.25 Y=1.25
99 X=-3.25 Y=1.75	100 X=-2.75 Y=1.75	101 X=-2.25 Y=1.75	102 X=-1.75 Y=1.75	103 X=-1.25 Y=1.75	104 X=-0.75 Y=1.75	105 X=-0.25 Y=1.75	106 X=0.25 Y=1.75	107 X=0.75 Y=1.75	108 X=1.25 Y=1.75	109 X=1.75 Y=1.75	110 X=2.25 Y=1.75	111 X=2.75 Y=1.75	112 X=3.25 Y=1.75

Figure 10—Plan view of the grid layout across the pillar for Boussinesq evaluation (Poulos and Davis, 1974). The measurement position was vertically above the centre of the grid (red)

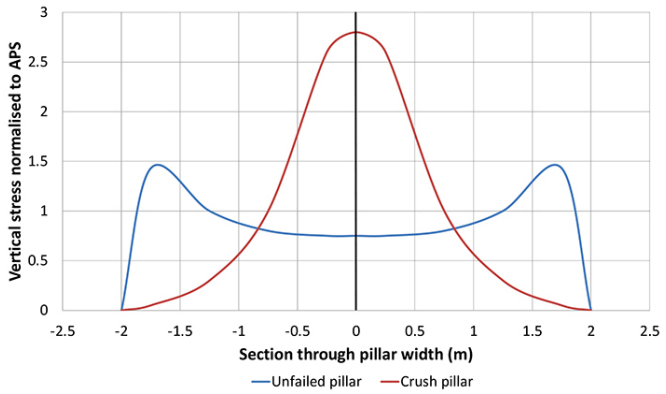

Figure 11—Typical stress profile assumed from Examine 2D elastic models (unfailed pillars) and Watson, Kuijpers, and Miovsky (2008) for crush pillars

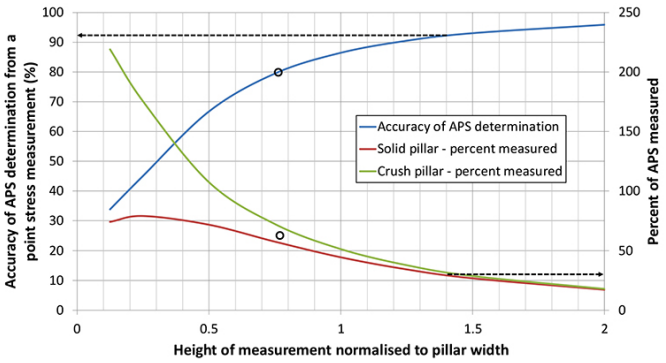

Figure 12—The accuracy of APS determination and percentage of the APS measured, as a function of height above the pillar centre. The results of the Boussinesq equation (Poulos and Davis, 1974), using the grid shown in Figure 10. The optimum height to avoid borehole breakout is shown by the dashed arrows. The accuracy of the optimum height on the original pillar width is shown by the circles

64 MPa. However, if the APS dropped to about 20 MPa after failure, which is shown by Merensky crush pillars of that size (Watson, Stacey, and Kuijpers, 2010), the cell would measure 8 MPa. The aim of the exercise would be to maximize the measured residual stress, but not to position the strain cells too close to the pillar so as to measure only a portion of the stress profile (and not the APS), or cause borehole breakout before pillar failure. The optimum cell position was found to be about 1.2 times the pillar width. However, the maximum stress at the measurement point needed to be kept to below 50 MPa to avoid borehole breakout. The height at which the critical 50 MPa value was reached was found to be about 1.4 times the pillar width. At this height, the stress measurement accuracy was about 92%, for the final pillar width of 3.94 m. However, for the same height of measurement, the accuracy was 80% for the initial 7.1 m wide pillar (shown by the circles in Figure 12). A compromise height of 6.2 m above the pillar was used to improve the stress measurements when the pillar was in its original size. This height was about 1.6 times the final pillar width and yielded a stress accuracy of about 94% at the final pillar width.

Instrumentation layout

Several strain cells were installed along the 7.7 m long borehole shown in Figure 13, to determine the APS level at the start of the monitoring period. A stress change measurement cell was installed at the final position at about 6.2 m above the pillar. Closure meter instruments were installed at the centres of the pillar sidewalls, in plan view.

During the narrowing of the pillar, pillar deformation was measured by closure stations on the up- and down-dip sides of the pillar. Once the pillar had been mined down to its planned size, two further closure meters were installed so that there was a station adjacent to each of the four pillar sidewalls. The closure results were averaged and used to determine the pillar strain.

Instrumentation results

Field stress measurements over the IP

At the start of the project, field stress measurements were done on the IP to determine the actual stress levels of the original 7.1 m × 9.3 m pillar. These measurements were made in the 7.7 m long hole used for the final stress change instrument (Figure 13). The vertical stress results are shown in Table IV. In Figure 14, these results are compared to the vertical elastic model results for the same borehole. All three of the measurement results were made above the UPC. Since the elastic model did

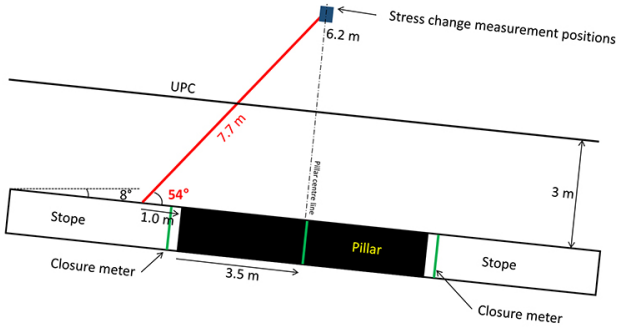

Figure 13—Instrumentation layout (section along reef dip)

Table IV

Results of the field stress measurements performed over the IP (a reliability index of less than 13 is considered acceptable (Coetzer, 2005))

Instrument no.	Rock type	σ_1 (MPa)	Direct of σ_1 (degr from north)	Dip of σ_1 (degr from horiz.)	σ_2 (MPa)	Direct of σ_2 (degr from north)	Dip of σ_2 (degr from horiz.)	σ_3 (MPa)	Direct of σ_3 (degr from north)	Dip of σ_3 (degr from horiz.)	Vert. strss (MPa)	Model stress (MPa)	Reliability index (%)	Young's modules (GPa) (at 50% of UCS)	Poisson's ratio (at 50% of UCS)
P1C-54-6.20 m	Spotted anorth-osite	55	192	4	19	98	50	16	285	40	18	16	4.8	85	0.38
P1b-54-6.42 m	Spotted anorth-osite	45	199	13	16	297	34	13	92	53	16	16	4.9	76	0.26
P1b-54-6.96 m	Spotted anorth-osite	66	198	10	21	290	9	13	62	77	15	15	7.6	130	0.26

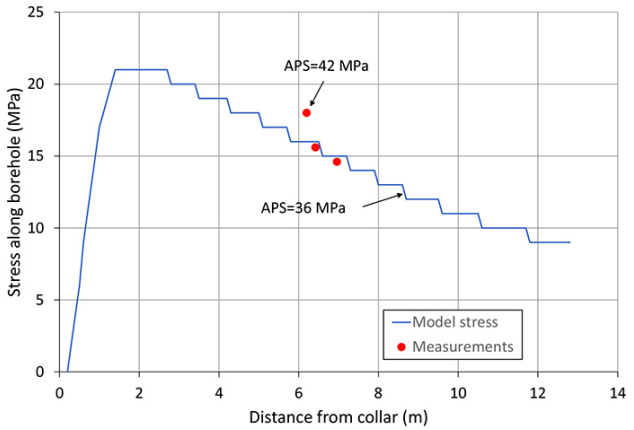

Figure 14—Stress measurements compared to elastic stresses along the borehole for an APS of 36 MPa

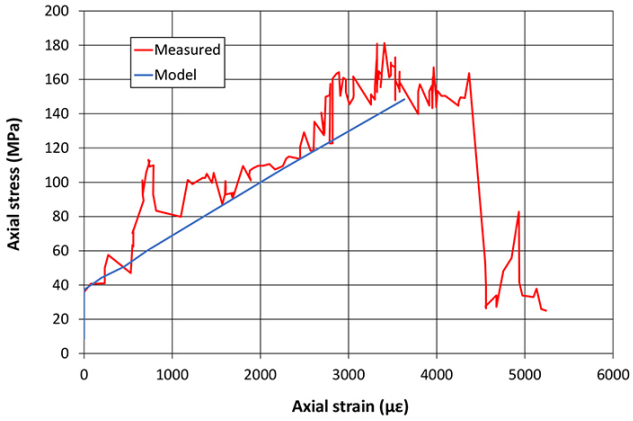

Figure 15—APS from the measurements at 6.2 m above the pillar and the elastic model results as a function of strain

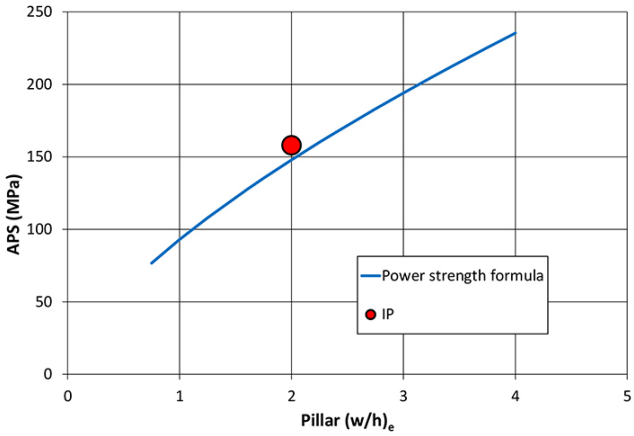

Figure 16—Comparison between the power APS formula and the underground measurement

not account for the UPC, it is clear from the good correlation between the measurements and the model, that the UPC did not significantly affect the stress results. At the time of the field stress measurements, the model predicted an APS of 36 MPa (starting stress), which was confirmed by the good correlation with the measurements in Figure 14.

Stress change measurements over the IP

The elastic model was used to determine both the APS and corresponding vertical stress at 6.2 m above the pillar centre, for various pillar sizes (to account for the pillar size reduction during monitoring). Factors were determined from the relationship between these two stresses to evaluate the measured stress change at each pillar size; *i.e.* these factors were used to back-analyse the APS from the vertical stress-change measurements. A final factor (once the narrowing of the IP was complete) was used to measure the stress build-up due to the mining of the surrounding pillars. The stress change measurements were added to the initial APS and a stress-strain curve was created using the total stress *versus* the accompanying closure results. Figure 15 shows the stress-strain curve for the IP using this evaluation process. Notice the similarity of the measurements to the elastic result produced by the numerical model, which is shown in the same figure.

Comparison between the instrumentation results and those from the PlatMine UG2 pillar strength formula

Since the IP was a rectangular pillar, an effective pillar width (w_e) was required to provide for the strengthening effects of the pillar length. The widely used 'perimeter rule', described by Wagner (1974), was used:

$$w_e \approx 2\,w\,L\,/(w+L) \qquad [4]$$

where w and L are the pillar width and length, respectively. Using Equation [4], the w_e/h ratio for the final IP was calculated to be 2.0. Using Equation [2], the strength was calculated to be 148 MPa. It is clear from Figure 16 that the measured stress at failure for the IP was close to the calculated strength.

Note the unexpectedly high residual strength for a pillar with a w/h ratio of 2.0. The curve suggests a residual strength of about 30 MPa, but further reductions in strength could have occurred with time if measuring had continued.

Implementation at Booysendal

Booysendal has been using the PlatMine pillar strength formula (Watson *et al.*, 2007), with a FoS of 1.6, for three years without a single pillar failure (*i.e.* Condition Codes CC3, CC4, or CC5). During this time, an area of 900 000 m² has been mined, amounting to about 3 670 pillars, designed on the Platmine formula (Watson *et al.*, 2007). These pillars were cut in the height range between 2.2 m and 2.8 m. The success of the PlatMine formula (Watson *et al.*, 2007) at Booysendal adds confidence to the validity of this formula within the range of the database. The formula provides for smaller pillars without compromising safety, within the range of the database.

As a direct result of implementing the PlatMine formula (Watson *et al.*, 2007) for pillar design, the mine will realize R20 billion (US$1.3 billion) in additional revenues over the 25-year life of the mine (Nothnagel, 2020), assuming a rand/dollar exchange rate of 15:1 (Exchangerates, 2020). The value was calculated using the January 2020 prices for the platinum group metals, produced by the mine (rands per ounce) and the average grade on the mine. Additional benefits include a further 2.6 years life-of-mine and improved efficiencies for underground transportation of ore (Nothnagel, 2020). The application of the 'new' formula fits the policies of the Minerals Council South Africa in almost every respect (van der Woude, 2019), without additional costs. There are also additional benefits.

- *Socio-economic impact*
  - A platinum ounce (includes the basket of platinum group metals for Booysendal) costs approximately R25 000 (van Schalkwyk, 2020) to produce. Due to the additional ounces achieved, R8.0 billion (approximately 60% of the cost) will be put back into society through procurement and labour, excluding royalties and taxes.
  - For every job in mining, at least two jobs are created up- and down-stream. The income of each mining employee supports five to ten dependants (Baxter, 2019).
- *Mineral resources*
  - Platinum resources are scarce, and social responsibility demands optimal extraction. The PlatMine formula (Watson *et al.*, 2007) allows a substantial increase in extraction ratios, particularly at deeper levels. One of the top ten risks facing mining is the replacement of production. This replacement is usually achieved by finding new orebodies, or extensions to existing workings. However, exploration is long-term and expensive. In this case, all costs have been paid and better utilization of the orebody is achieved.
- *Safety benefits*
  - Booysendal North Mine has shown that mechanized bord-and-pillar mining is a safe and productive mining method for the UG2 reef (Northam Platinum Limited, 2018). Booysendal has achieved three million fatality-free shifts, a significantly better safety record than the rest of the South African platinum mining industry (MOSH Learning Hub, 2019). The PlatMine formula (Watson *et a*l., 2007) will allow the mine to extend the same mining method to greater depths than the traditional formula (Malan and Napier, 2011). It will thus be possible to maintain a higher safety record than for the average South African platinum mines.

Conclusions

The instrumentation installed at the Booysendal Platinum Mine site successfully measured the stress/strain behaviour of a pillar. The measured failure stress was slightly higher than the strength calculated by the PlatMine formula (Watson *et al.*, 2007). In addition, the general slope of the measured stress/strain curve was similar to the elastic model produced by MAP3D (Wiles, 2017) and the deformation expected due to the measured elastic constants of the pillar material, suggesting a good set of measurements. An unexpectedly high initial residual strength of about 30 MPa was measured, but this stress may have reduced with time, after the monitoring period.

The significant number of pillars successfully mined on Booysendal using the PlatMine formula (Watson *et al.*, 2007) is further evidence of its legitimacy. Caution should, however, be exercised when applying this formula to w/h ratios and pillar heights outside the range of the database and in areas with different geotechnical and geomechanical properties.

The PlatMine formula (Watson *et al.*, 2007) will have a significant positive impact on the South African Bushveld Complex platinum mines that are mining the UG2 Reef. Pillars can be mined smaller without compromising safety, provided they fall within the range of the database. Booysendal is likely to realize an additional US$1.3 billion over the 25 year life-of-mine as a direct result of mining smaller pillars. The mine will also achieve other benefits such as an extension of the life-of-mine by 2.6 years and improved underground transportation efficiencies.

Recommendations

It is strongly recommended that similar investigations be conducted at various pillar heights and w/h ratios to confirm the PlatMine formula (Watson *et al.*, 2007).

Acknowledgements

The staff and management of Booysendal Platinum mine are thanked for their invaluable assistance and funding of the project. Mr Phillip Luwes is thanked for his patience and the arduous task of installing and manually reading the instrumentation over a period of about two years.

References

Baxter, R. 2019. What's happening economically and how is this impacting the mining industry? *Mining in SA today, Johannesburg Indaba*, October 2019: 2 pp

Coetzer, S.J. 2005. Personal communication.

Exchangerates. 2020. http://www.exchangerates.org.uk [accessed 26 February 2020].

Fernandes, N. 2020. Personal communication. Johannesburg.

Hedley, D.G.F. and Grant, F. 1972. Stope pillar design for the Elliot Lake uranium mines. *Bulletin of the Canadian Institute of Mining and Metallurgy*, vol. 65. pp. 37–44.

Mahlangu, M.P. 2020. Mandatory Code of Practice to combat rock fall and rock burst accidents in metalliferous mines at Booysendal (Pty) limited, Limpopo, South Africa.

Malan, D.F. and Napier, J.A.L. 2011. The design of stable pillars in the Bushveld Complex mines: A problem solved? *Journal of the Southern African Institute of Mining and Metallurgy*, vol. 111: pp. 821–836.

MOSH Learning Hub. 2019. Minerals Council of South Africa Safety Presentation. Falls of Ground COPA, Welkom.

Northam Platinum Limited. 2018. Annual Integrated Report 2018.: https://www.northam.co.za/procurement/127-investors-and-media/publications/719-annual-report [aAccessed: 7 February 2020]

Nothnagel, S.J. 2020. Personal commication.

Poulos, H.G. and Davis, E.H. 1974. Elastic Solutions for Soil and Rock Mechanics. Wiley, New York. 424 pp.

Spencer, D.A. 2009. Rock engineering designs for the North and South Sections of the Booysendal Project. BPM internal unpublished report.

Van der Woude S. 2019. Challenges in mining for the Fourth Industrial Revolution. *Mining Expo and Conference 2019*. Chamber of Mines of Namibia, Windhoek. pp. 22, 23, and 26.

Van Schalkwyk, L. 2020 Northam Platinum Limited condensed reviewed interim results for the six months ended 31 December 2019. https://www.northam.co.za/presentations [accessed: 2 March 2020]

Wagner, H. 1974. Determination of the complete load-deformation characteristics of coal pillars. *Proceedings of the 3rd International Congress on Rock Mechanics*, Denver, CO. International Society for Rock Mechanics. Vol. 2B, pp 1076-1082.

Wagner, H. 1980. Pillar design in coal mines. *Journal of the South African Institute of Mining and Metallurgy*, vol. 80. pp. 37-45.

Watson, B.P., Kataka, M.O., Leteane, F.P., and Kuijpers, J.S. 2007. Merensky and UG2 pillar strength back analyses. PlatMine 1.2, Johannesburg.

Watson, B.P., Kuijpers, J.S., and Miovsky, P. 2008. *In situ* measurements of pillar behaviour in the Bushveld Platinum deposits of South Africa. *Proceedings of the 42nd U.S. Rock Mechanics Symposium and 2nd U.S.*-Canada Rock Mechanics Symposium, San Francisco. American Rock Mechanics Association, Alexandria, VA. Paper no. ARMA-08-072

Watson, B.P., Stacey, A.T., and Kuijpers, J.S. 2010. Design of Merensky Reef crush pillars. *Journal of the South African Institute of Mining and Metallurgy*, vol. 110. pp. 581–591.

Watson, B.P., Lamos, R.A., and Roberts, D.P. 2021. PlatMine pillar strength formula for the UG2 Reef. *Journal of the Southern African Institute of Mining and Metallurgy*, vol.121, no. 8. pp. 437–448.

Wiles, T. 2017. MAP3D User's Manual version 65. Map3d International Ltd, Perth, Australia. ◆

NATIONAL & INTERNATIONAL ACTIVITIES

2021

20–22 September 2021 — **5th Young Professionals Online Conference 2021**
'A Showcase of Emerging Research and Innovation in the Minerals Industry'
Contact: Gugu Charlie
Tel: +27 11 834-1273/7, Fax: +27 11 838-5923/833-8156
E-mail: gugu@saimm.co.za, Website: http://www.saimm.co.za

23 September 2021 — **3rd Global Engineering Online Symposium**
'Bridging the gap between research (academia) and industry while transitioning into 4IR'
Contact: Gugu Charlie
Tel: +27 11 834-1273/7, Fax: +27 11 838-5923/833-8156
E-mail: gugu@saimm.co.za, Website: http://www.saimm.co.za

26–29 September 2021 — **The 16th International Ferroalloys Congress (INFACON XVI)**
Clarion Hotel & Congress, Trondheim, Norway
infacon2021@videre.ntnu.no

27–29 September 2021 — **XVI INFACON - International Ferroalloys Virtual Congress**
Trondheim, Norway
Contact: infacon2021@videre.ntnu.no
Website: https://www.sintef.no/Infacon/

18–19 October 2021 — **Southern African Rare Earths International Online Conference 2021**
Contact: Camielah Jardine
Tel: +27 11 834-1273/7, Fax: +27 11 838-5923/833-8156
E-mail: camielah@saimm.co.za, Website: http://www.saimm.co.za

25–29 October 2021 — **SAMCODES Online Conference 2021**
'*Good Practice and Lessons Learnt*'
Contact: Gugu Charlie
Tel: +27 11 834-1273/7, Fax: +27 11 838-5923/833-8156
E-mail: gugu@saimm.co.za, Website: http://www.saimm.co.za

11 November 2021 — **17TH Annual Online Student Colloquium 2021**
Contact: Gugu Charlie
Tel: +27 11 834-1273/7, Fax: +27 11 838-5923/833-8156
E-mail: gugu@saimm.co.za, Website: http://www.saimm.co.za

15, 17, 19, 22, 24, 26 November 2021 — **Global Tailings Standards and Opportunities Online Conference 2021**
'*For the Mine of the Future*'
Contact: Gugu Charlie
Tel: +27 11 834-1273/7, Fax: +27 11 838-5923/833-8156
E-mail: gugu@saimm.co.za, Website: http://www.saimm.co.za

2022

February 27–March 3, 2022 — **TMS Furnace Tapping 2022**
Anaheim Convention Center & Anaheim Marriott , Anaheim, California, USA
https://www.tms.org/AnnualMeeting/TMS2022/Programming/Furnace_Tapping_2022/AnnualMeeting/TMS2022/Programming/furnaceTapping.aspx?hkey=718f6af7-1852-445c-be82-596102913416

16–19 May 2022 — **8th Sulphur and Sulphuric Acid Conference 2022**
The Vineyard Hotel, Newlands, Cape Town, South Africa
Contact: Camielah Jardine
Tel: +27 11 834-1273/7, Fax: +27 11 838-5923/833-8156
E-mail: camielah@saimm.co.za, Website: http://www.saimm.co.za

20–27 May 2022 — **ALTA 2022 Hybrid Conference 2022**
Perth, Australia, Tel: +61 8 9389 1488
E-mail: alta@encanta.com.au, Website: www.encanta.com.au

14–16 June 2022 — **Water | Managing for the Future**
Vancouver, BC, Canada, https://www.mineconferences.com

14–16 June 2022 — **Copper Cobalt Africa** *In Association with* **The 10th Southern African Base Metals Conference**
Avani Victoria Falls Resort, Livingstone, Zambia
Contact: Camielah Jardine
Tel: +27 11 834-1273/7, Fax: +27 11 838-5923/833-8156
E-mail: camielah@saimm.co.za, Website: http://www.saimm.co.za

4–8 July 2022 — **32nd SOMP Annual Meeting and Conference 2022**
Windhoek Country Club & Resort, Windhoed, Namibia
Contact: Camielah Jardine
Tel: +27 11 834-1273/7, Fax: +27 11 838-5923/833-8156
E-mail: camielah@saimm.co.za, Website: http://www.saimm.co.za

9–13 July 2022 — **Sustainable Development in the Minerals Indistry (SDIMI) 2022 10th International Hybrid Conference**
Swakopmund Hotel and Entertainment Centre, Swakopmund, Namibia
Contact: Gugu Charlie
Tel: +27 11 834-1273/7, Fax: +27 11 838-5923/833-8156
E-mail: gugu@saimm.co.za, Website: http://www.saimm.co.za

21–25 August 2022 — **XXXI International Mineral Processing Congress 2022**
Melbourne, Australia + Online, www.impc2022.com

24–25 August 2022 — **Battery Materials Conference 2022**
Misty Hills Conference Venue, Muldersdrift, Johannesburg, South Africa
Contact: Camielah Jardine
Tel: +27 11 834-1273/7, Fax: +27 11 838-5923/833-8156
E-mail: camielah@saimm.co.za, Website: http://www.saimm.co.za

6–8 September 2022 — **PGM The 8th International Conference 2022**
Sun City, Rustenburg, South Africa
Contact: Camielah Jardine
Tel: +27 11 834-1273/7, Fax: +27 11 838-5923/833-8156
E-mail: camielah@saimm.co.za, Website: http://www.saimm.co.za

28–29 September 2022 — **Thermodynamic from Nanoscale to Operational Scale (THANOS) International Hybrid Conference 2022**
on Enhanced use of Thermodynamic Data in Pyrometallurgy Teaching and Research
Mintek, Randburg, South Africa
Contact: Camielah Jardine
Tel: +27 11 834-1273/7, Fax: +27 11 838-5923/833-8156
E-mail: camielah@saimm.co.za, Website: http://www.saimm.co.za

Company affiliates

The following organizations have been admitted to the Institute as Company Affiliates

3M South Africa (Pty) Limited
AECOM SA (Pty) Ltd
AEL Mining Services Limited
African Pegmatite (Pty) Ltd
Air Liquide (PTY) Ltd
Alexander Proudfoot Africa (Pty) Ltd
AMEC Foster Wheeler
AMIRA International Africa (Pty) Ltd
ANDRITZ Delkor (Pty) Ltd
Anlgo Operations Proprietary Limited
Anglogold Ashanti Ltd
Arcus Gibb (Pty) Ltd
ASPASA
Aurecon South Africa (Pty) Ltd
Aveng Engineering
Aveng Mining Shafts and Underground
Axiom Chemlab Supplies (Pty) Ltd
Axis House (Pty) Ltd
Bafokeng Rasimone Platinum Mine
Barloworld Equipment -Mining
BASF Holdings SA (Pty) Ltd
BCL Limited
Becker Mining (Pty) Ltd
BedRock Mining Support (Pty) Ltd
BHP Billiton Energy Coal SA Ltd
Blue Cube Systems (Pty) Ltd
Bluhm Burton Engineering (Pty) Ltd
Bond Equipment (Pty) Ltd
Bouygues Travaux Publics
Castle Lead Works
CDM Group
CGG Services SA
Coalmin Process Technologies CC
Concor Opencast Mining
Concor Technicrete
Council for Geoscience Library
CRONIMET Mining Processing SA (Pty) Ltd
CSIR Natural Resources and the Environment (NRE)
Data Mine SA
Digby Wells and Associates
DRA Mineral Projects (Pty) Ltd
DTP Mining - Bouygues Construction
Duraset
Elbroc Mining Products (Pty) Ltd
eThekwini Municipality
Ex Mente Technologies (Pty) Ltd
Expectra 2004 (Pty) Ltd
Exxaro Coal (Pty) Ltd
Exxaro Resources Limited
Filtaquip (Pty) Ltd
FLSmidth Minerals (Pty) Ltd
Fluor Daniel SA (Pty) Ltd
Franki Africa (Pty) Ltd-JHB
Fraser Alexander (Pty) Ltd
G H H Mining Machines (Pty) Ltd
Geobrugg Southern Africa (Pty) Ltd
Glencore
Gravitas Minerals (Pty) Ltd
Hall Core Drilling (Pty) Ltd
Hatch (Pty) Ltd
Herrenknecht AG
HPE Hydro Power Equipment (Pty) Ltd
Immersive Technologies
IMS Engineering (Pty) Ltd
Ingwenya Mineral Processing (Pty) Ltd
Ivanhoe Mines SA
Joy Global Inc.(Africa)
Kudumane Manganese Resources
Leica Geosystems (Pty) Ltd
Longyear South Africa (Pty) Ltd
Lull Storm Trading (Pty) Ltd
Maccaferri SA (Pty) Ltd
Magnetech (Pty) Ltd
MAGOTTEAUX (Pty) Ltd
Malvern Panalytical (Pty) Ltd
Maptek (Pty) Ltd
Maxam Dantex (Pty) Ltd
MBE Minerals SA Pty Ltd
MCC Contracts (Pty) Ltd
MD Mineral Technologies SA (Pty) Ltd
MDM Technical Africa (Pty) Ltd
Metalock Engineering RSA (Pty)Ltd
Metorex Limited
Metso Minerals (South Africa) Pty Ltd
Micromine Africa (Pty) Ltd
MineARC South Africa (Pty) Ltd
Minerals Council of South Africa
Minerals Operations Executive (Pty) Ltd
MineRP Holding (Pty) Ltd
Mining Projections Concepts
Mintek
MIP Process Technologies (Pty) Limited
MLB Investment CC
Modular Mining Systems Africa (Pty) Ltd
MSA Group (Pty) Ltd
Multotec (Pty) Ltd
Murray and Roberts Cementation
Nalco Africa (Pty) Ltd
Namakwa Sands(Pty) Ltd
Ncamiso Trading (Pty) Ltd
New Concept Mining (Pty) Limited
Northam Platinum Ltd - Zondereinde
Opermin Operational Excellence
OPTRON (Pty) Ltd
Paterson & Cooke Consulting Engineers (Pty) Ltd
Perkinelmer
Polysius A Division Of Thyssenkrupp Industrial Sol
Precious Metals Refiners
Rams Mining Technologies
Rand Refinery Limited
Redpath Mining (South Africa) (Pty) Ltd
Rocbolt Technologies
Rosond (Pty) Ltd
Royal Bafokeng Platinum
Roytec Global (Pty) Ltd
RungePincockMinarco Limited
Rustenburg Platinum Mines Limited
Salene Mining (Pty) Ltd
Sandvik Mining and Construction Delmas (Pty) Ltd
Sandvik Mining and Construction RSA(Pty) Ltd
SANIRE
Schauenburg (Pty) Ltd
Sebilo Resources (Pty) Ltd
SENET (Pty) Ltd
Senmin International (Pty) Ltd
SISA Inspection (Pty) Ltd
Smec South Africa
Sound Mining Solution (Pty) Ltd
SRK Consulting SA (Pty) Ltd
Time Mining and Processing (Pty) Ltd
Timrite (Pty) Ltd
Tomra (Pty) Ltd
Traka Africa (Pty) Ltd
Ukwazi Mining Solutions (Pty) Ltd
Umgeni Water
Webber Wentzel
Weir Minerals Africa
Welding Alloys South Africa
Worley

SAIMM
THE SOUTHERN AFRICAN INSTITUTE OF MINING AND METALLURGY

SAIMM ONLINE CONFERENCE

GLOBAL TAILINGS STANDARDS AND OPPORTUNITIES

FOR THE MINE OF THE FUTURE

15, 17, 19, 22, 24, 26 NOVEMBER 2021

IN PARTNERSHIP WITH

GLOBAL TAILINGS STANDARD BY

ICMM International Council on Mining & Metals

UN environment programme

PRI Principles for Responsible Investment

SUPPORTED BY

INTERNATIONAL MINE WATER ASSOCIATION

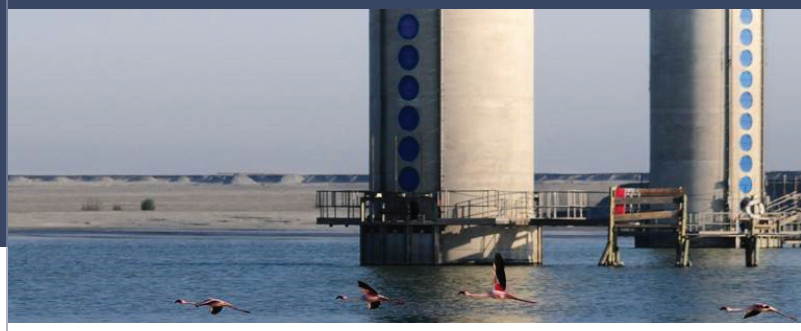

Tailings storage facilities have been a feature of mining operations around the globe since mining began. They are the depositories of waste or gangue material from mining operations and mineral processing plants, or the storage facilities for pollution control. In some cases, they may still contain low grade minerals, high grade fines that are not economically viable to treat. They may also contain reagents and other radioactive or potentially harmful minerals and chemicals, that could damage ecosystems in the event of their escape. Tailings facilities are each in a way unique, either in terms of location, terrain, design and construction. Furthermore, in terms of design and construction, debate occurs globally on the merits and demerits of upstream and downstream facilities, and wet or dry facilities.

Following failures of TSFs over many decades, but especially in the last few years, great pressure from civil society and the investment community has resulted in calls for more stringent standards and audits, as well as public disclosure of the results of risk analysis and monitoring.

This has culminated in the recent publication of the Global Industry Standard on Tailings Management by ICMM, UNEP and PRI as well as guidance by the International Commission on Large Dams (ICOLD). At the same time, the Global Mining Professionals Alliance has called on its members to participate actively on a Global Action on Tailings (GAT) group, to ensure cross fertilisation of knowledge and learnings about TSFs across the globe.

In addition, and in response to calls from the Church of England Pensions Board and the Council on Ethics for the Swedish Public Pension Funds, many mining companies conducted deep-dive self-audits during 2019 and 2020 which they published on their websites for public scrutiny.

In South Africa, the SAIMM has convened a Task Group which includes industry professionals, Academia, the SAIMM, and the South African Institute of Civil Engineers (SAICE). This group has formed the organizing committee for the presentation of this very important international conference.

KEYNOTE SPEAKERS:

Aidan Davy, *ICMM, United KIngdom*

Adam Matthews, *Chief Responsible Investment Officer, Church of England Pensions Board, United Kingdom*

Ross Cooper, *Sibanye Stillwater, South Africa*

Mariette Liefferink, *Federation for a Sustainable Environment, South Africa*

Alastair Macfarlane, *Mandela Mining Precinct, South Africa*

Luis Alberto Torres-Cruz, *University of the Witwatersrand, South Africa*

Isabelle Ramdoo, *International Institute for Sustainable Development, Switzerland*

Chris Anderson, *Yirri Global LLC, USA*

SPONSORS

GEO GROUP

AQUASENS™ Tailings Dam Sensors

FRASER ALEXANDER

IMPLATS EXCELLENCE IN PGMs

srk consulting

XROSSWATER GmbH Industrial Marine floating walkways

FOR FURTHER INFORMATION, CONTACT:

Gugu Charlie,
Conference Co-Ordinator

E-mail: gugu@saimm.co.za
Web: www.saimm.co.za

SAIMM ONLINE

COLLOQUIUM

17TH ANNUAL STUDENT COLLOQUIUM

Technological developments within mining and metals Industry through applied research

11 NOVEMBER 2021

CPD Points: 1 ECSA CPD Points

Students R150 (Inclusive of VAT)

Non-Students – R250 (Inclusive of VAT)

SUPPORTED BY

Online Registration Click Here

The Southern African Institute of Mining and Metallurgy has been organizing and presenting the annual Student Colloquium since 2002, to afford the best final-year mining and metallurgical students an opportunity to present their final year projects to an audience of mining and metallurgical industry experts.

These students are our future young professionals and will be fundamentally affected by how the industry operates. We have to support and assist our future young professionals! As Nelson Mandela observed: 'Education is the most powerful weapon which you can use to change the world'.

The SAIMM cordially invites our experts in the field to meet the fine calibre of young professionals who are about to embark on their careers in industry. There are 11 mining and 11 metallurgical presentations planned for the event, to be held online on 11 November 2021 . The top five in each discipline will have the opportunity to be published in the prestigious SAIMM Journal in April 2022. The presentations selected will be required to be submitted in the form of draft papers before 12 October 2021.

Our strategy is: To contribute to the nurturing of prosperous and empowered young professionals.

FOR FURTHER INFORMATION, CONTACT:

Gugu Charlie,
Conference Co-ordinator

E-mail: gugu@saimm.co.za
Web: www.saimm.co.za

YOUNG PROFESSIONALS COUNCIL

SAIMM
THE SOUTHERN AFRICAN INSTITUTE OF MINING AND METALLURGY